Synthesis and Characterization of Macrocyclic Complexes and Their Possible Applications

Surachai Kongchoo

A Thesis Submitted in Fulfillment of the Requirements for the Degree of Doctor of Philosophy in Chemistry

Prince of Songkla University

2017

Thesis Title	Synthesis and Characterization of Macrocyclic Complexes and Their Possible Applications
Author	Mr. Surachai Kongchoo
Major Program	Chemistry

Major Advisor

.....

(Assoc. Prof. Dr.Sumpun Wongnawa)

Co-advisor

.....

(Dr.Anob Kantacha)

Examining Committee :

.....Chairperson

(Asst. Prof. Dr. Chomchai Suksai)

.....Committee

(Assoc. Prof. Dr.Sumpun Wongnawa)

.....Committee

(Dr. Anob Kantacha)

.....Committee

(Asst. Prof. Dr. Kanidtha Hansongnern)

.....Committee

(Asst. Prof. Dr. Saowanit Saithong)

The Graduate School, Prince of Songkla University, has approved this thesis as fulfillment of the requirements for the Doctor of Philosophy Degree in Chemistry

.....

(Assoc. Prof. Dr.Teerapol Srichana)

Dean of Graduate School

This is to certify that the work here submitted is the result of the candidate's own investigations. Due acknowledgement has been made of any assistance received.

.....Signature
(Assoc. Prof. Dr.Sumpun Wongnawa)
Major Advisor

.....Signature
(Dr.Anob Kantacha)
Co-advisor

.....Signature
(Mr.Surachai Kongchoo)
Candidate

I hereby certify that this work has not been accepted in substance for any degree, and is not being currently submitted in candidature for any degree.

.....Signature
(Mr.Surachai Kongchoo)
Candidate

ชื่อวิทยานิพนธ์ การสังเคราะห์ และศึกษาคุณลักษณะของสารประกอบเชิงซ้อนที่มีลิแกนด์เป็นวงปิดและการใช้ประโยชน์

ผู้เขียน นายสุรชัย คงชู

สาขาวิชา เคมี

ปีการศึกษา 2559

บทคัดย่อ

สังเคราะห์สารประกอบเชิงซ้อนชนิดใหม่ของคอปเปอร์(II) และนิกเกิล(II) ทั้งหมด 15 ชนิด คือ $[CuL^{1}(ClO_4)_2]$ **(1)**, $[CuL^{2}(ClO_4)_2]$ **(2)**, $[CuL^{3}(ClO_4)_2]$ **(3)**, $[NiL^{3}](ClO_4)_2$ **(4)**, $[CuL^{4}(ClO_4)_2]$ **(5)**, $[CuL^{5}(ClO_4)_2]$ **(6)**, $[NiL^{5}](ClO_4)_2$ **(7)**, $[CuL^{6}(ClO_4)_2]$ **(8)**, $[CuL^{7}(ClO_4)_2]$ **(9)**, $[NiL^{7}](ClO_4)_2$ **(10)**, $[CuL^{8}(ClO_4)_2]$ **(11)**, $[CuL^{5}]_3[Fe(CN)_6]_3 \cdot 5H_2O$ **(12)**, $[NiL^{5}(4\text{-nba})_2] \cdot H_2O$ **(13)**, $[NiL^{3}(4\text{-nba})_2]$ **(14)** และ $[NiL^{5}(sal)_2]$ **(15)**, เมื่อ $L^{1,3,5,7}$ = 3,10-ไดแอลคิล-1,3,5,8,10,12-เฮกซะเอซาไซโคลเตตระเดคเคน, $L^{2,4,6,8}$ = 3,10-ไดแอลคิล-6,13-ไดเมทิล-1,3,5,8,10,12-เฮกซะเอซาไซโคลเตตระเดคเคน, 4-nba = *p*-ไนโตรเบนโซเอต และ sal = ซาลิไซเลต) และศึกษาคุณลักษณะทางโครงสร้างด้วยการวิเคราะห์หาเปอร์เซ็นต์ธาตุที่เป็นองค์ประกอบ และเทคนิคทางสเปกโทรสโกปี จากการศึกษาโครงสร้างผลึกของสารประกอบเชิงซ้อน **(5)**, **(7)**, **(8)**, **(12)** - **(15)** ด้วยเทคนิคการเลี้ยวเบนของรังสีเอกซ์บนผลึกเดี่ยว พบว่า สารประกอบเชิงซ้อน **(5)**, **(8)**, **(13)** - **(15)** มีโลหะศูนย์กลาง (ไอออนคอปเปอร์(II) หรือ ไอออนนิกเกิล(II)) ที่มีรูปทรงเรขาคณิตทรงแปดหน้าที่บิดเบี้ยว ในขณะที่สารประกอบเชิงซ้อน **(7)** เป็นรูปทรงเรขาคณิตแบบสี่เหลี่ยมแบนราบ ส่วนสารประกอบเชิงซ้อน **(12)** เป็นโลหะคู่ 2 ชนิดประกอบกันเป็นโครงสร้างแบบเพนตะนิวเคลียร์ Cu_3Fe_2 โดยใช้ลิแกนด์ไซยาไนด์เป็นสะพานเชื่อม ทำให้เกิดรูปทรงเรขาคณิตรอบอะตอมกลางที่แตกต่างกันสองชนิด คือ ทรงแปดหน้าและพีระมิดฐานสี่เหลี่ยม นอกจากนี้ได้ศึกษาการสลายตัวของสีย้อมเมทิล ออร์เรนจ์ โดยใช้โพแทสเซียม เปอร์ซัลเฟต (KPS) ร่วมกับสารประกอบเชิงซ้อน **(13)** (**(14)** หรือ **(15)**) พบว่า การสลายตัวของสีย้อมจะเกิดขึ้นอย่างสมบูรณ์ที่เวลาประมาณ 60 นาที เมื่อเปรียบเทียบกับสาร KPS เพียงอย่างเดียวภายใต้แสงยูวี สำหรับสารประกอบเชิงซ้อน **(3)** - **(10)** ได้ศึกษาฤทธิ์การต้านเชื้อแบคทีเรียบางชนิดทั้งแกรมบวกและแกรมลบ พบว่า มีประสิทธิภาพในการต้านเชื้อแบคทีเรียได้ทุกชนิดที่ความเข้มข้น 1 มิลลิกรัมต่อมิลลิลิตร

Thesis Title Synthesis and Characterization of Macrocyclic Complexes and Their Possible Applications
Author Mr. Surachai Kongchoo
Major Program Chemistry
Academic Year 2016

ABSTRACT

Fifteen new copper(II) and nickel(II) complexes with the composition $[CuL^1(ClO_4)_2]$ **(1)**, $[CuL^2(ClO_4)_2]$ **(2)**, $[CuL^3(ClO_4)_2]$ **(3)**, $[NiL^3](ClO_4)_2$ **(4)**, $[CuL^4(ClO_4)_2]$ **(5)**, $[CuL^5(ClO_4)_2]$ **(6)**, $[NiL^5](ClO_4)_2$ **(7)**, $[CuL^6(ClO_4)_2]$ **(8)**, $[CuL^7(ClO_4)_2]$ **(9)**, $[NiL^7](ClO_4)_2$ **(10)**, $[CuL^8(ClO_4)_2]$ **(11)**, $[CuL^5]_3[Fe(CN)_6]_3\cdot 5H_2O$ **(12)**, $[NiL^5(4\text{-nba})_2]\cdot H_2O$ **(13)**, $[NiL^3(4\text{-nba})_2]$ **(14)**, and $[NiL^5(sal)_2]$ **(15)**, ($L^{1,3,5,7}$ = 3,10-dialkyl-1,3,5,8,10,12-hexaazacyclotetradecane, $L^{2,4,6,8}$ = 3,10-dialkyl-6,13-dimethyl-1,3,5,-8,10,12-hexaazacyclotetradecane, 4-nba = *p*-nitrobenzoate, and sal = salicylate) have been synthesized and structurally studied by a combination of elemental analysis, spectroscopic techniques. The crystal structures of **(5)**, **(7)**, **(8)**, **(12) - (15)** were determined by single crystal X-ray diffraction measurements. Complexes **(5)**, **(8)**, **(13) - (15)** displayed a distorted octahedral coordination geometry environment for the copper(II) ions (or nickel(II) ions), while the complex **(7)** showed square-planar geometry. Complex **(12)** existed as cyano-bridged bimetallic of pentanuclear Cu_3Fe_2 with two different coordination modes of $[Fe(CN)_6]^{3-}$ through the Fe-C≡N-Cu linkages. In addition to, the degradation of methyl orange by potassium persulfate (KPS) in the presence of complex **(13)** (**(14)** or **(15)**) oxidation system was studied and found that it occurred to near completion in 60 min compared to only 55 % with KPS alone under UV light irradiation. Thus, this study showed that KPS and the complexes oxidation system could be an attractive choice for degradation of organic pollutants for environmental remediation. The complexes **(3) - (10)** were tested against different bacteria *in vitro* and were found to be potentially active in the concentration 1 mg mL^{-1}.

ACKNOWLEDGEMENTS

I would like to express my deepest respect and the most sincere appreciation to my supervisor Associate Professor Dr. Sumpun Wongnawa for generous support, his various suggestions, assistance in reading, correcting, criticizing the manuscript, and guidance throughout this work.

I am very grateful to thank my co-advisor Dr. Anob Kantacha (Department of Chemistry, Faculty of Science, Thaksin University) for the valuable comments on my thesis.

I am grateful to my examining committee, Assistant Professor Dr. Chomchai Suksai (Department of Chemistry, Faculty of Science, Burapha University), Assistant Professors Dr. Kanidtha Hansongnern and Dr. Saowanit Saithong (Department of Chemistry, Faculty of Science, Prince of Songkla University) for the kindness, comment, and helpful suggestion.

I am grateful to thank Assistant Professor Dr. Saowanit Saithong, who suggested research problem about single crystal X-ray diffraction analysis and the first article was published with great success.

A very special thank is due to Assistant Professor Dr. Kittipong Chainok (Department of Physics, Faculty of Science and Technology, Thammasat University) for providing single crystal X-ray diffractometer and sometimes organized workshops on solved and refinement of the crystal structures with *OLEX2* programe which is used in this thesis.

I am deeply indebted to the Songklanagarind Scholarship for Graduate Studies from the Prince of Songkla University and the Graduate School, Prince of Songkla University, for the partial supports of the research fund.

I would like to thank the Department of Chemistry, Faculty of Science, Prince of Songkla University, for all necessary laboratory facilities used throughout this research.

My deepest gratitude goes to my parents, brothers, and sisters for their unflagging love and support throughout my life; this work is simply impossible without them. I am forever grateful to them.

My heartfelt thanks also go to all dear friends. Finally, I thank all those who gave suggestions, advices, and guidance before and during the research. Omissions of references to any special help or suggestions are unintentional and I express my regret.

Surachai Kongchoo

CONTENTS

CONTENTS (CONTINUED)

CONTENTS (CONTINUED)

LIST OF TABLES

LIST OF TABLES (CONTINUED)

LIST OF FIGURES

LIST OF FIGURES (CONTINUED)

LIST OF FIGURES (CONTINUED)

LIST OF FIGURES (CONTINUED)

LIST OF FIGURES (CONTINUED)

LIST OF FIGURES (CONTINUED)

LIST OF FIGURES (CONTINUED)

LIST OF FIGURES (CONTINUED)

LIST OF SCHEMES

LIST OF ABBREVIATIONS AND SYMBOLS

B.M.	=	Bohr Magneton
nm	=	Nanometer
cm^{-1}	=	Wavenumber
K	=	Kelvin
mg	=	Milligram
mg L^{-1}	=	Milligram per liter
g L^{-1}	=	Gram per liter
1D	=	One-dimensional
2D	=	Two-dimensional
3D	=	Three-dimensional
MeCN	=	Acetonitrile
DMSO	=	Dimethyl sulfoxide
FT-IR	=	Fourier-Transformed Infrared
UV-Vis	=	Ultraviolet-Visible
EPR	=	Electron Paramagnetic Resonance
NMR	=	Nuclear Magnetic Resonance
TGA	=	Thermal Gravimetric Analyzer
ESI-MS	=	Electro Spray Ionization-Mass Spectroscopy
DRS	=	Diffused Reflectance Spectroscopy
PXRD	=	Powder X-ray Diffraction
MIC	=	Minimal Inhibitory Concentration
AOPs	=	Advanced Oxidation Processes
TOC	=	Total Organic Carbon
Ω^{-1} cm^2 M^{-1}	=	Per Ohm centimeter square per molar
4-nba	=	Para nitrobenzoate
sal	=	Salicylate
^oC	=	Degree Celsius
M.P.	=	Melting Point

LIST OF ABBREVIATIONS AND SYMBOLS (CONTINUED)

Calc.	=	Calculated values
Å	=	Angstrom unit
Z	=	Atomic of formula units per unit cell
R	=	Conventional residual, calculate from F_0-data
wR_2	=	Weight residual, calculate from F_0^2-data
τ values	=	Geometry index or structural parameter
ax	=	Axial position
eq	=	Equatorial plane
mer	=	Meridional isomer
fac	=	Facial isomer

CHAPTER 1

INTRODUCTION

1.1 Introduction

The metal(II) ion chemistry of macrocyclic ligands has now become a principle subdivision of inorganic chemistry and is a growing area of research in inorganic and bioinorganic chemistry. Macrocyclic ligands in inorganic chemistry are referred to 9-membered rings such as 1,4,7-triazacyclononane **(Figure 1A)** with nickel(II), copper(II), and zinc(II) complexes (Yang *et al*., 1976), 12-membered rings such as 1,4,7,10-tetraazacyclododecane or cyclen **(Figure 1B)** with copper(II) complexes (Goeta *et al*., 2000), 14-membered rings such as 1,4,8,11-tetraazacyclo-tetradecane or cyclam **(Figure 2A)** with nickel(II) complexes (Taraszewska *et al*., 2000), and 20-membered rings such as polyazomethines cyclic **(Figure 2B)** (Elizbarashvili *et al*., 2000). The homo- or hetero atom donors of macrocyclic ligands used to coordinate with metal(II) center are, for example, nitrogen, oxygen, sulfur, and phosphorus. In addition, classifications of types of macrocyclic ligands are tridentate, tetradentate, pentadentate, and so on depending on the number of binding sites. The other form of classifying them is as oxa (O), phospha (P), aza (N), sulfa (S), and a mixture of these depending on the kind of hetero atoms involved. The metal(II) complexes with macrocyclic ligands are important characteristics such as more stable than those with equivalent open chain ligands because macrocyclic effect, stability high oxidation states, high thermodynamic stability (Kamboj *et al*., 2016).

The first report of synthetic hexaazamacrocycle complexes was presented in 1988 when the successful synthesis of 14-membered hexaazamacrocycle by the metal template condensation reaction of ethylenediamine, formaldehyde, and ammonia in the presence of nickel(II) ion or copper(II) ion was discovered by Suh *et al*., 1988. Interest in the study of hexaazamacrocyclic metal(II) complexes with side chains is still growing due to their structural properties and unique coordination, their benefit as bioinorganic chemistry model for hemoglobin, vitamin B12, porphyrin, and

catalysis, and their rapidly developing area in view of their various applications such as radio pharmaceuticals and magnetic resonance imaging (MRI) contrast agents (León-Rodríguez *et al*., 2002), and as luminescent sensors (Bourdolle *et al*., 2011).

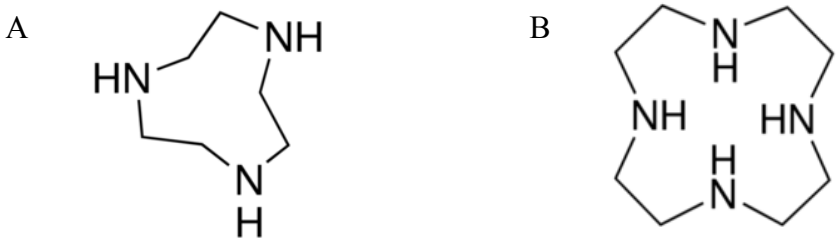

Figure 1. Macrocyclic ligands, (A) 1,4,7-triazacyclononane (Yang *et al*., 1976) and (B) 1,4,7,10-tetraazacyclododecane (Goeta *et al*., 2000).

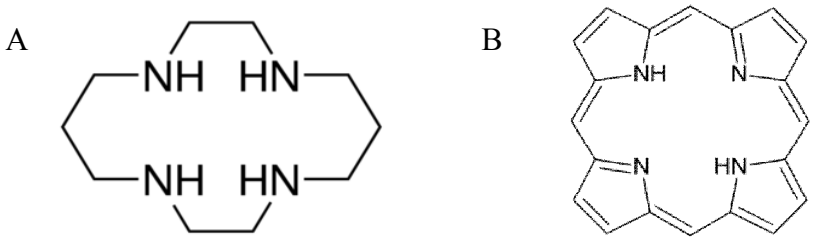

Figure 2. Macrocyclic ligands, (A) 1,4,8,11-tetraazacyclotetradecane (Taraszewska *et al*., 2000) and (B) polyazomethines cyclic (Elizbarashvili *et al*., 2000).

1.2 Synthesis of macrocyclic metal(II) complexes

The best method for synthesis of metal(II) complexes with hexaaza-macrocyclic ligands was by metal template condensation reactions. The term "template" has been widely used since early sixties. The routine use of metal template processes for obtaining several of hexaazamacrocyclic ligands were developed by Curtis *et al*., 1961 and Busch, 1963 also coined the template notion in coordination chemistry. Metal(II) template condensation reactions are simple "one-pot reactions" due to cheap and high yielding. Hexaazamacrocyclic complexes are better synthesized with the assist of metal(II) ions as template to direct the condensation reaction which finally ends with rings closure (Christensen *et al*., 1980).

Metal template condensation reactions of coordinated primary amines and formaldehyde in the presence of metal(II) ions are helpful for the preparation of saturated hexaazamacrocyclic complexes due to formaldehyde is a good reagent to connect two amine molecules containing N-CH_2-N linkage (Kang *et al*., 1990). The use of formaldehyde with "locking groups" in a metal template synthesis was widely used to the synthesis of hexaazamacrocycles with different pendant arms (Lindoy, 1989).

1.3 Copper(II) chemistry of macrocyclic complexes

The d^9 configuration of copper(II) ion with octahedral and tetragonal geometry is highly sensible to Jahn-Teller distortion effect. Octahedral Cu(II) complexes without any distortion are prospective to have only one *d-d* absorption band assignable to $^2E_g \rightarrow {}^2T_{2g}$ transition whereas for distorted octahedral Cu(II) complexes various weak absorption bands are given in a broad band around in the near IR region (Mohammed *et al*., 2015). Cu(II) complexes are usually found in tetragonal geometry with bond distances composed of four short in equatorial plane and two axially position elongated bonds because of the Jahn-Teller distortion effect. The tetragonally distorted of Cu(II) complexes display three absorption bands correspond to $^2B_{1g} \leftarrow {}^2A_{1g}$ ($d_x{}^2\text{-}_y{}^2 \leftarrow d_z{}^2$), $^2B_{1g} \leftarrow {}^2B_{2g}$ ($d_x{}^2\text{-}_y{}^2 \leftarrow d_{xy}$), and $^2B_{1g} \leftarrow {}^2E_g$ ($d_x{}^2\text{-}_y{}^2 \leftarrow d_{xz},d_{yz}$) transitions (Chandra *et al*., 2009). The spectra of copper(II) complexes have been vibronically corresponded to D_{4h} symmetry with a $d_x{}^2\text{-}_y{}^2$ ground state. The most active vibration in this point group is b_{1u} symmetry and its performance may occur from its being the only out-of-the xy plane vibration. The order of *d* orbitals levels in copper(II) complexes are as follow: $d_x{}^2\text{-}_y{}^2 > d_z{}^2 > d_{xy} > d_{xz},d_{yz}$ (Hathaway *et al*., 1970).

In the case of a square-planar geometry, the ground term is $^2B_{1g}$ and three *d-d* transition bands are assignable to $^2B_{1g} \rightarrow {}^2B_{2g}$, $^2B_{1g} \rightarrow {}^2A_{1g}$, and $^2B_{1g} \rightarrow {}^2E_g$ are obtained. Magnetic moments of many mononuclear copper(II) complexes are generally in the range 1.75-2.18 Bohr Magneton (B.M.). The low values are observed only in the case of polynuclear copper(II) complexes (Ramesh *et al*., 2016).

1.4 Nickel(II) chemistry of macrocyclic complexes

The nickel(II) ion has a d^8 configuration and forms a large number of complexes with several geometries such as four-coordinate square-planar (D_{4h}) or tetrahedral (T_d) (Li *et al*., 2003), and six-coordinate octahedral (O_h) (Choi *et al*., 2001). Octahedral Ni(II) complexes display three principle *d-d* electronic transition $^3A_{2g} \rightarrow {}^3T_{1g}$, $^3A_{2g} \rightarrow {}^3T_{2g}$, and $^3A_{2g} \rightarrow {}^3T_{1g}$. Two spin-forbidden transitions: $^3A_{2g} \rightarrow {}^1T_{2g}$ and $^3A_{2g} \rightarrow {}^1E_g$ are also obtained near the second spin-allowed transition and between second and third spin-allowed transition, respectively (Nair *et al*., 2014). Octahedral Ni(II) complexes have two unpaired electrons and thus have magnetic moments in the range 2.9-3.4 B.M. depending on the orbital angular momentum (L) contributions.

For tetrahedral nickel(II) complexes with $^3T_1$(F) ground state normally display four transitions: $^3T_1 \rightarrow {}^3A_2$, $^3T_1 \rightarrow {}^1E$, $^3T_1 \rightarrow {}^3T_1$ (P), and $^3T_2 \rightarrow {}^1T_1$. The absorption band $^3T_1 \rightarrow {}^3T_1$ (P) is a strong band of high absorbance intensity compared with other bands. The $^3T_1$ (F) ground state transition to the $^3T_1$ (P) arises in the visible region and has a strong absorption coefficient (ε) compared to the $^3A_{2g} \rightarrow {}^3T_{1g}$ transition in octahedral nickel(II) complexes.

In the case of square-planar nickel(II) complexes, the d_x^2-$_y^2$ orbital is uniquely high in energy and the eight electrons can dominate the other four *d*-orbitals but leave this strongly anti-bonding one vacant. Square-planar nickel(II) complexes reveal three spin-allowed *d-d* transition bands are attributed to $^1A_{1g} \rightarrow {}^1A_{2g}$, $^1A_{1g} \rightarrow {}^1B_{1g}$, and $^1A_{1g} \rightarrow {}^1E_g$. These complexes are frequently yellow, brown, and red due to the presence of the absorption band of medium intensity in the range 450-600 nm (Gaikwad *et al*., 2016).

1.5 Literature reviews

1.5.1 Hexaazamacrocycle copper(II) or nickel(II) complexes with the perchlorate anion coordination.

The copper(II) and nickel(II) complexes of hexaazamacrocyclic ligand with the perchlorate anion coordination have been extensively studied. In particular, the difference of pendant arms or side chain due to their interesting structural and chemical properties as follows:

Kang *et al*., 1999 have synthesized, characterized, and studied crystal structure of new $[Ni(H_2L^1)](ClO_4)_4$ (H_2L^1 = a protonated form of 1,8-*bis*(2-aminoethyl)-1,3,6,8,10,13-hexaazacyclotetradecane (L^1) containing two 2-aminoethyl pendant arms. The complex $[NiL^1]^{2+}$ existed in aqueous solution as a mixture of the square-planar and octahedral geometry $[NiL^1(H_2O)_2]^{2+}$ species. The addition of hydrochloric acid to aqueous solutions was to shift the equilibrium to favor the square-planar form. As a result, this complex was exchanged to increasing of the square-planar form. On the other hand, the addition of sodium hydroxide to the aqueous solutions of $[NiL^1]^{2+}$ increased the proportion of the octahedral form.

He *et al*., 2003 made a detailed study of a new copper(II) complexes: $[Cu(H_2L^1)](ClO_4)_4$ **(1)** and $[CuL^2](ClO_4)_2$ **(2)**, where L^1 = 1,8-*bis*(2-aminoethyl)-1,3,-6,8,10,13-hexaazacyclotetradecane and L^2 = 3;7-bis(2-aminoethyl)-1,3,5,7-tetraaza-bicyclo[3,3,2]decane from which they synthesized by the one-pot reaction of ethylenediamine and formaldehyde in the presence of the copper(II) ion. From the single crystal X-ray data, the crystal structure of **(1)** and **(2)** crystallized in the triclinic space group *P*-1 and monoclinic space group *C*c, respectively. The structure of **(1)** consisted one $[Cu(H_2L)]^{2+}$ cation and two perchlorate anions as shown in **Figure 3**. The crystal structure of **(2)** contained of one $[CuL^2]^{2+}$ cation and two perchlorate anions as shown in **Figure 4**.

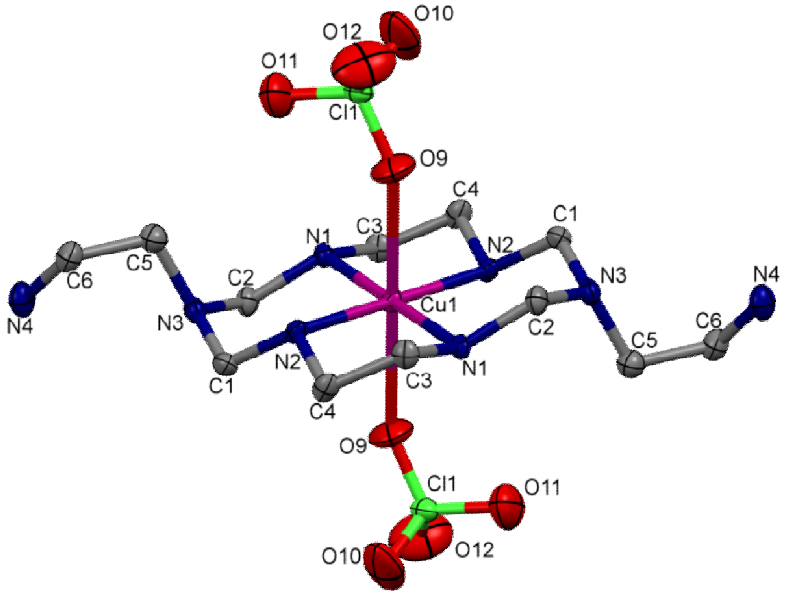

Figure 3. Crystal structure of the $[Cu(H_2L^1)(ClO_4)_2]^{2+}$ unit for **(1)**. All H atoms have been omitted for clarity (He *et al*., 2003).

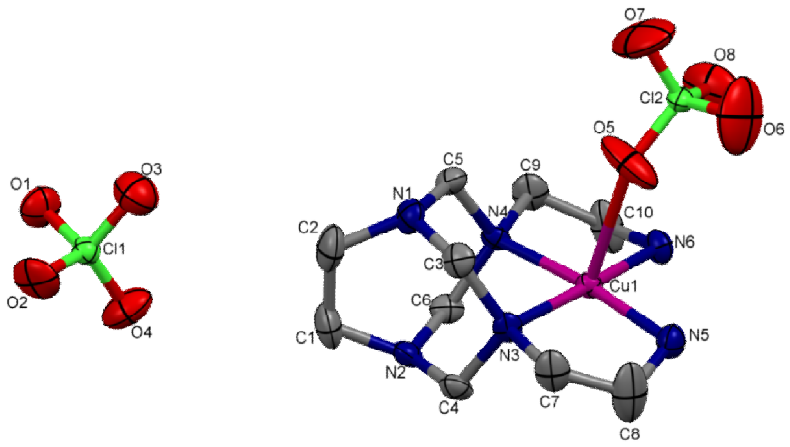

Figure 4. View of the structure for complex **(2)** (He *et al*., 2003).

Li *et al*., 2004 reported two new Ni(II) hexaazamacrocyclic complexes containing *n*-propyl and benzyl chain as pendant arms for complex **(1)** and **(2)**, respectively. The structure of $[Ni(C_{14}H_{34}N_6)](ClO_4)_2$ **(1)** consisted of $[Ni(C_{14}H_{34}N_6)]^{2+}$ cation and ClO_4^- anion as depicted in **Figure 5**. The Ni(II) ion was coordinated by four nitrogen atoms secondary amine of the hexaazamacrocycle in a square-planar geometry. There was hydrogen bonding between secondary nitrogen of the hexaazamacrocycle and the oxygen atom of the perchlorate anions. Complex **(2)** crystallized in the triclinic $P\bar{1}$ space group and asymmetric unit containing two independent half-molecules with the nickel(II) ions located on inversion centers. The nickel(II) ion had a distorted octahedral geometry with long Ni-$O_{perchlorate}$ bonds as shown in **Figure 6**.

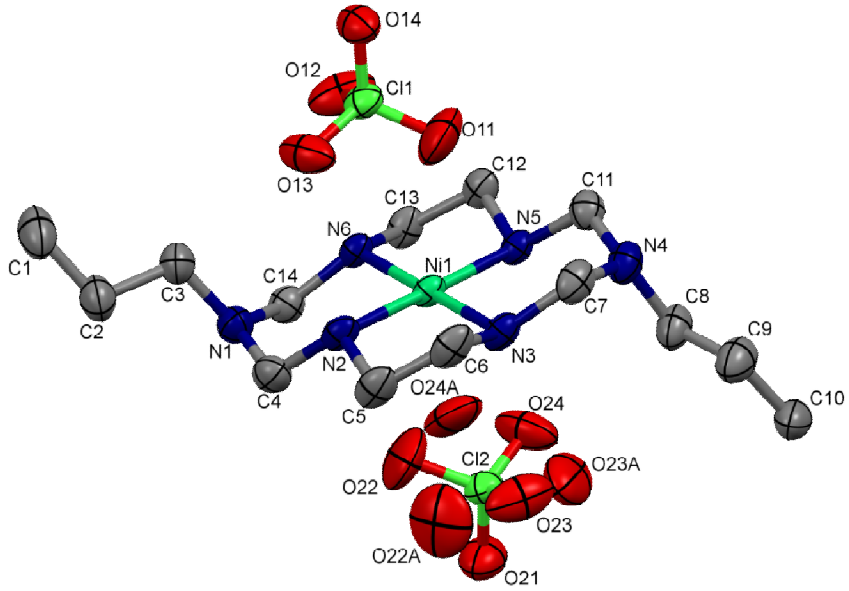

Figure 5. The crystal structure of $[Ni(C_{14}H_{34}N_6)](ClO_4)_2$ **(1)** with atomic labeling scheme. All H atoms have been omitted for clarity (Li *et al*., 2004).

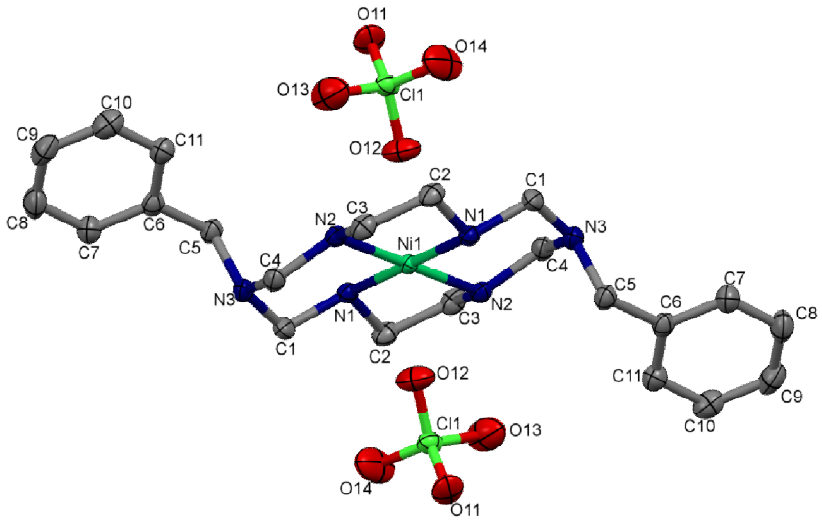

Figure 6. The crystal structure of $[Ni(C_{22}H_{34}N_6)](ClO_4)_2$ **(2)** with atomic labeling scheme. All H atoms have been omitted for clarity (Li *et al*., 2004).

Su *et al*., 2007 synthesized $[NiL](ClO_4)_2{\cdot}CH_3COCH_3$ **(1)** and $[CuL](ClO_4)_2{\cdot}CH_3COCH_3$ **(2)** (L = 3,10-bis(2-thiophenemethyl)-1,3,5,8,10,12-hexa-azacyclotetradecane and characterized by spectroscopic techniques and single crystal X-ray diffraction analyses. In complex **(1)**, the nickel(II) ion coordinated to four N atoms from the macrocyclic ligand in the equatorial position and two O atoms from the ClO_4^- anions in the axial position showing an elongated octahedral coordination geometry as illustrated in **Figure 7**. In complex **(2)**, the copper(II) ion coordinated to four N atoms from the macrocyclic ligand in the equatorial plane and two O atoms from the ClO_4^- anions in the axial position displaying an elongated octahedral coordination geometry as shown in **Figure 8**. The side chain thiophene groups of the adjacent macrocycles showed no π-π stacking interactions. All the perchlorate anions and acetone molecules showed hydrogen bonds interactions with the macrocyclic ligand. Two different molecular arrangements in which both the cations array in the style of M(1)M(2)M(1)... in series were observed.

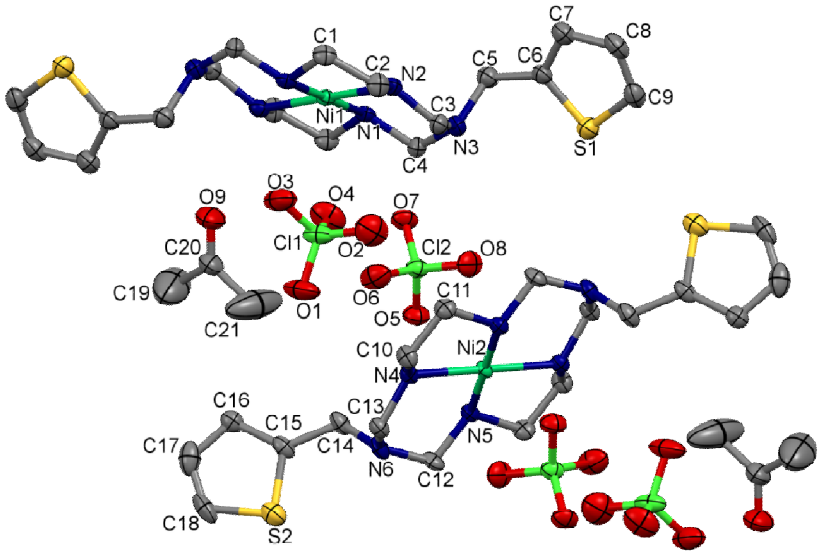

Figure 7. Crystal structure of $[NiL](ClO_4)_2 \cdot CH_3COCH_3$ **(1)** with the atomic numbering scheme (Su *et al.*, 2007).

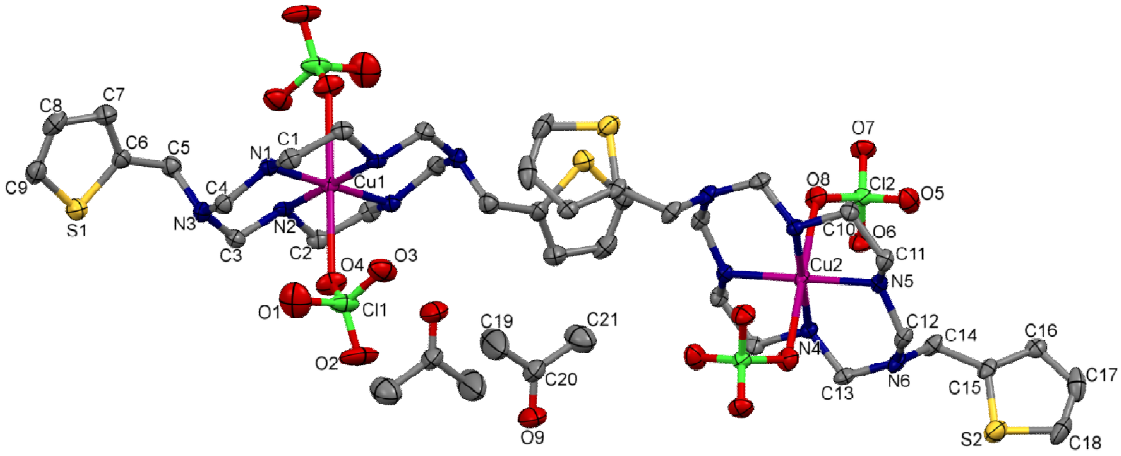

Figure 8. Crystal structure of $[CuL](ClO_4)_2 \cdot CH_3COCH_3$ **(2)** with the atomic numbering scheme (Su *et al.*, 2007).

Han *et al*., 2008 synthesized and characterized new macrocyclic nickel(II) complexes with α-methylbenzyl groups as chiral pendants. The crystal structure of $[Ni(L^{R,R})](ClO_4)_2$ **(1)** and $[Ni(L^{S,S})](ClO_4)_2$ **(2)**, where $L^{R,R/S,S}$ = 1,8-di((*R/S*)-α-methylbenzyl)-1,3,6,8,10,13-hexaazacyclotetradecane and analyzed by single crystal X-ray diffraction. Each complex had a square-planar coordination around the nickel(II) ion and intramolecular hydrogen bonds and π-π stacking interactions. The circular dichroism spectra **(Figure 9)** of $[Ni(L^{R,R})](ClO_4)_2$ **(1)** revealed a negative, positive Cotton effect and that of $[Ni(L^{S,S})](ClO_4)_2$ **(2)** exhibited an enantiomeric pattern. The observation of the CD pattern and the single crystal X-ray data clearly provided evidence for the chirality of **(1)** and **(2)**.

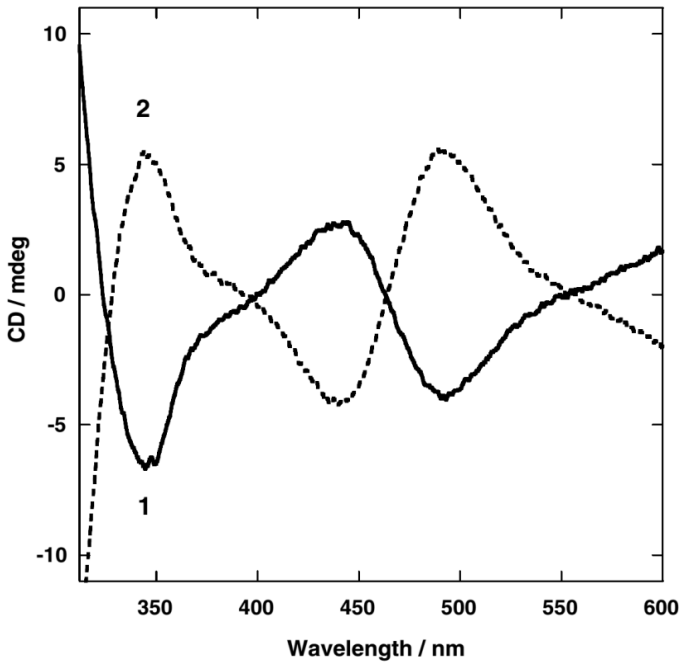

Figure 9. Circular dichroism spectra of **(1)** (*solid line*) and **(2)** (*dotted line*) (Han *et al*., 2008).

Husain *et al*., 2014 synthesized 14-membered hexaazamacrocyclic Cu(II) complex in the type $[CuL(ClO_4)_2]$ (L = 3,10-bis(benzyl)-1,3,5,8,10,12-hexaazacyclotetradecane by template condensation reaction and characterized by spectroscopic and single crystal X-ray techniques. The crystal structure **(Figure 10)** of

$[CuL(ClO_4)_2]$ showed axially elongated octahedral geometry with weakly coordinated perchlorate anions. The hexaazamacrocyclic ring consisted of six- and five-membered chelate rings in chair and gauche conformation, respectively. The spectral data corresponded to the result of X-ray diffraction analysis and the EPR spectra of $[CuL(ClO_4)_2]$ was axially distorted and consistent with a d_x^2-$_y^2$ ground state. The solid state spectra showed the arrangement of the coordination sphere as distorted octahedral while in solution a square-planar structure was detected.

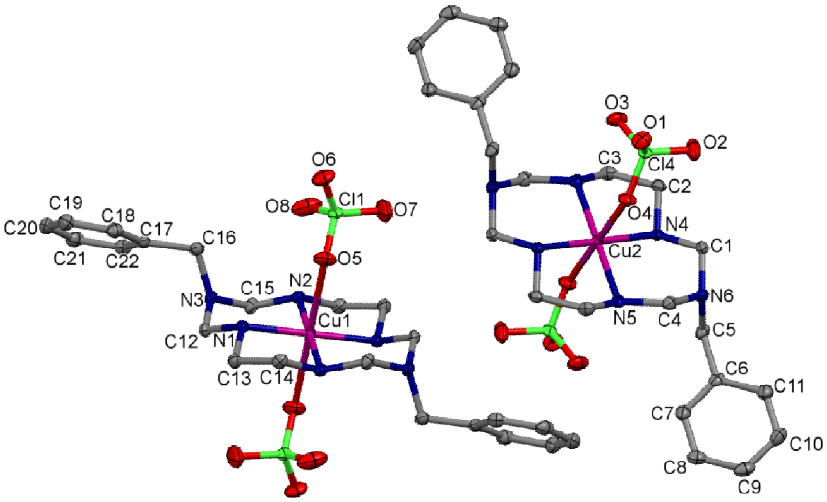

Figure 10. Crystal structure of $[CuL(ClO_4)_2]$ along with the atomic numbering scheme. All hydrogen atoms have been omitted for clarity (Husain *et al.*, 2014).

1.5.2 Hexaazamacrocycle nickel(II) complexes with the carboxylate anion coordination.

Ni(II) complexes with hexaazamacrocyclic ligands as a construction base were synthesized for self-assembly of several coordination polymers and multi-dimensional supramolecular networks. Such supramolecules have attracted many interests due to their potential applications in catalysis, gas sorption, ion-exchange, molecular magnets, optoelectronics, separation, sensor technology, and molecular devices. Among these, hexaazamacrocyclic nickel(II) complexes were used as very helpful building blocks due to availability of vacant sites at axial positions in the

square-planar geometry. In the assembly of the supramolecular framework other types of interaction, for instance hydrogen bonds, π-π stacking, and C-H···π interactions besides the metal-ligand coordination are used to induce intra- and intermolecular interactions. For example, in the supramolecular of hexaazamacrocyclic nickel(II) complexes with mono-, di-, and polycarboxylate ligand as follows:

Choi *et al.*, 1998 reported new supramolecular networks with brick wall and honeycomb structures in the types: $[Ni(C_{12}H_{30}N_6O_2)]_3[C_6H_3(COO)_3]_2{\cdot}18H_2O$ **(1)** and $[Ni(C_{12}H_{30}N_6O_2)]_3[C_6H_3(COO)_3]_2{\cdot}14H_2O{\cdot}2C_5H_5N$ **(2)** which were constructed by the self-assembly from $[Ni(C_{12}H_{30}N_6O_2)](ClO_4)_2$ complex containing hydroxyl pendant arms and 1,3,5-benzenetricarboxylate (BTC^{3-}) anion. From single crystal X-ray structures, each nickel(II) hexaazamacrocycle coordinated with two BTC^{3-} anions in the *trans* position and each BTC^{3-} anion bound to three nickel(II) hexaazamacrocyclic parts through C_1 symmetry in complex **(1) (Figure 11)** and C_3 symmetry in complex **(2)**. Variable-temperature (2-300 K) magnetic susceptibility measurements revealed that all complexes showed weak anti-ferromagnetic interactions between the $S = 1$ nickel(II) paramagnetic centers.

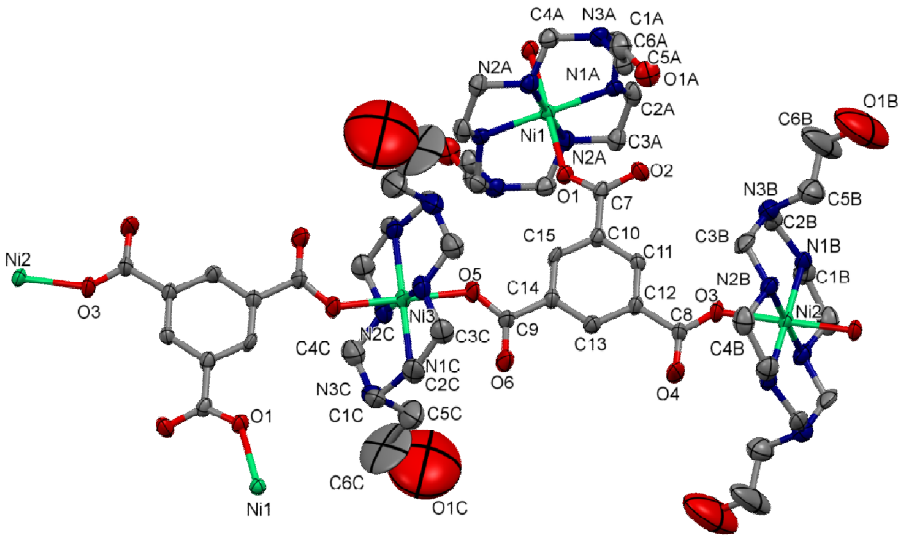

Figure 11. Crystal structure of the trinuclear unit of **(1)** with atomic labeling scheme. All hydrogen atoms and water molecules have been omitted for clarity (Choi *et al.*, 1998).

Choi *et al*., 1999 reported the synthesis of a novel type of $[Ni(C_{12}H_{30}N_6O_2)(C_8H_4O_4)]_n \cdot 4nH_2O$ which self-assembled from a precursor $[Ni(C_{12}H_{30}N_6O_2)](ClO_4)_2$ complex containing hydroxyl pendant arms and terephthalate (tp^{2-}) anion. In the symmetric unit of $[Ni(C_{12}H_{30}N_6O_2)(C_8H_4O_4)]_n \cdot 4nH_2O$, each $[Ni(C_{12}H_{30}N_6O_2)]^{2+}$ cation linked to two oxygen atoms from tp^{2-} anion at the *trans* position to form a distorted octahedral geometry. Each tp^{2-} connected to two Ni(II) ions in an *exo*-bidentate mode which resulted in the linear coordination polymer as depicted in **Figure 12**. In this structure the one-dimensional chains distributed to different directions were connected with the hydrogen bonding using the hydroxyl pendant arms and secondary amines from the hexaazamacrocycles leading to a three-dimensional network.

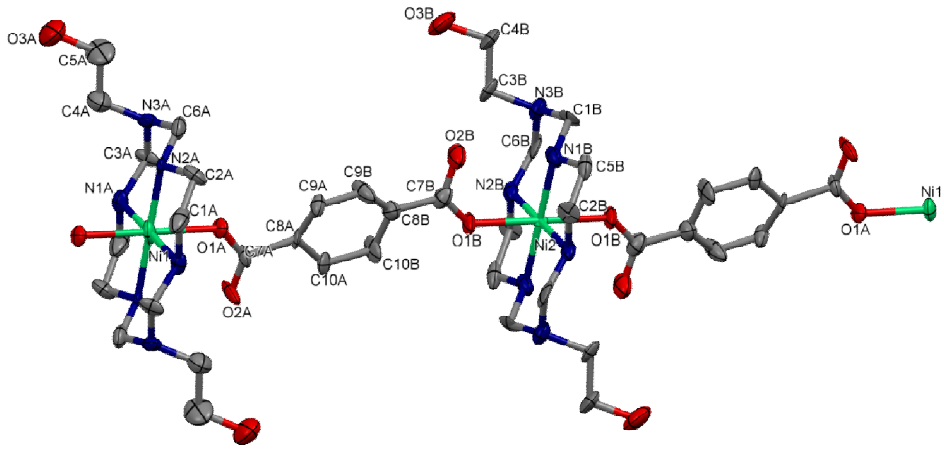

Figure 12. Crystal structure of the asymmetric unit of $[Ni(C_{12}H_{30}N_6O_2)(C_8H_4O_4)]_n \cdot 4nH_2O$ with atomic numbering scheme (Choi *et al*., 1999).

Xiang *et al*., 2001 prepared two nickel(II) complexes with the formula $[(NiL)_2(\mu\text{-ox})](ClO_4)_2$ (L = 3,10-bis(2-hydroxyethyl)-1,3,5,8,10,12-hexaazacyclotetra-decane and ox = oxalate anion and characterized by elemental analyses, spectroscopic techniques, and single crystal X-ray diffraction. The crystal structure of $[(NiL)_2(\mu\text{-ox})](ClO_4)_2$ contained one centrosymmetrical μ-oxalato bridged binuclear $[(NiL)_2(\mu\text{-ox})]^{2+}$ cation and two perchlorate anions. The ox^{2-} anions acted as a bis-bidentate ligand between two $[(NiL)_2(\mu\text{-ox})]^{2+}$ ions **(Figure 13)**. From spectroscopic data and X-ray diffraction results it was expected that the 14-membered hexaazamacrocycles

might adopt folded conformation in their octahedral geometry around the Ni(II) ion. Magnetic susceptibility measurements of $[(NiL)_2(\mu\text{-ox})](ClO_4)_2$ in the temperature range 5.1-300 K indicated that the two Ni(II) ions of the binuclear unit coupled to form anti-ferromagnetic with exchange coupling parameter (J) = -13.8 cm^{-1} and g = 2.05.

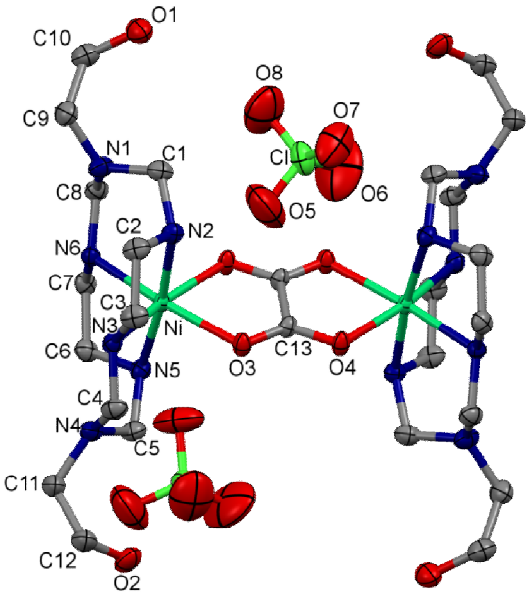

Figure 13. Crystal structure of $[(NiL)_2(\mu\text{-ox})](ClO_4)_2$ with atomic numbering scheme. All hydrogen atoms have been omitted for clarity (Xiang *et al*., 2001).

Min *et al*., 2001 reported the synthesis of the supramolecular complexes, $[Ni(C_{20}H_{32}N_8)(isonicotinate)_2]$ (**1**) and $[Ni(C_{20}H_{32}N_8)(BQDC)_2]\cdot 3H_2O$ (**2**) (BQDC = 2,2′-biquinoline-4,4′-dicarboxylate) by the self-assembly of a precursor $[Ni(C_{20}H_{32}N_8)](ClO_4)_2\cdot 2H_2O$ complex containing pyridyl rings as a pendant arms with isonicotinic acid and potassium 2,2'-biquinoline-4,4'-dicarboxylate, respectively. The crystal structure of **(1)** revealed that two isonicotinate anions linked to a nickel(II) hexaazamacrocyclic complex in axial positions as illustrated in **Figure 14**. The pyridine groups from isonicotinate ligands were linked in the offset face-to-face π-π stacking interaction leading to a one-dimensional chain network. The crystal structure of **(2)** shows that each $BQDC^{2-}$ anion bound two nickel(II) hexaazamacrocyclic complexes and each nickel(II) hexaazamacrocyclic unit coordinated to two $BQDC^{2-}$

anions in axial positions to form a one-dimensional chain network as illustrated in **Figure 15**. The 1D chain consisted of the intramolecular hydrogen bonding as well as the interchain offset face-to-face π-π stacking interactions between the pyridyl rings from hexaazamacrocycle and the $BQDC^{2-}$ anions leading to a 2D sheet.

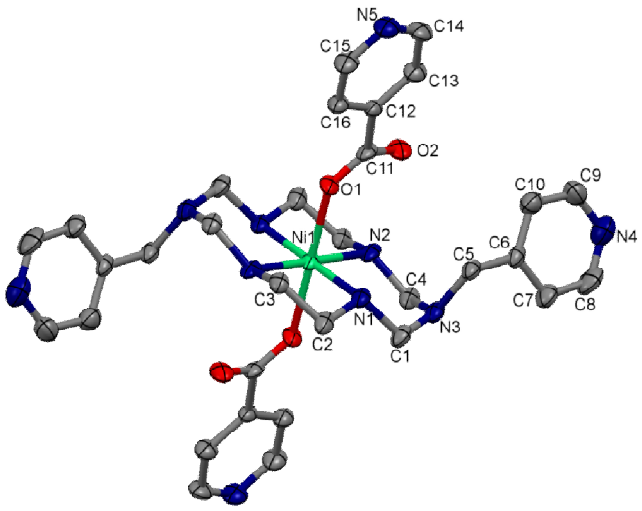

Figure 14. Crystal structure of **(1)** with atomic numbering scheme. All hydrogen atoms have been omitted for clarity (Min *et al*., 2001).

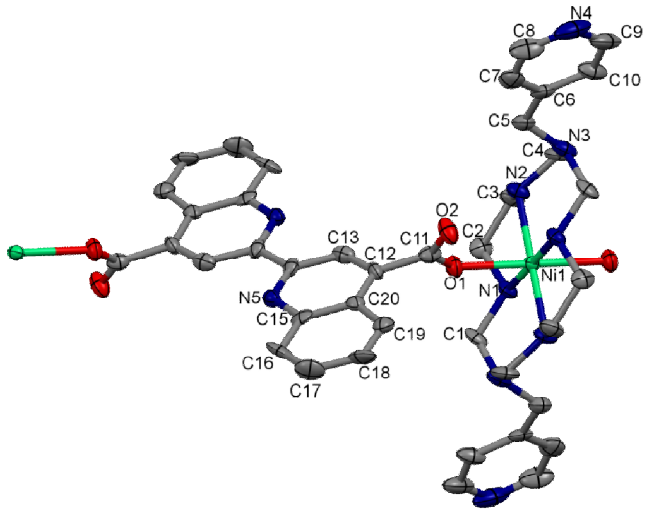

Figure 15. Crystal structure of **(2)** with atomic numbering scheme. All H-atoms and two water molecules have been omitted for clarity (Min *et al*., 2001).

Kim *et al*., 2002 have synthesized $\{[Ni(L)]\cdot(btc^{2-})\}_n$ **(1)** and $[Ni(L)]\cdot(btc^{2-})\cdot(btc)$ **(2)**, where L = 3,10-bis(2-hydroxy- ethyl)-1,3,5,8,10,12,-hexaazacyclotetradecane and btc = 1,2,4,5-benzenetetracarboxylic acid, from the reaction between $[Ni(L)Cl_2]$ containing methyl group as pendant arms and btc ligand. These structures were characterized by elemental analyses, spectroscopy, and single crystal X-ray diffraction methods. The orange crystals of **(1)** involved a one-dimension polymeric chain with $[Ni(L)]^{2+}$ cation and bridging btc^{2-} anions. The coordination geometry of **(1)** was a square-planar with four Ni-N bonds and weak interactions between the oxygen atoms from btc^{2-} anions with the nickel(II) ions as shown in **Figure 16**. The yellow crystals of **(2)** had a monomeric structure which included a $[Ni(L)]^{2+}$ cation while btc^{2-} acted as a counter anion, and a free acid as depicted in **Figure 17**. The nickel(II) coordination geometry of **(2)** was a square-planar, where tetra-valent Ni(II) ion was bounded to four nitrogen atoms of the hexaazamacrocycle. Moreover, the presence of counter anion and the free acid resulted in various hydrogen bonding interactions.

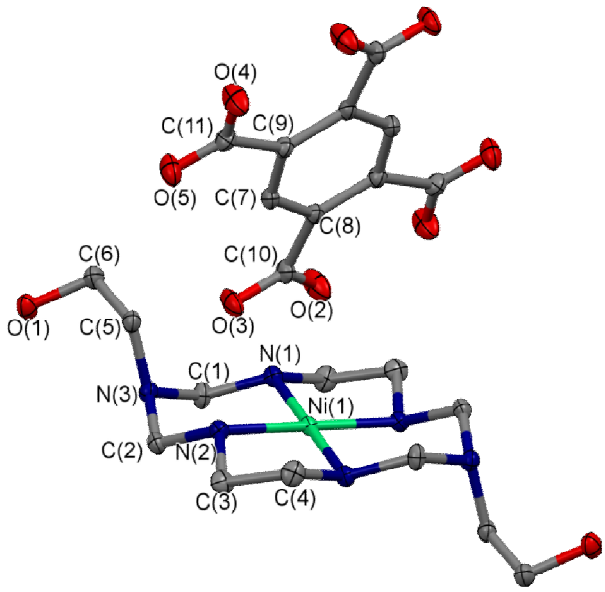

Figure 16. Crystal structure of $\{[Ni(L)]\cdot(btc^{2-})\}_n$ **(1)** with atomic numbering scheme. All hydrogen atoms have been omitted for clarity (Kim *et al*., 2002).

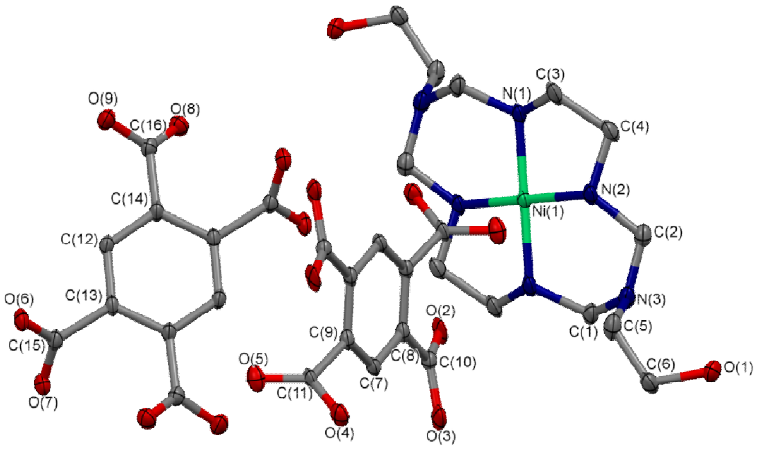

Figure 17. Crystal structure of [Ni(L)]·(btc^{2-})·(btc) **(2)** with atomic numbering scheme. All hydrogen atoms have been omitted for clarity (Kim *et al*., 2002).

Han *et al*., 2011 reported synthesis of new nickel(II) complex with the composition [Ni(L)(tp)]·$6H_2O$, tp = terephthalate and L = 3,10-bis{3-(1-imidazolyl)propyl}-1,3,5,8,10,12-hexaazacyclotetradecane and characterized by a combination of analytical, spectroscopic techniques, and X-ray diffraction methods. The structure of [Ni(L)(tp)]·$6H_2O$ contained one-dimensional polymeric formed from $[Ni(L)]^{2+}$ cation, the bridging terephthalate anions, and six lattices water molecules as shown in **Figure 18**.

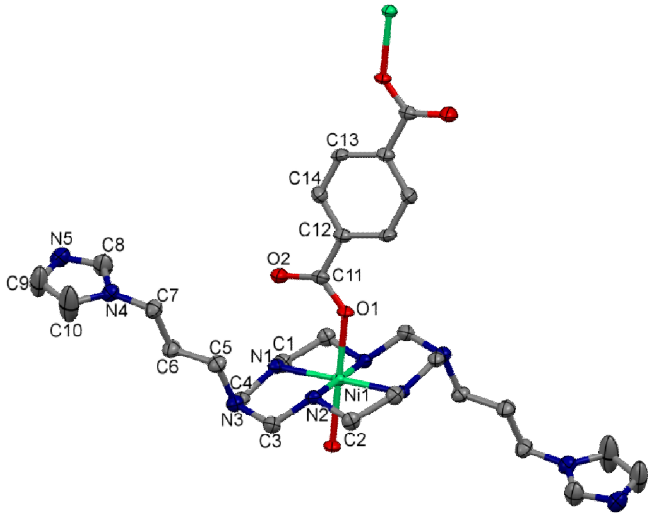

Figure 18. Crystal structure of [Ni(L)(tp)]·$6H_2O$ with atom-labeling scheme. Hydrogen atoms and lattices water molecule are omitted for clarity (Han *et al*., 2011).

Park *et al*., 2015 studied self-assembled complex $[Ni(L)(pab)_2]\cdot 2CH_3CN$ (L = 1,8-dipentyl-1,3,6,8,10,13-hexaazacyclotetradecane and pab = 4-(phenylazo)benzoate) by the reaction of 4-(phenylazo)benzoic acid with a precursor $[Ni(L)](ClO_4)_2$ complex. This complex was characterized by elemental analyses, FT-IR, UV-Vis, photoluminescence, and single crystal X-ray diffraction. Orange crystals of nickel(II) complex were obtained by layering of $MeCN/H_2O$ solution of Hpab into MeCN solution of a precursor $[Ni(L)](ClO_4)_2$ complex. The coordination geometry around nickel(II) ion was a tetragonally distorted octahedron by binding to four nitrogen atoms from the hexaazamacrocyclic ligand in equatorial plane and two oxygen atoms from the pab^- anions in axial position as shown in **Figure 19**. The linked pab^- anions involved in hydrogen bonding interactions with the adjacent pab^- anions giving a one-dimensional ribbon-like structure. Moreover, the photo-luminescence behaviors of $[Ni(L)(pab)_2]\cdot 2CH_3CN$ revealed that no fluorescence bands were quenched due to the coordination of pab^- anion to nickel(II) ion.

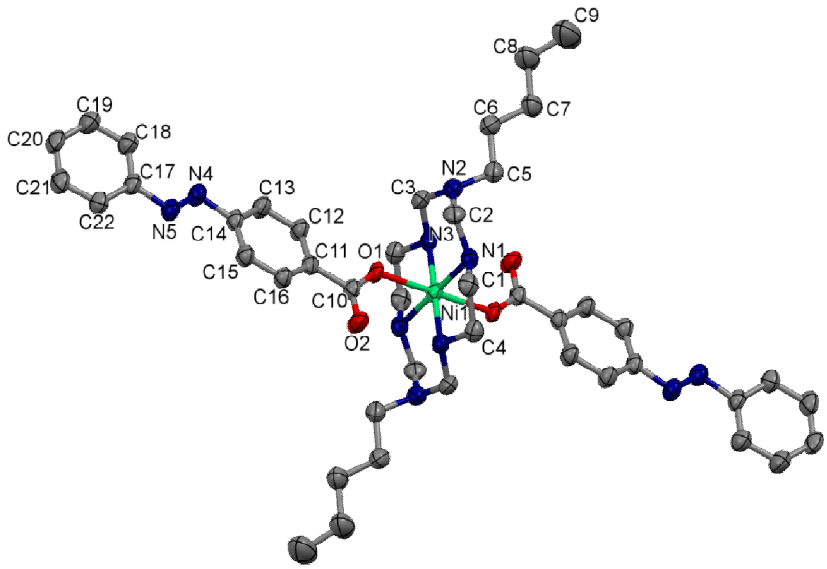

Figure 19. Crystal structure view of $[Ni(L)(pab)_2]\cdot 2CH_3CN$. H atoms and MeCN molecules are omitted for clarity (Park *et al*., 2015).

Shin *et al*., 2016 synthesized three supramolecular complexes, $[Ni(C_{16}H_{38}N_6)(2,7\text{-NDC})]$ **(1)**, $[Ni(C_{16}H_{38}N_6)(H_2O)_2]$ $[Ni(C_{16}H_{38}N_6)(1,3,5\text{-BTC})_2]$ **(2)**, and $[Ni(C_{16}H_{38}N_6)(\text{nicotinate})_2]$ **(3)** through self-assembly of a precursor $[Ni(C_{16}H_{38}N_6)](ClO_4)_2$ complex containing butyl pendant groups. All complexes were characterized by elemental analyses, FT-IR, magnetic properties, and single crystal X-ray diffraction analysis. For complex **(1)**, the $[Ni(C_{16}H_{38}N_6)]^{2+}$ cation coordinated to two 2,7-NDC^{2-} anions in the axial position and each 2,7-NDC^{2-} anion coordinated to two adjacent $[Ni(C_{16}H_{38}N_6)]^{2+}$ units with *syn-syn* and *syn-anti* orientations to form one-dimensional zigzag chain as depicted in **Figure 20**. Complex **(1)** showed very weak anti-ferromagnetic interactions *via* the bridged 2,7-NDC^{2-} anion within the one-dimensional zigzag chains. Complex **(2)** contained two nickel(II) hexaazamacrocyclic cations and one nickel(II) hexaazamacrocyclic anions. Each nickel(II) ion in the cation and anion parts linked with four nitrogen atoms from hexaazamacrocyclic ligand at the equatorial plane and two oxygen atoms of the water molecules or BTC^{3-} anion in the axial positions to form a distorted octahedral geometry as depicted in **Figure 21**. In complex **(3)**, the coordination environment around the nickel(II) ion was a distorted octahedral geometry through the connection with four nitrogen atoms from the hexaazamacrocyclic ligand at the equatorial plane and two nicotinate anions in the axial positions as illustrated in **Figure 22**.

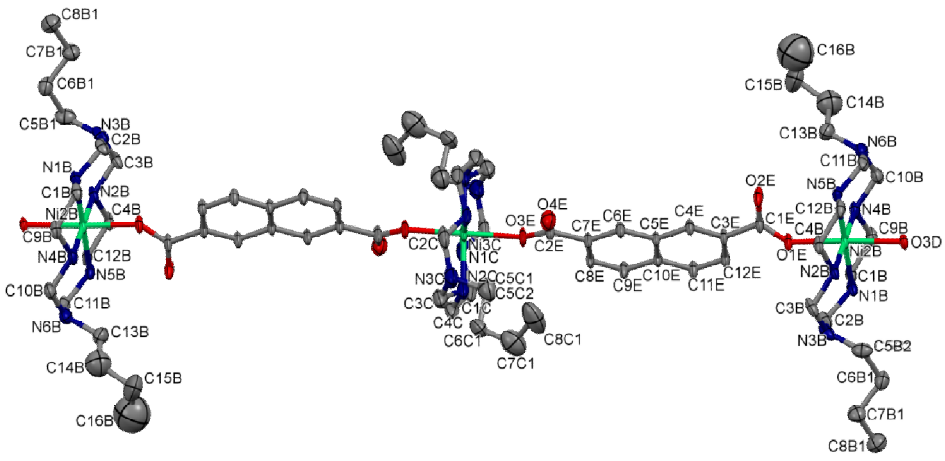

Figure 20. Crystal structure view of $[Ni(C_{16}H_{38}N_6)(2,7\text{-NDC})]$ **(1)**. Hydrogen atoms and solvent are omitted for clarity (Shin *et al*., 2016).

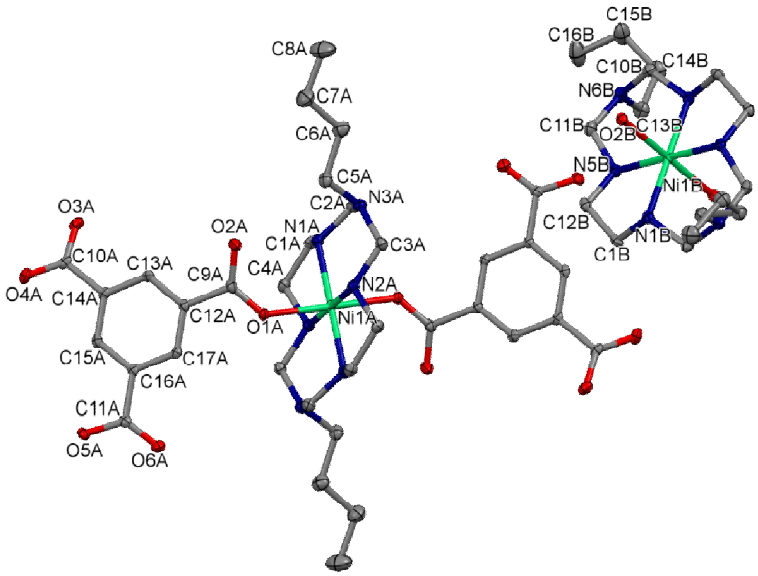

Figure 21. Crystal structure view of [Ni($C_{16}H_{38}N_6$)(H_2O)$_2$] [Ni($C_{16}H_{38}N_6$)(1,3,5-BTC)$_2$] **(2)**. Hydrogen atoms are omitted for clarity (Shin *et al*., 2016).

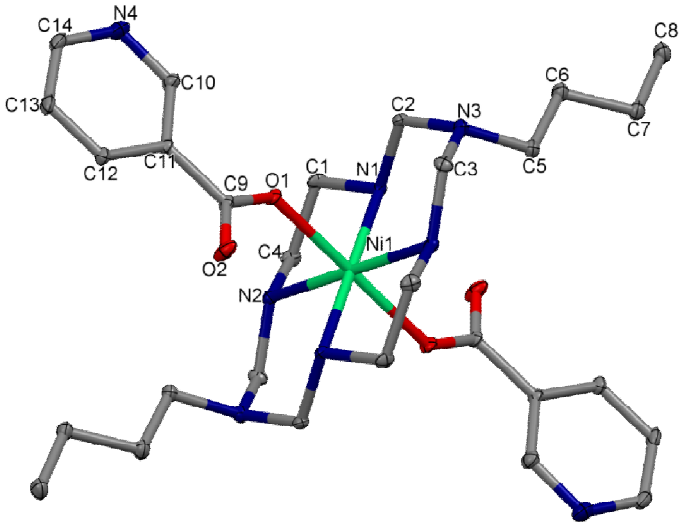

Figure 22. Crystal structure view of [Ni($C_{16}H_{38}N_6$)(nicotinate)$_2$] **(3)**. Hydrogen atoms are omitted for clarity (Shin *et al*., 2016).

1.5.3 Copper(II) complexes of hexaazamacrocyclic ligands with the $[Fe(CN)_6]^{3-}$ anion coordination.

The coordination chemistry of cyanide-bridged bimetallic complexes, particularly ferricyanides and ferrocyanides, derived from $[M(CN)_6]^{n-}$ (M = Fe, Cr, Mn, and Co), have received great interest because of their potential applications for technologically helpful such as photochemical properties, electrochemical, magnetic behavior, electronic states, and catalytic materials. The terminal nitrogen atoms of the cyanide ligands of hexacyanoferrate(III) are strong donor atoms that could link two metal ions. Cyanide-bridged transition metal complexes of 3d-3d or 4f-3d electron configurations have extended arrays of $[M(CN)_6]^{n-}$ building blocks with metal complexes containing hexaazamacrocyclic ligand. A variety of extended structures such as a one-dimensional (1D) zigzag chain or rope ladder; two-dimension (2D) square, sheet, and honeycomb, and three-dimensional (3D) cubane structures have been observed. Since copper(II) ions usually have four-, five-, or six-coordination, it is expected that the coupling of the Cu complexes with $[Fe(CN)_6]^{n-}$ can give rise to a large diversity of structural architectures and physical properties. Following are examples of related reports of these complexes.

Lu *et al*., 1999 reported a new three-dimension network structure with the formula $[CuL(H_2O)_2]\{[CuL][Fe(CN)_6]\}_2 \cdot 2H_2O$, where L = 3,10-bis(2-hydroxy-ethyl)-1,3,5,8,10,12-hexaazacyclotetradecane was synthesized from the reaction of $[CuL]Cl_2$ and $K_3[Fe(CN)_6]$. X-ray crystallography indicated that the structure consisted of a 1D zigzag chain of $[CuL(H_2O)_2]^{2+}$ cations and $\{[CuL][Fe(CN)_6]\}_2^{2-}$ anions as shown in **Figure 23**. The 1D zigzag chain extented via Cu-CN-Fe-CN-Cu coordinates. The adjacent two polymer chains were connected by the O-H···N≡C-hydrogen bonding between $[CuL(H_2O)_2]^{2+}$ cation and $[Fe(CN)_6]^{3-}$ anion leading to a three-dimension supramolecular structure. The magnetic susceptibility measurements displayed no exchange magnetic interaction between the Cu^{2+} and Fe^{3+} ions due to the weak coordination of bridged-cyanide ion group in the axial position of the Cu(II) ion.

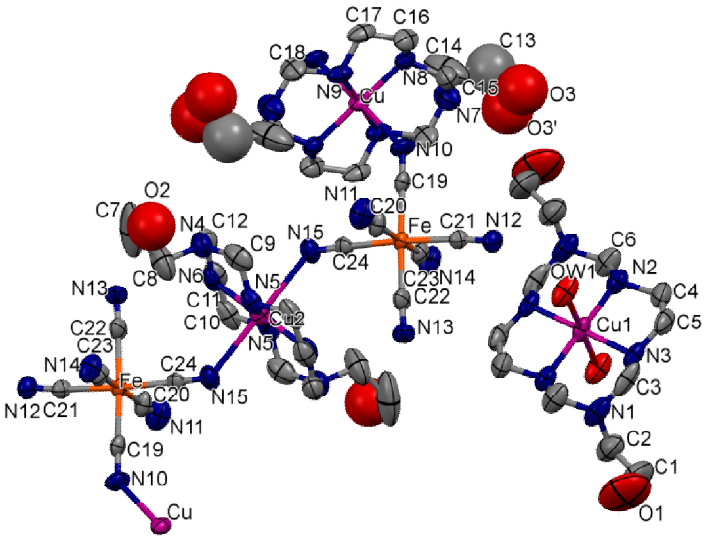

Figure 23. Crystal structure of $[CuL(H_2O)_2]\{[CuL][Fe(CN)_6]\}_2 \cdot 2H_2O$. Hydrogen atoms and two lattice water molecules are omitted for clarity (Lu *et al*., 1999).

Zhang *et al*., 2002 reported novel $[Cu(L)Fe(CN)_5NO]$ which was synthesized by the reaction of $[Cu(L)]Cl_2$, where L = 3,10-bis(2-hydroxymethyl)-1,3,5,8,10,12-hexaazacyclotetradecane with $Na_2[Fe(CN)_5NO] \cdot 2H_2O$ in water. This structure was characterized by elemental analysis, FT-IR, single crystal X-ray diffraction, and magnetic susceptibility measurements. Single crystal analysis indicated that the $[Cu(L)Fe(CN)_5NO]$ complex was the first structurally dinuclear $Cu^{II}Fe^{II}$ complex based on nitropusside to be reported. The crystal structure of $[Cu(L)Fe(CN)_5NO]$ indicated that the complex was created on dinuclear units linked by an elongated Cu(1)···N(1a) contact resulting in a 1D extended chain structure. The copper(II) ion showed a square-pyramidal structure with four nitrogen atoms from the hexaazamacrocyclic ligand at the equatorial planes and one nitrogen atom from the cyanide group at the axial positions. As usual, the $[Fe(CN)_5NO]^{2-}$ anion displayed a distorted octahedral structure. Variable temperature magnetic susceptibility measurements revealed very weak antiferromagnetic interactions between the Cu^{2+} ions.

Zhou *et al*., 2003 reported new complex $[Cu(H_2L)][Fe(CN)_5(NO)]_2 \cdot 4H_2O$, L = 3,10-bis(2-aminoethyl)-1,3,5,8,10,12-hexaazacyclotetradecane which was prepared and characterized by elemental analyses, FT-IR, electronic absorption, EPR,

and single crystal X-ray diffraction. This structure, the first example of trinuclear nitroprusside-bridged $CuFe_2$ complex, had its central copper(II) atom coordinated to four nitrogen atoms of the hexaazamacrocyclic ligand at the equatorial plane and two nitrogen atoms from two cyanide-bridges in the *trans* positions to form distorted octahedral geometry **(Figure 24)**. The axial position N-Cu-N connection was almost vertical to the equatorial plane assigned by the four binding nitrogen atoms of hexaazamacrocyclic ligand. The units connected with hydrogen bonds into three-dimension networks.

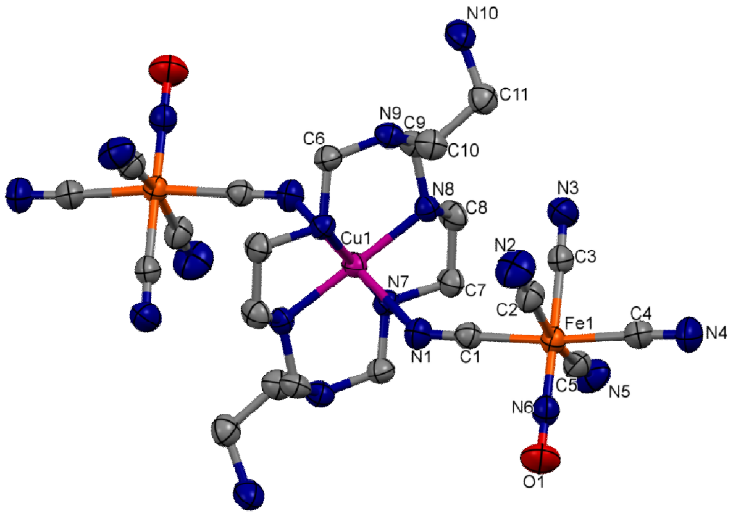

Figure 24. Crystal structure of $[Cu(H_2L)][Fe(CN)_5(NO)]_2 \cdot 4H_2O$. Hydrogen atoms and four lattice water molecules are omitted for clarity (Zhou *et al*., 2003).

Shen *et al*., 2004 synthesized and studied crystal structure of the bimetallic title complex, $[Cu(L)Fe(CN)_5(NO)]$, where L = 1,8-bis(2-hydroxyethyl)-1,-3,6,8,10,13-hexaazacyclotetradecane. As shown in **Figure 25**, the asymmetric unit contains one $[Cu(L)]^{2+}$ cation connected to an $[Fe(CN)_5(NO)]^{2-}$ anion. Two nitrogen atoms from the cyanide in *cis* position coordinate to the adjacent copper(II) atoms forming a 1D zigzag polymeric chain. The coordination around the Cu(II) atom was elongated octahedral. The equatorial plane was created by the coordination of four secondary nitrogen atoms from the hexaazamacrocyclic ligand with two nitrogen atoms of the cyanide groups at the axial positions. The Fe(II) ion was in a slightly deformed octahedral geometry. The basal plane was defined by four cyanide carbon

atoms, and the two axial sites were occupied by the cyanide carbon atom and the nitrosyl nitrogen atom. The 1D zigzag chains were connected to form a 3D networks through N-H···N and O-H···N hydrogen bonding interactions.

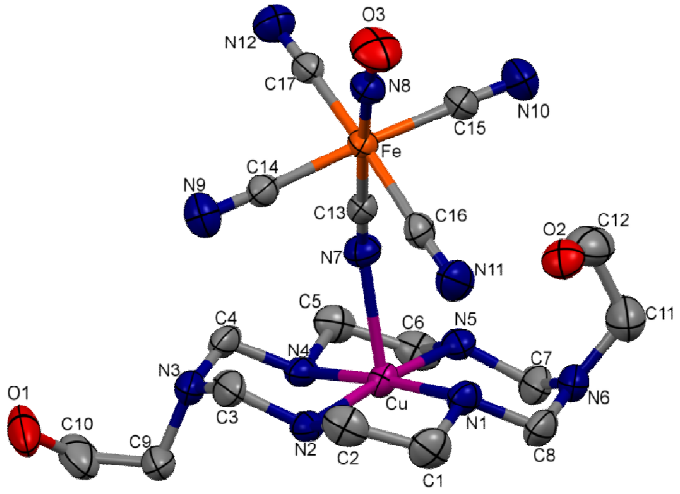

Figure 25. Crystal structure of $[Cu(L)Fe(CN)_5(NO)]$. Hydrogen atoms are omitted for clarity (Shen *et al*., 2004).

Shen *et al*., 2008 reported the synthesis of a novel cyano-bridged assembly $[CuL^4]_3[Fe(CN)_6]_2{\cdot}2H_2O$, where L = 3,10-dibutyl-1,3,5,8,10,12-hexaaza-cyclotetradecane and characterized by elemental analyses, FT-IR, ICP, single crystal X-ray analysis, and magnetic properties. It had a unique polymeric structure containing two-dimensional infinite layer and pentanuclear Cu_3Fe_2 chain-like unit. Each $[Fe(CN)_6]^{3-}$ anion within the 2D layer bound to three $[CuL^4]^{2+}$ cations through three *mer*-cyanide groups and each $[CuL^4]^{2+}$ cation is connected with two $[Fe(CN)_6]^{3-}$ anions in *trans* positions leading to a two-dimensional ring-like dodecanuclear networks. The three copper(II) ions were elongated octahedral coordination geometry of which the equatorial planes linked to four nitrogen atoms from ligand L^4 and the axial positions linked to two nitrogen atoms of the cyanide groups. The fact that the $Cu\text{-}N_{axial}$ bond distances are much longer than the $Cu\text{-}N_{equatorial}$ distances could be assigned to the Jahn-Teller effects of copper(II) ion. Magnetic properties on this complex showed the presence of a weak anti-ferromagnetic interaction between the adjacent Cu(II) and Fe(III) ions via cyano-bridged.

Cha *et al*., 2009 synthesized a new branch-like 1D coordination polymer, $[Cu^{II}(L)]_3[Fe^{III}(CN)_6]_2 \cdot 8H_2O$ (L = 6,13-dimethyl-6-nitro-1,4,8,11-tetraaza-bicyclo[11.1.1]pentadecane) by a precursor azamacrocyclic copper(II) complex with $K_3[Fe(CN)_6]$ in H_2O/CH_3OH. This structure was characterized by FT-IR, elemental analyses, single crystal X-ray crystallography, and magnetic susceptibility studies. As shown in **Figure 26**, the core structure of the complex consisted of three $[Cu^{II}(L)]^{2+}$ cations, two $[Fe^{III}(CN)_6]^{3-}$ anions, and eight water molecules as lattice solvent. The crystal structure displayed one $[Fe(CN)_6]^{3-}$ anions utilizing three *fac*-cyanides to link to three $[Cu^{II}(L)]^{2+}$ cations in *trans* position. The Cu(1) ion showed a square pyramidal coordination configuration with the four secondary nitrogen atoms from the ligand L in the equatorial plane and one nitrogen atom of the cyanide group at the apical directions, while both Cu(2) and Cu(3) ions showed distorted octahedral geometry with the four nitrogen atoms from the ligand L and two nitrogen atoms of the $[Fe^{III}(CN)_6]^{3-}$ anions. The complex revealed weak ferromagnetic coupling between the Cu(II) ion and low spin Fe(III) ion within the one-dimensional branch-like chain structure.

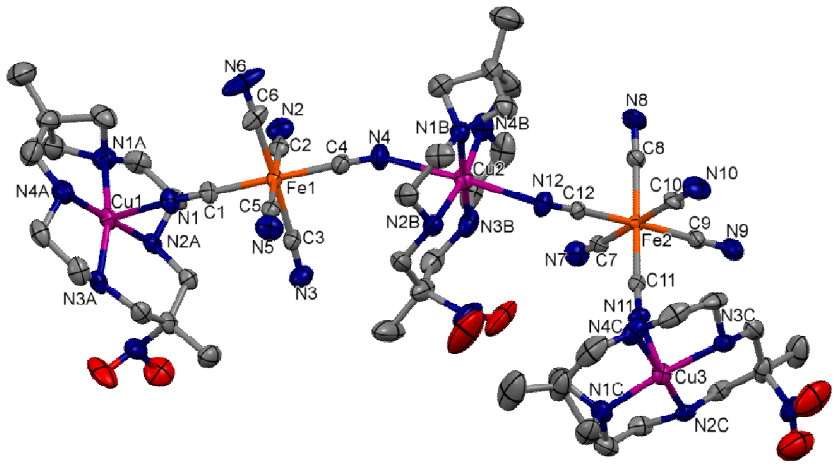

Figure 26. Crystal structure of $[Cu^{II}(L)]_3[Fe^{III}(CN)_6]_2 \cdot 8H_2O$. Hydrogen atoms and water molecule are omitted for clarity (Cha *et al*., 2009).

Lim *et al*., 2011 synthesized two two-dimensional complexes with honeycomb-like structures of $[Fe(CN)_6]_2[Cu(L^1)]_3 \cdot 6H_2O$ **(1)** and a pentanuclear cluster of $\{[Fe(CN)_6]_2[Cu(L^2)]_3\}[Cu(L^2)(H_2O)_2](ClO_4)_2 \cdot 4H_2O$ **(2)** by reacting Cu(II)

macrocycle ligands with methyl (for **1**) or ethyl (for **2**) side groups and $[Fe(CN)_6]^{3-}$ anions. Complexes **(1)** and **(2)** were characterized by elemental analyses, FT-IR, single crystal X-ray crystallography, and magnetic susceptibility measurements. The crystal structure of **(1)**, the iron(III) ion coordination geometry could be described as an octahedral connected with six cyanide groups and the copper(II) macrocycle fragment with the methyl side group. The evidence of Jahn-Teller effects was observed from larger Cu-N_{axial} distances than Cu-$N_{equatorial}$ bond distances **(Figure 27)**. The structure of **(1)** can be seen as a two-dimensional honeycomb-like due to the $[Fe(CN)_6]^{3-}$ ions were positioned at the corners of a hexagon and copper(II) macrocyclic moieties composed the edges of the hexagon. The structure of **(2)** is showns in **Figure 28**. The pentanuclear Cu_3Fe_2 bimetallic was linked by the coordination of ClO_4^- anions at the axial positions of the terminal copper(II) macrocyclic. The isolated $[Cu(L^2)(H_2O)]^{2+}$ cation present in the structure played the role to confirm charge balance. The Cu(2) ion was surrounded by four equatorial nitrogen atoms of the ligand L^2 and two axial nitrogen atoms of the cyanide ligands. The Cu(3) atom showed a Jahn-Teller effect. The magnetic data revealed that ferromagnetic couplings passed between Fe(III) ion and Cu(II) ion via the cyanide links.

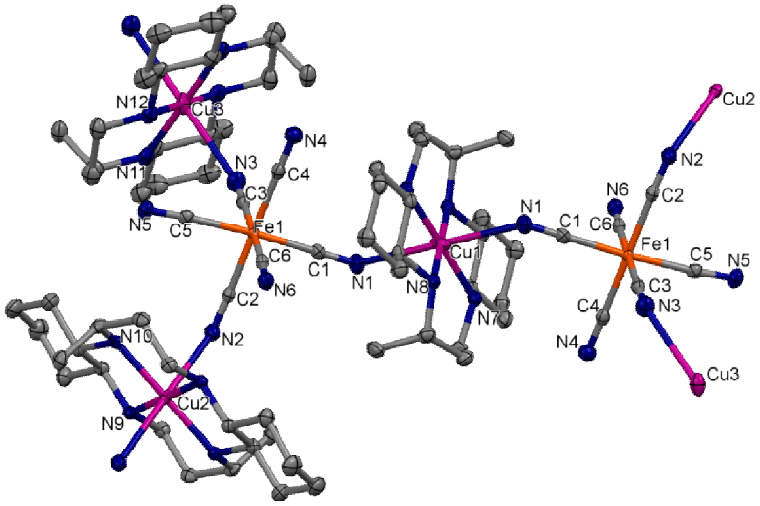

Figure 27. Crystal structure of **(1)** with the atom-labeling scheme. Hydrogen atoms and water molecule are omitted for clarity (Lim *et al*., 2011).

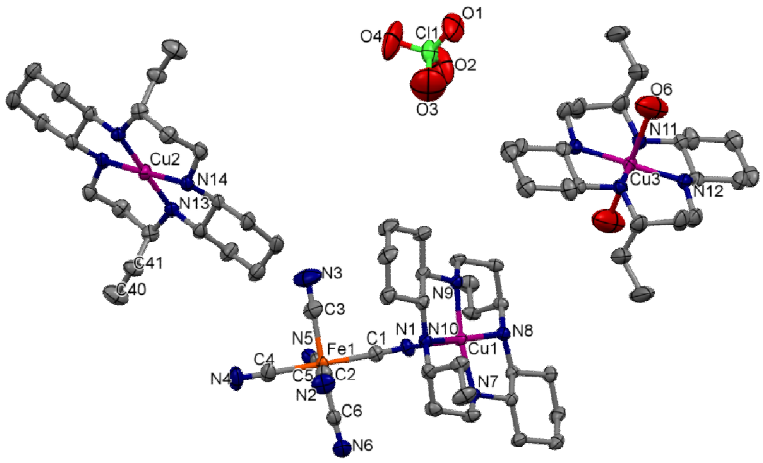

Figure 28. Crystal structure of **(2)** with the atom-labeling scheme. H-atoms and lattice water molecule are omitted for clarity (Lim *et al*., 2011).

1.5.4 Hexaazamacrocycle Copper(II) and nickel(II) complexes and their antibacterial activity

The appearance of antibiotic resistant pathogens and the persisting emphasis on health care has aroused a renewed attention in the design and development of novel and highly effective antibacterial delegates with increase capacity against the resistant bacterial strains. To revise this problem the structural modification of existing antibacterial drugs are being surveyed to which resistance has developed along with the development of thoroughly novel types of antibacterial agents (Stănilă *et al*., 2011). In many case, the metal chelates were found to have higher antibacterial activity than the chelating agents itself. In particularly, transition metal complexes of tetradentate nitrogen-donor atoms ligand have received much interest recently because the increase thermodynamic and kinetic stability of the resulting complexes (Degagsa *et al*., 2013).

Biologically, the copper(II) ion is preferred due to the lower toxicity and also found in the metallothionein in the cytosol and albumin in the plasma. For the copper(II) ion, the adventage in stability has been realized based on the Irving-Williams series. In general, a given ligand will form increasingly stable in octahedral complexes because of the lower dissociation constant (K_d) with the divalent cations.

(Olar *et al*., 2010). Furthermore, the nickel(II) ion is also an essential element related in life process in supporting the absorption of iron element, the increase of red blood cell (RBC), and the synthesis of some enzymes in body; and its complexes show interesting binding and cleavage reactivity with nucleic acids (Gurumoorthy *et al*., 2012). As for ligands, those having the ability to link as chelate and to create neutral species are preferred in order to improve the complexes lipophilicity and thus allow the biological membranes across (Olar *et al*., 2010). Moreover, the factors such as types of metal(II) salt, the electron density, coordination potential, dipole moment, conductance also affect its overall biological activity (Jain *et al*., 2016).

The synthesis, crystal structures, physico-chemical properties, and biological activities of hexaazamacrocyclic ligand and some of its metal complexes, have been previously reported as follows.

Shakir *et al*., 2006 reported the synthesis of a series of 14 and 16-membered hexaaza-macrocyclic complexes by a reaction of 1,2-diaminoethane or 1,3-diaminopropane, formaldehyde, and hydrazine hydrate in the presence of M(II) salts transition (M = Co(II), Ni(II), Cu(II), and Zn(II)) using template condensation reaction method. The products were characterized by elemental analyses, FT-IR, ^{1}H-NMR, EPR, electronic spectra, conductivity, and magnetic susceptibility measurement to determine the overall geometry and stereochemistry of the complexes. The obtained complexes were: $[CoL^{1}(NO_3)_2$ **(1)**, $[NiL^{1}(NO_3)_2$ **(2)**, $[ZnL^{1}(NO_3)_2$ **(3)**, $[CuL^{1}](NO_3)_2$ **(4)**, $[CoL^{2}Cl_2]$ **(5)**, $[NiL^{2}Cl_2]$ **(6)**, $[ZnL^{2}Cl_2]$ **(7)**, and $[CuL^{2}]Cl_2$ **(8)**, where L^{1} = 1,3,5,8,10,12-hexaaza-3,10-*N*,*N*′-diaminocyclodecatetrane and L^{2} = 1,3,5,9,11,13-hexaaza-3,11-*N*,*N*′-diaminocyclodecahexane. An octahedral geometry was proposed for all complexes, except **(4)** and **(8)**, which the copper(II) ion coordinated to four nitrogen atoms from macrocycle to form square-planar complexes. All complexes were tested against different fungi (*C. albicans* and *C. neoformans*) and bacteria (*S. typhimurium* and *E. coli*), by using agar well diffusion method. These complexes showed activity at the concentration dose of 5 mg mL^{-1}, as depicted in **Figures 29** and **30**.

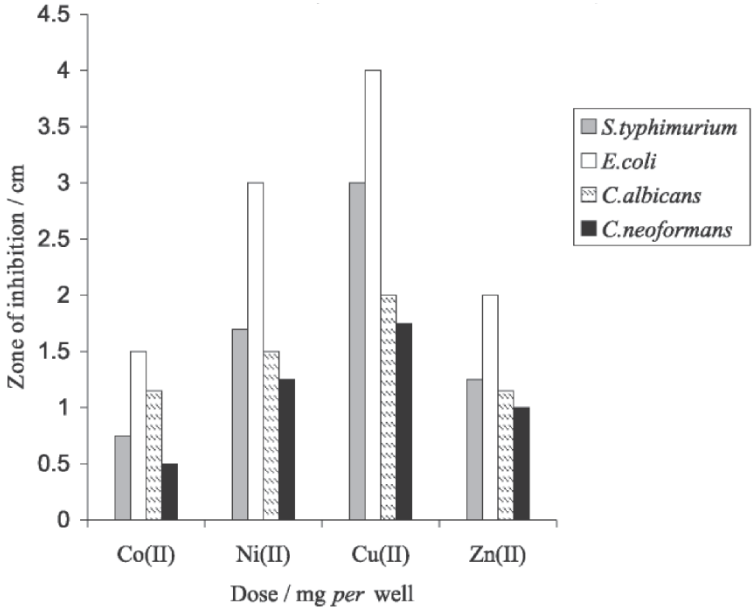

Figure 29. The antimicrobial screening of 14-membered hexaazamacrocyclic complexes (Shakir *et al*., 2006).

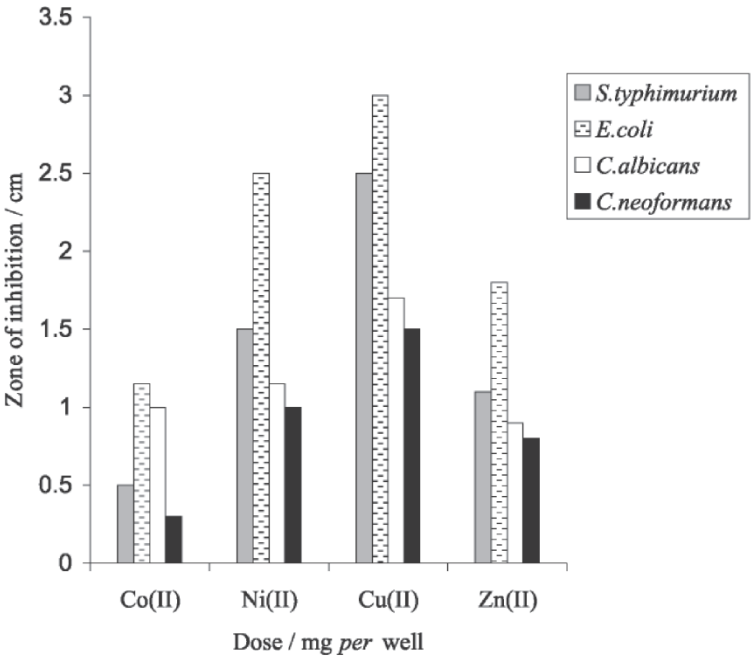

Figure 30. The antimicrobial screening of 16-membered hexaazamacrocyclic complexes (Shakir *et al*., 2006).

Olar *et al*., 2010 reported a novel complexes of type $[Cu(HTBG)_2]Cl_2$ **(1)**, $[Cu(TBG)_2]\cdot 3H_2O$ **(2)**, and $[CuL]\cdot nH_2O$ **(3)**. All complexes were characterized by elemental analyses, FT-IR, electronic spectra, TGA, cyclic voltammetry, and X-ray powder diffraction. The thermal analyses of complexes were studied of which the final product of decomposition was CuO. The *in vitro* qualitative and quantitative antimicrobial activity assays showed that the complexes exhibited a good antimicrobial activity against gram positive and gram negative strains. Besides, some complexes restrained the ability of *P. aeruginosa* and *S. aureus* to colonize the inert substratum.

Husain *et al*., 2011 reported synthesis of two new monomeric Cu(II) complexes with hexaazamacrocyclic ligand of the types $[CuL(ClO_4)_2]$ **(1)** and $[CuL(PF_6)_2]$ **(2)**, where L = 3,10-bisbenzyl-6,13-dimethyl-1,3,5,8,10,12-hexaaza-cyclotetradecane by one-pot template reaction. Complexes were characterized by spectroscopic method and single crystal X-ray crystallography. The crystallographic asymmetric unit of **(1)** consisted of one $[CuL]^{2+}$ cation and two ClO_4^- anions as depicted in **Figure 31**. The Cu(II) atom was in a distorted octahedral geometry binding to four secondary amine nitrogen atoms from the hexaazamacrocycle in the equatorial plane and two oxygen atoms form the perchlorate anions in the axial position. The crystal structure of **(2)** along with the atom-labeling scheme is shown in **Figure 32**. It was crystallized in the monoclinic and space group *P*2(1)/n. The crystal structure of **(2)** consisted of one $[CuL]^{2+}$ cation and two PF_6^- anions. The copper(II) atom was a distorted octahedral by binding with four secondary amine nitrogen (N_4) atoms at the equatorial plane and two fluorine atoms (F_2) of the two hexafluorophosphate anions in the axial positions. The complex **(1)** was tested for antimicrobial activity against three bacterial (*E. coli*, *B. thuringiensis*, and *P. aeruginosa*) and three fungal (*A. nigrus*, *F. oxysporum*, and *P. chrysogenum*) by the well-diffusion method. The results showed that complex **(1)** had higher antibacterial activity against all the bacterial than the tetracycline (as standard drug) as shown in **Table 1**. In case of antifungal activity, it was found to be effective against *P. chrysogenum* and *F. oxysporum*, but lower activity against *A. nigrus*.

Table 1. Mean zone of inhibition (mm ± SD) (Husain *et al*., 2011).

Antibacterial assay		
Bacterial	$[CuL(ClO_4)_2]$	Tetracycline
E. coli	27.0 ± 0.6	17.0 ± 0.5
P. aeruginosa	23.1 ± 0.3	15.0 ± 0.5
B. thuringiensis	25.0 ± 0.6	18.0 ± 0.4
Antifungal assay		
Fungi	$[CuL(ClO_4)_2]$	Tetracycline
A. nigrus	14.0 ± 0.6	18.0 ± 0.4
F. oxysporum	14.1 ± 0.3	14.2 ± 0.4
P. chrysogenum	18.0 ± 0.6	20.0 ± 0.5

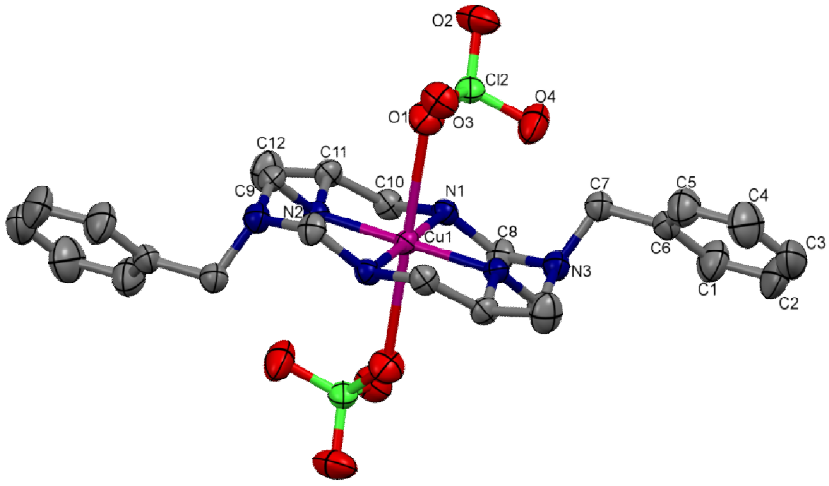

Figure 31. The crystal structure of $[CuL(ClO_4)_2]$ **(1)**, along with the atomic-labeling scheme. Hydrogen atoms have been omitted for clarity (Husain *et al*., 2011).

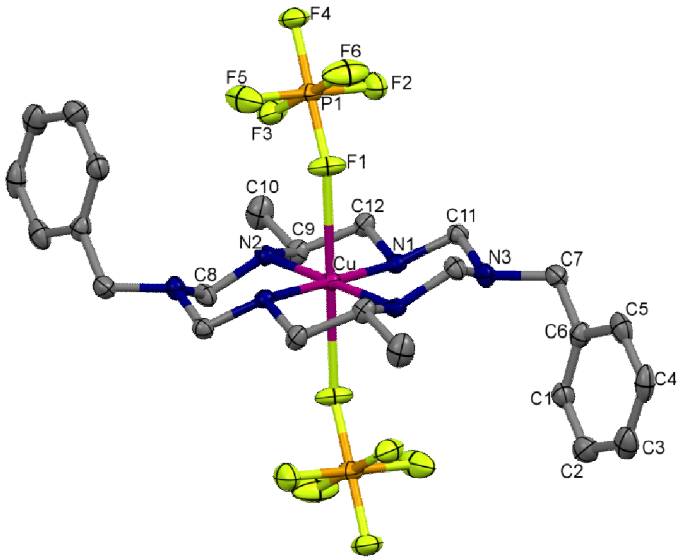

Figure 32. The crystal structure of $[CuL(PF_6)_2]$ **(2)**, along with the atomic-labeling scheme. Hydrogen atoms have been omitted for clarity (Husain *et al*., 2011).

Pătraşcu *et al*., 2013 synthesized a new series of type $MLCl_2 \cdot nH_2O$ (where M = Ni(II), n = 6; Cu(II), n = 1.5; Zn(II) n = 1 and L = 1,8-bis(3'-ketopyridil)-1,3,6,8,10,13-hexaazacyclotetradecane) by template condensation reaction and characterized by elemental analysis, FT-IR, ESI-MS, NMR, electronic absorption, EPR spectroscopy, X-ray powder diffraction as well as magnetic properties at room temperature. Electronic absorption spectra showed that Ni(II) ions adopted an octahedral coordination geometry, whereas the surrounding of Cu(II) ion was square-pyramidal geometry. The octahedral geometry of Zn(II) ion was confirmed by the combination of molar conductance, NMR spectra, ESI-MS spectra, and thermal studies. The proposed stereochemistry was furthermore confirmed by ESI-MS, magnetic moments, and EPR spectra at ambient temperature. The water dissociated in one or two processes while the oxidative degradation of the ligand and chloride elimination occured in two steps. The final residues contained stable metallic oxides as checked by X-ray powder diffraction. The evaluation about the antimicrobial activities of the newly synthesized complexes was carried out against: *P. aeruginosa*, *E. coli*, *E. cloacae*, *S. aureus*, *B. subtilis*, and *C. albicans*. The results of antimicrobial activity revealed that the novel synthesized complexes had an inhibitory effect against gram positive bacteria strains *S. aureus* and *B. subtilis* and also against fungal strain

C. albicans. In the case of bacteria strains, the studied complexes were more active against *B. subtilis* as shown in **Table 2**. The assays showed that the complexes displayed a very good antifungal activity as evidenced by their low MIC values. In addition, the tests showed that the complexes did not exhibit an inhibitory effect against gram negative strains.

Table 2. The MIC (μg mL^{-1}) values for complexes (Pătraşcu *et al*., 2013).

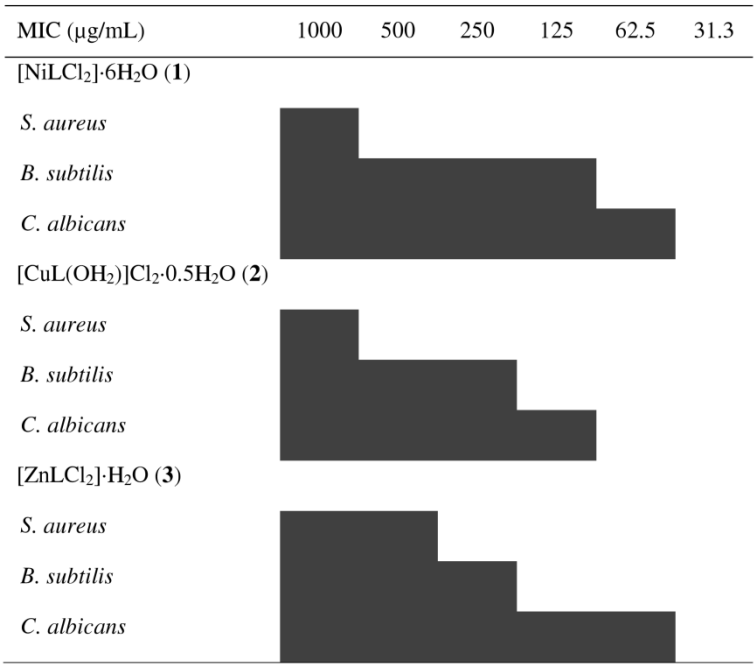

1.5.5 Hexaazamacrocycle Nickel(II) complexes and their catalytic studies

The increasing world population with growing industrial demands has led to a situation where protection of the environment has become a major problem and an importance factor for several industrial processes. In particularly, the dye pollutants from textile industry are an important source of environmental contaminations. This colored wastewater imposes a major problem for the industry as well as a serious threat to the environment. A number of studies have been carried out in which chemical and physical processes such as electrochemical process, ion-exchange, flocculation and coagulation techniques, biological treatment, adsorption on activated carbon are applied for color removal from textile wastewater.

Moreover, the advanced oxidation processes, or the so-called “AOPs”, have been widely studied for the treatment of industrial wastewaters. In general, AOPs are mainly based on the generation of the highly reactive oxidizing species, hydroxyl radical, which may be generated by various methods such as UV photolysis of hydrogen peroxide/ozone (H_2O_2/O_3) (Sánchez-Poli *et al*., 2006), photochemical catalysis (UV/TiO_2) (Singh *et al*., 2010), Fenton’s reaction (Liu *et al*., 2016), and persulfate oxidation (Fukuzumi *et al*., 2016). The activated persulfate oxidation uses persulfate ion ($S_2O_8^{2-}$) which is also known as peroxydisulfate or peroxodisulfate. Persulfate salts of ammonium persulfate ($(NH_4)_2S_2O_8$), sodium persulfate ($Na_2S_2O_8$), and potassium persulfate ($K_2S_2O_8$) dissociate in water to yield the persulfate anion which is one of the strong oxidation species with high potential (E^o = 2.01 V) compared with H_2O_2 (E^o = 1.76 V). It shows some advantages over other oxidants as a solid chemical at room temperature with the ease of storage and transport, high stability, high aqueous solubility, and relatively low cost. There are several methods to activate the persulfate anions, such as thermal activation (Huang *et al*., 2005), UV irradiation (Peternel *et al*., 2013), base activation, and activation with transition metal catalysts (Xiao-Bing *et al*., 2016), to generate reactive sulfate radicals ($SO_4^{\cdot-}$). Activation of persulfate by metal ion catalysis occurs by an oxidation-reduction reaction in which low valent metal ions (M^{n+}) act as electron donors. Transition metal complexes with hexaazamacrocyclic ligands have been extensively studied and generated continuous interest because of the rich metal coordination chemistry as summarized in the following paragraphs.

Gokulakrishnan *et al*., 2012 investigated the degradation of malachite green (MG) by potassium persulfate (KPS) and KPS in the presence of $[NiL](ClO_4)_2$ **(1)** (where L = 1,8-dimethyl-1,3,6,8,10,13-hexaazacyclotetradecane) using UV-Vis spectroscopy and HPLC methods. MG and its structurally related *N*-demethylated species were nearly completely degraded by using KPS alone. Absorbance spectra of these bands decreased when addition of KPS to MG with a major decrease in absorbance at 618 nm, and change to almost zero at approximately ~60 min as shown in **Figure 33**. Remarkably, degradation of MG by KPS and complex **(1)** oxidation system was found to occur at pH range 3-9 with enhanced rate as compared to KPS

alone while the Fenton process as well as ozonation process was mainly effective under acidic conditions. Degradation of MG by KPS in the presence of Fe(II) ion was incomplete, whereas addition of Ni(II) ions had no significant effect on degradation of MG by KPS. Degradation of MG by KPS was based on the concentration of MG, KPS, and complex **(1)**. The results of microbial assay showed removal of antibacterial activity of MG after treatment indicating that this oxidation system has potentiality to decrease toxicity of MG significantly towards *E. coli* bacteria. Furthermore, TOC analysis revealed the ability of KPS, and KPS in the presence of complex **(1)** to decrease total organic carbon of MG dye. Hydroxyl adducts of MG, DLBP, and BPA intermediates were determined in degraded solution by LC-ESI-MS analysis. From the above data, important possible reactions for degradation of MG by KPS and complex **(1)** were proposed **(Figure 34)** to comprise of main reactions such as *N*-demethylation, hydroxyl adducts formation and removal of benzene ring.

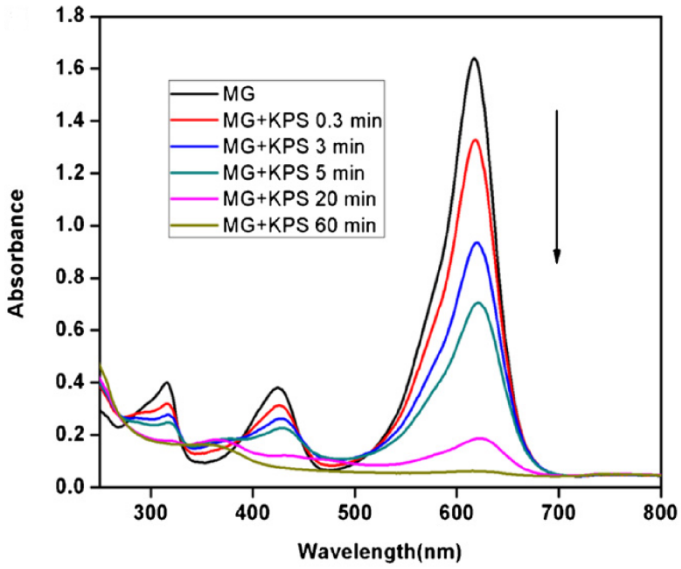

Figure 33. Absorption spectrum of MG (10 mg L^{-1}) after addition of KPS (1 g L^{-1}) at different time intervals (Gokulakrishnan *et al*., 2012).

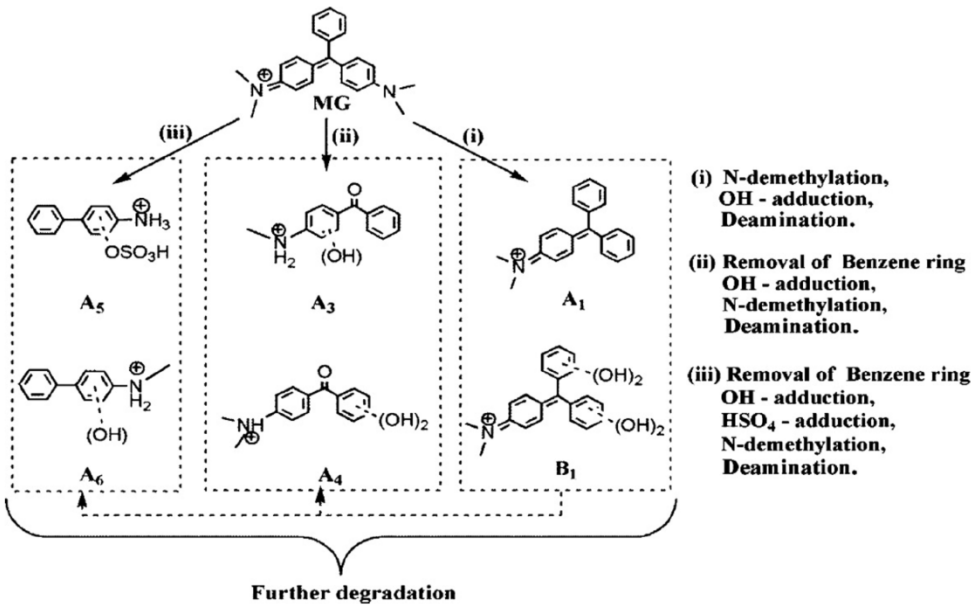

Figure 34. Possible reactions in degradation of MG by KPS in presence of complex **(1)** (Gokulakrishnan *et al*., 2012).

Gokulakrishnan *et al*., 2015 made a detailed study of a homogeneous $[NiL](ClO_4)_2$ **(1)** activated persulfate (PS) and degradation of methyl orange (MO) is shown in **Figure 35**. Absorption spectra showed that the degradation of MO by PS was slow and incomplete after 60 min of reaction. Moreover, methyl orange dye was rapidly degraded by PS in the presence of $[NiL](ClO_4)_2$ **(1)** within 10 min, with a pseudo-first order rate constant value (k) = 3.9 ± 0.07 s^{-1}. It was observed that $NiCl_2 \cdot 6H_2O$ (without hexaazamacrocyclic ligand) had no effect on the degradation of MO as depicted in **Figure 36**. Furthermore, the solid of **(1)** - AC was recycled to activate PS and degrade methyl orange without significant losing of nickel into the solution. Besides, the amberlite (Am) was useful in a metal complex activated PS based advanced oxidation processes for adsorptive recovery of the complex and for the recycle of the complex in homogeneous form after the ion exchange process. These results showed the application of adsorbents to recovery and recycle a metal complex based PS activator. Recycle and recovery of a metal complex based PS activator is advantageous in PS based advanced oxidation processes for the remediation of natural or water pollutants from industries and other sources.

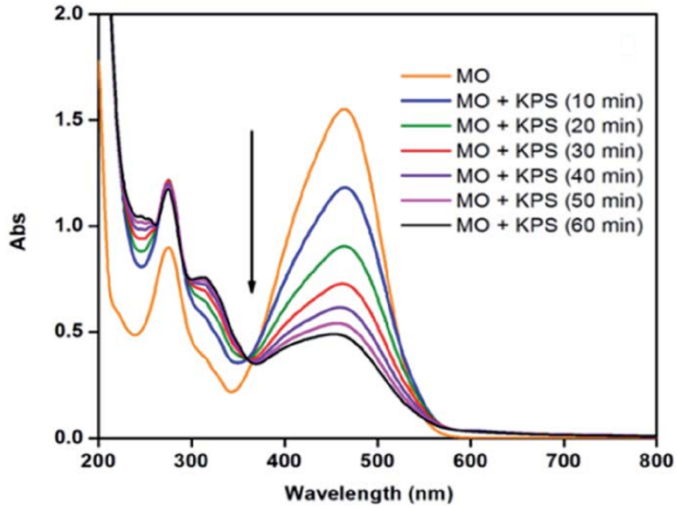

Figure 35. Absorption spectra showing the degradation of MO by PS (Gokulakrishnan *et al*., 2015).

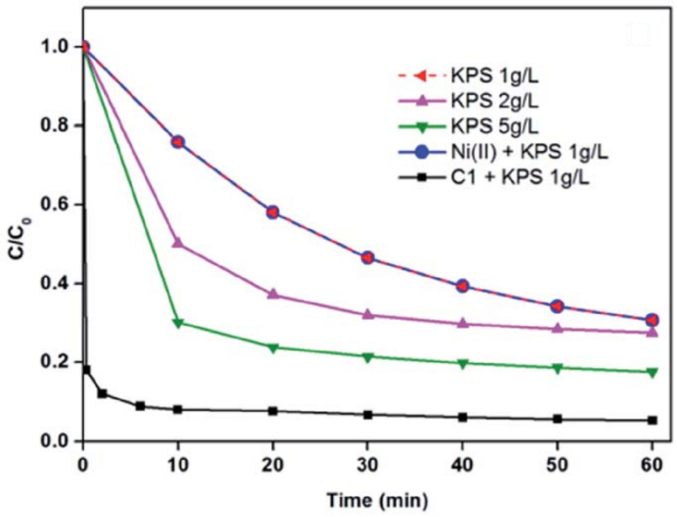

Figure 36. C/C_0 plot showing the degradation of MO in the presence of PS, PS + **(1)**, and $NiCl_2 \cdot 6H_2O$ + PS (Gokulakrishnan *et al*., 2015).

1.6 Types of hexaazamacrocyclic ligands used in this thesis

In this work, the researcher used hexaazamacrocyclic ligands with different pendant-arms and bidentate ligands **(Figures 37-44)**, such as 3,10-dicyclohexyl-1,3,5,8,10,12-hexaazacyclotetradecane (L^1), 3,10-dicyclohexyl-6,13-dimethyl-1,3,5,-8,10,12-hexaazacyclotetradecane (L^2), 3,10-dioctyl-1,3,5,8,10,12-hexaazacyclotetra-decane (L^3), 6,13-dimethyl-3,10-dioctyl-1,3,5,8,10,12-hexaazacyclotetradecane (L^4), 3,10-diisobutyl-1,3,5,8,10,12-hexaazacyclotetradecane (L^5), 3,10-diisobutyl-6,13-di-methyl-1,3,5,8,10,12-hexaazacyclotetradecane (L^6), 3,10-bis(2-ethylhexyl)-1,3,5,8,-10,12-hexaazacyclotetradecane (L^7), and 3,10-bis(2-ethylhexyl)-6,13-dimethyl-1,3,5,-8,10,12-hexaazacyclotetradecane (L^8).

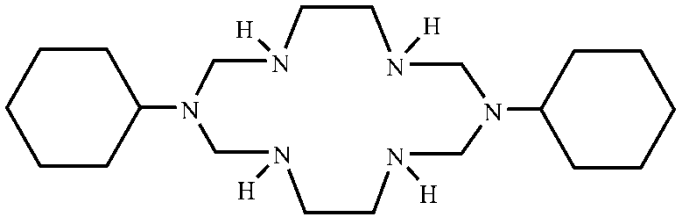

Figure 37. Structure of 3,10-dicyclohexyl-1,3,5,8,10,12-hexaazacyclotetradecane (L^1) ligand.

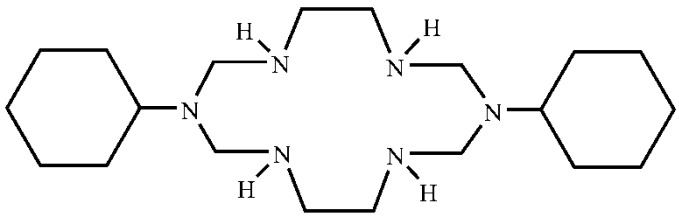

Figure 38. Structure of 3,10-dicyclohexyl-6,13-dimethyl-1,3,5,8,10,12-hexaazacyclo-tetradecane (L^2) ligand.

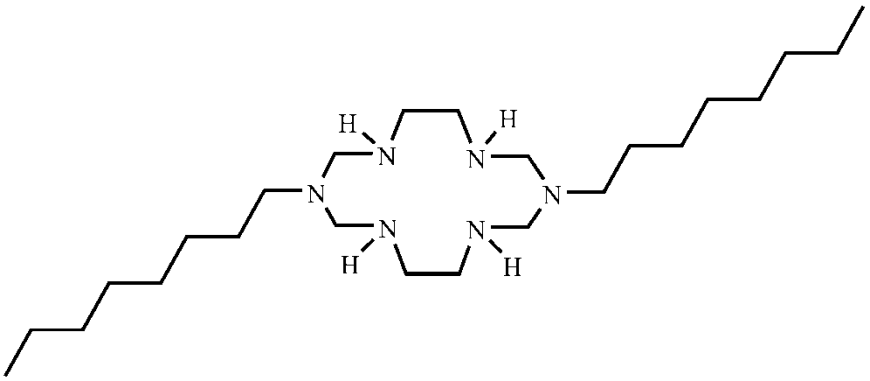

Figure 39. Structure of 3,10-dioctyl-1,3,5,8,10,12-hexaazacyclotetradecane (L^3) ligand.

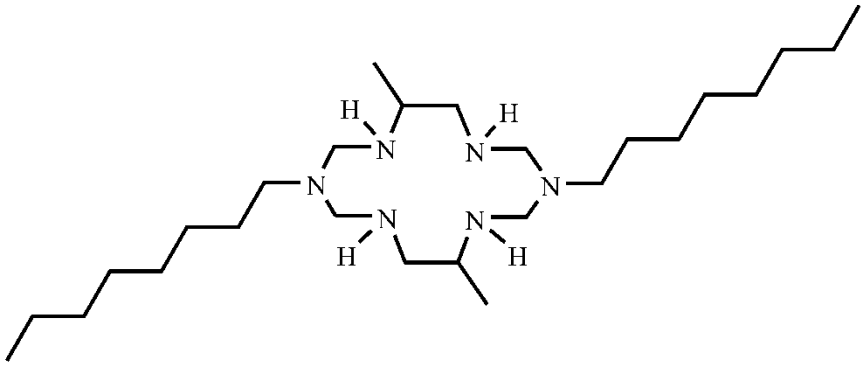

Figure 40. Structure of 6,13-dimethyl-3,10-dioctyl-1,3,5,8,10,12-hexaazacyclotetradecane (L^4) ligand.

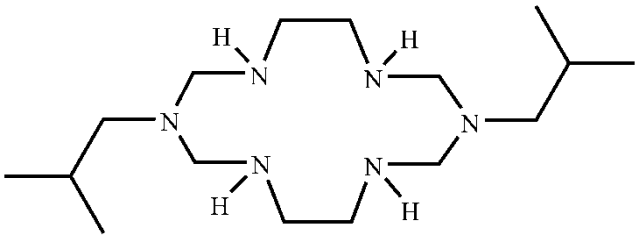

Figure 41. Structure of 3,10-diisobutyl-1,3,5,8,10,12-hexaazacyclotetradecane (L^5) ligand.

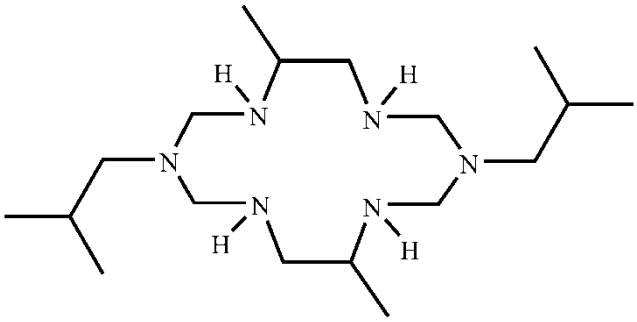

Figure 42. Structure of 3,10-diisobutyl-6,13-dimethyl-1,3,5,8,10,12-hexaazacyclotetradecane (L^6) ligand.

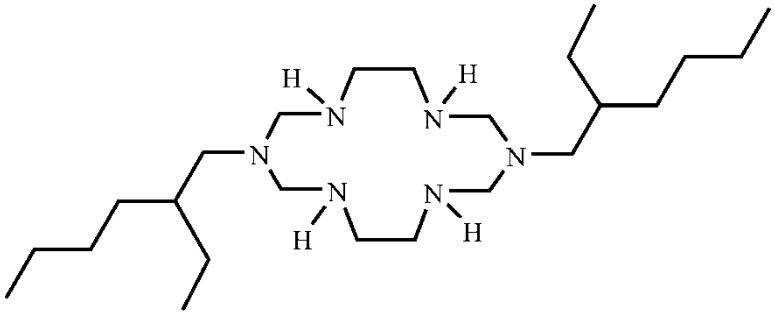

Figure 43. Structure of 3,10-bis(2-ethylhexyl)-1,3,5,8,-10,12-hexaazacyclotetradecane (L^7) ligand.

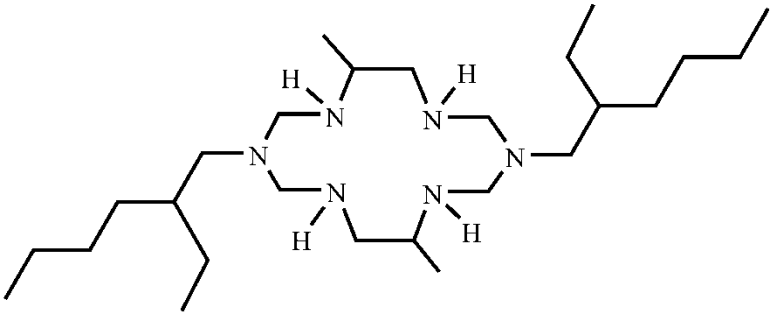

Figure 44. Structure of 3,10-bis(2-ethylhexyl)-6,13-dimethyl-1,3,5,8,-10,12-hexaazacyclotetradecane (L^8) ligand.

1.7 Objectives

1.7.1 To synthesize new Cu(II) and Ni(II) complexes of the 14-membered hexaazamacrocyclic ligand by a one-pot condensation reaction.

1.7.2 To characterize the as-synthesized complexes by various physico-chemical methods and spectroscopic techniques.

1.7.3 To determine the crystal structures of complexes by single crystal X-ray diffraction analysis.

1.7.4 To study the catalytic performances of the synthesized complexes activated by persulfate (from KPS) for the degradation of methyl orange (MO).

1.7.5 To study the antibacterial activities of the synthesized complexes by agar disc diffusion method.

CHAPTER 2

RESEARCH METHODOLOGY

2.1 Materials and chemicals

1. Copper(II) chloride dihydrate ($CuCl_2 \cdot 2H_2O$), Analytical reagent, Univar, Ajax Finechem, Australia.
2. Copper(II) acetate monohydrate ($Cu(CH_3COO)_2 \cdot H_2O$), Analytical reagent, Univar, Ajax Finechem, Australia.
3. Nickel(II) chloride hexahydrate ($NiCl_2 \cdot 6H_2O$), Analytical reagent, Univar, Ajax Finechem, Australia.
4. Nickel(II) acetate tetrahydrate ($Ni(CH_3COO)_2 \cdot 4H_2O$), Laboratory reagent, BHD, England.
5. Ethylenediamine ($C_2H_8N_2$), Analytical reagent, Fluka, USA.
6. 1,2-Diaminopropane ($C_3H_{10}N_2$), Analytical reagent, Merck, Germany.
7. Cyclohexylamine ($C_6H_{13}N$), Reagent plus grade, Sigma-Aldrich, USA.
8. Octylamine ($C_8H_{19}N$), Analytical reagent, Sigma-Aldrich, USA.
9. *Iso*-butylamine ($C_4H_{11}N$), Analytical reagent, Fluka, USA.
10. 2-Ethyl-1-hexylamine ($C_8H_{19}N$), Analytical reagent, Sigma-Aldrich, USA.
11. Potassium hexacyanoferrate(III) ($K_3[Fe(CN)_6]$, Laboratory reagent, Unilab, Ajax Finechem, Australia.
12. 4-Nitrobenzoic acid ($C_7H_5NO_4$), General purpose reagent, LabChem, Ajax Finechem, Australia.
13. Aspirin ($C_9H_8O_4$), Analytical reagent, Sigma-Aldrich, USA.

14. Formaldehyde (CH_2O), Analytical science, LabScan, Thailand.
15. Perchloric acid (70%, $HClO_4$), Analytical reagent, Univar, Ajax Finechem, Australia.
16. Absolute ethanol (99.9%, C_2H_6O), American Chemical Society (ACS) reagent, Merck, Germany.
17. Dimethyl sulfoxide (C_2H_6OS), Analytical reagent, RCI LabScan, Thailand.
18. Dimethylformamide (C_3H_7NO), Analytical reagent, RCI LabScan, Thailand.
19. Acetonitrile (C_2H_3N), Analytical reagent, RCI LabScan, Thailand.
20. Acetone (C_3H_6O), Analytical reagent, RCI LabScan, Thailand.
21. Triethylamine ($C_6H_{15}N$), Analytical reagent, Sigma-Aldrich, USA.
22. Potassium persulfate ($K_2S_2O_8$), Laboratory reagent, Unilab, Ajax Finechem, Australia.
23. Methyl orange ($C_{14}H_{14}N_3NaO_3S$), American Chemical Society reagent, Merck, Germany.
24. Nutrient agar (NA), Microbiology grade, Sigma-Aldrich, USA.
25. Universal indicator, Merck, Germany.

2.2 Instruments

1. Elemental analyzer (C, H and N), CE Instruments Flash EA 1112 Series, Thermo Quest, Italy.
2. Fourier-transformed infrared spectrophotometer (FT-IR), Perkin-Elmer Spectrum One, USA.

3. Liquid chromatography-mass spectrometer (LC-MS), 2690, LCT, Waters, Micromass, U.K. and was recorded by electrospray ionization Positive mode (ESI^+) technique.
4. Thermalgravimetric analyzer (TGA), Perkin-Elmer, USA.
5. Ultraviolet-Visible spectrophotometer (UV-Vis), Shimadzu-1600, Japan.
6. Solid state UV-Vis diffused reflectance spectra (DRS), Shimadzu 2450 PC, Japan.
7. Powder X-ray diffractometer (PXRD), X'pert MPD, Philips, Netherlands.
8. Single crystal X-ray diffractometer (SCXRD), Bruker APEX CCD, Department of Chemistry, Faculty of Science, Prince of Songkla University and Bruker APEXII D8 QUEST CMOS, Department of Physics, Faculty of Science and Technology, Thammasat University.
9. Analytical balance, Mettler Toledo, AE200 with significant of ±0.0001 g.
10. Centrifuge, Hettich, EBA 20, Germany.
11. Oven, Griffin, for drying the samples prior to spectroscopy measurement.
12. Magnetic stirrer, Heidolph, MR3001, USA.
13. Photoreactor compartment (0.9 m x 0.9 m x 0.9 m) containing five fluorescent blacklight tubes, 20 Watts, F20T12-BLB, GE, USA.

2.3 Synthesis of the complexes

1. Synthesis of $[CuL^1(ClO_4)_2]$ **(1)**

To a stirred solution of copper(II) chloride dihydrate (1 mmol) and ethylenediamine (2 mmol) in absolute ethanol (10 mL) added dropwise a solution of formaldehyde (4 mmol) and cyclohexylamine (2 mmol) in absolute ethanol (10 mL). The reaction mixture was refluxed for 24 h. The hot solution was filtered, cooled, and

perchloric acid (70%, 2 mL) was added slowly. The pink powder formed was filtered off, washed with absolute ethanol, and dried in air.

2. Synthesis of $[CuL^2(ClO_4)_2]$ **(2)**

To a stirred solution of copper(II) acetate monohydrate (1 mmol) and 1,2-diaminopropane (2 mmol) in absolute ethanol (10 mL) added dropwise a solution of formaldehyde (4 mmol) and cyclohexylamine (2 mmol) in absolute ethanol (10 mL). The reaction mixture was refluxed for 48 h. The hot solution was filtered, cooled, and perchloric acid (70%, 2 mL) was added slowly and the formation of a red precipitate resulted. The precipitate was filtered off and washed with absolute ethanol, and dried in air.

3. Synthesis of $[CuL^3(ClO_4)_2]$ **(3)** and $[NiL^3](ClO_4)_2$ **(4)**

To a stirred solution of copper(II) chloride dihydrate (1 mmol) and ethylenediamine (2 mmol) in absolute ethanol (10 mL) added dropwise a solution of formaldehyde (4 mmol) and octylamine (2 mmol) in absolute ethanol (10 mL). The reaction mixture was refluxed for 24 h. The hot solution was filtered, cooled, and perchloric acid (70%, 2 mL) was added slowly. The precipitate formed was filtered off, washed with absolute ethanol, and dried in air.

The complex **(4)** was prepared using the same procedure described for the complex **(3)** using nickel(II) chloride hexahydrate instead of copper(II) chloride dihydrate.

4. Synthesis of $[CuL^4(ClO_4)_2]$ **(5)**

To a stirred solution of copper(II) acetate monohydrate (1 mmol) and 1,2-diaminopropane (2 mmol) in absolute ethanol (10 mL) added dropwise a solution of formaldehyde (4 mmol) and octylamine (2 mmol) in absolute ethanol (10 mL). The reaction mixture was refluxed for 48 h. The hot solution was filtered, cooled, and perchloric acid (70%, 2 mL) was added slowly. After about 5 days, many purple-red single crystals formed which were filtered off and washed with absolute ethanol, and dried in air.

5. Synthesis of $[CuL^5(ClO_4)_2]$ **(6)** and $[NiL^5](ClO_4)_2$ **(7)**

To a stirred solution of copper(II) acetate monohydrate (1 mmol) and ethylenediamine (2 mmol) in absolute ethanol (10 mL) added dropwise a solution of formaldehyde (4 mmol) and *iso*-butylamine (2 mmol) in absolute ethanol (10 mL). The reaction mixture was refluxed for 24 h. The hot solution was filtered, cooled, and perchloric acid (70%, 2 mL) was added slowly. The pink precipitate formed was filtered off, washed with absolute ethanol, and dried in air.

The complex **(7)** was prepared using the same procedure described for the complex **(6)** using nickel(II) chloride hexahydrate instead of copper(II) chloride dihydrate. Yellow single crystals were obtained after a few days at room temperature.

6. Synthesis of $[CuL^6(ClO_4)_2]$ **(8)**

The complex **(8)** was prepared using the same procedure described for the complex **(6)** using 1,2-diaminopropane instead of ethylenediamine.

7. Synthesis of $[CuL^7(ClO_4)_2]$ **(9)** and $[NiL^7](ClO_4)_2$ **(10)**

To a stirred solution of copper(II) acetate monohydrate (1 mmol) and ethylenediamine (2 mmol) in absolute ethanol (10 mL) added dropwise a solution of formaldehyde (4 mmol) and 2-ethyl-1-hexylamine (2 mmol) in absolute ethanol (10 mL). The reaction mixture was refluxed for 24 h. The hot solution was filtered, cooled, and perchloric acid (70%, 2 mL) was added slowly. The precipitate formed was filtered off, washed with absolute ethanol, and dried in air.

The complex **(10)** was prepared using the same procedure described for the complex **(9)** using nickel(II) chloride hexahydrate instead of copper(II) chloride dihydrate.

7. Synthesis of $[CuL^8(ClO_4)_2]$ **(11)**

The complex **(11)** was prepared using the same procedure described for the complex **(9)** using 1,2-diaminopropane instead of ethylenediamine.

8. Synthesis of $[CuL^5]_3[Fe(CN)_6]_2 \cdot 5H_2O$ **(12)**

To an aqueous solution (15 mL) of potassium hexacyanoferrate(III) (0.10 mmol) was added to a DMF solution (15 mL) containing complex **(6)** (0.10 mmol) with stirring at room temperature. The brown color precipitate thus produced was filtered off and washed several times with water, and dried in air. Well shaped brown single crystals suitable for single crystal X-ray determination were grown at room temperature by the slow diffusion of two solutions of the reactants into a H-tube.

9. Synthesis of $[NiL^5(4\text{-nba})_2] \cdot H_2O$ **(13)**, $[NiL^3(4\text{-nba})_2]$ **(14)**, and $[NiL^5(sal)_2]$ **(15)**

The complex **(7)** (0.088 mmol) was dissolved in 10 mL of MeCN and was added to a solution of *p*-nitrobenzoic acid (0.180 mmol) in 8 mL of mixed MeCN/H_2O (1:1 v/v) followed by addition of an excess triethylamine (0.02 mL). The mixture was stirred for 3 hour at room temperature and was filtered to remove insoluble material. The filtrate was left to stand at ambient temperature until the orange crystals formed.

The complex **(14)** was prepared using the same procedure described for the complex **(13)** using precursor of the complex **(4)** instead of the complex **(7)**.

The complex **(15)** was prepared using the same procedure described for the complex **(13)** using aspirin instead of *p*-nitrobenzoic acid.

2.4 Characterization of the complexes

1. Elemental analyzer

The elemental analysis (C, H and N) was obtained on a Flash EA 1112 Series CHNS analyzer by standard methods (Tubitak Marmara Research Center).

2. Fourier-transformed infrared spectrophotometer

FT-IR spectra of solid complexes were obtained in the form of KBr disc in the range 400-4000 cm^{-1}.

3. Electrospray ionization mass spectrometer

All complexes (LC-MS) were carried out on a tandem time-of-flight (Q-TOF) instrument, equipped with a pneumatically assisted electrospray ion source (Micromass, U.K.) operated in positive mode (ESI^+). The solutions of all complexes were prepared in acetonitrile solvent and were introduced using a syringe pump with a flow rate 5 μl/min. The mass spectrum corresponding to the complex species were identified by analyzing their specific isotopic profile due the different Cu (or Ni) isotopes (e.g. ^{63}Cu, ^{65}Cu and ^{58}Ni, ^{60}Ni). The stoichiometries of the molecular associations were determined in accordance with the greater isotopic peak (e.g. ^{63}Cu and ^{58}Ni).

4. Thermalgravimetric analyzer

For all complexes, about 0.255-4.125 mg of sample was used. The heating rate was 10 °C/min, the temperature ranged from 50 to 1,000 °C, and the system was purged with gas nitrogen (N_2).

5. Ultraviolet-visible spectrophotometer

Electronic spectra were obtained in solution form by dissolving all complexes in dimethyl sulfoxide at room temperature. The spectra were recoded in the range 400-800 nm with a Shimadzu-1600 UV-visible double beam spectrophotometer.

6. Solid state UV-Vis spectrophotometer

Solid state UV-Vis diffused reflectance spectra of complexes (diluted with $BaSO_4$) were recorded with a Shimadzu 2450 PC spectrophotometer.

7. Powder X-ray diffractometer

The PXRD patterns of the complexes were made using X-ray diffractometer with CuK_α radiation (λ = 0.154 nm) at an ambient temperature. The following conditions were used: a voltage of 40 kV, a current of 30 mA, a scanning speed of 3 °/min over in the 2θ range between 5-90 ° with a step of 0.05 °. To obtain the PXRD patterns, Mercury (version 3.8) software has been used for the simulation of theoretical peaks using single-crystal X-ray diffraction data. This data confirms the purity of all complexes.

8. Single crystal X-ray analysis

Suitable single crystals of complex **(5)** was collected on a Bruker APEX CCD area-detector equipped with graphite-monochromated (Department of Chemistry, Faculty of Science, Prince of Songkla University) using Mo Kα radiation (λ = 0.7103 Å) at 293(2) K. Data reduction was preformed by using *SIANT* 5.12 program and a semi-empirical absorption-correction (multi-scan, *SADABS*). The structure **(5)** was solved by direct method using SHELXL and refined by a full-matrix least-squares procedure based on F^2. X-ray data for complexes **(7)**, **(8),** and **(12) - (15)** were collected on Bruker APEXII D8 QUEST CMOS (Department of Physics, Faculty of Science and Technology, Thammasat University) with Mo Kα radiation (λ = 0.71073 Å) in the ω scanning mode at 298(2) K. Data reduction was preformed by using *SIANT* program and a semi-empirical absorption-correction (multi-scan, *SADABS*) based on the intensities of equivalent reflections. The structures were solved by direct method using *OLEX2* program and refined by a full-matrix least-squares procedure based on F^2. All non-hydrogen atoms were found from the different map and refined with anisotropic displacement parameters. All hydrogen atoms on carbon atoms were constrained at calculated positions and refined as riding atoms. The molecular structures with atomic labeling scheme and the crystal packing were drawn by Mercury 3.8 program.

2.5 Study on antibacterial activity

Antibacterial activity was tested at the Scientific Equipment Center, Faculty of Science, King Mongkut's Institute of Technology Ladkrabang. The complexes were screened for their antibacterial activity against one gram-positive (*Staphylococcus aureus* (*S. aureus*), ATCC 25923) and two gram-negative (*Escherichia coli* (*E. coli*), ATCC 25922 and *Pseudomonas aeruginosa* (*P. aeruginosa*), ATCC 27853). Penicilin (10 μg) and Gentamicin (10 μg) were used as the reference antibacterial agent. Each complex was dissolved in DMSO at a concentration of 1 mg mL^{-1}. The inoculums were prepared using a 4-6 hours broth culture of each bacterium and adjusted to a turbidity equivalent to a 0.5 McFarland standard containing approximately 10^4-10^6 CFU mL^{-1}. A sterile cotton swab was dipped into the inoculums and the surface of the nutrient agar (NA) was inoculated by streaking the swab. The paper disks impregnated with the test complexes were placed on the solidified medium. The plates were incubated immediately at 37 ^oC for 24 h. The antibacterial activity was evaluated by measuring the diameter of zones showing complete inhibition (mm). Percentage of inhibition was determined by comparing between the distance of the each complex and positive control as follows (Mulaudzi *et al*., 2011):

$$\%\text{inhibition} = \left(\frac{\text{Diameter of the sample}}{\text{Diameter of the positive control}} \right) \times 100$$

2.6 Catalytic studies

Methyl orange (MO) was selected as model organic dye pollutants to investigate the photocatalytic activity of the complexes **(13) - (15)**. The degradation reaction with each complex was tested in a 150 mL beaker containing 100 mL aqueous solution of methyl orange (3 x 10^{-5} mol L^{-1}), 50 mg of $K_2S_2O_8$, and 50 mg of each complex as catalyst. The mixture was placed and magnetically stirred inside a black box containing 5 fluorescent blacklight (20 W) tubes having maximum wavelength at 366 nm. The distance between the UV source and reaction beaker was

30 cm. The box was tightly closed during the experiment to prevent UV light leakage or interference from ambient light. At given time intervals, 3 mL aliquot each was taken out and centrifuged to remove the catalyst particles, then analyzed by UV-Vis spectrophotometer at the maximum wavelength of 464 nm. The comparative blank experiments without the complexes as catalyst, and with only KPS were carried out under the same conditions. The degradation efficiency of methyl orange is defined as follows:

$$\text{Degradation efficiency (\%)} = \frac{C_0 - C_t}{C_0} \times 100$$

where C_0 (mol L^{-1}) is the initial concentration of methyl orange, and C_t (mol L^{-1}) is the concentration of methyl orange at reaction time t (min).

CHAPTER 3

RESULTS AND DISCUSSION

In this work, the researcher reports research results of several complexes of Cu(II) and Ni(II) involving the syntheses, characterizations, crystal structures, and applications for antibacterial activity and catalytic property. The antibacterial activities of the complexes **(3)** - **(10)** were measured against gram-positive and gram-negative bacterial. The catalytic activities of the complexes **(13)** - **(15)** were tested in the reaction to catalyze potassium persulfate in the degradation of methyl orange dye as follows.

3.1 Synthesis and physicochemical characterization of the complexes

The complexes **(1)** - **(11)** of hexaazamacrocyclic ligand were synthesized utilizing a template reaction, or the so-called "one-pot condensation", containing $MX_2 \cdot nH_2O$ (M = Cu(II) or Ni(II), X = Cl^- or CH_3COO^-, n = 1, 2, 4, 6), ethylenediamine or 1,2-diaminopropane, formaldehyde, and primary amines such as cyclohexylamine, octylamine, and *iso*-butylamine as shown in **Schemes 1** and **2**. The complexes **(1)** - **(11)** were soluble in common solvents such as acetonitrile, dimethylformamide, acetone, and dimethylsulfoxide. The molar conductivity (Λ_m) of the Cu(II) complexes were 43 **(1)**, 55 **(2)**, 61 **(3)**, 41 **(5)**, 59 **(6)**, 44 **(8)**, 62 **(9)**, and 65 **(11)** Ω^{-1} cm^2 M^{-1} indicating a non-electrolytic nature. The molar conductance values of the Ni(II) complexes were 250 **(4)**, 248 **(7)**, and 261 **(10)** Ω^{-1} cm^2 M^{-1} corresponding to 1:2 electrolytes. The elemental analyses of the complexes **(1)** - **(11)** and some physical properties are summarized in **Table 3**.

The mechanism routes of the complexes **(1)** - **(11)** are shown in **Scheme 3**. The initial ethylenedimaine-Cu(II) complexes (or Ni(II) complexes) reacted with formaldehyde to form an imine. And then, the imine was connected by the primary amine ($R\text{-}NH_2$) to form a *gem*-diamine which later condensed with another imine to form the five- and six-membered rings.

The complex **(12)** was obtained as brown single crystals by slow diffusion of **(6)** and potassium hexacyanoferrate(III) *via* a H-tube at ambient temperature. It was insoluble in most organic and inorganic solvents. The elemental analysis, % yield, melting point, and color are shown in **Table 3**.

The complexes **(13)** and **(14)** were synthesized in mixed MeCN/H_2O solvents from **(7)** (for **13**) or **(4)** (for **14**) with *p*-nitrobenzoic acid and adjusted the pH using triethylamine. Both complexes were insoluble in common inorganic and organic solvents. The elemental analyses, % yield, melting point, and color are shown in **Table 3**.

The complex **(15)** was obtained in a procedure similar to the synthesis of **(13)** except using aspirin instead of *p*-nitrobenzoic acid. During the reaction of the complex **(15)**, the acetoxy group of the aspirinate ligand underwent hydrolysis process resulting in the cleavage of a covalent bond in a molecule to give the salicylate ligand which was confirmed in the crystal structure by single crystal X-ray diffraction analysis. Complex **(15)** was insoluble in common inorganic and organic solvents. The elemental analyses, % yield, melting point, and color are shown in **Table 3**.

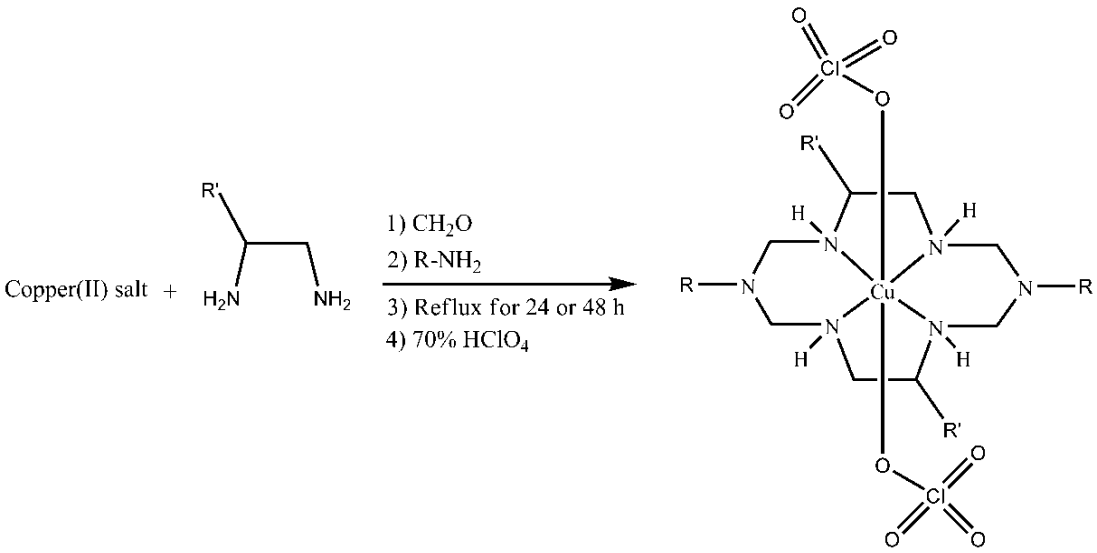

Scheme 1. Synthesis of the Cu(II) complexes **(1)** - **(3)**, **(5)**, **(6)**, **(8)**, **(9)**, and **(11)**.

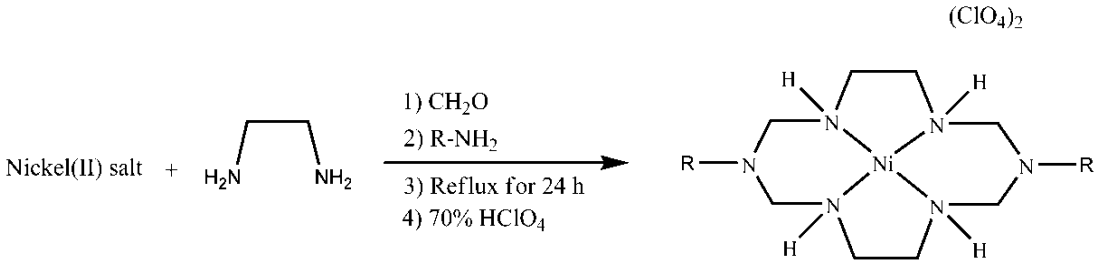

Scheme 2. Synthesis of the Ni(II) complexes **(4)**, **(7)**, and **(10)**.

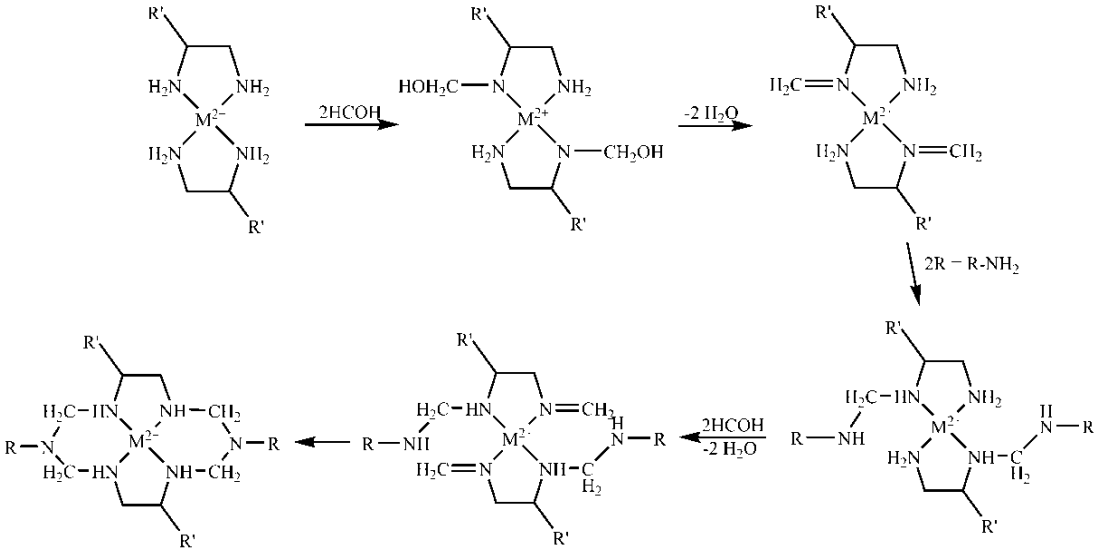

Scheme 3. Proposed mechanism routes of complexes **(1)** - **(11)**.

Table 3. Melting point (^oC), % yield, color, and elemental analyses data of the complexes.

Complexes	Color	M.P.	Yield	Found (*Calc.*) %		
				C	H	N
$[CuL^1(ClO_4)_2]$ **(1)**	Pink	242-244	30	35.62 (35.58)	6.48 (6.51)	13.48 (13.62)
$[CuL^2(ClO_4)_2]$ **(2)**	Red	254-257	25	40.34 (40.26)	7.11 (7.06)	12.29 (12.17)
$[CuL^3(ClO_4)_2]$ **(3)**	Pink	263-265	75	41.56 (41.72)	7.81 (7.88)	12.52 (12.17)

Table 3 (continued). Melting point (^{o}C), % yield, color, and elemental analyses data of the complexes.

Complexes	Color	M.P.	Yield	Found (*Calc.*) %		
				C	H	N
$[NiL^3](ClO_4)_2$ **(4)**	Yellow	278-280	50	41.62 (41.92)	7.81 (7.87)	12.36 (12.25)
$[CuL^4(ClO_4)_2]$ **(5)**	Red	266-267	35	43.95 (43.54)	8.08 (8.15)	11.84 (11.71)
$[CuL^5(ClO_4)_2]$ **(6)**	Pink	262-264	75	32.43 (32.60)	6.42 (6.66)	14.79 (14.80)
$[NiL^5](ClO_4)_2$ **(7)**	Yellow	275-277	80	33.13 (33.61)	6.51 (6.65)	14.77 (14.71)
$[CuL^6(ClO_4)_2]$ **(8)**	Red	264-265	65	35.70 (35.73)	6.87 (6.90)	13.81 (13.89)
$[CuL^7(ClO_4)_2]$ **(9)**	Pink	263-264	52	41.08 (41.76)	7.72 (7.88)	12.28 (12.17)
$[NiL^7](ClO_4)_2$ **(10)**	Yellow	277-278	73	41.92 (41.90)	7.90 (7.90)	12.39 (12.35)
$[CuL^8(ClO_4)_2]$ **(11)**	Pink	279-281	38	43.96 (43.55)	8.09 (8.16)	11.84 (11.73)
$[CuL^5]_3[Fe(CN)_6]_2{\cdot}5H_2O$ **(12)**	Brown	289-291	44	44.05 (44.10)	6.90 (6.92)	25.68 (25.70)
$[NiL^5(4\text{-nba})_2]{\cdot}H_2O$ **(13)**	Orange	263-265	63	50.55 (50.51)	6.53 (6.49)	15.77 (15.71)
$[NiL^3(4\text{-nba})_2]$ **(14)**	Orange	277-278	65	55.82 (55.84)	7.64 (7.65)	11.84 (11.87)
$[NiL^5(sal)_2]$ **(15)**	Purple	274-276	47	55.66 (55.69)	7.47 (7.49)	12.98 (12.99)

3.2 FT-IR spectral studies

FT-IR spectroscopic technique is used to investigate the functional groups in the powders and crystals. The FT-IR spectra of the complexes **(1)** - **(15)** showed several absorption bands in the mid-infrared region due to vibrations such as stretching and bending of organic ligands and the data are summarized in **Table 4**. All FT-IR spectra of complexes showed common absorption bands of the stretching vibration mode in the region 3206-3288 cm^{-1}, corresponding to the presence

secondary amine (-NH) group of the hexaazamacrocyclic ligand and also confirmed that the condensation reaction had occurred. In addition, the absence of ν(C=O) of aldehydic moiety bands in the range 1720-1740 cm^{-1} was another evidence confirming the condensation reaction (Shakir *et al*., 2006). All the complexes show absorption bands in the region 2925-2963 cm^{-1} which were assignable to ν(C-H) stretching vibration. The copper(II) and nickel(II) complexes **(1) - (11) (Figure 45-55)** showed the presence of perchlorate ions was supported by the absorption bands in the region 1020-1090 cm^{-1} and 1091-1121 cm^{-1} which were assigned to stretching vibration of the ClO_4^- ions and a strong band in the region 621-628 cm^{-1} was assigned to δ(ClO_4^-) bending (Kim *et al*., 2013). The weak absorption bands in the region 420-485 cm^{-1} of the complexes **(1) - (15)** were assigned to ν(M-N).

FT-IR spectrum of the complex **(12)** showed the splitting of the cyanide groups ν(C≡N) absorption bands in the range 2097, 2117 cm^{-1} corresponding to the presence of both cyanide bridged and cyanide terminal ligand, respectively **(Figure 56)**. Similar vibration frequencies were reported in the literatures for cyano-bridged complexes (Kou *et al*., 2001 and Kou *et al*., 2004). The absence of absorption bands at 1091-1121 cm^{-1} and 621-628 cm^{-1} confirmed to absence of perchlorate ion in the crystal structure, consistent with the results of single crystal X-ray diffraction analysis.

The FT-IR spectra **(Figures 57** and **58)** of the complexes **(13)** and **(14)** showed bands of the nitro group (-NO_2) of 4-nba ligand occurred at 1341 and 1340 cm^{-1}, respectively (Choi *et al*., 1999). The very strong bands of the carboxylato group (C=O) at 1592 and 1593 cm^{-1}, respectively, were characteristic of the 4-nba ion in the monodentate carboxylate coordination (Zeleňák *et al*., 2007). The bands of the perchlorate ions disappeared due to the perchlorate being replaced by 4-nba ion.

In the FT-IR spectrum **(Figures 59)** of the complex **(15)**, a strong band at 3359 cm^{-1} was assigned to the hydroxyl group. The appearance of a strong intensity band at 1597 cm^{-1} was assigned to the carboxylate group coordinated to the nickel(II) ion in a monodentate mode.

Table 4. FT-IR absorption data and assignments of **(1) - (15)**.

Complexes	Vibrational frequencies (cm^{-1})								
	ν(N-H)	ν(C-H)	ν(C≡N)	ν(C=O)	ν(NO_2)	ν(Cl-O)	δ(Cl-O)	ν(M-O)	ν(M-N)
$[CuL^1(ClO_4)_2]$ **(1)**	3249 s	2933 s	-	-	-	1090 m, 1116 w	628 s	529 w	441 w
$[CuL^2(ClO_4)_2]$ **(2)**	3234 s	2928 s	-	-	-	1081 w, 1118 w	624 s	521 w	456 w
$[CuL^3(ClO_4)_2]$ **(3)**	3241 s	2927 s	-	-	-	1067 m, 1121 w	623 s	512 w	471 w
$[NiL^3](ClO_4)_2$ **(4)**	3206 s	2927 s	-	-	-	1093 w, 1118 m	622 s	-	485 w
$[CuL^4(ClO_4)_2]$ **(5)**	3241 s	2932 s	-	-	-	1030 m, 1091 w	623 s	557 w	454 w
$[CuL^5(ClO_4)_2]$ **(6)**	3244 s	2961 s	-	-	-	1080 m, 1119 w	627 s	550 w	443 w
$[NiL^5](ClO_4)_2$ **(7)**	3208 s	2958 s	-	-	-	1089 w, 1116 w	624 s	-	434 w
$[CuL^6(ClO_4)_2]$ **(8)**	3241 s	2963 s	-	-	-	1064 w, 1114 w	622 s	565 w	420 w
$[CuL^7(ClO_4)_2]$ **(9)**	3243 s	2961 s	-	-	-	1068 w, 1121 w	622 s	526 w	444 w
$[NiL^7](ClO_4)_2$ **(10)**	3206 s	2962 s	-	-	-	1020 w, 1115 w	622 s	507 w	443 w
$[CuL^8(ClO_4)_2]$ **(11)**	3242 s	2960 s	-	-	-	1068 w, 1121 w	621 s	556 w	423 w
$[CuL^5]_3[Fe(CN)_6]_3 \cdot 5H_2O$ **(12)**	3247 s	2956 s	2097 m, 2117 m	-	-	-	-	-	421 w
$[NiL^5(4\text{-nba})_2] \cdot H_2O$ **(13)**	3288 s	2957 s	-	1592 s	1341 s	-	-	518 w	426 w
$[NiL^3(4\text{-nba})_2]$ **(14)**	3186 s	2925 s	-	1593 s	1340 s	-	-	517 w	429 w
$[NiL^5(sal)_2]$ **(15)**	3193 s	2931 s	-	1597 s	-	-	-	518 w	427 w

ν = Stretching vibration; δ = Bending vibration; s = Strong intensity band; m = Medium intensity band; w = Weak intensity band

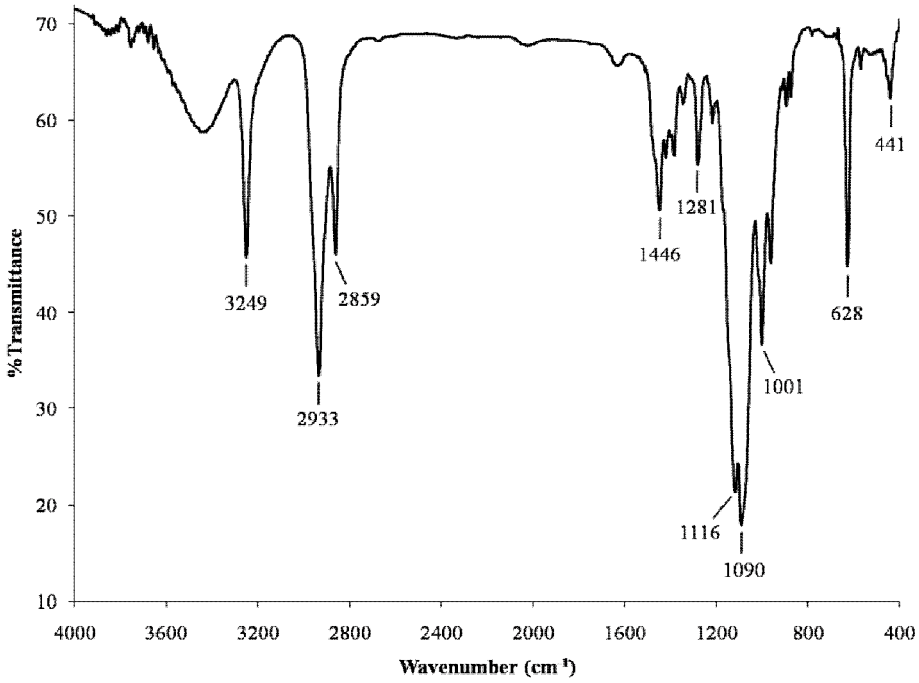

Figure 45. FT-IR spectra of $[CuL^{1}(ClO_4)_2]$ **(1)**.

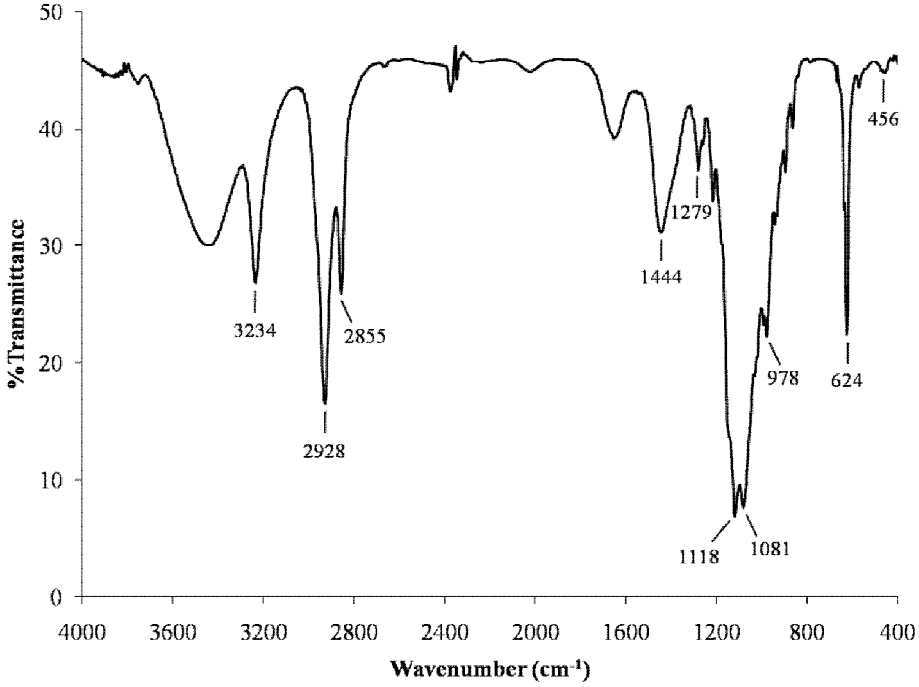

Figure 46. FT-IR spectra of $[CuL^{2}(ClO_4)_2]$ **(2)**.

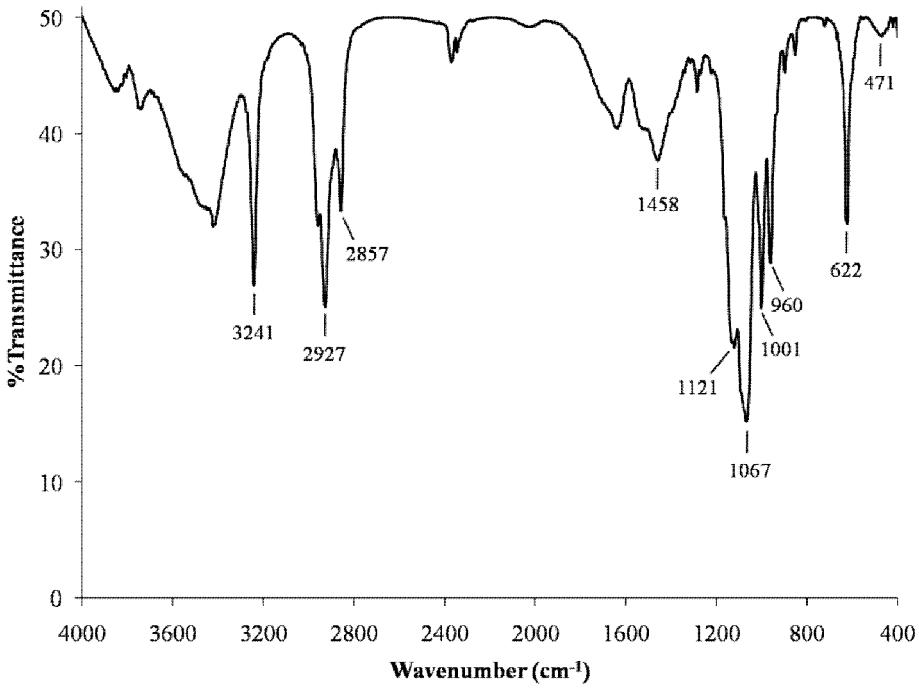

Figure 47. FT-IR spectra of $[CuL^3(ClO_4)_2]$ **(3)**.

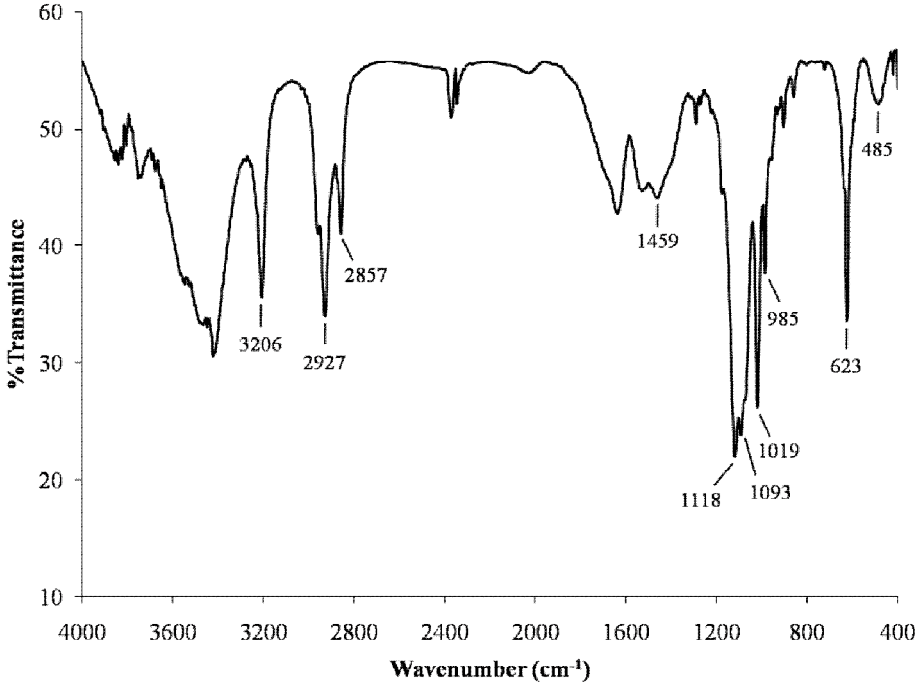

Figure 48. FT-IR spectra of $[NiL^3](ClO_4)_2$ **(4)**.

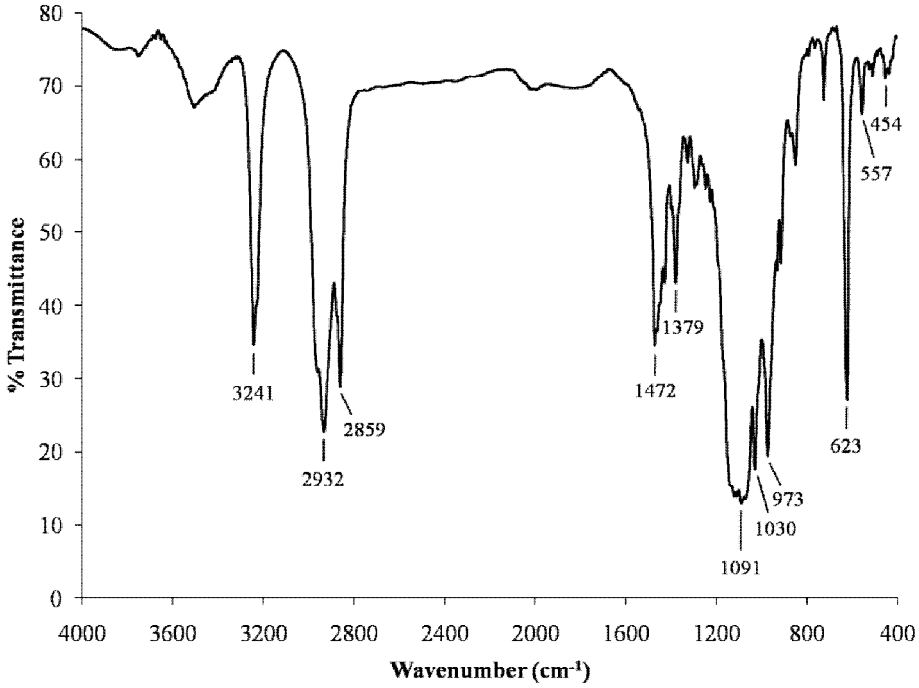

Figure 49. FT-IR spectra of $[CuL^4(ClO_4)_2]$ **(5)**.

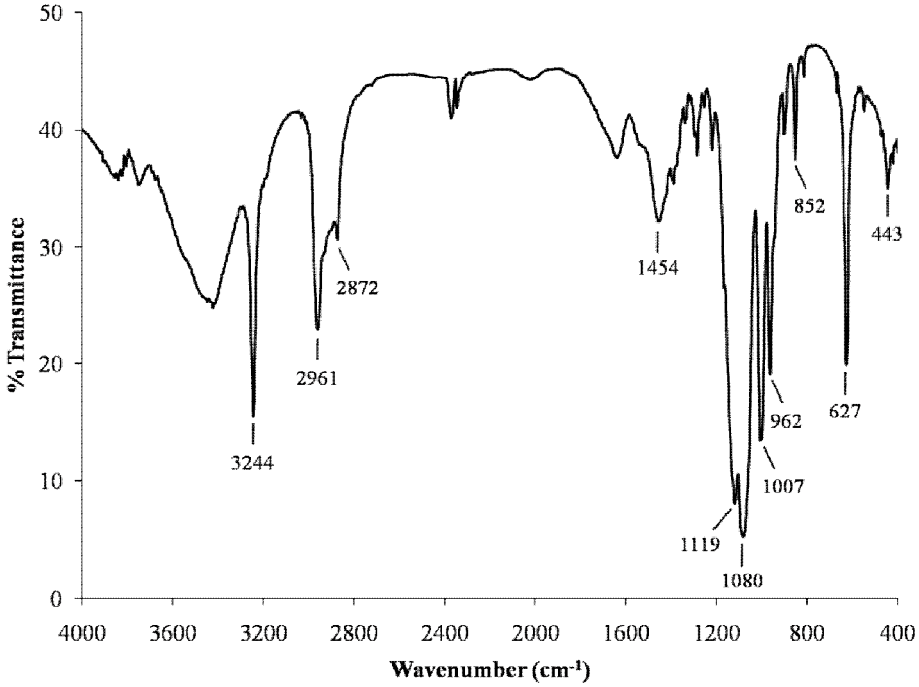

Figure 50. FT-IR spectra of $[CuL^5(ClO_4)_2]$ **(6)**.

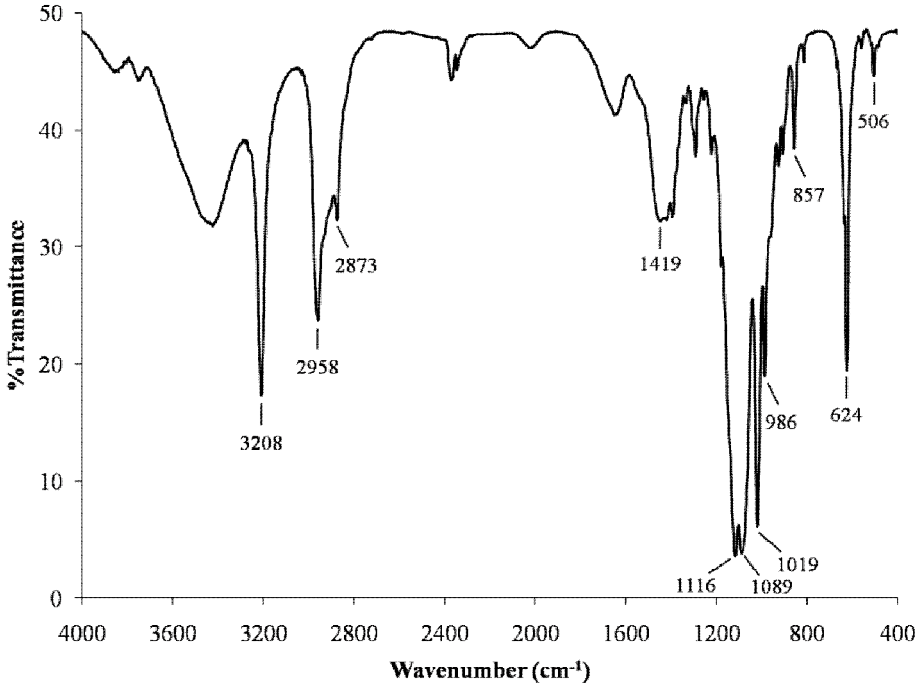

Figure 51. FT-IR spectra of $[NiL^5](ClO_4)_2$ **(7)**.

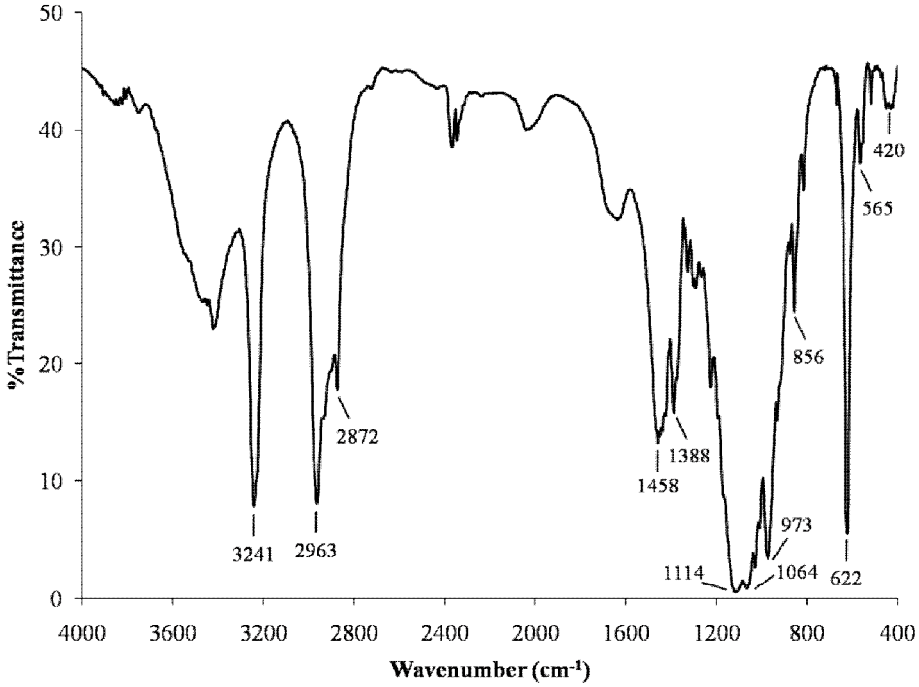

Figure 52. FT-IR spectra of $[CuL^6(ClO_4)_2]$ **(8)**.

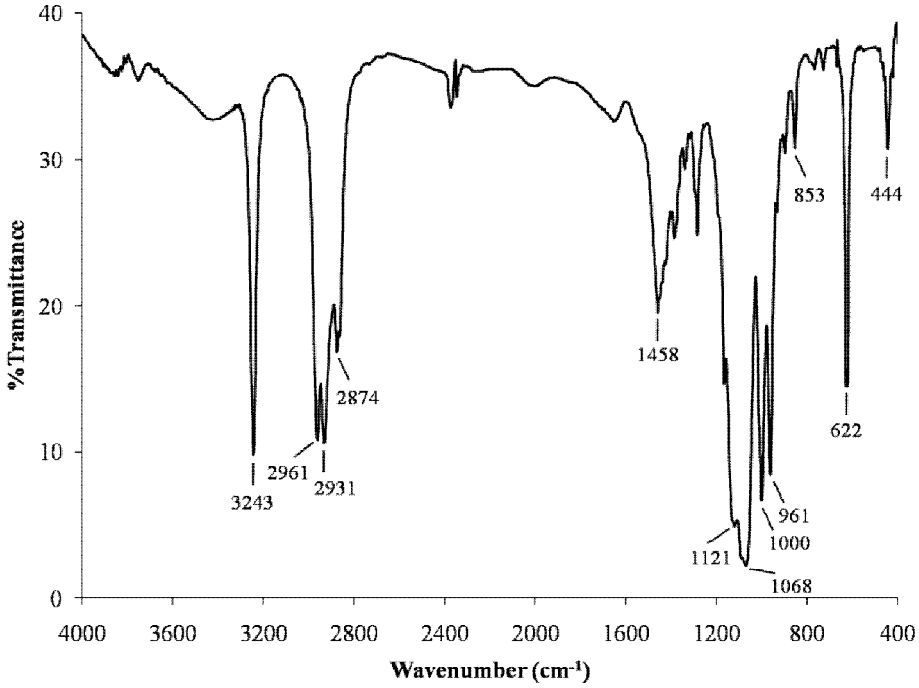

Figure 53. FT-IR spectra of $[CuL^7(ClO_4)_2]$ **(9)**.

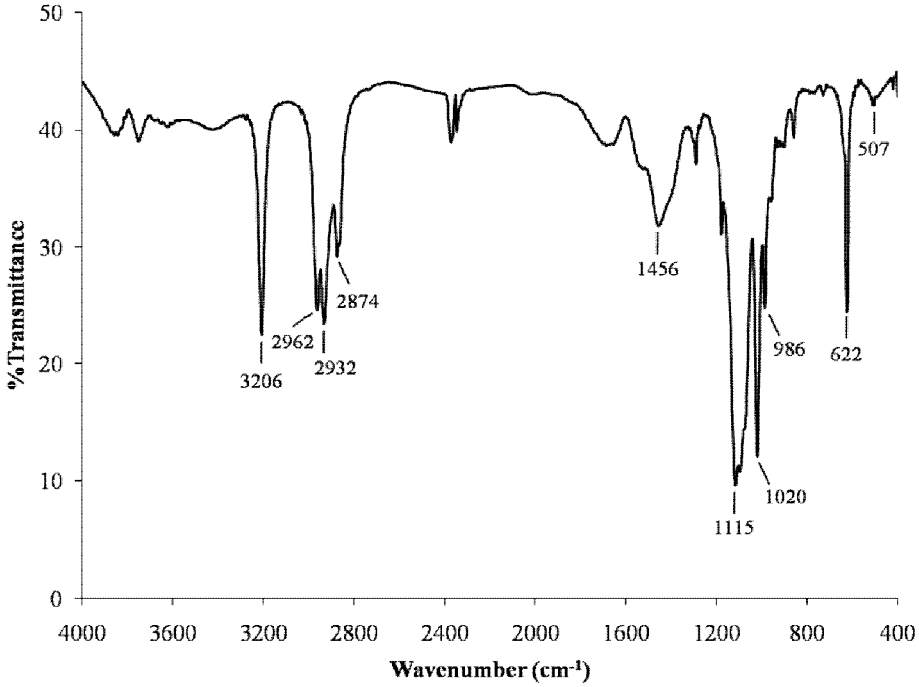

Figure 54. FT-IR spectra of $[NiL^7](ClO_4)_2$ **(10)**.

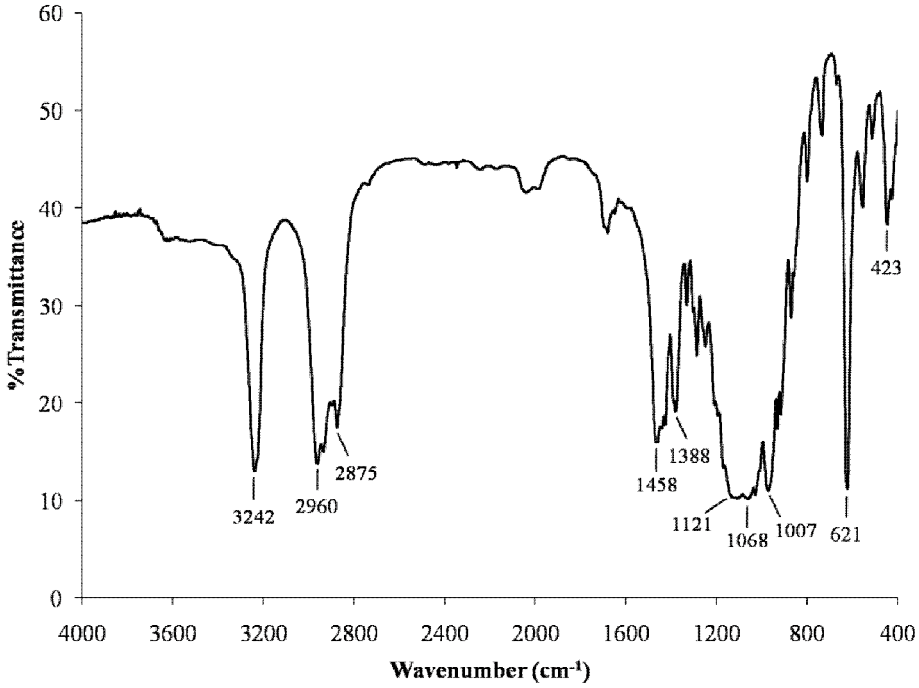

Figure 55. FT-IR spectra of $[CuL^{8}(ClO_4)_2]$ **(11)**.

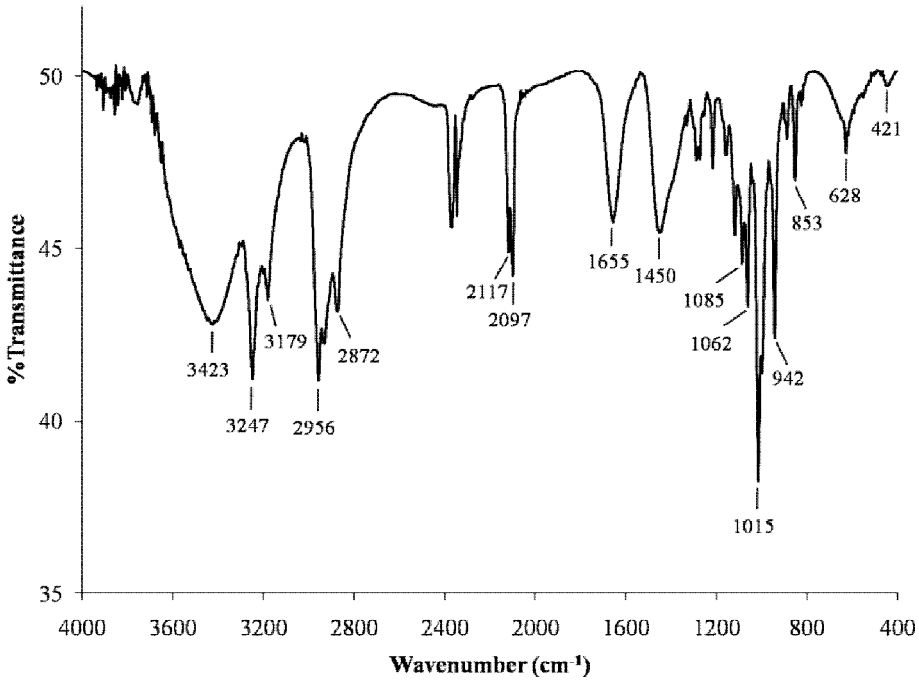

Figure 56. FT-IR spectra of $[CuL^{5}]_3[Fe(CN)_6]_2 \cdot 5H_2O$ **(12)**.

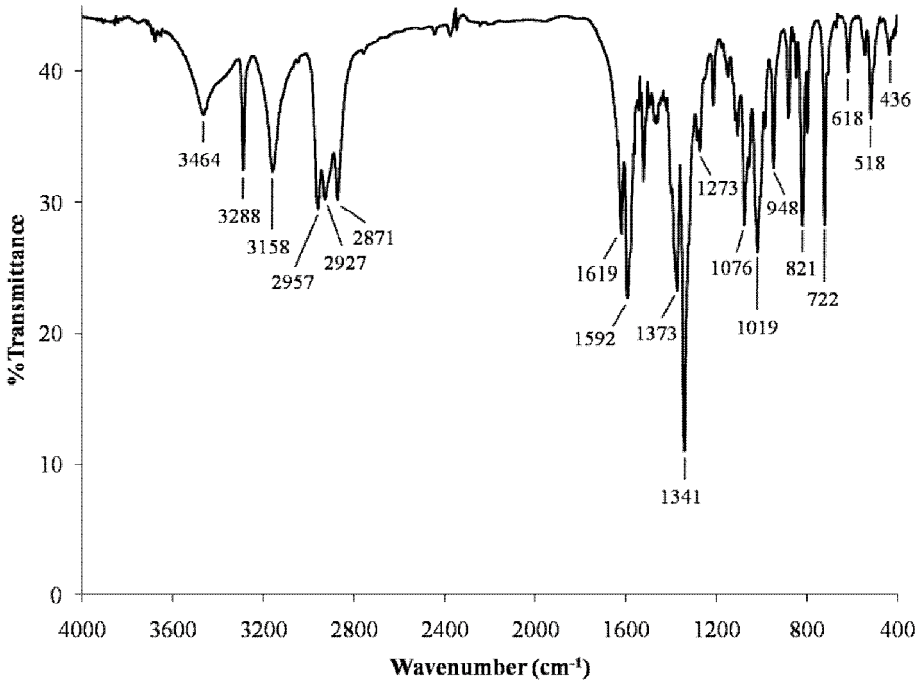

Figure 57. FT-IR spectra of $[NiL^5(4\text{-nba})_2]\cdot H_2O$ **(13)**.

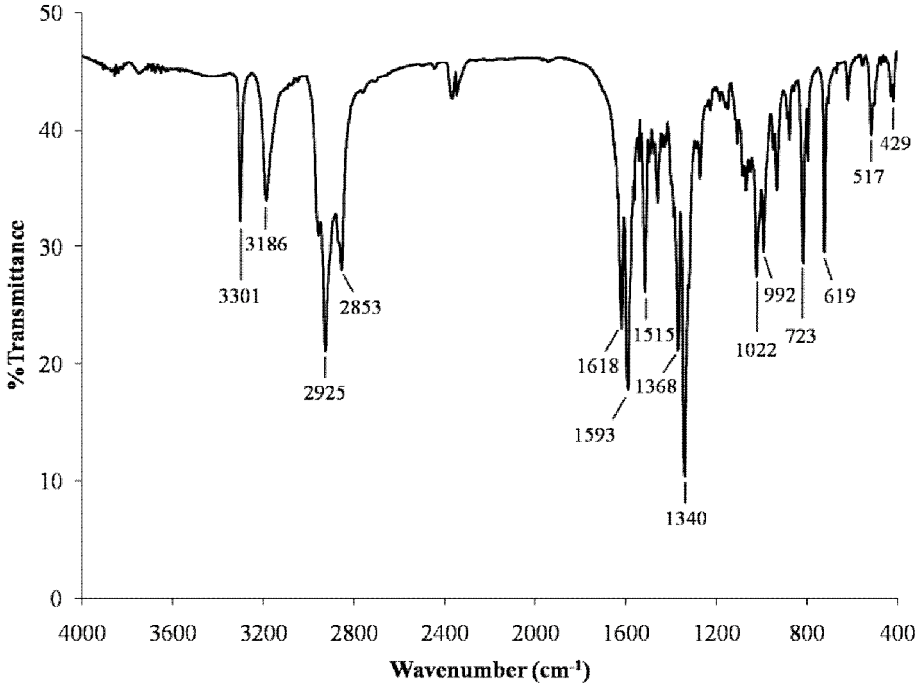

Figure 58. FT-IR spectra of $[NiL^3(4\text{-nba})_2]$ **(14)**.

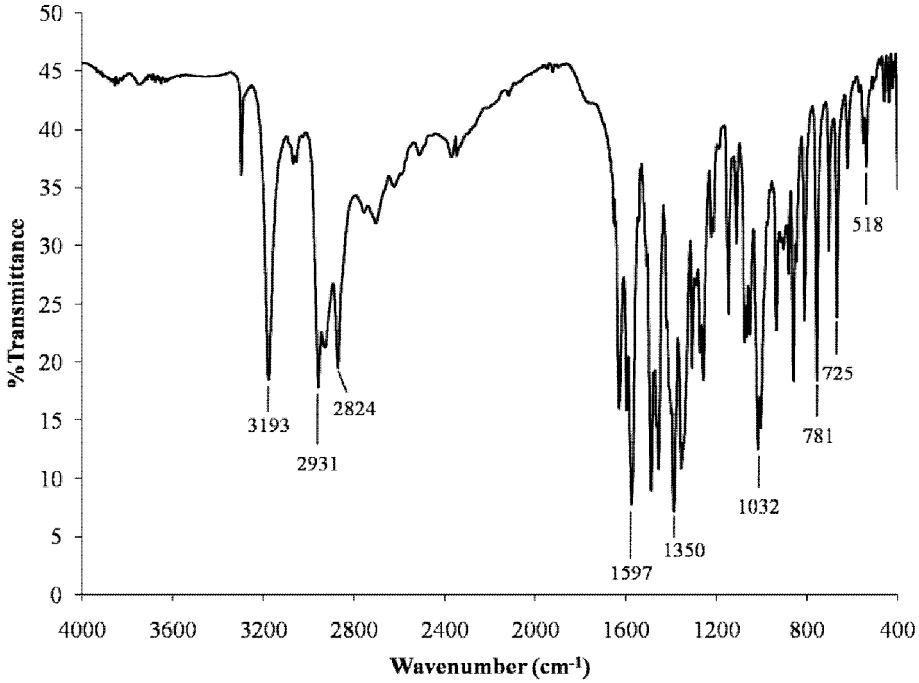

Figure 59. FT-IR spectra of $[NiL^5(sal)_2]$ **(15)**.

3.3 Electronic absorption spectral measurement

The electronic absorption spectra of complexes **(1)** - **(11)** were obtained in DMSO solution at ambient temperature and are illustrated in **Figures 60** and **61**. The solid-state electronic spectra of the complex **(12)** by the diffused reflectance (DRS) spectroscopic method at room temperature are shown in **Figure 62**. The electronic spectral data of complexes **(1)** - **(12)** were summarized in **Table 5**. The six-coordinated copper(II) complexes are d^9 configuration which can have either the D_{4h} or C_{4v} symmetry with the energy levels (E_g and T_{2g}) of ^2D free ion term symbol (Cho *et al.*, 2003). This results in three spin allowed transitions namely: $^2B_{1g} \rightarrow {}^2A_{1g}$ ($d_x{}^2\text{-}_y{}^2 \leftarrow d_z{}^2$), $^2B_{1g} \rightarrow {}^2B_{2g}$ ($d_x{}^2\text{-}_y{}^2 \leftarrow d_{xy}$), and $^2B_{1g} \rightarrow {}^2Eg$ ($d_x{}^2\text{-}_y{}^2 \leftarrow d_{xy}$, d_{yz}). The energy levels sequence will depend on the total of tetragonal distortion from ligand field and Jahn-Teller effects (Chandra *et al.*, 2009). The electronic spectra of copper(II) complexes showed a single *d-d* transition band in the range 500-512 nm and were assigned to $^2B_{1g} \rightarrow {}^2B_{2g}$ transition of the tetragonally distorted octahedral. The distortion was confirmed by the X-ray diffraction data of the Cu(II) complexes

(5) and **(8)** that the Cu-$O_{perchlorate}$ bonds in axial position were longer than the Cu-N_{amines} bonds in equatorial plane due to the Jahn-Teller distortion with z-out elongation.

The nickel(II) complexes were four-coordinated d^8 configuration with low-spin square-planar geometry in the D_{4h} symmetry with the energy level (E_g and T_{2g}) of ^3F free ion term symbol. This resulted in two spin allowed transitions namely: $^1A_{1g} \rightarrow {}^1A_{2g}$ ($b_{2g} \rightarrow b_{1g}$) and $^1A_{1g} \rightarrow {}^1B_{1g}$ ($a_{1g} \rightarrow b_{1g}$) transitions (Odola *et al.*, 2011 and Sujatha *et al.*, 2009). All the Ni(II) complexes showed two *d-d* transitions absorption bands in the range 449-452 nm and a broad shoulder bands at 632-634 nm attributed to $^1A_{1g} \rightarrow {}^1A_{2g}$ and $^1A_{1g} \rightarrow {}^1B_{1g}$ electronic transitions, respectively, according to the square-planar geometry. This geometry around nickel(II) ion was confirmed by single crystal X-ray diffraction analysis of complex **(7)** that the Ni-$O_{perchlorate}$ bonds in axial position were longer than the Ni-N_{amines} bonds in equatorial plane.

Solid state DRS of the complex **(12)** revealed a shoulder absorption band at 530 nm in the visible region which could be assigned to *d-d* transition occurred from overlay between Cu^{2+} and Fe^{3+} ions. The absorption band at 530 nm of the complex **(12)** was comparable to the absorption band at 514 nm of complex **(6)** precursor. Substitution of hexacyanoferrate(III) for perchlorate ligand shifted the band by 16 nm towards longer wavelength was described as stabilization of the Fe^{3+} *d*-orbital because the weakening of the σ-donor types of the cyanide ligands (Uddin *et al.*, 2013). Other absorption bands below 380 nm were assigned to $\pi \rightarrow \pi^*$, $n \rightarrow \pi^*$, and $n \rightarrow \sigma^*$ transitions and the maximum absorption band at 431 nm was assigned to the ligand-to-metal charge transfer (LMCT) due to the presence of $[Fe(CN)_6]^{3-}$ ions (Uddin *et al.*, 2014).

Table 5. Electronic spectral data of complexes **(1)** - **(12)**.

Complexes	λ_{max} (nm)	ε (L mol^{-1} cm^{-1})
$[CuL^1(ClO_4)_2]$ **(1)**	514	32
$[CuL^2(ClO_4)_2]$ **(2)**	512	35
$[CuL^3(ClO_4)_2]$ **(3)**	500	40
$[NiL^3](ClO_4)_2$ **(4)**	452, 634	37
$[CuL^4(ClO_4)_2]$ **(5)**	500	60
$[CuL^5(ClO_4)_2]$ **(6)**	514	38
$[NiL^5](ClO_4)_2$ **(7)**	450, 632	29
$[CuL^6(ClO_4)_2]$ **(8)**	516	39
$[CuL^7(ClO_4)_2]$ **(9)**	504	37
$[NiL^7](ClO_4)_2$ **(10)**	449, 633	38
$[CuL^8(ClO_4)_2]$ **(11)**	512	38
$[CuL^5]_3[Fe(CN)_6]_2 \cdot 5H_2O$ **(12)**	431, 530	-

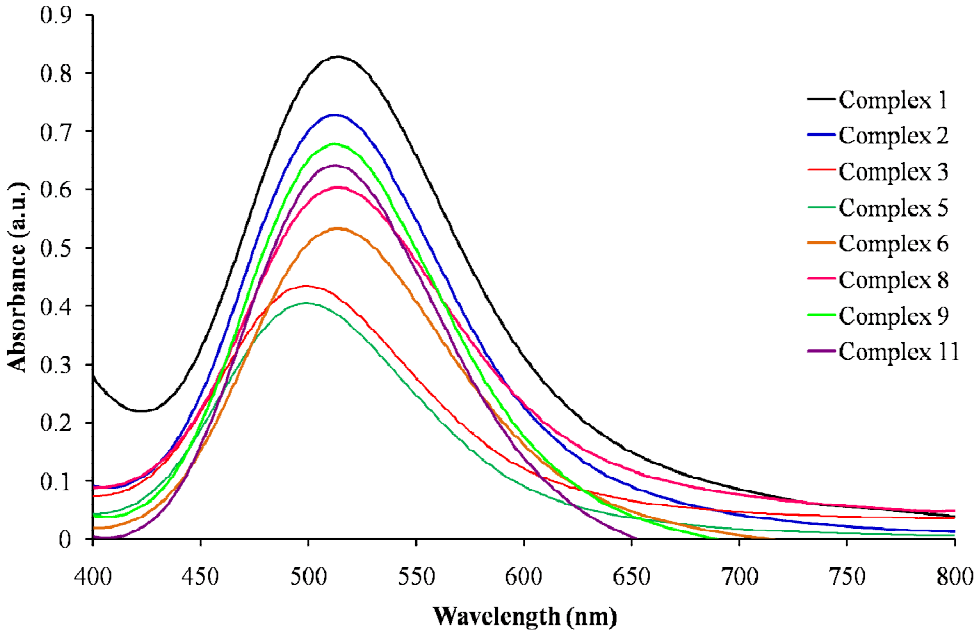

Figure 60. UV-Visible spectra of the Cu(II) complexes **(1)**, **(2)**, **(3)**, **(5)**, **(6)**, **(8)**, **(9)**, and **(11)**.

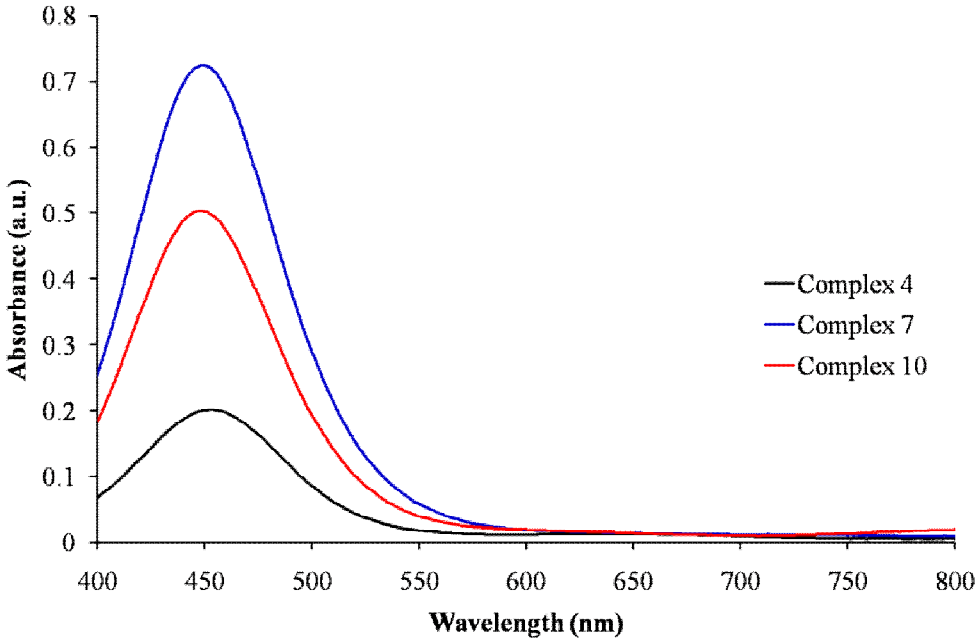

Figure 61. UV-Visible spectra of the Ni(II) complexes **(4)**, **(7)**, and **(10)**.

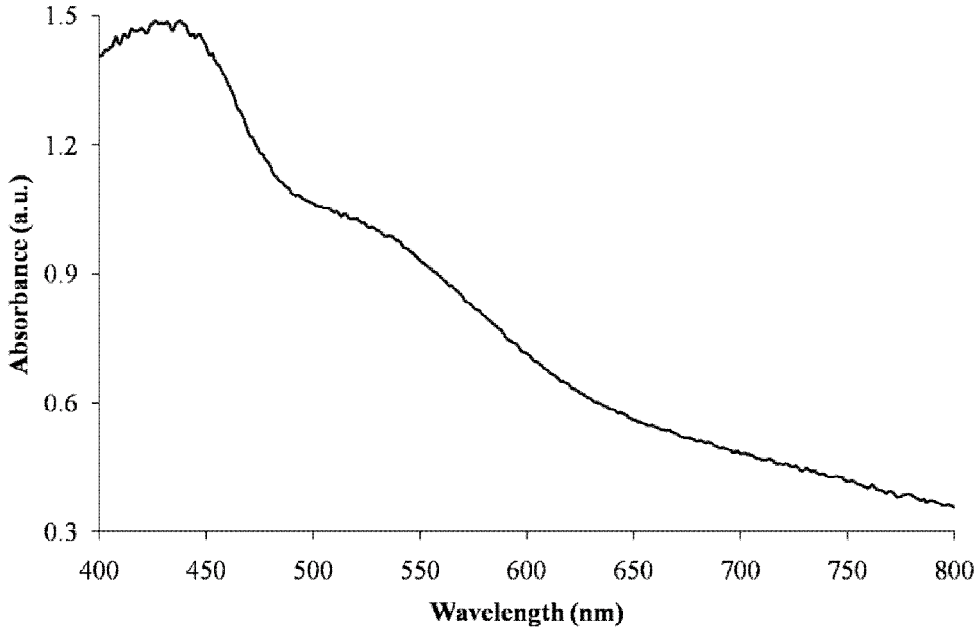

Figure 62. Solid-state UV-Visible spectra of the Cu(II)-Fe(III) complex **(12)**.

3.4 Thermogravimetric analysis

TGA curves of all complexes were recorded from 50-1,000 ^{o}C under flowing nitrogen (N_2) gas atmosphere. The thermograms of Cu(II) complexes are given in **Figure 63**.

The thermal release of the complex **(1)** occurred in four stages. The first stage was under the temperature range 198-332 ^{o}C and corresponding to the loss of two perchlorate ions with weight losses 31.65 % (calculated 31.66 %). The second stage was under the temperature range 332-596 ^{o}C corresponding to the loss of two cyclohexyl molecules with weight losses 26.46 % (calculated 26.41 %). The third stage was within a temperature range 596-808 ^{o}C, and was attributed to the loss of hexaazamacrocyclic moiety with weight losses 31.87 (calculated 31.82 %). Finally, the decomposition of the complex **(1)** at temperature above 808 ^{o}C which the weight of the residue 10.02 % corresponding to copper(II) oxide (calculated 10.10 %).

In the thermogram of the complex **(3)**, there was a weight loss of 45.20 % within the temperature range 253-480 ^{o}C attributable to the release of two perchlorate anions and one octyl molecule (calculated 45.18 %). The next step, weight loss between 480-807 ^{o}C of 45.40 % (calculated 45.33 %) corresponded to the loss of one octyl molecule and hexaazamacrocyclic moiety. The final residue was copper(II) oxide with weight loss of 9.40 % (calculated 9.23 %).

For complex **(5)**, the first weight loss of 28.9 % (calculated 27.8 %) was in the range 120-250 ^{o}C corresponding to the loss of two perchlorate ions. On further heating, the second weight loss was observed in the range 250-860 ^{o}C with the loss of hexaazamacrocyclic ligands. After decomposition of the complex at high temperature above 1000 ^{o}C, the weight of the residue (taken as copper(II) oxide) was 25.1 % (calculated 24.4 %).

TGA curve of the complex **(6)** revealed four steps of weight losses. The first weight loss (26.46 %) appeared in the temperature range 200-260 ^{o}C corresponding to the loss of one *iso*-butyl molecule and one perchlorate anion (calculated 26.97 %). The second step occurred at 260-320 ^{o}C (21.07 %)

corresponding to the loss of one perchlorate anion (calculated 21.11 %). The third step at 320-530 °C with a weight loss of 12.49 % corresponded to the weight loss of one *iso*-butyl molecule (calculated 12.57 %). The final residue, presumably copper(II) oxide, was obtained with weight loss of 15.34 % (calculated 15.56 %).

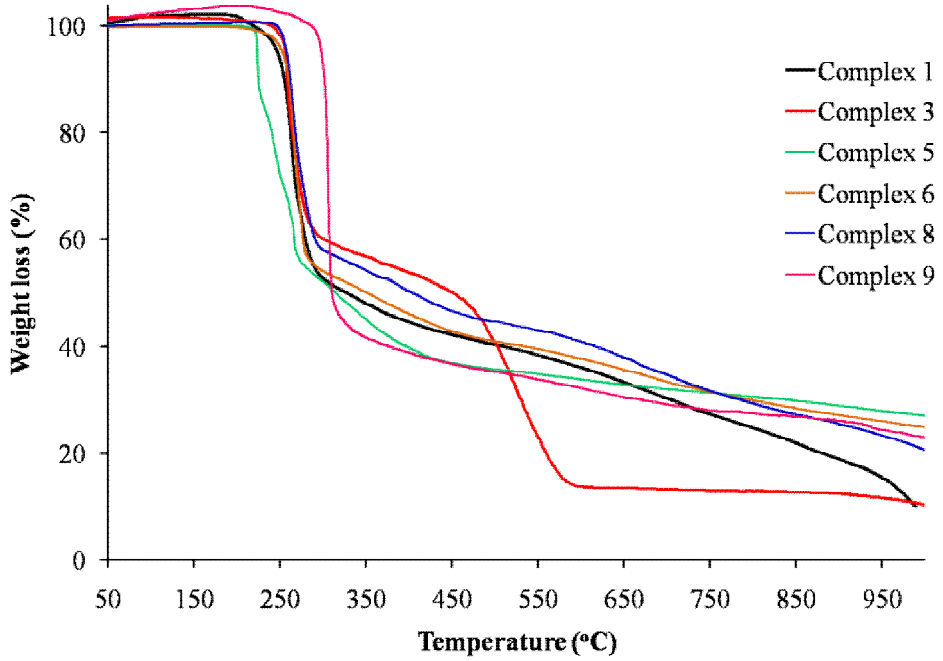

Figure 63. TGA curves of Cu(II) complexes **(1)**, **(3)**, **(5)**, **(6)**, **(8)**, and **(9)**.

The TGA degradation of the complex **(8)** displayed four decomposition steps. The first step appeared at 256-282 °C with a weight loss of 32.92 % (calculated 32.94 %) which corresponded to the loss of two perchlorate anions. The second step decomposition temperature was in the range 282-362 °C with a weight loss of 18.91 % (calculated 18.87 %) corresponding to the loss of two *iso*-butyl molecules. The third step in the temperature range of 362-630 °C with a weight loss of 33.15 % (calculated 33.10 %) corresponded to the loss of hexaazamacrocyclic moiety. The final product was copper(II) oxide.

The TGA curve of the complex **(9)** showed the first weight loss of 61.26 % (calculated 61.28 %) in the range 300-430 °C corresponding to the loss of two perchlorate anions and two 2-ethyl-1-hexyl molecules. The second weight loss of

29.02 % (calculated 28.98 %) in the range 430-783 ^{o}C corresponded to the loss of hexaazamacrocyclic moiety. The residual weight loss of 9.72 % corresponded to values calculated for copper(II) oxide of 9.20 %.

The thermograms of Ni(II) complexes are illustrated in **Figure 64**. The TGA curve of the complex **(4)** showed the weight loss of 29.11 % (calculated 29.12 %) from 271-286 ^{o}C corresponding to the release of two perchlorate anions. With the increase temperature, the second step weight loss of 32.84 % (calculated 32.78 %) was observed at 286-559 ^{o}C resulting from the decomposition of two octyl molecules. With the rise in temperature, the weight loss of 29.31 % (calculated 32.78 %) at 559-709 ^{o}C corresponded to the loss of hexaazamacrocyclic moiety. The last step at over 709 ^{o}C, the nickel(II) oxide residue with weight loss of 8.74 % (calculated 8.83 %) was obtained.

In the thermogram of the complex **(7)**, the initial weight loss of 35.03 % (calculated 34.84 %) at 264-285 ^{o}C corresponded to release of the two perchlorate counter ions molecules. The next weight loss due to the loss of two *iso*-butyl molecules in the region 285-472 ^{o}C was 30.78 % (calculated 30.72 %). Moreover, the thermogram of the hexaazamacrocyclic ligand showed decomposition curve in the region 472-750 ^{o}C with weight loss of 77.98 % (calculated 77.87 %). The final product was nickel(II) oxide.

The thermal degradation of the complex **(10)** occurred in three stages. The initial stage was within the temperature range of 279-513 ^{o}C and corresponded to the loss of two perchlorate anions and two 2-ethyl-1-hexyl molecules with weight loss of 61.95 % (calculated 61.90 %). The second stage occurred between 513-765 ^{o}C and was attributed to loss of hexaazamacrocyclic ligand with weight loss of 29.32 % (calculated 29.72 %). Finally, the nickel(II) oxide residue with weight loss of 8.73 % (calculated 8.59 %) remained over 765 ^{o}C.

The TGA curve of the complex **(13)** showed the first weight loss of 1.26 % (calculated 1.26 %) due to elimination of a water molecule at 49-175 ^{o}C. It showed a further weight loss of 46.57 % (calculated 1.26 %) in the range 175-330 ^{o}C due to the loss of *p*-nitrobenzoate ligand. The subsequent steps, the weight loss of

16.01 % (calculated 15.98 %) occurred within the range 330-385 °C corresponded to the release of the *iso*-butyl molecules. The fourth step of 28.07 % at 385-657 °C corresponded to loss of hexaazamacrocyclic moiety (calculated 28.03 %). The final product was nickel(II) oxide.

Decomposition of complex **(14)** composed of the first weight loss 50.98 % in the range 230-323 °C corresponding to the loss of the hexaazamacrocyclic ligand (calculated 51.92 %). On further heating, the second weight loss (40.61 %) was observed in the range 323-900 °C with the loss of *p*-nitrobenzoate ligand (calculated 39.82 %). Final residue, presumably a nickel(II) oxide, 8.41 % was obtained (calculated: 8.26 %).

The two steps decomposition was observed for complex **(15)** from the TGA curve with the first weight loss of 47.93 % which occurred within the range 249-355 °C corresponding to the release of the hexaazamacrocyclic ligand (calculated 48.22%). The second step weight loss of 41.87 % took place at 355-900 °C ascribable to the loss of salicylate ligand (calculated 42.66 %). The remaining weight, corresponding to nickel(II) oxide, was 10.20 % (calculated 9.12 %).

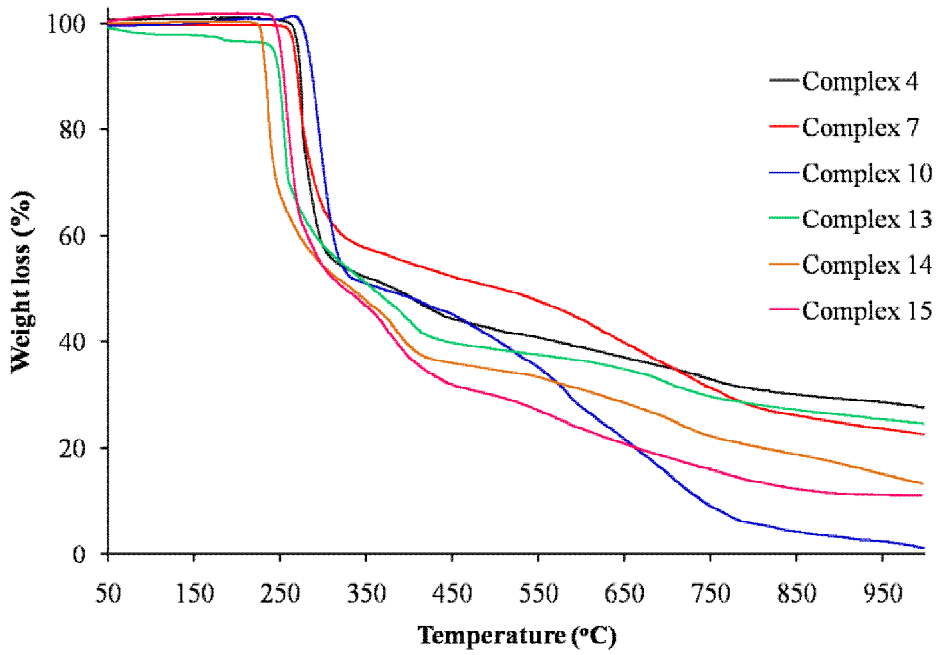

Figure 64. TGA curves of Ni(II) complexes **(4)**, **(7)**, **(10)**, **(13)**, **(14)**, and **(15)**.

The TGA decomposition curve **(Figure 65)** of the complex **(12)** showed four steps of dissociation in TGA curve. The first decomposition began in the temperature range 120-200 ^{o}C with the weight loss of 5.06 % (calculated 5.46 %) corresponding to release of five lattice water molecules. The second weight loss of 40.37 % at 200-285 ^{o}C was assigned to the loss of hexaazamacrocyclic ligand and cyanide groups (calculated 40.20 %). The third step of 20.54 % at 285-600 ^{o}C corresponded to loss of one hexaazamacrocyclic ligand (calculated 20.15 %). The remaining mass of 2.47 % (calculated 2.51 %), mixture product of CuO + Fe_2O_3, was obtained above 600 ^{o}C.

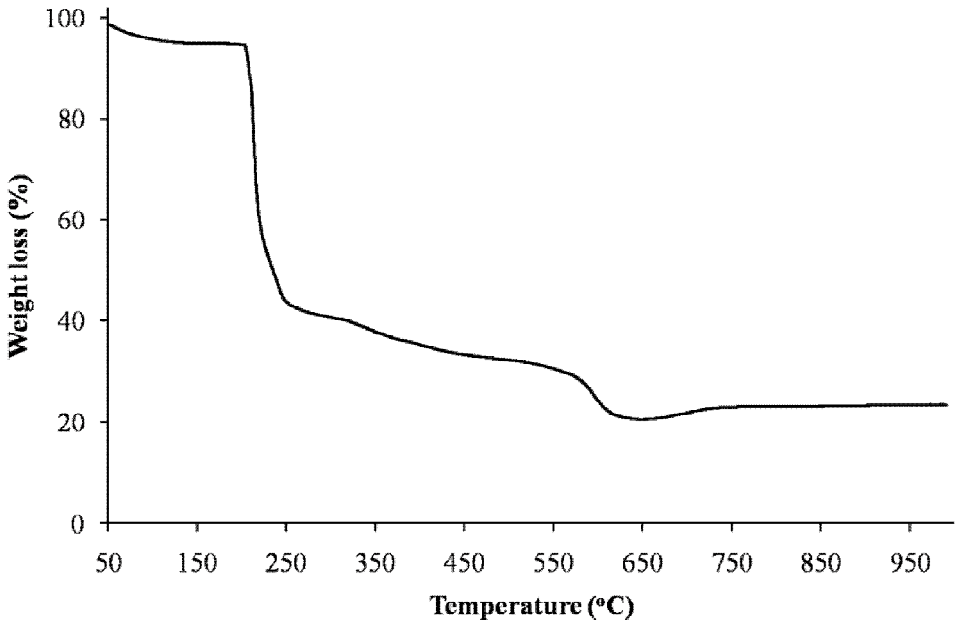

Figure 65. TGA curve of Cu(II)-Fe(III) complex **(12)**.

3.5 ESI-MS analysis

ESI-MS spectra were used to confirm the molecular formula of the complexes **(1)** - **(11)**. The copper(II) complexes revealed belonged to a doublet peak of ^{63}Cu and ^{65}Cu isotopes and the higher peak value of *m/z* are those existing the major isotope (^{63}Cu) (Chu *et al*., 2001). Copper has two stable isotopes of mass ^{63}Cu and ^{65}Cu which have average abundances of 69.17 % and 30.83 %, respectively

(Pokrovsky *et al*., 2008). The nickel(II) complexes showed a doublet peak of ^{58}Ni and ^{60}Ni isotopes with and the high *m/z* value belonged to the major isotope (^{58}Ni) (Taner, 2014 and Shih *et al*., 2015). Nickel has five stable isotopes of mass ^{58}Ni, ^{60}Ni, ^{61}Ni, ^{62}Ni, and ^{64}Ni, which have average abundances of 68.1 %, 26.2 %, 1.1 %, 3.6 %, and 0.9 %, respectively (Bullen *et al*., 2011).

In the mass spectrum **(Figure 66)** of the complex **(1)**, a molecular ion peak was observed at *m/z* 464.3 (100 %) corresponding to $[Cu(C_8H_{20}N_6)(ClO_4)_2\text{-}2H]$. The first fragmentation of the complex **(1)** occurred due to the cleavage of one perchlorate ion from $[Cu(C_{20}H_{42}N_6)(ClO_4)_2]$ to give $[Cu(C_{20}H_{42}N_6)(ClO_4)]^+$ ion with *m/z* at 528.3 (90 %). The $[Cu(C_{20}H_{42}N_6)(ClO_4)]^+$ ion further released one perchlorate ion forming $[Cu(C_{20}H_{42}N_6)]^{2+}$ ion with their peak *m/z* at 428.3 (80 %). The $[Cu(C_{20}H_{42}N_6)]^{2+}$ ion further fragmented to give smaller fragments $[Cu(C_{13}H_{29}N_5)]^{2+}$ ion with values *m/z* = 317.2 (81 %) and $[Cu(C_{12}H_{25}N_3)]^{2+}$ ion with values *m/z* = 273.2 (5 %), respectively. This mass spectrum fragmentation pattern **(Figure 67)** is in agreement with the structure of the complex **(1)**.

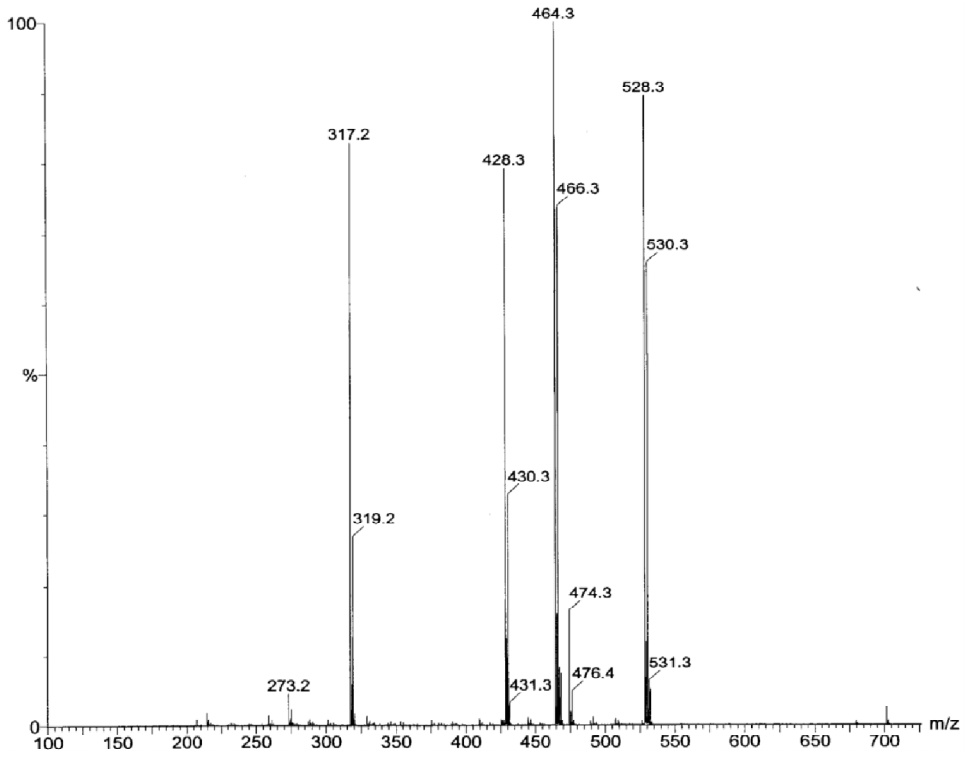

Figure 66. ESI mass spectra of the $[CuL^1(ClO_4)_2]$ **(1)**.

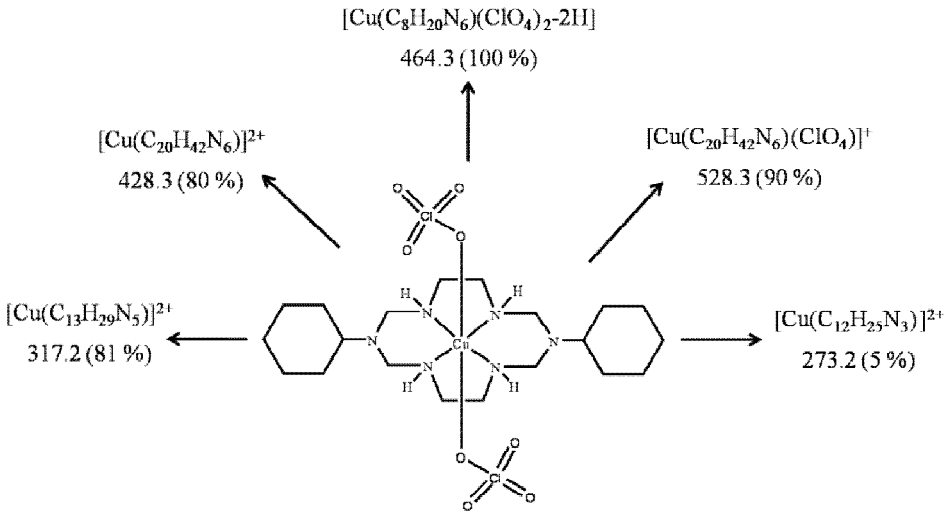

Figure 67. Fragmentation patterns of the $[CuL^1(ClO_4)_2]$ **(1)**.

The mass spectrum **(Figure 68)** of the complex **(2)** showed peaks at *m/z* value 556.3 (100 %), 467.5 (5 %), and 273.5 (4 %) corresponding to the $[Cu(C_{22}H_{46}N_6)(ClO_4)]^+$, $[Cu(C_{16}H_{30}N_6)(ClO_4)\text{-}2H]^+$, and $[Cu(C_{10}H_{19}N_5)]^{2+}$ species, respectively. This mass spectrum fragmentation pattern is in conformity with the structure of the complex **(2)** as shown in **Figure 69**.

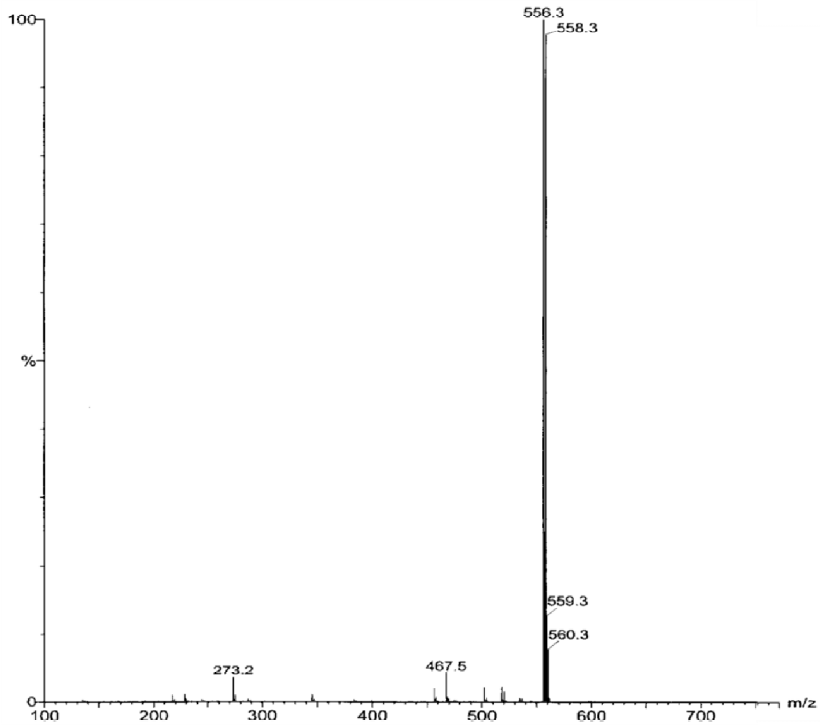

Figure 68. ESI mass spectra of the $[CuL^2(ClO_4)_2]$ **(2)**.

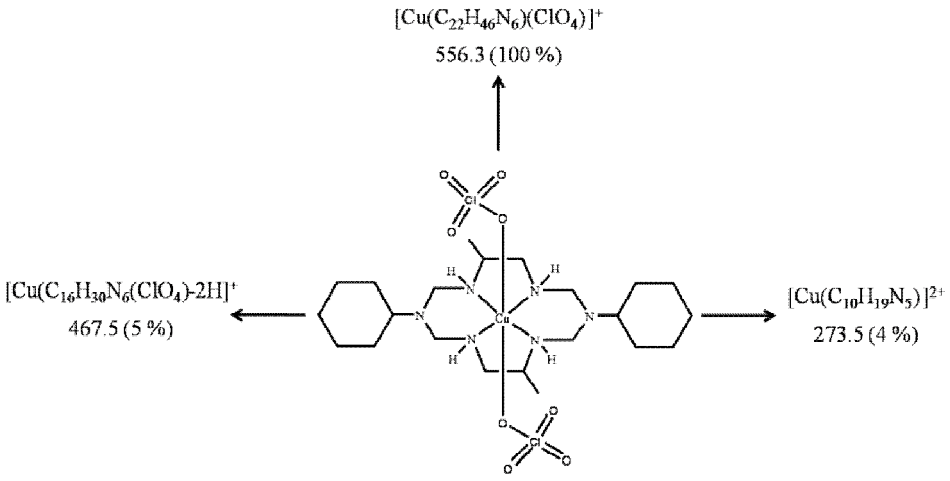

Figure 69. Fragmentation patterns of the $[CuL^2(ClO_4)_2]$ **(2)**.

In the mass spectrum **(Figure 70)** of the complex **(3)** a molecular ion peak at *m/z* 588.3 (100 %) was observed corresponding to the $[Cu(C_{24}H_{54}N_6)(ClO_4)]^+$ ion. The fragmentation peaks at *m/z* 289.9 (27 %), 190.1 (28 %), and 142.2 (25 %) were ascribed to the cleavage of $[Cu(C_5H_{11}N_4)(ClO_4)]^+$, $[Cu(C_5H_{11}N_4)]^{2+}$, and $[Cu(C_3H_2N_3)]^{2+}$, respectively. This mass spectrum fragmentation pattern is in conformity with the structure of the complex **(2)** as depicted in **Figure 71**.

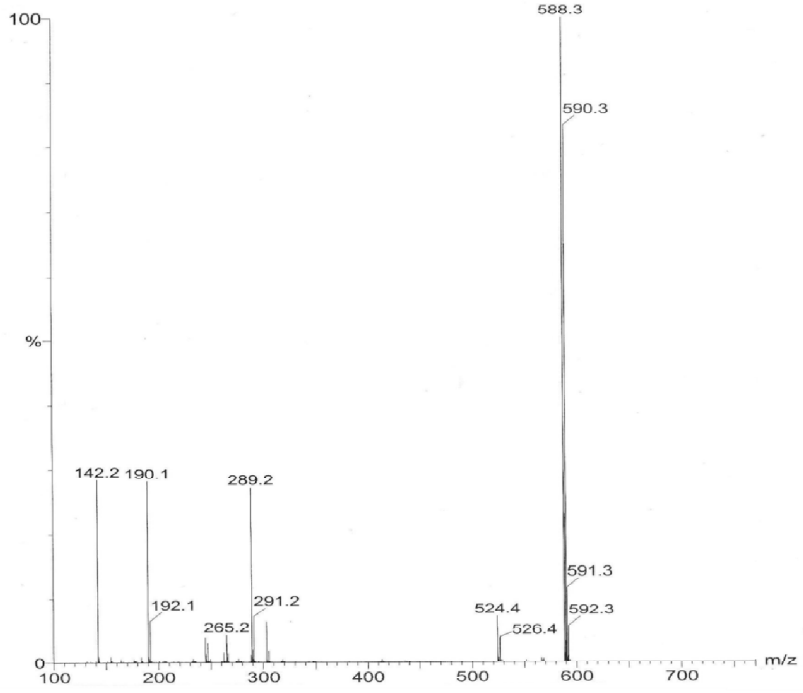

Figure 70. ESI mass spectra of the $[CuL^3(ClO_4)_2]$ **(3)**.

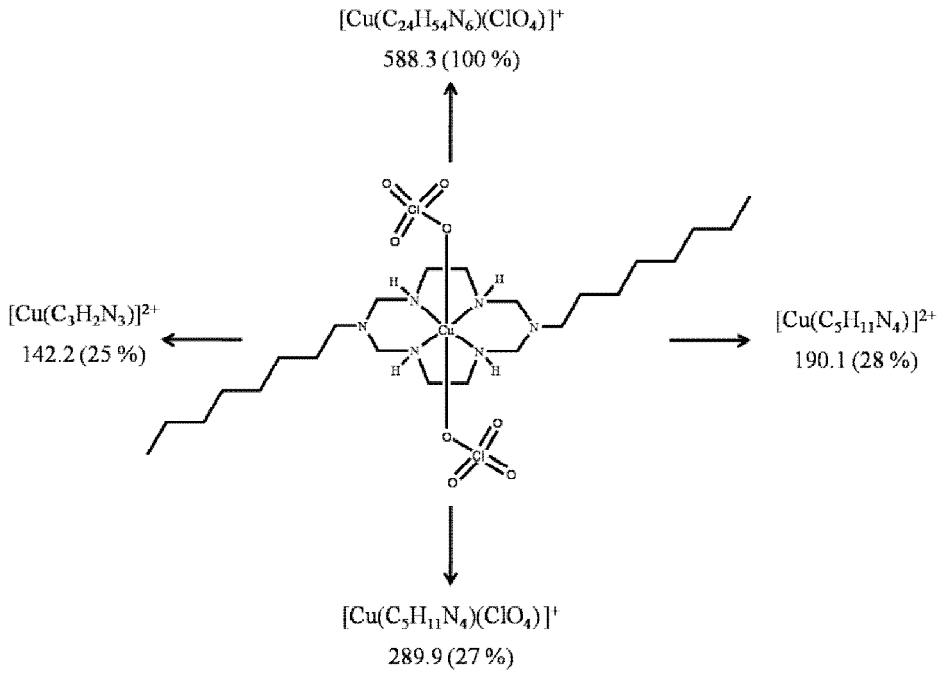

Figure 71. Fragmentation patterns of the $[CuL^3(ClO_4)_2]$ **(3)**.

In the mass spectrum **(Figure 72)** of the complex **(4)**, a molecular ion peak at *m/z* 583.3 (100 %) was assigned to $[Ni(C_{24}H_{54}N_6)]^+ClO_4^-$. The first dissociation of the complex **(4)** was the cleavage of one perchlorate ion from the $[Ni(C_{24}H_{54}N_6)](ClO_4)_2$. This form further degraded with the loss of one perchlorate ion forming $[Ni(C_{15}H_{35}N_5)]^{2+}$ species with the peak *m/z* at 342.2 (13 %). The $[Ni(C_{15}H_{35}N_5)]^{2+}$ ion with the continuous fragments were assignable to $[Ni(C_6H_{16}N_4)]^{2+}$ ion with values *m/z* = 201.1 (69 %), $[Ni(C_4H_{11}N_3)]^{2+}$ with *m/z* = 158.0 (8 %), and $[Ni(C_4H_{10}N_2)]^{2+}$ ion with *m/z* = 142.2 (11 %). The dissociation pattern is consistent with the structure of the complex **(4)** as presented in **Figure 73**. Similarly mass spectrum pattern was observed in metal(II) complexes with hexaaza-macrocyclic ligands reported by Sujatha *et al*., 2009.

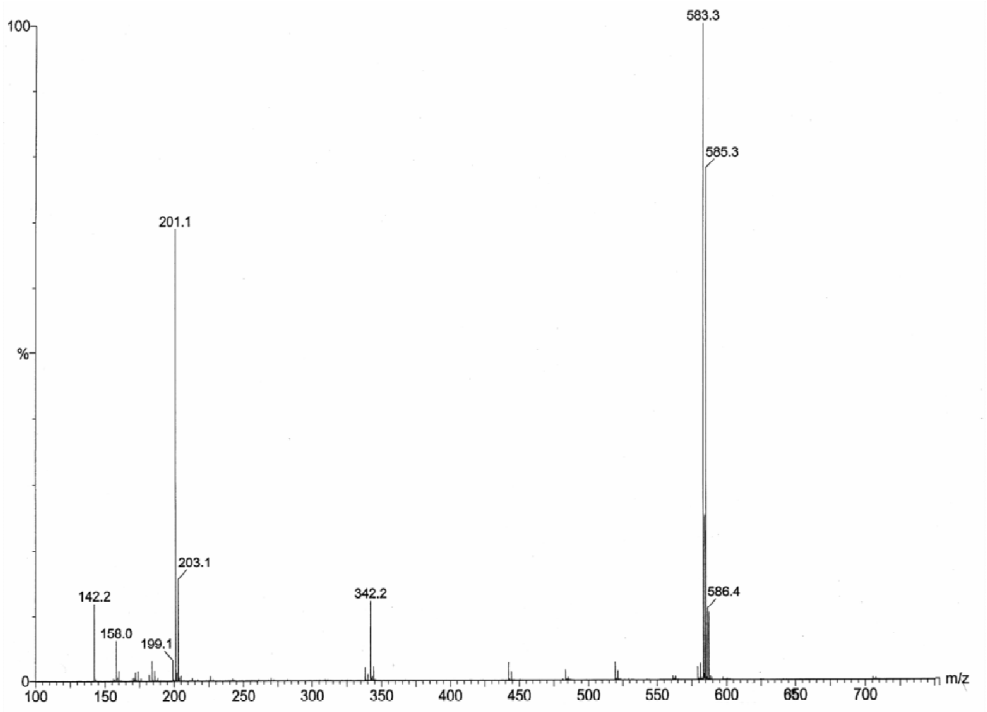

Figure 72. ESI mass spectra of the $[NiL^3](ClO_4)_2$ **(4)**.

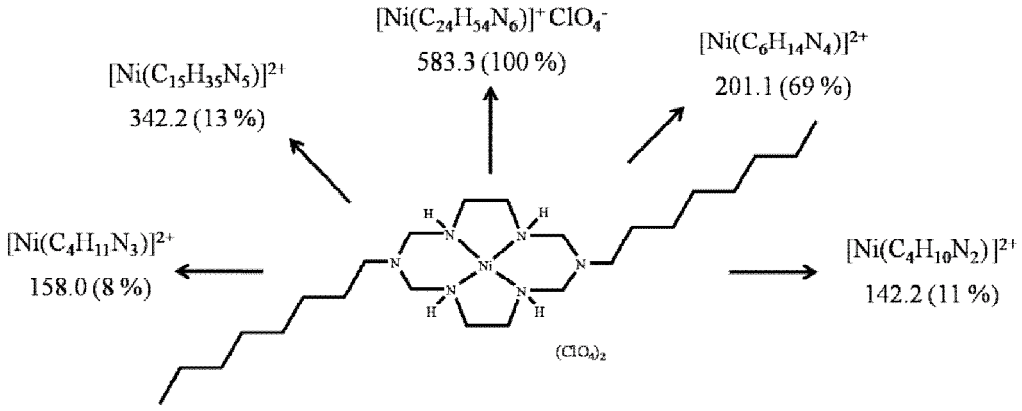

Figure 73. Fragmentation patterns of the $[NiL^3](ClO_4)_2$ **(4)**.

The mass spectrum of the complex **(5)** showed molecular ion peak at m/z = 618.3 (100 %) corresponding to the $[Cu(C_{26}H_{58}N_6)(ClO_4)\text{-}H]^+$ as shown in **Figure 74**. Other fragments of the complex gave peaks with various intensities at different *m/z* values as shown in **Figure 75**. The mass spectral data of complex agreed with the formula of the complex with crystal structure received from X-ray crystallography.

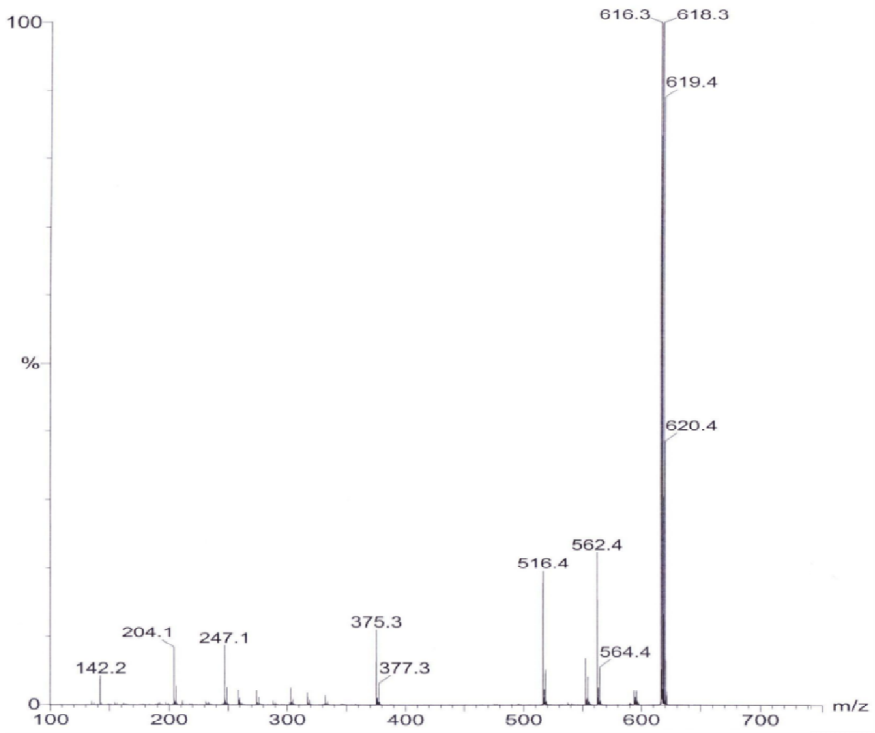

Figure 74. ESI mass spectra of the $[CuL^4(ClO_4)_2]$ **(5)**.

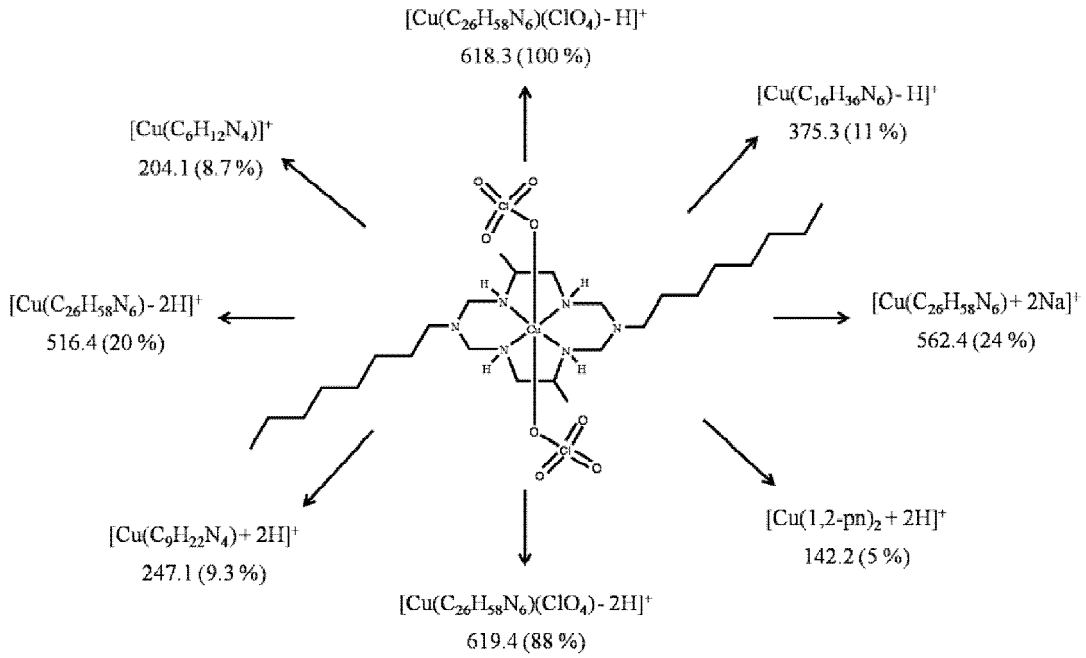

Figure 75. Fragmentation patterns of the $[CuL^4(ClO_4)_2]$ **(5)**.

The mass spectrum of the complex **(6)** **(Figure 76)** showed its molecular ion peak at *m/z* 476.1 (100 %) corresponding to $[Cu(C_{16}H_{38}N_6)(ClO_4)]^+$. Other molecular ion peaks were also detected. The scheme as shown in **Figure 77** represents the proposed fragmentation pattern of the complex **(6)**.

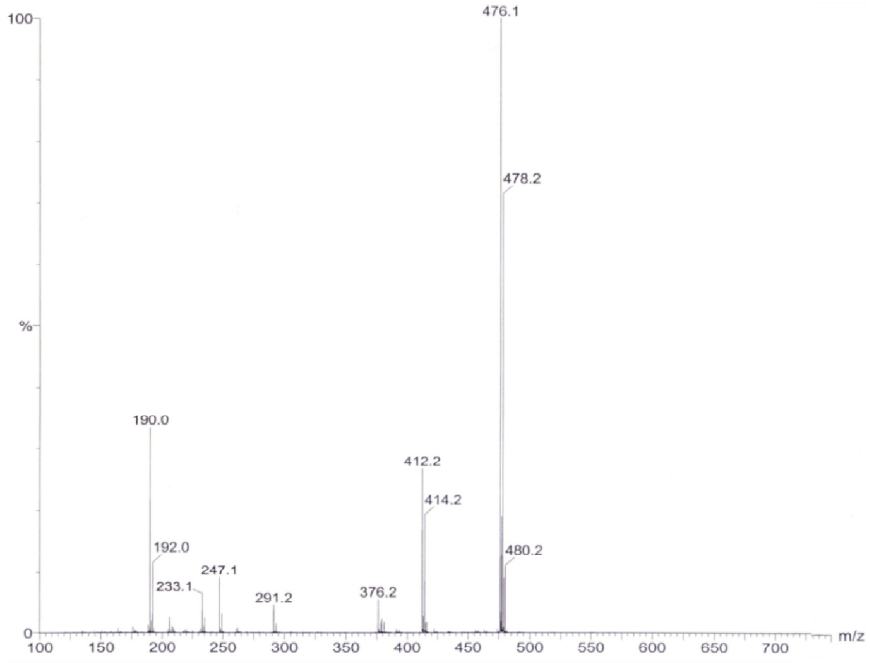

Figure 76. ESI mass spectra of the $[CuL^5(ClO_4)_2]$ **(6)**.

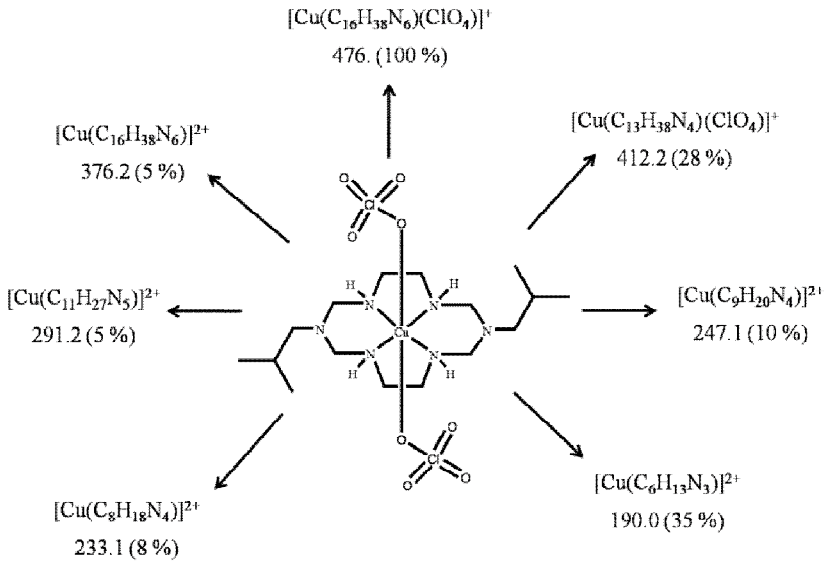

Figure 77. Fragmentation patterns of the $[CuL^5(ClO_4)_2]$ **(6)**.

In the mass spectrum **(Figure 78)** of the complex **(7)** the molecular ion peak was observed at *m/z* 471.2 (100 %) corresponding to $[Ni(C_{16}H_{38}N_6)]^+ ClO_4^-$. Other molecular ion peaks were also detected. The scheme as shown in **Figure 79** represents the proposed fragmentation pattern of the complex **(7)**. The mass spectral data of complex matched with the formula of the crystal structure from X-ray diffraction analysis.

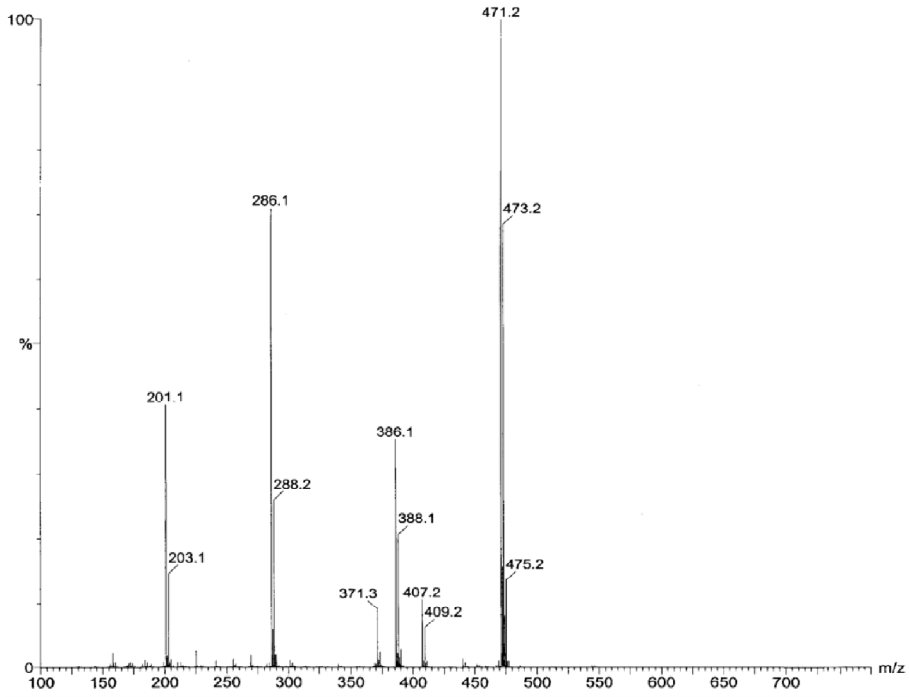

Figure 78. ESI mass spectra of the $[NiL^5](ClO_4)_2$ **(7)**.

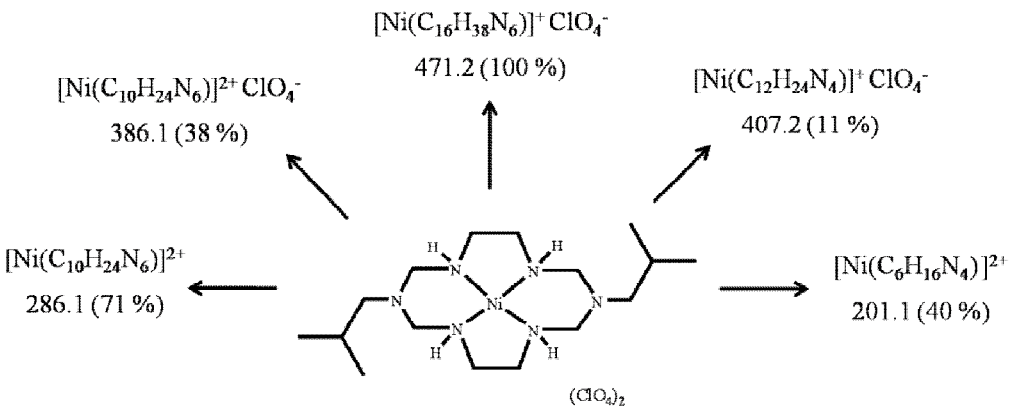

Figure 79. Fragmentation patterns of the $[NiL^5](ClO_4)_2$ **(7)**.

In **Figure 80** the mass spectrum of the complex **(8)** exhibited parent ion peak at *m/z* 504.2 (100 %) due to $[Cu(C_{18}H_{42}N_6)(ClO_4)]$. The release of C_4H_{14} radical gave the fragment ion peak shown at *m/z* 440.3 (15 %). Further, this molecular ion underwent dissociation by the loss of perchlorate ion and the $C_5H_6N_2$ molecule together giving a fragment ion peak at *m/z* 204.1 (11 %). This fragment ion on further cleavage of CH_3 radical gave a peak appeared at m/z 191.9 (9 %). The scheme as shown in **Figure 81** represents the proposed fragmentation pattern of the complex **(8)**. The mass spectral data of complex consistent with the crystal structure from X-ray diffraction data.

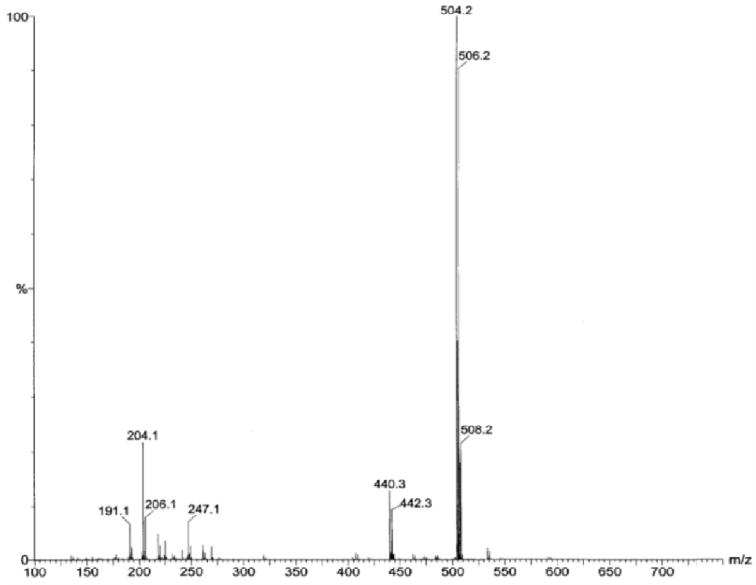

Figure 80. ESI mass spectra of $[CuL^6(ClO_4)_2]$ **(8)**.

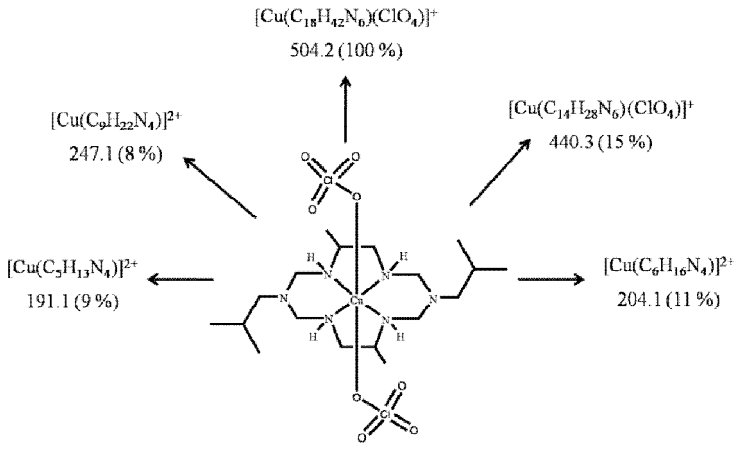

Figure 81. Fragmentation patterns of the $[CuL^6(ClO_4)_2]$ **(8)**.

The mass spectrum of the complex **(9) (Figure 82)** revealed a molecular ion peak at *m/z* 590.3 (100 %) attributed to $[Cu(C_{24}H_{54}N_6)(ClO_4)]^+$. Several peaks were also obtained, e.g., fragment ion peak at *m/z* 524.3 (40 %), 303.2 (9 %), 289.2 (8 %), 262.1 (4 %), and 190.0 (40 %). The scheme as shown in **Figure 83** represents the proposed fragmentation pattern of the complex **(9)**.

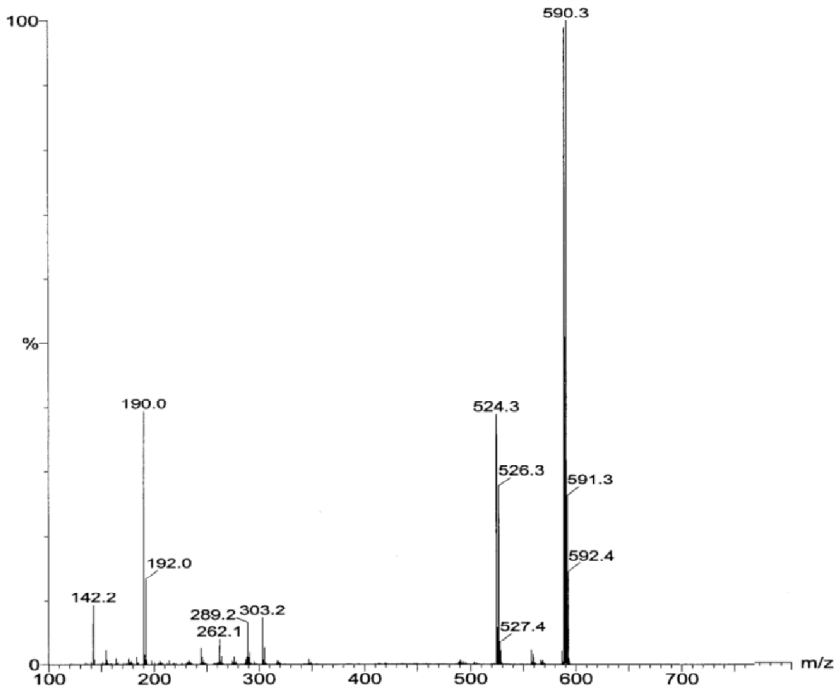

Figure 82. ESI mass spectra of $[CuL^7(ClO_4)_2]$ **(9)**.

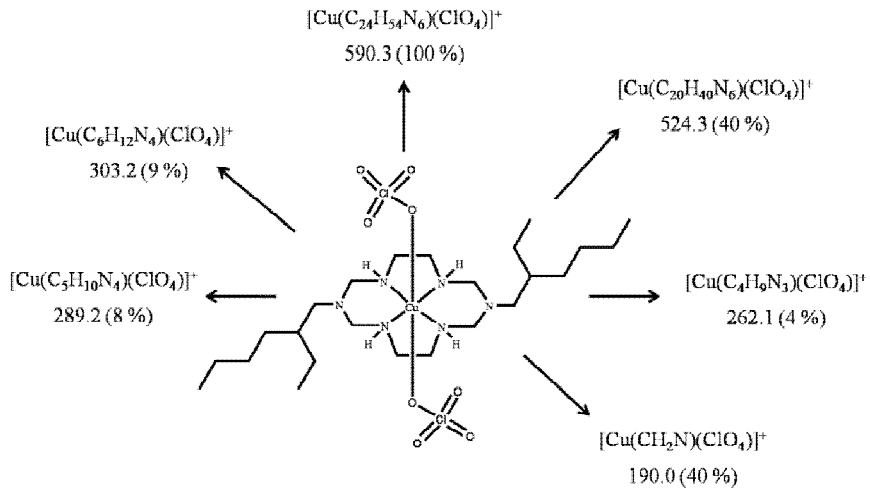

Figure 83. Fragmentation patterns of the $[CuL^7(ClO_4)_2]$ **(9)**.

The mass spectrum **(Figure 84)** of the complex **(10)** showed a molecular ion peak at *m/z* 583.3 (100 %) corresponding to $[Ni(C_{24}H_{54}N_6)]^+ ClO_4^-$. Other peaks were also observed in dissociation peak at m/z 552.3 (12 %), 519.4 (4 %), 483.4 (5 %), 342.2 (15 %), 201.1 (59 %), and 142.2 (4 %), which were consistent with the fragmentation and confirmation the identity of the proposed structure **(Figure 85)**.

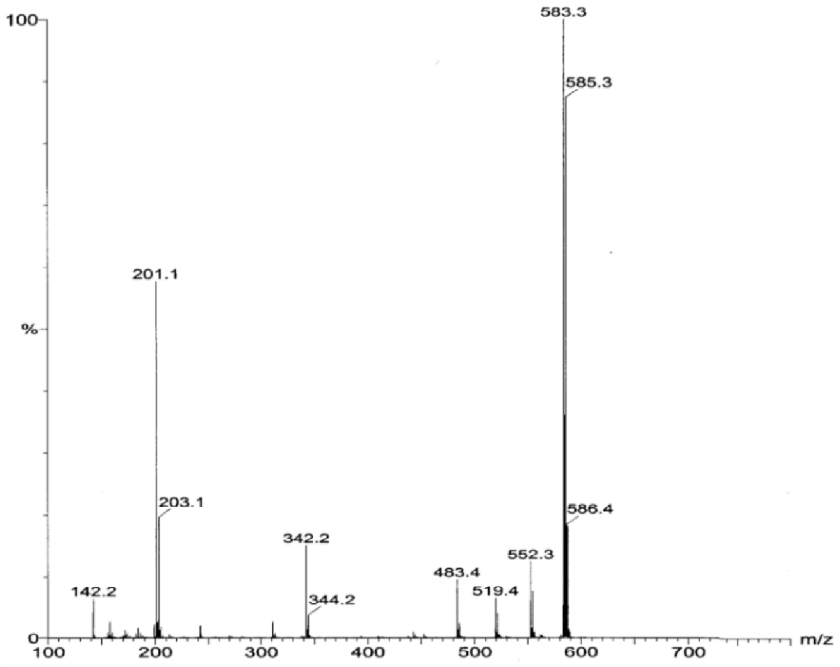

Figure 84. ESI mass spectra of $[NiL^7](ClO_4)_2$ **(10)**.

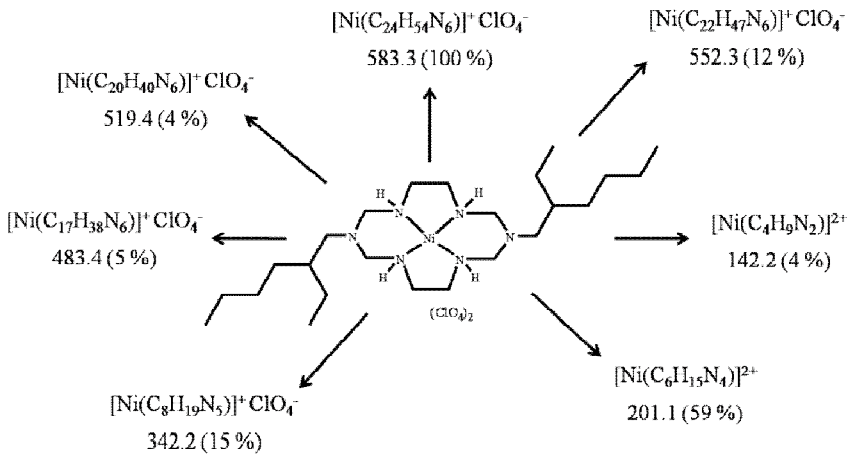

Figure 85. Fragmentation patterns of the $[NiL^7](ClO_4)_2$ **(10)**.

The mass spectrum **(Figure 86)** of the complex **(11)** showed a parent ion peak at *m/z* 616.4 (100 %) and was assigned to $[Cu(C_{26}H_{58}N_6)(ClO_4)]^+$. The fragment ion peak at m/z 562.5 (3 %) corresponding to $[Cu(C_{22}H_{50}N_6)(ClO_4)]^+$. The scheme as shown in **Figure 87** represents the proposed fragmentation pattern of the complex **(11)**.

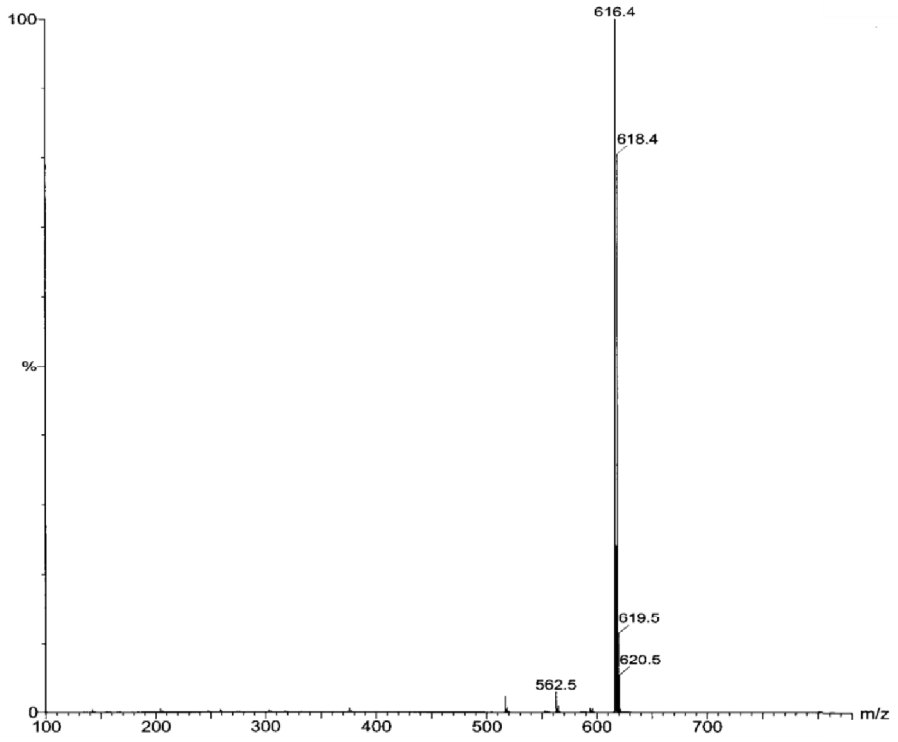

Figure 86. ESI mass spectra of the $[CuL^8(ClO_4)_2]$ **(11)**.

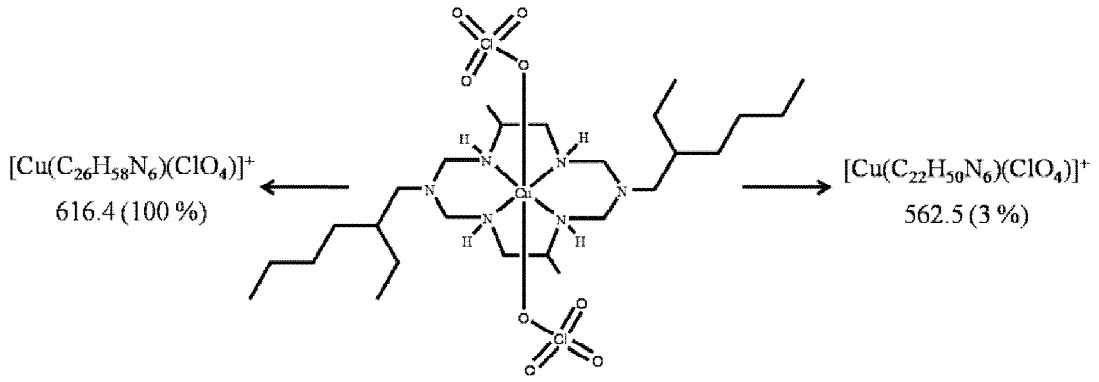

Figure 87. Fragmentation patterns of the $[CuL^8(ClO_4)_2]$ **(11)**.

3.6 Powder X-ray diffraction studies

The purity of the synthesized complexes **(5)**, **(7)**, **(8)**, **(12)**, **(13)**, **(14)**, and **(15)** were checked by powder X-ray diffraction technique. In the case of the complex **(6)**, attempt to obtain single crystal by recrystallization was unsuccessful, so the data of single crystal of complex **(7)** was used instead as both complexes have similar structure. The resulting PXRD patterns are shown in **Figures 88-95**. The as-synthesized PXRD patterns of the bulk powder of the complexes (black) were in good agreement with the simulated PXRD pattern derived from the single crystal X-ray data by Mercury 3.8 program (red) confirming phase purity of the bulk samples.

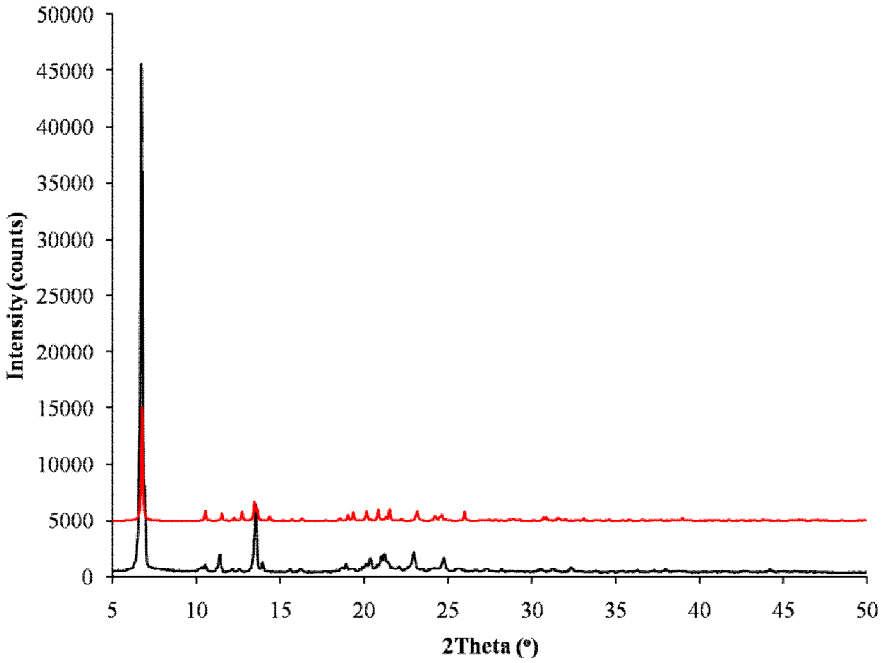

Figure 88. The PXRD pattern of $[CuL^4(ClO_4)_2]$ **(5)**.

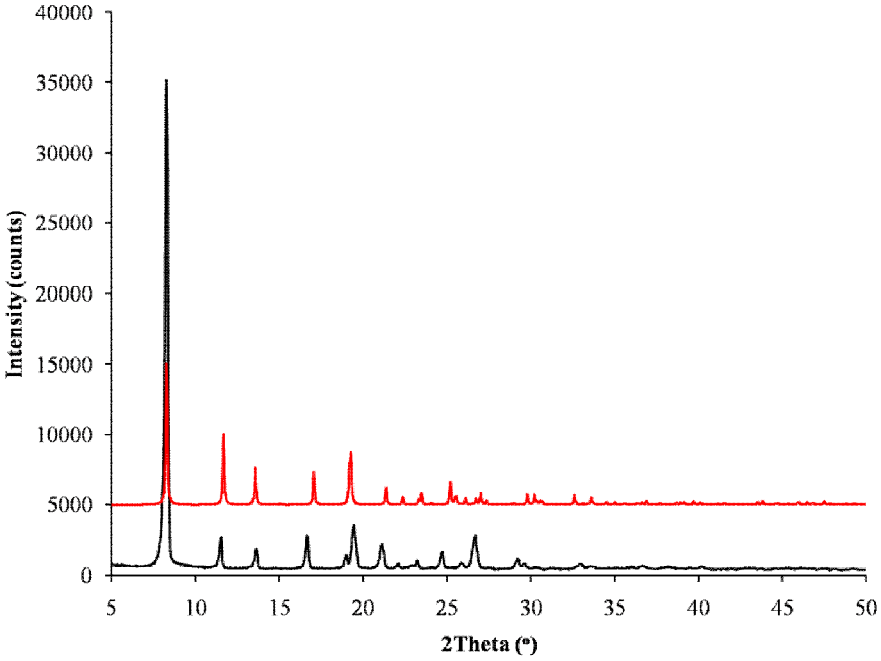

Figure 89. The PXRD pattern of $[CuL^5(ClO_4)_2]$ **(6)**.

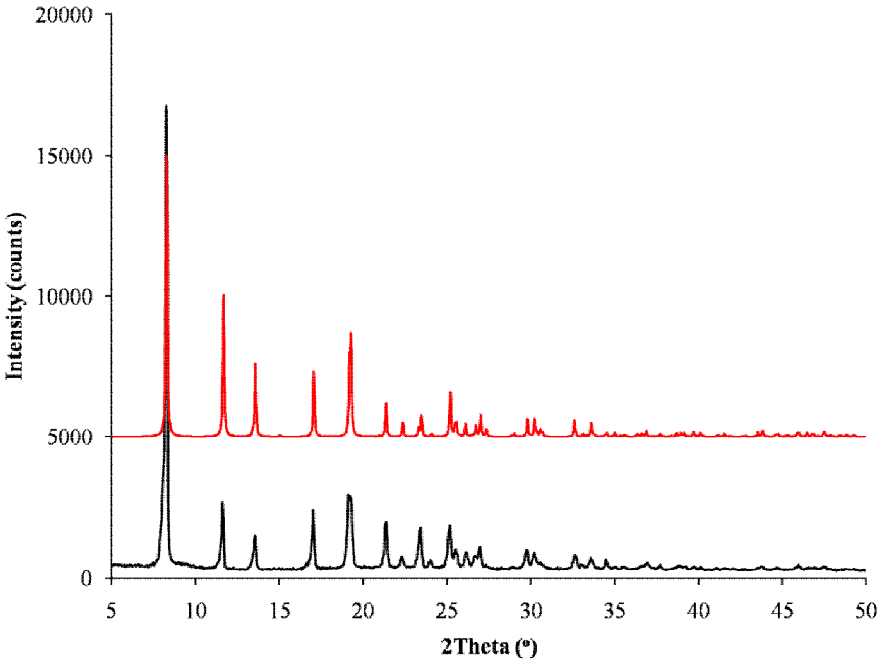

Figure 90. The PXRD pattern of $[NiL^5](ClO_4)_2$ **(7)**.

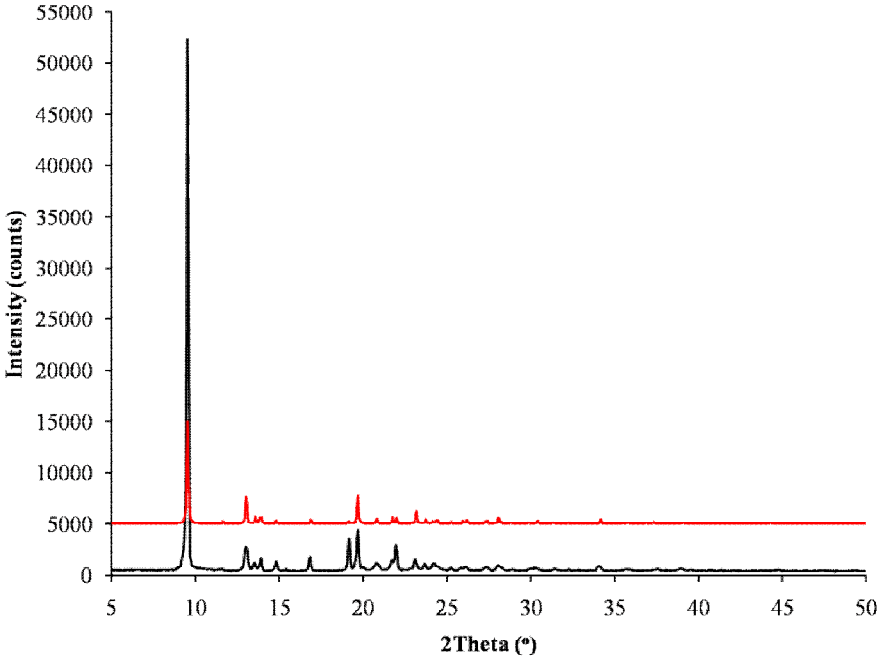

Figure 91. The PXRD pattern of $[CuL^{6}(ClO_4)_2]$ **(8)**.

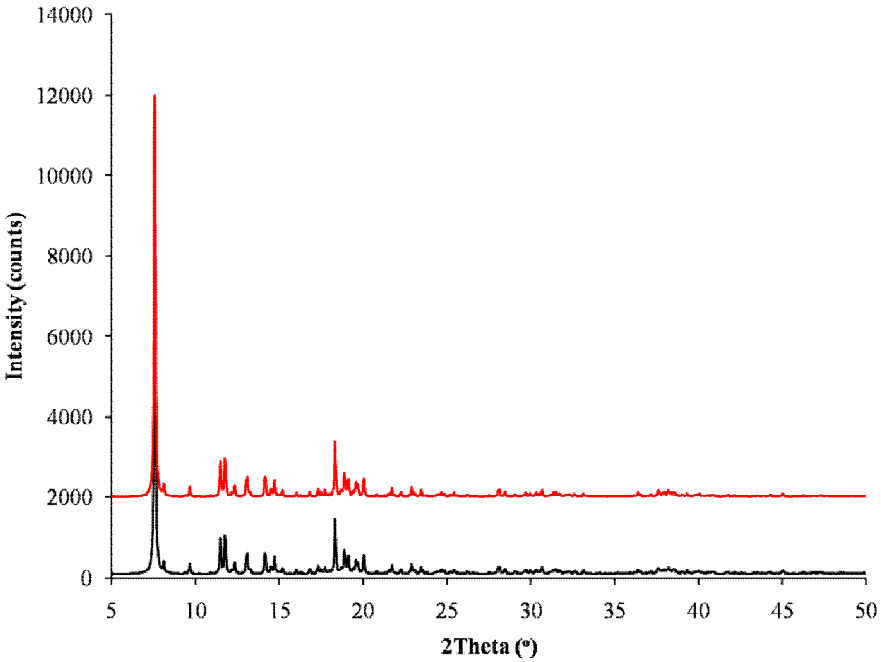

Figure 92. The PXRD pattern of $[CuL^{5}]_3[Fe(CN)_6]_2 \cdot 5H_2O$ **(12)**.

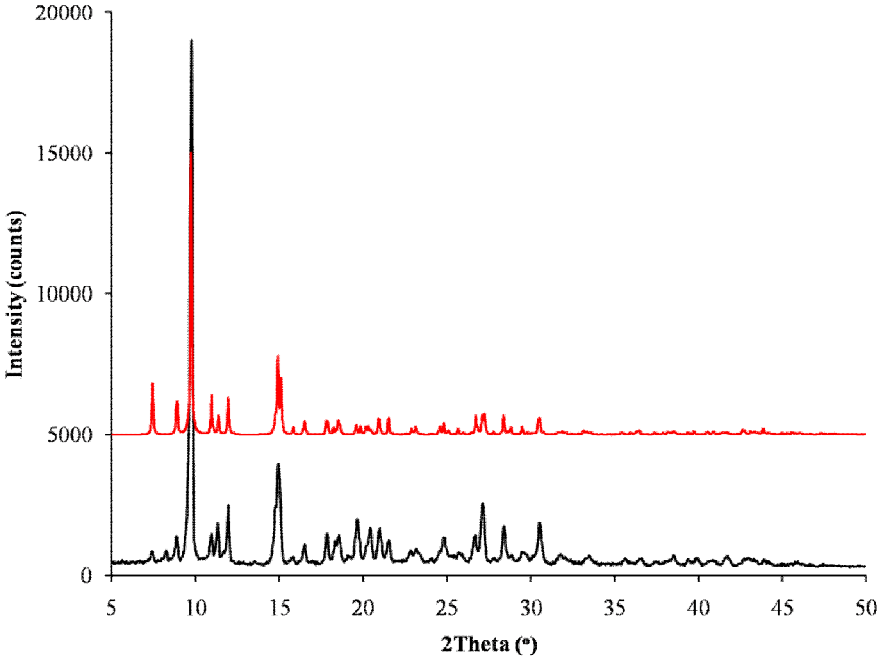

Figure 93. The PXRD pattern of $[NiL^5(4\text{-nba})_2]\cdot H_2O$ **(13)**.

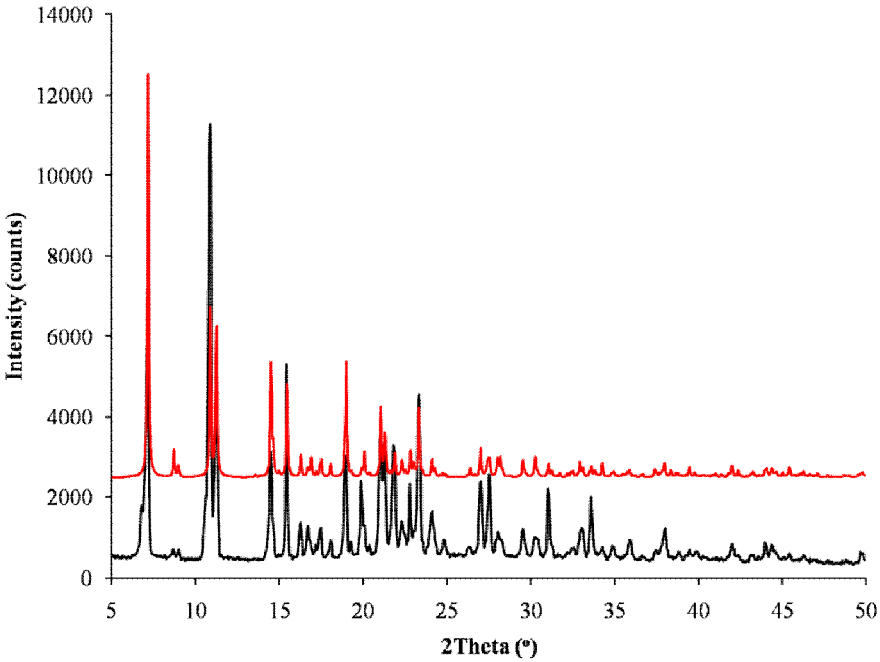

Figure 94. The PXRD pattern of $[NiL^3(4\text{-nba})_2]$ **(14)**.

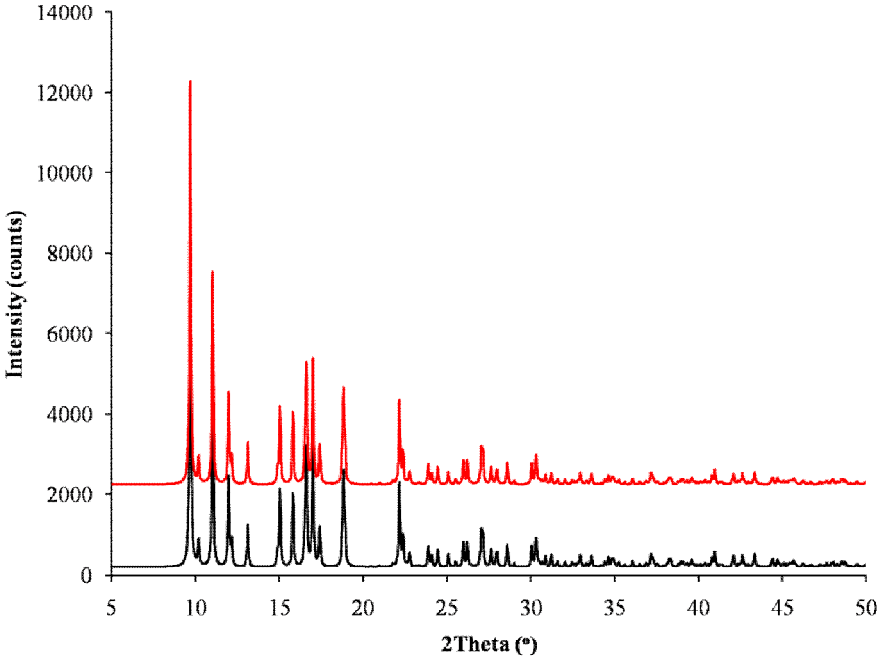

Figure 95. The PXRD pattern of $[NiL^5(sal)_2]$ **(15)**.

3.7 X-ray crystallography

3.7.1 Crystal structure description of the $[CuL^4(ClO_4)_2]$ (5)

The crystallographic data and the result of refinement parameters observed from single crystal X-ray diffraction analysis of the complex **(5)** is summarized in **Table 6** with the selected bond distances and bond angles are listed in **Tables 7** and **8**, respectively. Complex **(5)** crystallized in the triclinic $P\bar{1}$ space group with one formula unit per unit cell **(Figure 97)** and the asymmetric unit of the complex **(5)** composed of one $[CuL^4]^{2+}$ cation and two perchlorate anions as depicted in **Figure 96**. Copper(II) atom in the asymmetric unit located in the crystallographic $\bar{1}$ inversion center and coordinated to four secondary amines nitrogen atoms of the hexaazamacrocyclic ligand [Cu(1)-N(1) = 2.002(3) Å, Cu(1)-N(1)#1 = 2.002(3) Å, Cu(1)-N(2) = 2.013(3) Å, and Cu(1)-N(2)#1 = 2.013(3) Å] at the equatorial positions and two oxygen atoms of perchlorate anions at the axial position [Cu(1)-O(3) = 2.592(3) Å and Cu(1)-O(3)#1 = 2.592(3) Å]. The Cu-O bonds were significantly

longer than those to the nitrogen atoms in the equatorial positions, however, slightly shorter than Cu-O distances in $[CuL^{R,R}(ClO_4)_2$ and $[CuL^{S,S}(ClO_4)_2$ at 2.639(7) Å and 2.610(7) Å, respectively ($L^{R,R/S,S}$ = 1,8-di((*R/S*-α-methylbenzyl)-1,3,6,8,10,13-hexaazacyclotetradecane) (Shin *et al*., 2012). The geometry around copper(II) ion was explained as an elongated octahedron in the z-axis due to the Jahn-Teller distortion.

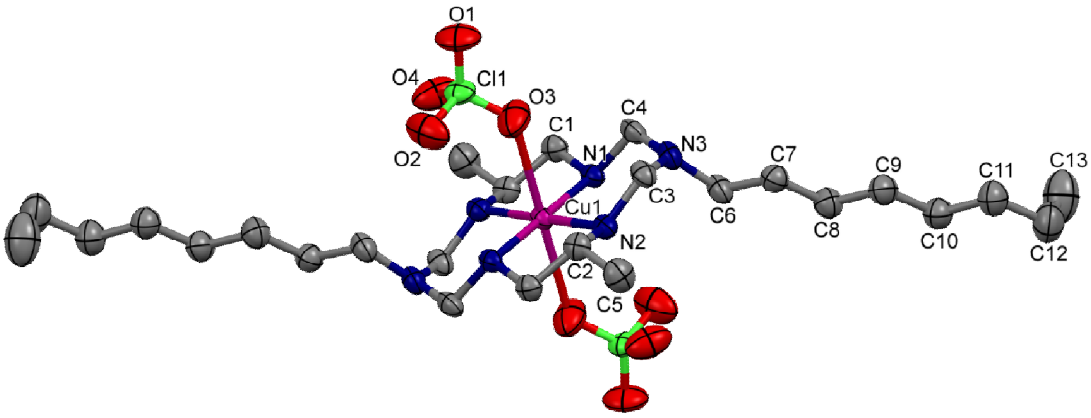

Figure 96. The crystal structure of the $[CuL^4(ClO_4)_2]$ **(5)**, along with atomic numbering scheme (H atoms omitted for clarity).

The six-membered chelate rings relating with the C(3) and C(4) atoms adopted a chair conformation with the chelate angles N(1)-Cu(1)-N(2) = 94.14(13)°. In contrast, the five-membered chelate rings involving the C(1) and C(2) atoms adopted a gauche conformation with the chelate angles N(1)-Cu(1)-N(2)#1 = 85.86(13)°. The C(3)-N(3) and C(4)-N(3) bond distances were 1.512(5) Å and 1.400(5) Å, respectively. The average C(3)-N(3)-C(4) bond angle involving the tertiary nitrogen atom N(3) was 116.8(3)° which revealed a significant proportion of sp^2 hybridization for the nitrogen atom. The ClO_4^- anions at Cl(1) showed a rather distorted tetrahedron. The Cl-O distances different from 1.376(4) to 1.433(4) Å while bond angles varied from 101.1(3) to 116.6(3)° were similar to those reported in the literatures (Husain *et al*., 2011 and Beltrán *et al*., 1999).

The mononuclear structure of complex **(5)** exhibited intramolecular the N-H···O hydrogen bonding interactions between the secondary amines of the hexaazamacrocycle and the oxygen atoms of perchlorate anions to form an infinite

one-dimensional chain along *c* axis as shown in **Figure 98**. The hydrogen bonding interaction parameters are given in **Table 9**.

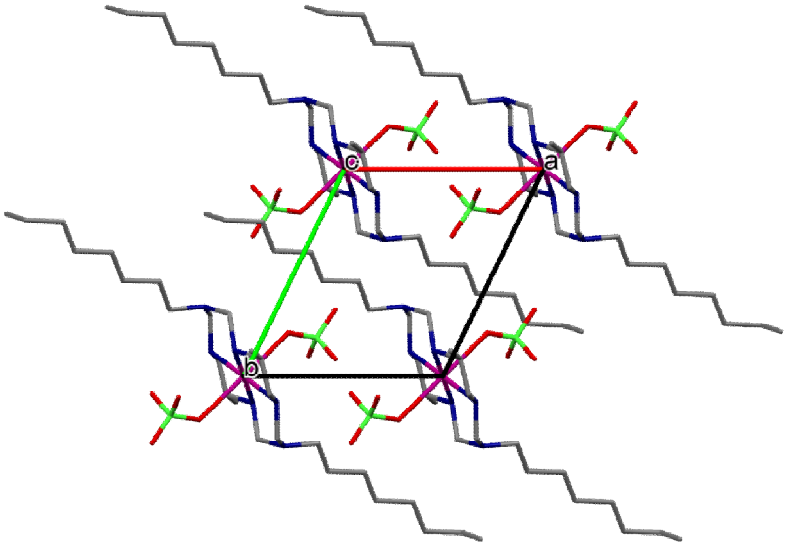

Figure 97. View of the unit cell packing of the $[CuL^4(ClO_4)_2]$ **(5)**, plotted down *c* axis.

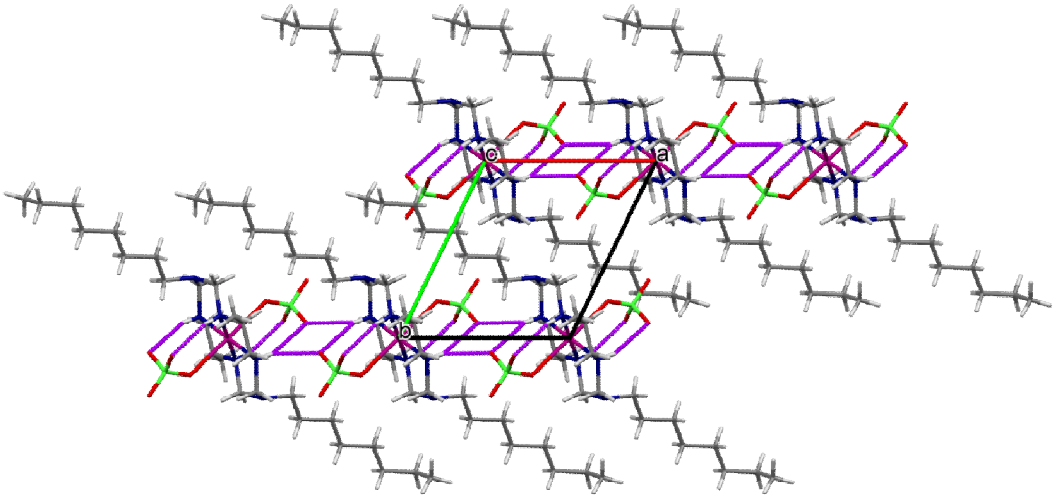

Figure 98. One-dimensional hydrogen bonding interaction of the $[CuL^4(ClO_4)_2]$ **(5)**, plotted down *c* axis (shown as *dashed lines*).

Table 6. Crystallographic data and structure refinement of **(5)**.

Identification code	$[CuL^4(ClO_4)_2]$ **(5)**	
Empirical formula	$C_{26}H_{58}Cl_2CuN_6O_8$	
Formula weight	717.22	
Temperature	296.2 K	
Wavelength	0.71073 Å	
Crystal system	Triclinic	
Space group	$P\bar{1}$	
Unit cell dimensions	a = 8.1307(6) Å	α = 95.932(2)°
	b = 9.3579(7) Å	β = 98.579(2)°
	c = 13.3930(10) Å	γ = 114.478(2)°
Volume	901.48(12) Å^3	
Z	1	
Density (Calculated)	1.321 Mg/m^3	
Absorption coefficient	0.804 mm^{-1}	
F(000)	383	
Crystal size	0.335 x 0.107 x 0.071 mm^3	
θ range for data collection	1.564 to 24.997°	
Index ranges	$-9 \leq h \leq 9$, $-11 \leq k \leq 11$, $-15 \leq l \leq 15$	
Reflection collected	9637	
Independent reflections	3185 [R_{int} = 0.0308]	
Completeness to θ	100 % (θ = 24.997°)	
Absorption correction	Semi-empirical from equivalents	
Refinement method	Full-matrix least-squares on F^2	
Data / restraints / parameters	3185 / 2 / 204	
Goodness-of-fit on F^2	1.042	
Final R indices [$I > 2\sigma(I)$]	R_1 = 0.0559, wR_2 = 0.1459	
R indices (all data)	R_1 = 0.0681, wR_2 = 0.1561	
Largest diff. peak and hole	0.568 and -0.381 e.Å^{-3}	

Table 7. Selected bond distances (Å) of **(5)**.

Cu(1)-N(1)	2.002(3)	Cu(1)-N(1)#1	2.002(3)
Cu(1)-N(2)	2.013(3)	Cu(1)-N(2)#1	2.013(3)
N(1)-C(1)	1.461(5)	N(1)-C(4)	1.521(5)
N(2)-C(2)	1.488(5)	N(2)-C(3)	1.512(5)
N(3)-C(4)	1.400(5)	N(3)-C(3)	1.419(5)
Cl(1)-O(1)	1.376(4)	Cl(1)-O(2)	1.433(4)
Cl(1)-O(3)	1.385(4)	Cl(1)-O(4)	1.408(4)

Symmetry transformations used to generate equivalent atoms: #1 -x+2, -y+2, -z+1

Table 8. Selected bond angles (^{o}) of **(5)**.

N(1)-Cu(1)-N(1)#1	180.0	N(2)-Cu(1)-N(2)#1	180.00(10)
N(1)-Cu(1)-N(2)	94.14(13)	N(1)#1-Cu(1)-N(2)#1	94.14(13)
N(1)-Cu(1)-N(2)#1	85.86(13)	N(1)#1-Cu(1)-N(2)	85.86(13)
C(4)-N(3)-C(3)	116.8(3)	C(3)-N(3)-C(6)	117.7(4)
C(2)-N(2)-C(3)	113.8(3)	C(2)-N(2)-Cu(1)	107.8(2)
O(3)-Cl(1)-O(2)	101.1(3)	O(1)-Cl(1)-O(3)	116.6(3)

Symmetry transformations used to generate equivalent atoms: #1 -x+2, -y+2, -z+1

Table 9. Hydrogen bonds (Å and ^{o}) of **(5)**.

D-H···A	d(D-H)	d(H···A)	d(D···A)	<(DHA)
C(3)-H(3B)...O(3)#1	0.97	2.64	3.274(6)	122.8
C(4)-H(4A)...O(3)#1	0.97	2.58	3.232(6)	124.6
N(1)-H(1)···O(2)	0.851(19)	2.59(3)	3.369(6)	153(4)
N(1)-H(1)···O(2)#2	0.851(19)	2.41(3)	3.099(5)	138(4)
N(2)-H(2)...Cl(1)	0.852(18)	2.99(3)	3.686(3)	140(3)
N(2)-H(2)...O(4)	0.852(18)	2.25(2)	3.078(5)	164(4)

Symmetry transformations used to generate equivalent atoms: #1 -x+2,-y+2,-z+1
#2 -x+1,-y+2,-z+1

3.7.2 Crystal structure description of the $[NiL^5](ClO_4)_2$ (7)

The crystallographic data and the result of refinement parameters observed from single crystal X-ray diffraction analysis of the complex **(7)** is summarized in **Table 10** with the selected bond distances, and bond angles are listed in **Tables 11** and **12**, respectively. Complex **(7)** crystallized in the monoclinic *C*2/*m* space group with one formula unit per unit cell **(Figure 99)** and the asymmetric unit of the complex **(7)** composed of one $[NiL^5]^{2+}$ cation and two perchlorate counter anions as illustrated in **Figure 100**. One nickel(II) atom coordinated with four secondary amines nitrogen atoms of the hexaazamacrocyclic ligand occupying the equatorial position. The average Ni–N bond lengths were close to that of 1.936 Å which was the square-planar hexaazamacrocyclic nickel(II) complex, but slightly shorter than that of 2.0-2.1 Å which was six-coordinated macrocyclic nickel(II) polymer (Lu *et al*., 2003). Two oxygen atoms from the perchlorate anions at the axial sites and the distances between Ni(1) and O(1) atoms was 2.960(8) Å which was longer than the average Ni-O bond distance of the hexaazamacrocyclic nickel(II) with carboxylate ligands (Kim *et al*., 2006 and Park *et al*., 2015). The result showed that there was no coordination bond between the nickel(II) ion and the perchlorate anions.

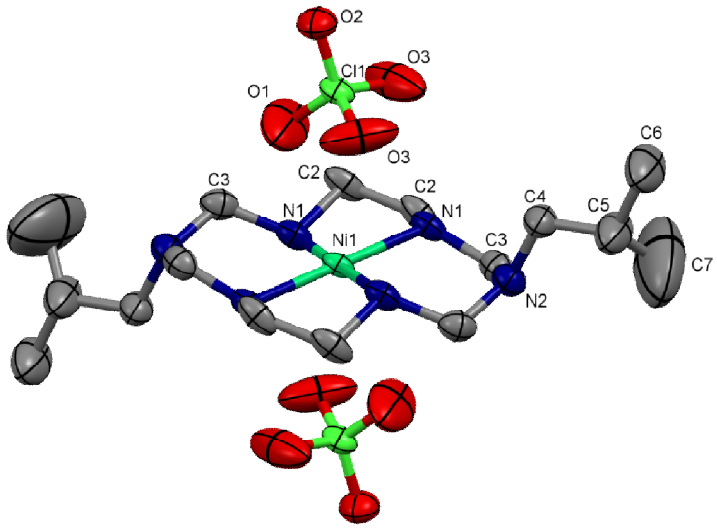

Figure 99. The crystal structure of the $[NiL^5](ClO_4)_2$ **(7)**, along with atomic numbering scheme (H atoms omitted for clarity).

The six-membered chelate rings relating with the C(3) and C(3)#3 atoms adopted a chair conformation and the chelate angles N(1)#1-Ni(1)-N(1)#2 = 92.53(16)°. In contrast, the five-membered chelate rings involving the C(2) and C(2) #1 atoms adopted a gauche conformation and the chelate angles N(1)-Ni(1)-N(1)#1 = 87.47(16)°. The C(3)-N(2) and C(3)#3-N(2) bond distances were 1.414(5) Å and the average C(3)-N(2)-C(3)#3 bond angle involving the tertiary nitrogen atom N(3) was 114.5(4)°, which revealed significant proportion of sp^2 hybridization for the nitrogen atom. The ClO_4^- anions at Cl(1) showed a rather distorted tetrahedron. The Cl-O distances varied from 1.341(6) to 1.411(4) Å while bond angles from 107.1(6) to 115.8(4)° which were similar to those reported in the literatures (Husain *et al.*, 2011 and Beltrán *et al.*, 1999).

Analysis of the crystal packing showed that mononuclear units were held together by intermolecular hydrogen bonds involving the N(1)#1-H(1)#1···O(3)#1 and N(1)#2-H(1)#2···O(3)#2 with *d*(D···A) = 3.157 Å, *d*(H···A) = 2.313 Å, ∠(D-H···A) = 154.35° to form an infinite one-dimensional chain along *b* axis as shown in **Figure 101**.

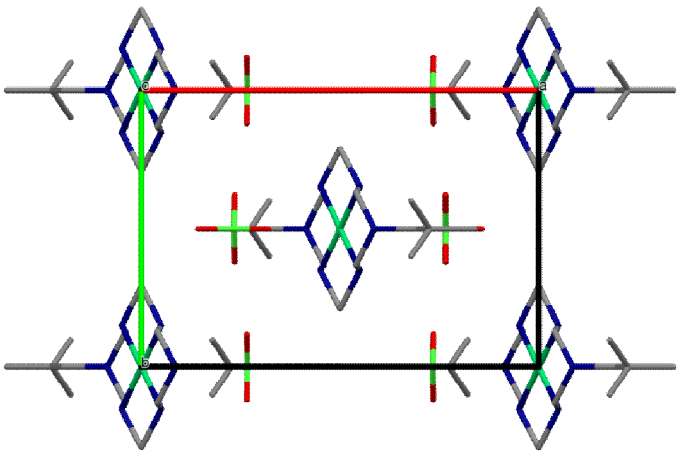

Figure 100. View of the unit cell packing of $[NiL^5](ClO_4)_2$ **(7)**, plotted down *c* axis.

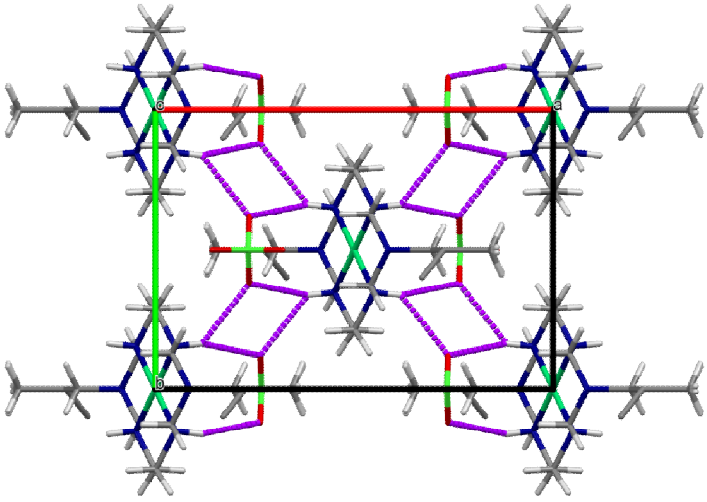

Figure 101. One-dimensional hydrogen bonding interaction of $[NiL^5](ClO_4)_2$ **(7)**, plotted down *b* axis (shown as *dashed lines*).

Table 10. Crystallographic data and structure refinement of **(7)**.

Identification code	$[NiL^5](ClO_4)_2$ **(7)**	
Empirical formula	$C_{16}H_{38}Cl_2NiN_6O_8$	
Formula weight	571.15	
Temperature	273.2 K	
Wavelength	0.71073 Å	
Crystal system	Monoclinic	
Space group	*C*2/*m*	
Unit cell dimensions	a = 13.4278(6) Å	$\alpha = 90.^{o}$
	b = 9.2421(4) Å	$\beta = 100.8420(10)^{o}$
	c = 10.8592(5) Å	$\gamma = 90^{o}$
Volume	1323.58(10) $Å^3$	
Z	2	
Density (Calculated)	1.496 Mg/m^3	
Absorption coefficient	0.987 mm^{-1}	
F(000)	628	
Crystal size	0.25 x 0.21 x 0.21 mm^3	

Table 10 (continued). Crystallographic data and structure refinement of **(7)**.

θ range for data collection	3.09 to 26.73°
Index ranges	$-16 \leq h \leq 16$, $-11 \leq k \leq 11$, $-13 \leq l \leq 13$
Reflection collected	17433
Independent reflections	1495 [$R_{int} = 0.0220$]
Completeness to θ	99.8 % ($\theta = 26.73°$)
Absorption correction	Semi-empirical from equivalents
Refinement method	Full-matrix least-squares on F^2
Data / restraints / parameters	1495 / 0 / 93
Goodness-of-fit on F^2	1.070
Final R indices [$I > 2\sigma(I)$]	$R_1 = 0.0541$, $wR_2 = 0.1687$
R indices (all data)	$R_1 = 0.0575$, $wR_2 = 0.1723$
Largest diff. peak and hole	0.85 and -0.44 e.Å^{-3}

Table 11. Selected bond distances (Å) of **(7)**.

Ni(1)-N(1)	1.936(3)	Ni(1)-N(1)#1	1.936(3)
Ni(1)-N(1)#2	1.936(3)	Ni(1)-N(1)#3	1.936(3)
N(1)-C(2)	1.485(4)	N(1)-C(3)	1.491(5)
N(1)-C(3)	1.491(5)	N(2)-C(3)#3	1.414(5)
N(2)-C(4)	1.466(7)	C(4)-C(5)	1.425(10)

Symmetry transformations used to generate equivalent atoms: #1 1-x,+y,1-z, #2 1-x,1-y,1-z, #3 +x,1-y,+z

Table 12. Selected bond angles (°) of **(7)**.

N(1)#1-Ni(1)-N(1)#2	92.53(16)	N(1)#1-Ni(1)-N(1)#3	180.0
N(1)-Ni(1)-N(1)#1	87.47(16)	N(1)#3-Ni(1)-O(1)	85.13(12)
N(1)#2-Ni(1)-O(1)	94.87(12)	C(2)-N(1)-Ni(1)	107.3(2)
C(3)-N(2)-C(3)#3	114.5(4)	N(2)-C(3)-N(1)	114.3(3)
N(1)-C(2)-C(2)#1	106.7(3)	C(5)-C(4)-N(2)	114.6(5)

Symmetry transformations used to generate equivalent atoms: #1 1-x,+y,1-z, #2 1-x,1-y,1-z, #3 +x,1-y,+z

3.7.3 Crystal structure description of the $[CuL^6(ClO_4)_2]$ (8)

The crystallographic data and the results of refinement parameters observed from single crystal X-ray diffraction analysis of the complex **(8)** is summarized in **Table 13** with the selected bond distances, and bond angles are listed in **Table 14** and **15**, respectively. Complex **(8)** crystallized in the monoclinic $P2_1/n$ space group with one formula unit per unit cell **(Figure 103)** and the asymmetric unit of the complex **(8)** composed of one $[CuL^6]^{2+}$ cation and two perchlorate anions as shown in **Figure 102**. The copper(II) atom was (N_4 + O_2) coordinated with four secondary amines nitrogen atoms of the hexaazamacrocyclic ligand [Cu(1)-N(1) = 1.989(5) Å, Cu(1)-N(1)#1 = 1.989(5) Å, Cu(1)-N(2) = 2.028(4) Å, and Cu(1)-N(2)#1 = 2.028(4) Å] occupying the equatorial position and two oxygen atoms of perchlorate anions at the axial position [Cu(1)-O(1) = 2.575(5) Å and Cu(1)-O(1)#1 = 2.575(5) Å]. The Cu-O distance significantly longer than the Cu-N distances in the equatorial position, but slightly shorter than Cu-O distances in $[CuL(ClO_4)_2]$ at 2.651 Å, where L = 3,10-bis(benzyl)1,3,5,8,10,12-hexaazacyclotetradecane (Husain *et al.*, 2012). The geometry around copper(II) ion was explained as an elongated distorted octahedron in the z-axis due to the Jahn-Teller distortion.

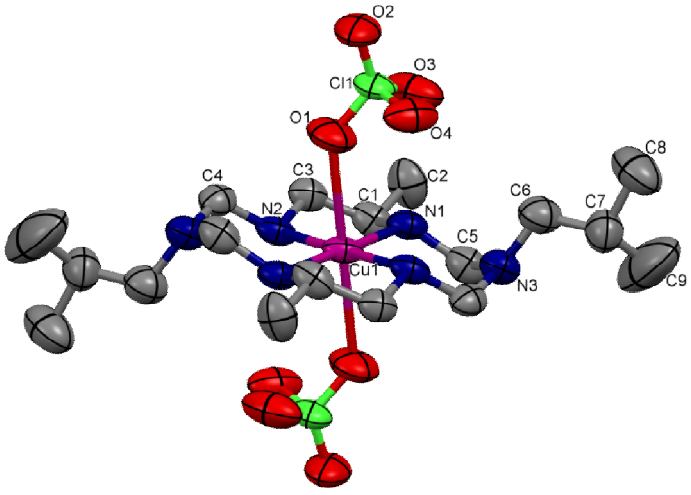

Figure 102. The crystal structure of the $[CuL^6(ClO_4)_2]$ **(8)**, along with atomic numbering scheme (H atoms omitted for clarity).

The six-membered chelate rings relating with the C(4) and C(5) atoms adopted a chair conformation and the chelate angles N(1)-Cu(1)-N(2) = 93.1(2)°. In contrast, the five-membered chelate rings involving the C(1) and C(3) atoms adopted a gauche conformation and the chelate angles N(1)#1-Cu(1)-N(2) = 86.9(2)°. The C(4)-N(3) and C(5)-N(3) bond distances were 1.409(9) Å and 1.431(10) Å, respectively and the average C(4)-N(3)-C(5) bond angle involving the tertiary nitrogen atom N(3) was 114.7(6)°, which revealed significant proportion of sp^2 hybridization for the nitrogen atom. The ClO_4^- anions at Cl(1) showed a rather distorted tetrahedron. The Cl-O distances varied from 1.355(5) to 1.394(19) Å while bond angles from 101.1(3) to 116.6(3)°. Those values were similar to those reported in the literatures (Husain *et al*., 2011 and Beltrán *et al*., 1999).

Analysis of the crystal packing showed that mononuclear units were held together by intermolecular hydrogen bonds involving the N(1)-H(1)···O(3) with *d*(D···A) = 3.042 Å, *d*(H···A) = 2.185 Å, ∠(D-H···A) = 156.69° and N(2)-H(2)···O(4) with *d*(D···A) = 3.288 Å, *d*(H···A) = 2.454 Å, ∠(D-H···A) = 152.55° to form an infinite one-dimensional chain.

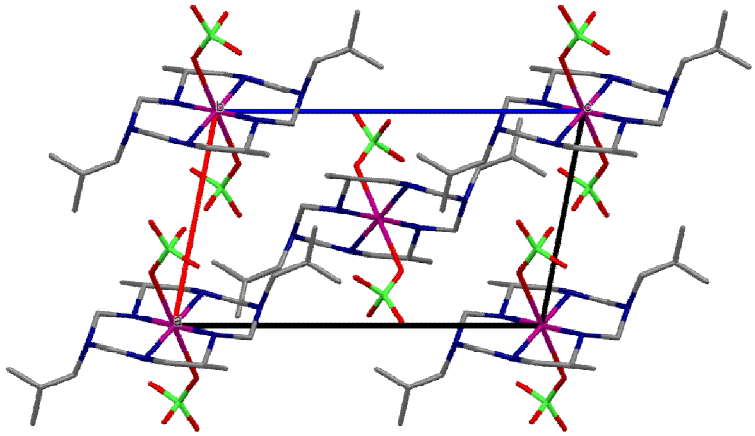

Figure 103. View of the unit cell packing of $[CuL^6(ClO_4)_2]$ **(8)**, plotted down *b* axis.

Table 13. Crystallographic data and structure refinement of **(8)**.

Identification code	$[CuL^6(ClO_4)_2]$ **(8)**	
Empirical formula	$C_{18}H_{42}Cl_2CuN_6O_8$	
Formula weight	605.02	
Temperature	273.2 K	
Wavelength	0.71073 Å	
Crystal system	Monoclinic	
Space group	$P2_1/n$	
Unit cell dimensions	a = 8.1991(3) Å	$\alpha = 90^o$
	b = 12.6880(5) Å	$\beta = 101.132(1)^o$
	c = 13.8100(7) Å	$\gamma = 90^o$
Volume	1409.63(10) $Å^3$	
Z	2	
Density (Calculated)	1.425 Mg/m^3	
Absorption coefficient	1.014 mm^{-1}	
$F(000)$	639.5	
Crystal size	0.30 x 0.25 x 0.20 mm^3	
θ range for data collection	3 to 27.55^o	
Index ranges	$-10 \leq h \leq 10$, $-16 \leq k \leq 16$, $-17 \leq l \leq 17$	
Reflection collected	36380	
Independent reflections	3239 [R_{int} = 0.0420]	
Completeness to θ	99.5 % (θ = 27.55^o)	
Absorption correction	Semi-empirical from equivalents	
Refinement method	Full-matrix least-squares on F^2	
Data / restraints / parameters	3239 / 0 / 182	
Goodness-of-fit on F^2	1.101	
Final R indices [$I > 2\sigma(I)$]	R_1 = 0.0857, wR_2 = 0.2317	
R indices (all data)	R_1 = 0.1274, wR_2 = 0.2831	
Largest diff. peak and hole	1.03 and -0.41 e.$Å^{-3}$	

Table 14. Selected bond distances (Å) of **(8)**.

Cu(1)-N(1)	1.989(5)	Cu(1)-N(1)#1	1.989(5)
Cu(1)-N(2)	2.028(4)	Cu(1)-N(2)	2.028(4)
Cu(1)-O(1)	2.575(5)	Cu(1)-O(1)#1	2.575(5)
N(1)-C(5)	1.493(9)	N(2)-C(3)	1.442(7)
N(3)-C(4)	1.409(9)	N(3)-C(5)	1.431(10)
Cl(1)-O(1)	1.363(6)	Cl(1)-O(2)	1.355(5)
Cl(1)-O(3)	1.394(5)	Cl(1)-O(4)	1.358(4)

Symmetry transformations used to generate equivalent atoms: #1 1-x, 1-y, 1-z

Table 15. Selected bond angles (°) of **(8)**.

N(1)-Cu(1)-N(1)#1	180.0	N(2)-Cu(1)-N(2)#1	180.0
N(1)-Cu(1)-N(2)	93.1(2)	N(1)#1-Cu(1)-N(2)#1	93.1(2)
O(1)-Cu(1)-O(1)#1	180.0	N(1)#1-Cu(1)-O(1)	87.7(2)
N(1)-Cu(1)-O(1)	92.3(2)	C(4)-N(3)-C(5)	114.7(6)
C(4)-N(3)-C(6)	115.6(7)	C(5)-N(3)-C(6)	121.5(7)
N(2)-C(4)-N(3)	115.1(6)	N(1)-C(5)-N(3)	114.4(6)
C(6)-C(7)-C(8)	108.4(10)	C(8)-C(7)-C(9)	107.8(14)

Symmetry transformations used to generate equivalent atoms: #1 1-x, 1-y, 1-z

3.7.4 Crystal structure description of the $[CuL^5]_3[Fe(CN)_6]_2 \cdot 5H_2O$ (12)

The crystal structure of the $[CuL^5]_3[Fe(CN)_6]_2 \cdot 5H_2O$ **(12)** had a disordered solvent water molecules occupancy. An acceptable model for the disordered solvent water molecules were not found, so the disordered density was masked out by using solvent mask route in *OLEX2*. Moreover, this structure implicated orientation disorder of carbon atoms. The molecule was refined at two positions, the major position of the atoms C(16A) = 51 %, C(17A) = 51 %, C(18A) = 51 %, C(20A) = 56.7 %, C(21A) = 56.7 %, and C(22A) = 56.7 % and the minor position of the atoms C(16B) = 49 %, C(17B) = 49 %, C(18B) = 49 %, C(20B) = 43.3 %, C(21B) = 43.3 %, and C(22B) = 43.3 %.

The crystallographic data and the results of refinement parameters are summarized in **Table 16** with the selected bond lengths and bond angle**s** are listed in **Tables 17** and **18**, respectively. The molecular structure of **(12)** is presented in **Figure 104**, together with the atomic labeling scheme and the unit cell packing diagram are illustrated in **Figure 105**. X-ray crystallographic study revealed that complex **(12)** belonged to the monoclinic system with space group $P2_1/n$. The asymmetric unit of **(12)** consisted of core structure of three $[CuL^5]^{2+}$ cations, two $[Fe(CN)_6]^{3-}$ anions, and five water molecules as lattice solvent. Addison *et al*., 1984 have explained the geometry index or structural parameter (τ) to differentiate the geometry of the coordination center to be a square pyramidal (SP) or trigonal bipyramidal (TBP). The τ parameter was calculated as: $\tau = (\beta-\alpha)/60^o$, where β and α are the two greatest valence angles of the coordination center. In general, if τ close to 0 indicates an ideal square pyramidal geometry, while if τ close to 1 indicates ideal trigonal bipyramidal geometry (Samanta *et al*., 2007). In this research, the value of τ was 0.115 pointing to the central Cu(1) atom (five-coordination) should adopt a square pyramidal geometry to four nitrogen atoms of the macrocyclic ligand with the average Cu(1)-$N_{macrocyclic}$ bond lengths of 2.013(3) Å and one nitrogen atom of cyanide ligand from $[Fe(CN)_6]^{3-}$ anion with the Cu(1)-N(1) distance of 2.303(3) Å. The Cu(2) center displayed distorted octahedral geometry with the equatorial positions consisted of four nitrogen atoms of the hexaazamacrocyclic ligand with the average Cu(2)-N_{eq} bond distances of 2.009(3) Å and the axial positions linked to two nitrogen atoms from cyanide ions with the Cu(2)-N_{ax} distances of 2.579(3) Å. The data showed that the Cu(2)-N_{ax} distances were much longer than the Cu(2)-N_{eq} distances which could be due to the Jahn-Teller distortion of the d^9 configuration of the Cu^{2+} ion. In the crystal structure, each Fe^{3+} ion coordinated to six carbon atoms from the cyanide ligands in an octahedral geometry. The bond angles of the *cis*-N-C-Fe for the terminal cyanide ligands were *app.* 177.0 ^{o} and those for the bridging cyanide ligands were slightly bent to *app.* 176.2 ^{o}. The cyanide-bridged with the bond distances of N(1)-C(0AA) = 1.144(4) Å, N(2)-C(1AA) = 1.149(4) Å and the terminal cyanide ligands were in the range 1.146(5)-1.154(5) Å which was in the normal range for low spin cyanide complexes of Fe^{3+} ion.

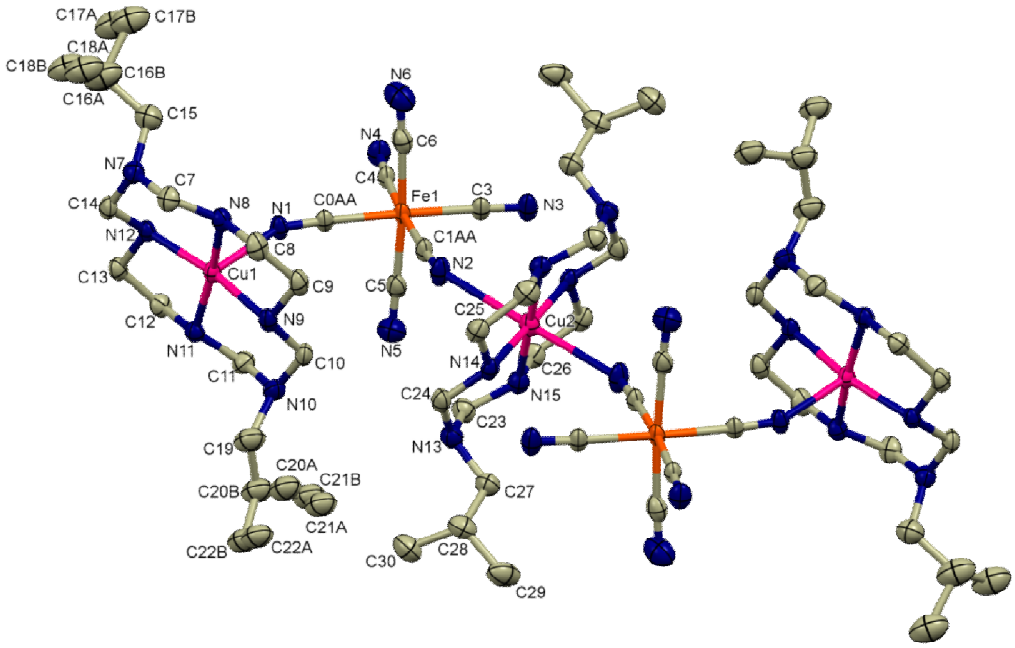

Figure 104. The crystal structure of the $[CuL^5]_3[Fe(CN)_6]_2{\cdot}5H_2O$ **(12)** with the atomic labeling scheme (All H atoms and solvent molecules omitted for clarity).

There have been several reports on reactions between $[Fe(CN)_6]^{3-}$ anions and $[ML]^{2+}$ cations (M = Cu^{2+} or Ni^{2+} and L = 3,10-dialkyl-1,3,5,8,10,12-hexaazacyclotetradecane) adducts where the $[Fe(CN)_6]^{3-}$ showed different coordination modes depending on the substituted pendant arm of hexaazamacrocyclic ligand (L). For example, when using ligand L^1 = 3,10-dibutyl-1,3,5,8,10,12-hexaazacyclotetradecane, the complex $[CuL^1]_3[Fe(CN)_6]_2{\cdot}2H_2O$ (Shen *et al*., 2008) is obtained, in which each $[Fe(CN)_6]^{3-}$ anion coordinated with three $[CuL^1]^{2+}$ cations through three *mer*-CN^- groups and resulted in a two-dimension ring-like dodecanuclear structure. On the other hand, if the ligand L^2 was used instead of L^1, a new complex $[NiL^2][Fe(CN)_6]$ (L^2 = 3,10-diethyl-1,3,5,8,10,12-hexaazacyclotetra-decane) was obtained (Kou *et al*., 2000), where each $[Fe(CN)_6]^{3-}$ unit used three *mer*-C≡N groups to connect with three *trans*-$[NiL^2]^{2+}$ units leading to a brick wall-like structure. Therefore, this result indicated that the pendant arms in the hexaazamacrocyclic ligands could determine the structural forms of the giving complexes.

Hydrogen bonding interactions were observed between the hydrogen atoms (H(9), H(11), and H(14)) from secondary amine (N(9), N(11), and N(14)) of the hexaazamacrocyclic ligand with the nitrogen atoms (N(3) and N(4)) of the terminal cyanide ligands with the contacts of N(9)-H(9)···N(3) = 2.453 Å, N(11)-H(11)···N(4) = 2.565 Å, and N(14)-H(14)···N(3) = 2.419 Å leading to a two-dimension chain like supramolecular interactions as depicted in **Figure 106**.

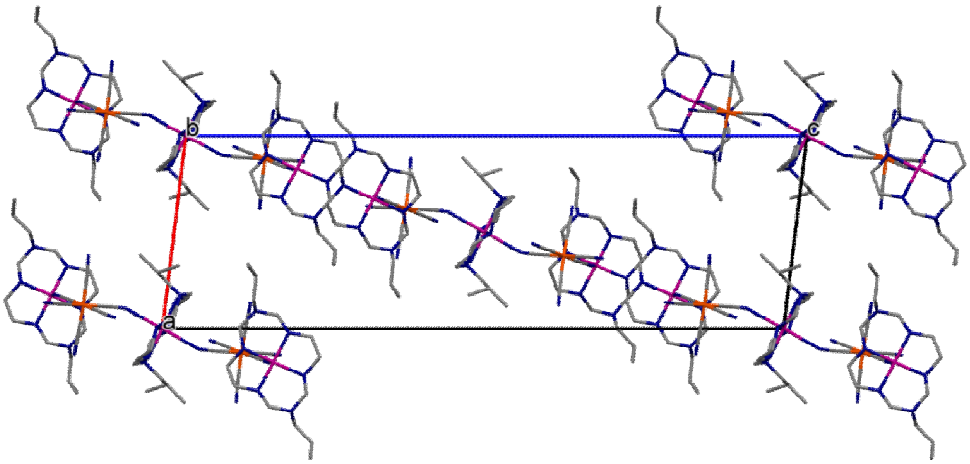

Figure 105. The unit cell packing of the $[CuL^5]_3[Fe(CN)_6]_2{\cdot}5H_2O$ **(12)**, plotted along the *b* axis (All H atoms and solvent molecules omitted for clarity)..

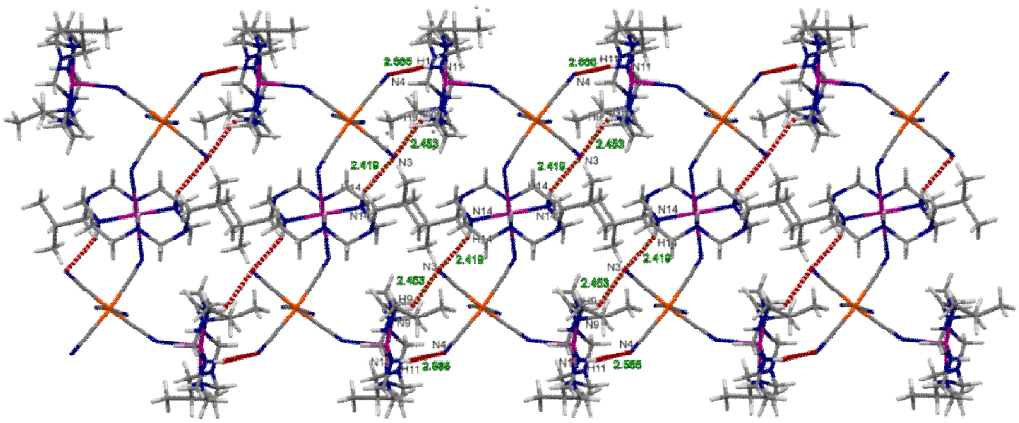

Figure 106. The 2D supramolecular structure of the $[CuL^5]_3[Fe(CN)_6]_2{\cdot}5H_2O$ **(12)**, showing hydrogen bonding (N-H···N) are indicated by dashed lines, plotted along *a*-axis.

Table 16. Crystallographic data and structure refinement of **(12)**.

Identification code	$[CuL^5]_3[Fe(CN)_6]_2 \cdot 5H_2O$ **(12)**	
Empirical formula	$C_{60}H_{112}Cu_3Fe_2N_{30}$	
Formula weight	1556.12	
Temperature	298.2 K	
Wavelength	0.71073 Å	
Crystal system	Monoclinic	
Space group	$P2_1/n$	
Unit cell dimensions	a = 11.8658(5) Å	$\alpha = 90.0^o$
	b = 9.7447(3) Å	$\beta = 96.8990(12)^o$
	c = 37.7968(14) Å	$\gamma = 90.0^o$
Volume	4338.7(3) $Å^3$	
Z	2	
Density (Calculated)	1.191 Mg/m^3	
Absorption coefficient	1.100 mm^{-1}	
$F(000)$	1642	
Crystal size	0.30 x 0.28 x 0.20 mm^3	
θ range for data collection	3.01 to 25.75°	
Index ranges	$-14 \leq h \leq 14$, $-11 \leq k \leq 11$, $-46 \leq l \leq 46$	
Reflection collected	57347	
Independent reflections	8205 [R_{int} = 0.0737]	
Completeness to θ	98.8 % (θ = 25.75°)	
Absorption correction	Semi-empirical from equivalents	
Refinement method	Full-matrix least-squares on F^2	
Data / restraints / parameters	8205 / 135 / 430	
Goodness-of-fit on F^2	1.021	
Final R indices [$I > 2\sigma(I)$]	R_1 = 0.0491, wR_2 = 0.1241	
R indices (all data)	R_1 = 0.0775, wR_2 = 0.1340	
Largest diff. peak and hole	0.57 and -0.40 e.$Å^{-3}$	

Table 17. Selected bond distances (Å) of **(12)**.

Cu(1)-N(1)	2.303(3)	Cu(1)-N(8)	2.009(3)
Cu(1)-N(9)	2.013(3)	Cu(1)-N(11)	2.008(3)
Cu(1)-N(12)	2.022(3)	Cu(2)-N(14)	2.011(3)
Cu(2)-N(14)#1	2.011(3)	Cu(2)-N(15)	2.007(3)
Cu(2)-N(15)#1	2.007(3)	Fe(1)-C(0AA)	1.941(3)
Fe(1)-C(1AA)	1.944(3)	Fe(1)-C(3)	1.942(3)
Fe(1)-C(4)	1.944(3)	Fe(1)-C(5)	1.941(3)
Fe(1)-C(6)	1.940(3)	N(1)-C(0AA)	1.144(4)
N(1)-C(1AA)	1.149(4)	N(1)-C(3)	1.147(4)
N(1)-C(4)	1.154(4)	N(1)-C(5)	1.146(4)

Symmetry transformations used to generate equivalent atoms: #1 1-x, 1-y, 1-z

Table 18. Selected bond angles (^{o}) of **(12)**.

N(8)-Cu(1)-N(1)	92.85(11)	N(8)-Cu(1)-N(9)	85.63(12)
N(8)-Cu(1)-N(12)	94.67(11)	N(9)-Cu(1)-N(1)	93.13(10)
N(9)-Cu(1)-N(12)	170.77(10)	N(11)-Cu(1)-N(1)	97.00(11)
N(11)-Cu(1)-N(9)	92.56(12)	N(11)-Cu(1)-N(12)	85.57(11)
N(14)#1-Cu(2)-N(2)	87.83(10)	N(15)-Cu(2)-N(2)	86.61(12)
N(14)#1-Cu(2)-N(14)	179.99(1)	N(15)#1-Cu(2)-N(15)	180.00(1)
C(0AA)-Fe(1)-C(1AA)	90.94(13)	C(0AA)-Fe(1)-C(4)	93.55(12)
C(1AA)-Fe(1)-C(4)	175.63(13)	C(3)-Fe(1)-C(1AA)	86.60(13)
C(3)-Fe(1)-C(4)	89.11(13)	C(5)-Fe(1)-C(3)	92.08(16)
C(6)-Fe(1)-C(0AA)	88.73(15)	C(6)-Fe(1)-C(3)	91.91(16)
C(6)-Fe(1)-C(4)	87.23(16)	C(6)-Fe(1)-C(5)	175.85(16)

Symmetry transformations used to generate equivalent atoms: #1 1-x, 1-y, 1-z

3.7.5 Crystal structure description of the $[NiL^5(4\text{-nba})_2]\cdot H_2O$ (13)

The crystal structure of **(13)** is shown in **Figure 107**. The crystallographic data and the result of refinements and the selected bond lengths and angles are listed in **Tables 19-21**, respectively. Complex **(13)** crystallized in the monoclinic *C*2/*c* space group and each unit cell **(Figure 108)** included two independent molecules. The coordination geometry around the nickel(II) ion was a distorted octahedral in which each Ni(1) or Ni(2) ion was coordinated to the four secondary amine atoms of the hexaazamacrocycle in the planes and two oxygen atoms from two *p*-nitrobenzoate anions at the axial positions. The average bond length of Ni(1)-N_{eq} and Ni(2)-N_{eq} in the square-planar part were 2.0638(17) Å and 2.0528(18) Å, respectively. The average bond lengths, Ni(1)-O_{ax} = 2.1309(13) Å and Ni(2)-O_{ax} = 2.1319(14) Å were within the previously reported values, for example, the complexes $[Ni(C_{16}H_{38}N_6)(2,7\text{-NDC})]$ and $[Ni(C_{16}H_{38}N_6)(nicotinate)_2]$; Ni-$O_{ax}$ = 2.132(1) Å (Shin *et al*., 2016).

The core of the nickel(II) hexaazamacrocyclic unit in **(13)** adopted the most stable *trans*-III (*R,R,S,S*) conformation with two chair six-membered chelate rings relating with the C(3) and C(4) or C(16) and C(17) atoms and the chelate average angles N(1)-Ni(2)-N(2)#2 = 94.50(8)^o and N(4)-Ni(1)-N(5) = 93.96(7)^o and two gauche five-membered chelate rings relating to the C(1) and C(2) or C(18) and C(19) atoms and the chelate average angles N(1)-Ni(2)-N(2) = 85.50(8)^o and N(4)-Ni(1)-N(5)#1 = 86.04(7)^o. The C(3)-N(3), C(4)-N(3), C(16)-N(6), and C(17)-N(6) bond distances were 1.422(4) Å, 1.443(3) Å, 1.437(3) Å, and 1.438(3) Å, respectively. The C(3)-N(3)-C(4) and C(16)-N(6)-C(17) bond angles involving the tertiary nitrogen atom N(3) or N(6) were 116.2(2)^o and 116.18(17)^o showing a significant proportion of sp^2 hybridization for the nitrogen atoms which were similar to the literature report (Han *et al*., 2008).

Figure 109 shows a 1D chain-like structure of **(13)** with the interactions of two types namely: intra- and intermolecular interactions. The intramolecular hydrogen bonding interaction between the uncoordinated carboxylate oxygen atoms (O(6) and O(3)) of the *p*-nitrobenzoate ligand and the secondary amines

(-NH) of the hexaazamacrocyclic ligand to form a six-membered chelate rings (N(2)-H(2)···O(6) = 2.039 Å, ∠N(2)-H(2)-O(6) = 151.31° and (N(5)-H(5)···O(3) = 2.081 Å, ∠N(5)-H(5)-O(3) = 148.49°. The intermolecular interactions were connected by the offset face-to-face π-π stacking between the aromatic groups of the *p*-nitrobenzoate ligand in one chain and another aromatic group of the *p*-nitrobenzoate ligand in adjacent chain. The inter-planar separations of the benzene rings was 3.797-3.855 Å (centroid···centroid = 3.802 and 3.852 Å). The shortest Ni(1)···Ni(1) or Ni(2)···Ni(2) lengths within the chain-like was 12.829 Å and the separation Ni(1)···Ni(2) between the chain-like was 8.401 Å, respectively.

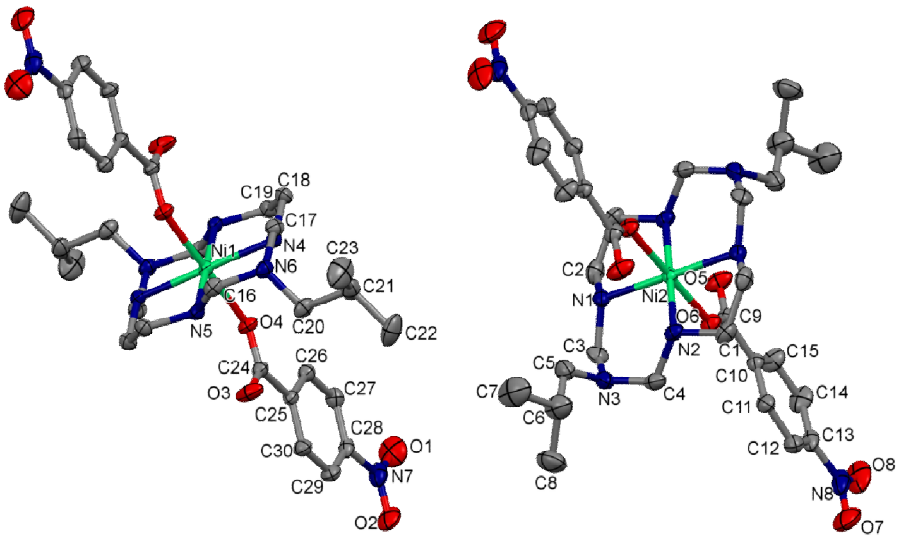

Figure 107. The crystal structure of the $[NiL^5(4\text{-nba})_2]\cdot H_2O$ **(13)** with the atomic labeling scheme (All H atoms and solvent molecules omitted for clarity).

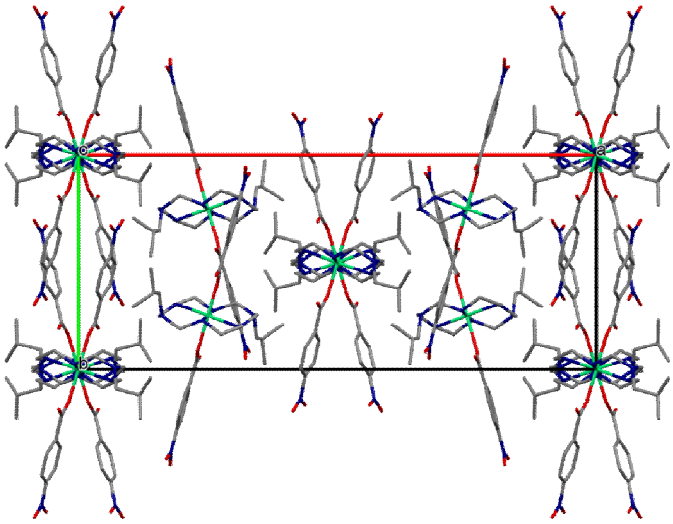

Figure 108. The unit cell packing of the $[NiL^5(4\text{-nba})_2]\cdot H_2O$ **(13)**, plotted down *c* axis (All H atoms and solvent molecules omitted for clarity).

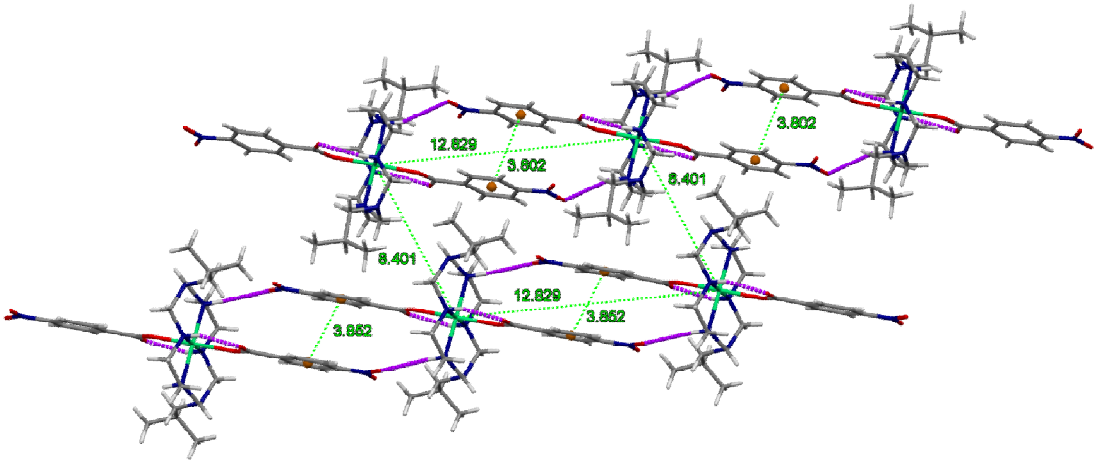

Figure 109. One-dimension of the $[NiL^5(4\text{-nba})_2]\cdot H_2O$ **(13)** showing intra- and intermolecular hydrogen bonds (N-H···O) and π-π stacking interactions are indicated by *dashed lines*.

Table 19. Crystallographic data and structure refinement of **(13)**.

Identification code	$[NiL^5(4\text{-nba})_2]\cdot H_2O$ **(13)**	
Empirical formula	$C_{60}H_{90}Ni_2N_{16}O_{16}$	
Formula weight	1408.86	
Temperature	273.2 K	
Wavelength	0.71073 Å	
Crystal system	Monoclinic	
Space group	*C*2/*c*	
Unit cell dimensions	a = 31.0572(12) Å	$\alpha = 90.0^o$
	b = 12.8285(4) Å	$\beta = 90.7760(10)^o$
	c = 18.1320(7) Å	$\gamma = 90.0^o$
Volume	7223.4(5) $Å^3$	
Z	4	
Density (Calculated)	1.296 Mg/m^3	
Absorption coefficient	0.594 mm^{-1}	
F(000)	2984	
Crystal size	0.35 x 0.24 x 0.20 mm^3	
θ range for data collection	3.37 to 26.52°	
Index ranges	$-38 \le h \le 38$, $-16 \le k \le 14$, $-22 \le l \le 22$	
Reflection collected	70377	
Independent reflections	7449 [R_{int} = 0.0576]	
Completeness to θ	99.3 % ($\theta = 26.52^o$)	
Absorption correction	Semi-empirical from equivalents	
Refinement method	Full-matrix least-squares on F^2	
Data / restraints / parameters	7449 / 0 / 431	
Goodness-of-fit on F^2	1.054	
Final *R* indices [$I > 2\sigma(I)$]	R_1 = 0.0426, wR_2 = 0.1079	
R indices (all data)	R_1 = 0.0631, wR_2 = 0.1154	
Largest diff. peak and hole	0.50 and -0.28 e.$Å^{-3}$	

Table 20. Selected bond distances (Å) of **(13)**.

Ni(1)-N(4)	2.0608(16)	Ni(1)-N(4)#1	2.0609(16)
Ni(1)-N(5)	2.0668(17)	Ni(1)-N(5)#1	2.0668(17)
Ni(1)-O(4)	2.1309(13)	Ni(1)-O(4)#1	2.1310(13)
Ni(2)-N(1)	2.0577(18)	Ni(2)-N(1)#2	2.0578(18)
Ni(2)-N(2)	2.0478(18)	Ni(2)-N(2)#2	2.0478(18)
Ni(2)-O(5)	2.1320(14)	Ni(2)-O(5)#2	2.1319(14)
N(7)-O(1)	1.211(3)	N(7)-O(2)	1.215(3)
N(8)-O(7)	1.188(4)	N(8)-O(8)	1.224(4)
C(9)-O(5)	1.259(3)	C(24)-O(3)	1.237(3)
C(9)-O(6)	1.238(3)	C(24)-O(4)	1.255(2)

Symmetry transformations used to generate equivalent atoms: #1 -x, -y, -z; #2 ½-x, 3/2-y, -z

Table 21. Selected bond angles (^{o}) of **(13)**.

N(4)-Ni(1)-N(4)#1	180.0(3)	N(5)-Ni(1)-N(5)#1	180.0
N(4)-Ni(1)-N(5)	93.96(7)	N(1)-Ni(1)-N(5)#1	86.04(7)
N(1)-Ni(2)-N(1)#1	180.0	N(2)-Ni(2)-N(2)	180.0
N(1)-Ni(2)-N(2)#2	94.50(8)	N(1)-Ni(2)-N(2)	85.50(8)
C(3)-N(3)-C(4)	116.2(2)	C(16)-N(6)-C(17)	116.18(17)
O(4)-Ni(1)-O(4)#1	180.00(8)	O(5)-Ni(2)-O(5)#2	180.0
O(5)-C(9)-O(6)	126.9(2)	O(3)-C(24)-O(4)	126.37(19)
O(1)-N(7)-O(2)	123.1(2)	O(7)-N(8)-O(8)	123.5(3)
Ni(1)-O(4)-C(24)	133.47(14)	Ni(2)-O(5)-C(9)	133.17(15)

Symmetry transformations used to generate equivalent atoms: #1 -x, -y, -z; #2 ½-x, 3/2-y, -z

3.7.6 Crystal structure description of the $[NiL^3(4\text{-nba})_2]$ (14)

Crystallographic data and the details of the data collection are listed in **Table 22** and selected bond distances and angles of **(14)** are listed in **Tables 23** and **24**. The crystal structure of **(14)** and atom labeling scheme are depicted in **Figure 110**. The complex crystallized in a monoclinic system with a *C*2/*c* space group. The crystallographic asymmetric unit of $[NiL^3(4\text{-nba})_2]$ **(14)** consisted of one $[NiL^3]^{2+}$ cation and two *p*-nitro benzoate anions. The Ni(II) ion showed a distorted octahedron coordination geometry by binding to four secondary nitrogen atoms of the hexaazamacrocycle with the bond distances of Ni(1)-N(1) = 2.056(19) Å and Ni(1)-N(3) = 2.072(2) Å occuppying the equatorial position, and two oxygen atoms of p-nitrobenzoate anions at the axial positions with the bond distance of Ni(1)-O(1) = 2.1407(15) Å. The average C-N bond distances relating the tertiary atoms (N(2)) was 1.445(3) Å and the angles C(2)-N(2)-C(3), C(2)-N(2)-C(5), and C(3)-N(2)-C(5) were 117.26(19), 115.3(2), and 116.7(2)°, respectively which revealed significant proportion of sp^2-like hybridization for the nitrogen atoms. These values were within of those reported by Husain *et al.*, 2011 and Han *et al.*, 2008. The six-membered chelate rings connecting the C(2) and C(3) atoms adopted a chair conformation with the chelate angle N(1)-Ni(1)-N(3) = 93.98(8)°, whereas five-membered rings connecting the C(4)-C(4)#1 atoms adopted a gauche conformation with the chelate angel N(3)-Ni(1)-N(3)#1 = 86.09(11)°. **Figure 111** shows the packing diagrams of **(14)**, viewed along the *c* axis.

Complex **(14)** has involved one intramolecular N-H···O hydrogen bonds between the secondary amine of the hexaazamacrocycle and the oxygen atoms of carbonyl group on the *p*-nitrobenzoate anions: N(1)-H(1)···O(2) = 2.07Å and ∠(N1)-(H1)-(O2) = 148.8°. Moreover, the intermolecular N-H···O hydrogen bonds between the nitrogen atoms of secondary amine groups and the oxygen atoms of nitro group on the *p*-nitrobenzoate anions: N(3)-H(3)···O(4)#1 = 2.28 Å and ∠(N3)-(H3)-(O4)#1 = 145.3°. The average bond lengths and bond angles of **(14)** were very similar to those of previously reported $[Ni(C_{16}H_{38}N_6)(nicotinate)_2]$ complex (Shin *et al.*, 2016). Furthermore, the aromatic rings of *p*-nitrobenzoic anions were linked by face-to-face π-π stacking interaction. Between the monomeric structure units, there are π-π

stacking interactions of d(4-nba$_{centroid}$-4-nba$_{centroid}$ = 3.894 Å, which leads to one-dimensional zigzag-like structure when viewed along the crystallographic *c* axis as illustrated in **Figure 112**. This distance values between the aromatic rings of the carboxylate anions were comparable to those of the previously reported in related complexes: [Cu(L)(H_2btc)$_2$] (L = 3,10-bis(2-hydroxyethyl)-1,3,5,8,10,12-hexaaza-cyclotetradecane); d(centroid···centroid) = 3.489 Å (Tao *et al*., 2012), [Ni($L^{R,R}$)]-(ClO_4)$_2$ ($L^{R,R}$ = 1,8-di((*R*)-α-methylnaphthyl)-1,3,6,8,10,13-hexaazacyclotetradecane); d(centroid···centroid) = 3.817 Å (Min *et al*., 2013), and [Ni($C_{20}H_{32}N_8$)-(isonicotinate)$_2$]; d(centroid···centroid) = 3.673 Å (Min *et al*., 2001), [Ni(L)(tp)]·6H_2O (L = 3,10-bis{3-(1-imidazolyl)propyl}-1,3,5,8,10,12-hexaazacyclotetradecane and tp = terephthalate); d(centroid···centroid) = 4.175 Å (Han *et al*., 2011).

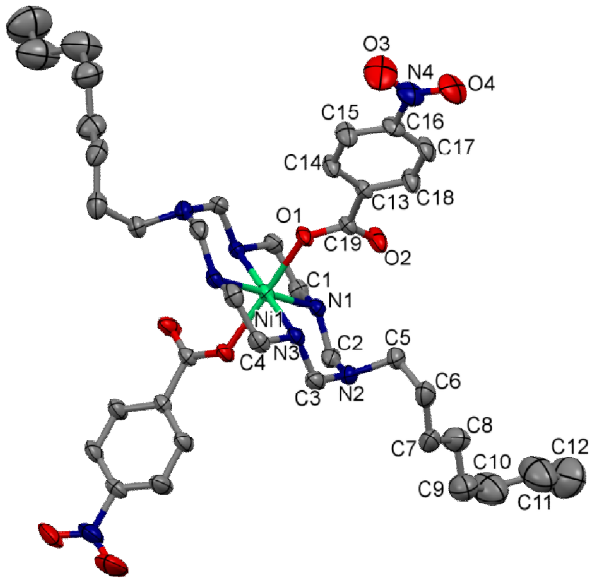

Figure 110. The crystal structure of the [NiL^3(4-nba)$_2$] **(14)**, along with atomic numbering scheme (All H atoms omitted for clarity).

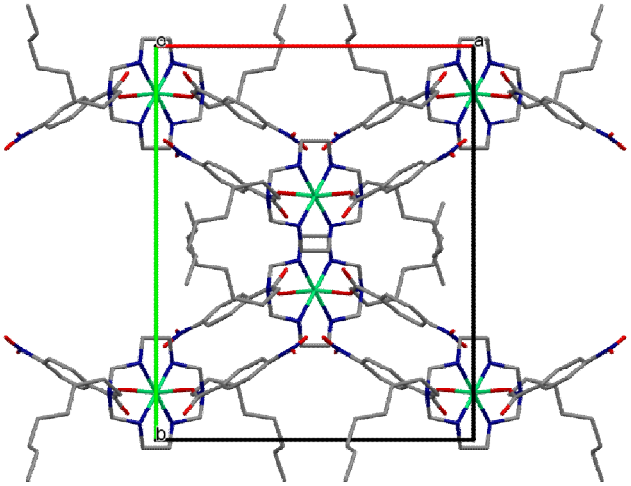

Figure 111. View of the unit cell packing of [NiL^3(4-nba)$_2$] **(14)**, plotted down *c* axis. (All H atoms omitted for clarity).

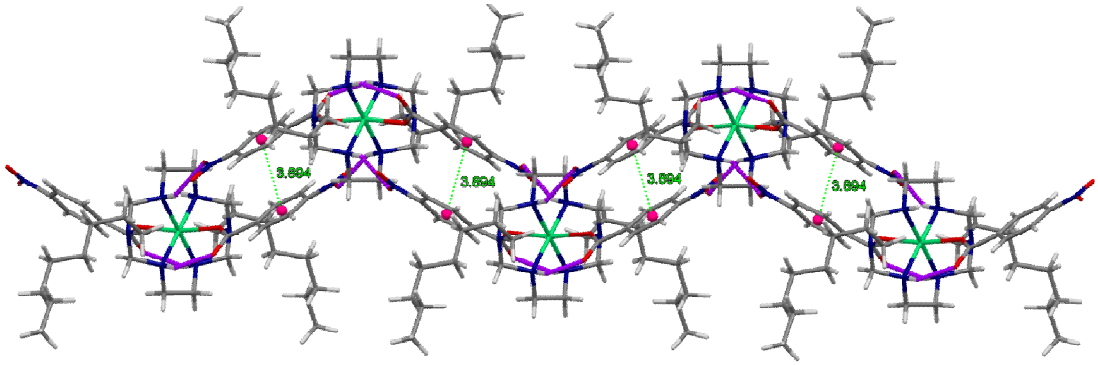

Figure 112. One-dimension of the [NiL^3(4-nba)$_2$] **(14)** showing intra- and intermolecular hydrogen bonds (N-H···O) and π-π stacking interactions, plotted down *c* axis (shown as *dashed lines*).

Table 22. Crystallographic data and structure refinement of **(14)**.

Identification code	$[NiL^3(4\text{-nba})_2]$ **(14)**	
Empirical formula	$C_{28}H_{62}NiN_8O_8$	
Formula weight	817.66	
Temperature	298.0 K	
Wavelength	0.71073 Å	
Crystal system	Monoclinic	
Space group	*C*2/*c*	
Unit cell dimensions	a = 16.434(4) Å	$\alpha = 90.0^o$
	b = 19.624(5) Å	$\beta = 106.258(7)^o$
	c = 13.596(3) Å	$\gamma = 90.0^o$
Volume	4209.3(17) $Å^3$	
Z	8	
Density (Calculated)	1.290 Mg/m^3	
Absorption coefficient	0.519 mm^{-1}	
F(000)	1752	
Crystal size	0.25 x 0.243 x 0.20 mm^3	
θ range for data collection	2.51 to 25.71°	
Index ranges	$-20 \le h \le 19$, $-23 \le k \le 23$, $-16 \le l \le 16$	
Reflection collected	34431	
Independent reflections	4008 [R_{int} = 0.0586]	
Completeness to θ	99.8 % (θ = 25.71°)	
Absorption correction	Semi-empirical from equivalents	
Refinement method	Full-matrix least-squares on F^2	
Data / restraints / parameters	4008 / 9 / 250	
Goodness-of-fit on F^2	1.045	
Final *R* indices [$I > 2\sigma(I)$]	R_1 = 0.0431, wR_2 = 0.1060	
R indices (all data)	R_1 = 0.0615, wR_2 = 0.1174	
Largest diff. peak and hole	0.39 and -0.25 e.$Å^{-3}$	

Table 23. Selected bond distances (Å) of **(14)**.

Ni(1)-N(1)	2.056(19)	Ni(1)-N(1)#1	2.056(19)
Ni(1)-N(3)	2.072(2)	Ni(1)-N(3)#1	2.072(2)
Ni(1)-O(1)	2.141(15)	Ni(1)-O(1)#1	2.141(15)
N(2)-C(2)	1.425(3)	N(2)-C(3)	1.436(3)
N(2)-C(5)	1.475(3)	C(1)-C(1)#1	1.514(5)
C(19)-O(1)	1.263(3)	C(4)-C(4)#1	1.518(5)
C(19)-O(2)	1.232(3)	N(4)-O(3)	1.207(4)
N(4)-O(4)	1.214(3)	N(4)-C(16)	1.473(3)
C(1)-C(1)#1	1.514(5)	C(4)-C(4)	1.518(5)
C(5)-C(6)	1.492(4)	C(6)-C(7)	1.494(5)
C(10)-C(11)	1.444(7)	C(13)-C(14)	1.371(3)
C(15)-C(16)	1.370(4)	C(17)-C(18)	1.385(4)

Symmetry transformations used to generate equivalent atoms: #1 1-x, +y, ½-z

Table 24. Selected bond angles (^{o}) of **(14)**.

N(1)-Ni(1)-N(1)#1	85.96(11)	N(1)-Ni(1)-N(3)	93.98(8)
N(1)-Ni(1)-N(3)#1	179.58(7)	N(1)#1-Ni(1)-N(3)	179.57(7)
O(1)-Ni(1)-O(1)#1	171.31(9)	N(1)-Ni(1)-O(1)	94.20(7)
O(3)-N(4)-O(4)	123.6(3)	O(2)-C(19)-O(1)	126.7(2)
C(2)-N(2)-C(3)	117.26(19)	C(2)-N(2)-C(5)	115.3(2)
C(3)-N(2)-C(5)	116.7(2)	C(19)-O(1)-Ni(1)	131.96(15)
O(3)-N(4)-C(16)	118.2(3)	O(4)-N(4)-C(16)	118.2(3)
O(2)-C(19)-O(1)	126.7(2)	O(2)-O(19)-C(13)	117.9(2)
C(1)-N(1)-Ni(1)	105.91(14)	C(1)-N(1)-C(2)	114.12(18)
O(3)-N(4)-O(4)	123.6(3)	C(11)-C(10)-C(9)	115.6(5)
C(13)-C(18)-C(17)	120.8(3)	O(1)-C(19)-C(13)	115.4(2)
O(2)-C(19)-O(1)	126.7(2)	O(2)-C(19)-C(13)	117.9(2)

Symmetry transformations used to generate equivalent atoms: #1 1-x, +y, ½-z

3.7.7 Crystal structure description of the $[NiL^5(sal)_2]$ (15)

A summary of selected crystallographic data for **(15)** are given in **Table 25** while the structure is displayed in **Figure 113** and the selected bond lengths and angles are listed in **Tables 26** and **27**, respectively. The complex **(15)** crystallized in the monoclinic system with space group $P2_1/n$. The structure asymmetric unit of **(15)** consisted of a basis $[NiL^5]^{2+}$ cationic complex (L^5 = 3,10-diisobutyl-1,3,5,8,10,-12-hexaazacyclotetradecane) and two salicylate anions. The molecular packing arrangement of **(15)** viewed along the *a* axis is displayed in **Figure 113**. In the crystal structure of **(15)**, each nickel(II) ion had a distorted octahedral geometry with the two secondary and two tertiary amines of the hexaazamacrocycle and two salicylate anions. The Ni(1)-N(2) (tertiary amines) distance of 3.301 Å was significantly longer than the average Ni(1)-N(1) and Ni(1)-N(3) (secondary amines) distances of 2.055 Å indicating no participation in the coordination. The average Ni-N distance (2.096 Å) in NiN_4 plane was significantly longer than in the square-planar geometry of $[Ni(L^{R,R})](ClO_4)_2$ complex ($L^{R,R}$ = 1,8-di((*R*)-α-methylnaphthyl)-1,3,6,8,10,13-hexa-azacyclotetradecane) (Ni-N = 1.941 Å) (Min *et al*., 2013) but was similar to that observed for the octahedral nickel(II) complexes with 14-membered hexaaza-macrocyclic ligands (Kang *et al*., 1999). Moreover, C-N (tertiary amines) bond distances were much shorter than other C-N single bond distances indicating possibility of the sp^2-like hybridization of the uncoordinated tertiary nitrogen. The bond angles of the six-membered rings (N(1)-Ni(1)-N(3) = 94.10(7)^o and $N(1)^i$-Ni(1)-$N(3)^i$ = 94.11(7)^o) were large than those of the five-membered rings (N(3)-Ni(1)-$N(1)^i$ and $N(3)^i$-Ni(1)-N(1) = 85.89(7)^o). The axial positions average Ni(1)-O(1) bonds were not perpendicular to the NiN_4 equatorial plane as the $O(1)_{ax}$-Ni(1)-N_{eq} angles ranging from 88.80(7)-93.09(6)^o.

Interestingly, the secondary amines of the hexaazamacrocyclic ligand formed intramolecular hydrogen bonds with carboxylate oxygen atoms N(3)-H(3A)···O(2)#1 = 2.019(2) Å and ∠N(3)-H(3A)-O(2)#1 = 152.3(7)^o; symmetry code: #1 2-x, 1-y, 1-z and hydrogen atoms of the hydroxyl groups of the salicylate ligand O(3)-H(3)···O(2) = 1.766(3) Å and ∠O(3)-H(3)-O(2) = 147.3(4)^o, as shown in **Figure 114**.

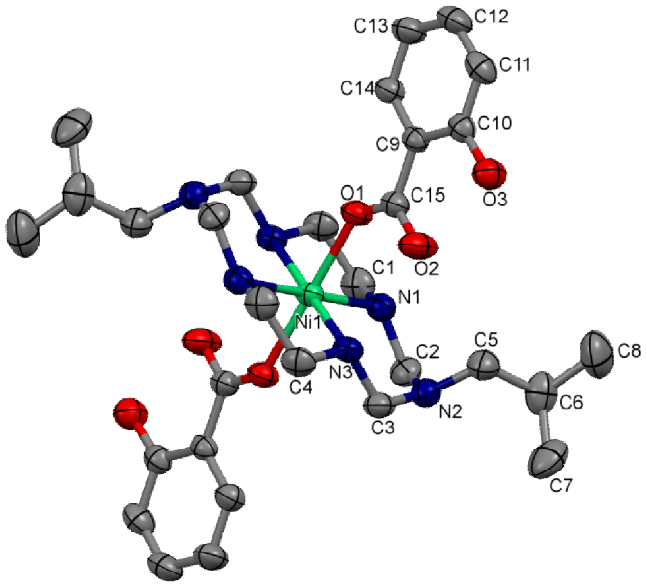

Figure 113. The crystal structure of the $[NiL^5(sal)_2]$ **(15)**, along with atomic numbering scheme (All H atoms omitted for clarity).

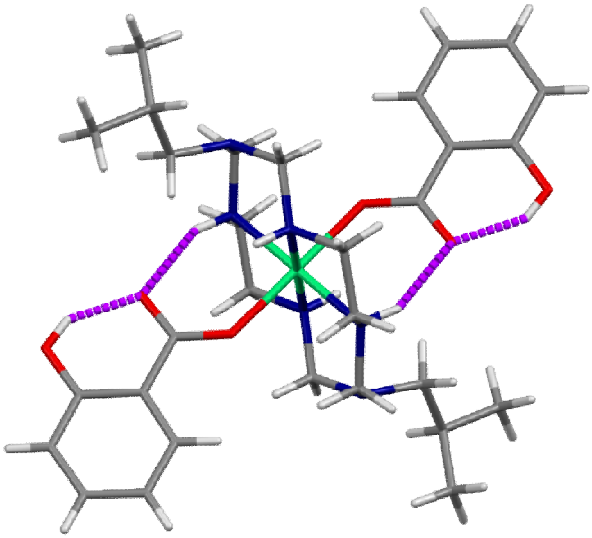

Figure 114. Intramolecular hydrogen bonds interaction of $[NiL^5(sal)_2]$ **(15)**, (*dashed lines*).

Table 25. Crystallographic data and structure refinement of **(15)**.

Identification code	$[NiL^5(sal)_2]$ **(15)**	
Empirical formula	$C_{30}H_{48}NiN_6O_6$	
Formula weight	647.45	
Temperature	298.0 K	
Wavelength	0.71073 Å	
Crystal system	Monoclinic	
Space group	$P2_1/n$	
Unit cell dimensions	a = 8.7283(4) Å	$\alpha = 90.0^o$
	b = 17.3360(7) Å	$\beta = 110.915(1)^o$
	c = 11.4701(5) Å	$\gamma = 90.0^o$
Volume	1621.23(12) $Å^3$	
Z	2	
Density (Calculated)	1.326 Mg/m^3	
Absorption coefficient	0.684 mm^{-1}	
$F(000)$	693	
Crystal size	0.40 x 0.32 x 0.32 mm^3	
θ range for data collection	3.02 to 26.38^o	
Index ranges	$-10 \leq h \leq 10$, $-21 \leq k \leq 21$, $-14 \leq l \leq 14$	
Reflection collected	21925	
Independent reflections	3306 [R_{int} = 0.0446]	
Completeness to θ	99.7 % ($\theta = 26.38^o$)	
Absorption correction	Semi-empirical from equivalents	
Refinement method	Full-matrix least-squares on F^2	
Data / restraints / parameters	3306 / 0 / 198	
Goodness-of-fit on F^2	1.063	
Final R indices [$I > 2\sigma(I)$]	R_1 = 0.0391, wR_2 = 0.0885	
R indices (all data)	R_1 = 0.0622, wR_2 = 0.1006	
Largest diff. peak and hole	0.39 and -0.24 e.$Å^{-3}$	

Table 26. Selected bond distances (Å) of **(15)**.

Ni(1)-N(1)	2.057(18)	Ni(1)-N(1)#1	2.057(18)
Ni(1)-N(3)	2.052(18)	Ni(1)-N(3)#1	2.052(18)
N(2)-C(2)	1.424(3)	N(2)-C(3)	1.428(3)
N(2)-C(5)	1.471(3)	O(3)-C(10)	1.3473(3)
O(1)-C(15)	1.251(3)	O(2)-C(15)	1.259(3)
N(1)-C(1)	1.479(3)	N(1)-C(2)	1.493(3)
N(3)-C(3)	1.486(3)	N(3)-C(4)	1.471(3)

Symmetry transformations used to generate equivalent atoms: #1 2-x, 1-y, 1-z

Table 27. Selected bond angles (^{o}) of **(15)**.

N(3)-Ni(1)-N(1)	94.12(7)	N(3)#1-Ni(1)-N(1)#1	94.12(7)
N(1)-Ni(1)-N(1)#1	180.0	O(1)#1-Ni(1)-O(1)	180.0
N(3)-Ni(1)-O(1)	86.86(6)	N(3)-Ni(1)-N(1)#1	85.88(7)
C(4)-N(3)-C(3)	114.59(17)	C(3)-N(3)-Ni(1)#1	114.38(14)
O(2)-C(15)-O(1)	124.4(2)	C(9)-C(15)-O(1)	118.7(2)
O(9)-C(15)-O(2)	116.8(2)	C(10)-C(11)-O(3)	118.4(2)

Symmetry transformations used to generate equivalent atoms: #1 2-x, 1-y, 1-z

3.8 Catalytic properties

Persulfate oxidation, a member in the class of advance oxidation process, has been applied to degrade organic dyes such as congo red (Wang *et al*., 2014 and Li *et al*., 2015), crystal violet (Gokulakrishnan *et al*., 2012), methylene blue (Huan *et al*., 2016), and methyl orange (Jiao *et al*., 2012 and Gokulakrishnan *et al*., 2015). The uncatalyzed degradation reaction had very low efficiency. In the presence of catalyst, persulfate oxidation process produced strongly oxidizing sulfate radicals. In this work, the degradation efficiency of the catalytic oxidation of methyl orange was studied using potassium persulfate (KPS) as an oxidant and complexes **(13) - (15)** as heterogeneous catalysts. The degradation of methyl orange with KPS alone was

slow with almost no change in color even up to 80 min of reaction as shown in **Figure 115**. However, when each complex of **(13) - (15)** was added the reaction took place almost immediately as indicated by the color change of methyl orange dye.

Under the same conditions, the degradation efficiency **(Figure 116)** of **(14)** was higher than that of **(13**) and **(15)**. This could be due to the directionality of metal-ligand interactions and the supramolecular interactions leading to formation of channels that could be accessed from the exterior allowing electron transfer and the incorporation of substrates inside the crystal. The presence of lipophilic side chains of the hexaazamacrocyclic ligand did not affect the electron transfer process at the nickel ion center (Haines *et al*., 2003). Other factors that could affect the degradation of organic dyes, such as central metal atoms (Ming *et al*., 2015), molecular structures or supramolecular architectures (Qin *et al*., 2013), and thermal stability of the structures (Feng *et al*., 2014). The reaction that used **(13)** and **(14)** as catalyst could degrade 90 % and 96 % of methyl orange in 60 min but only 83 % with **(15)**. With KPS alone, in the same time period, the degradation was only 55 %. This could be the result of the presence of each complex **(13) - (15)** facilitated the generation of sulfate radicals from KPS to proceed more effectively. The mechanism has been proposed that during the oxidation processes in aqueous solution, the $S_2O_8^{2-}$ anion accepted electron from Ni^{2+} complex *via* ion-pair mechanism leading to the formation of the Ni^{3+} species. In this work, the complexes **(13) - (15)** behaved as heterogeneous catalyst. Nonetheless, the researcher deemed that the same mechanism still can be applied, i.e., the surface adsorbed $S_2O_8^{2-}$ ion accepted electron from solid complexes **(13) - (15)** leading to the formation of transient Ni^{3+} in the solid complex which was quickly reduced back to Ni^{2+} complex again. Simultaneously, the generated sulfate radicals went on to degrade the organic dyes. The mechanism involving chemical transformation steps of persulfate anion was proposed by Gokulakrishnan *et al*. 2012 as follows:

$$[Ni^{(II)}L]^{2+} + S_2O_8^{2-} \leftrightarrow \{Ni^{(II)}L^{2+} + S_2O_8^{2-}\} \text{ ion-pair} \quad (1)$$

$$\{Ni^{(II)}L^{2+} + S_2O_8^{2-}\} \rightarrow [Ni^{(III)}L(SO_4)]^{+} + SO_4^{\cdot -} \quad (2)$$

$$[Ni^{(II)}L]^{2+} + SO_4^{\cdot -} \rightarrow [Ni^{(III)}L(SO_4)]^{+} \quad (3)$$

$SO_4^{\cdot -}$ + organic dyes → oxidative degradation (4)

$SO_4^{\cdot -} + H_2O \leftrightarrow OH^{\cdot} + H^+ + SO_4^{2-}$ (5)

$OH^{\cdot}$ + organic dyes → oxidative degradation (6)

$[Ni^{(III)}L(SO_4)]^+$ + organic dyes → $[Ni^{(II)}L]^{2+} + SO_4^{\cdot -}$ oxidative degradation (7)

where L = hexaazamacrocyclic ligand

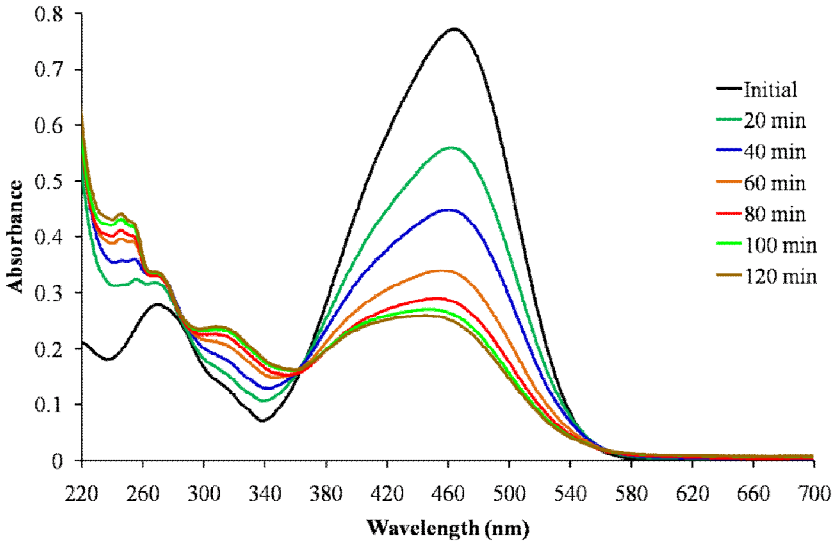

Figure 115. Absorption spectra showing the degradation of methyl orange by KPS under UV irradiation.

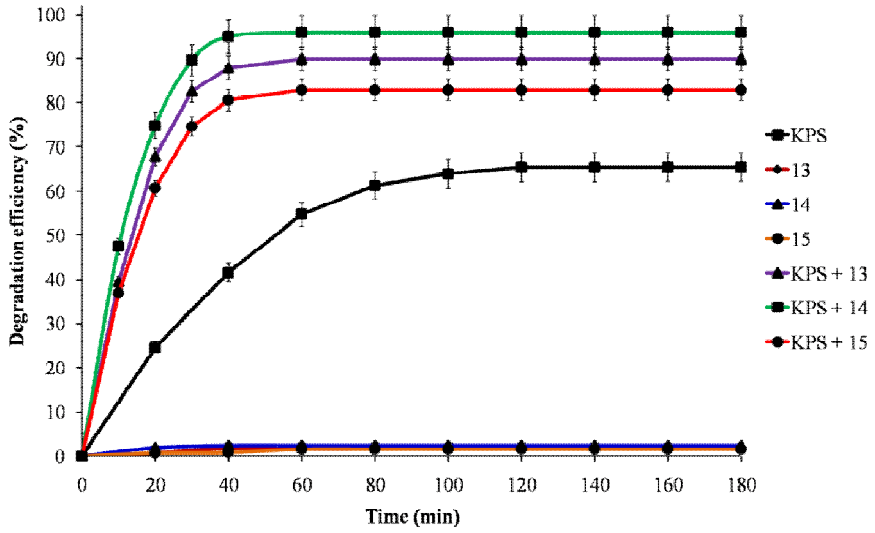

Figure 116. Degradation efficiency (%) of methyl orange versus reaction time under UV irradiation.

3.9 Recyclability of the catalysts

Each catalyst **(13)** - **(15)** was very robust as they remained unscratched through 5 cycles of reuses. During the photodegradation tests, the catalyst could be simply isolated by centrifugation and reused by adding it into the freshly-prepared methyl orange solution to start the next round of photodegradation reaction. The extent of methyl orange degradation remained almost unchanged throughout 5 cycles of tests and not significantly lower than when it was first used **(Figure 117)**. The FT-IR spectra of the each catalyst **(13)** - **(15)** isolated after the 5^{th} cycle matched well with the initial spectra of all complexes **(Figures 118-120)**. The color of **(13)** and **(14)** remained unchanged both before and after the reaction whereas the color of **(15)** after used became almost undistinguishable paler than before used **(Figure 121).** All these results indicated that the **(13)** - **(15)** are attractive catalyst in terms of efficiency and robustness, especially complexes **(13)** and **(14)** which showed higher efficiency than **(15)** while all the other data remained the same.

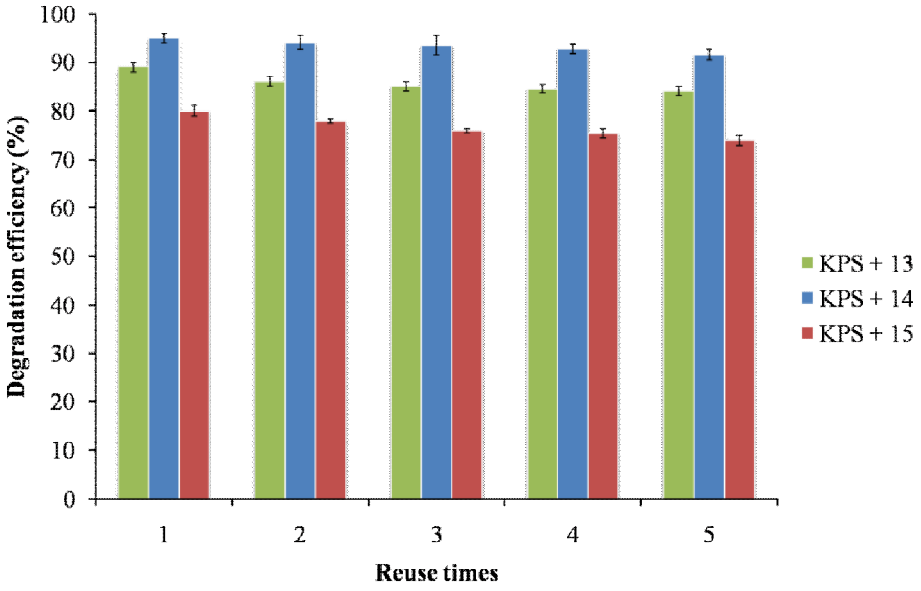

Figure 117. The recyclability of complexes **(13), (14)** and **(15)** with KPS as oxidant for the photodegradation of methyl orange under UV irradiation.

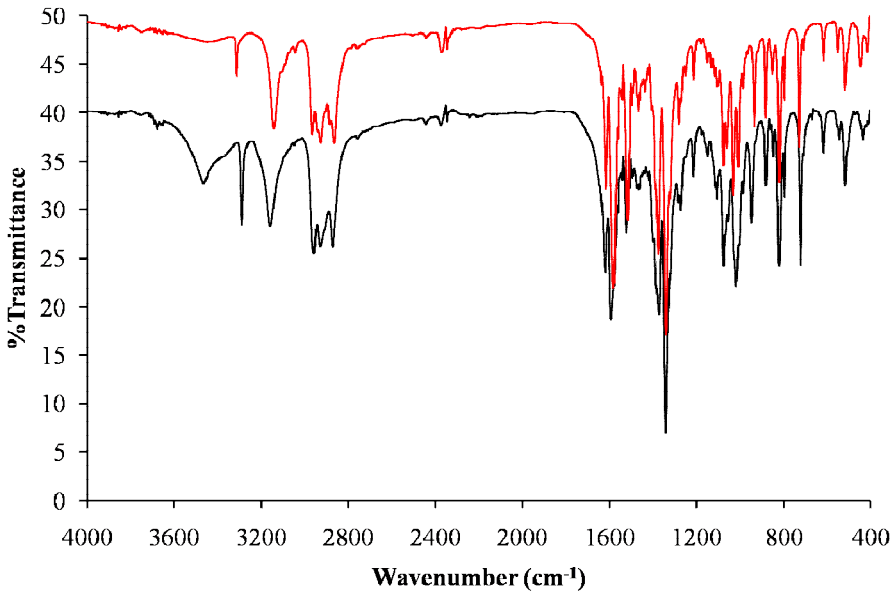

Figure 118. FT-IR spectra of complex **(13)** before (Black) and after (Red) 5 recycles.

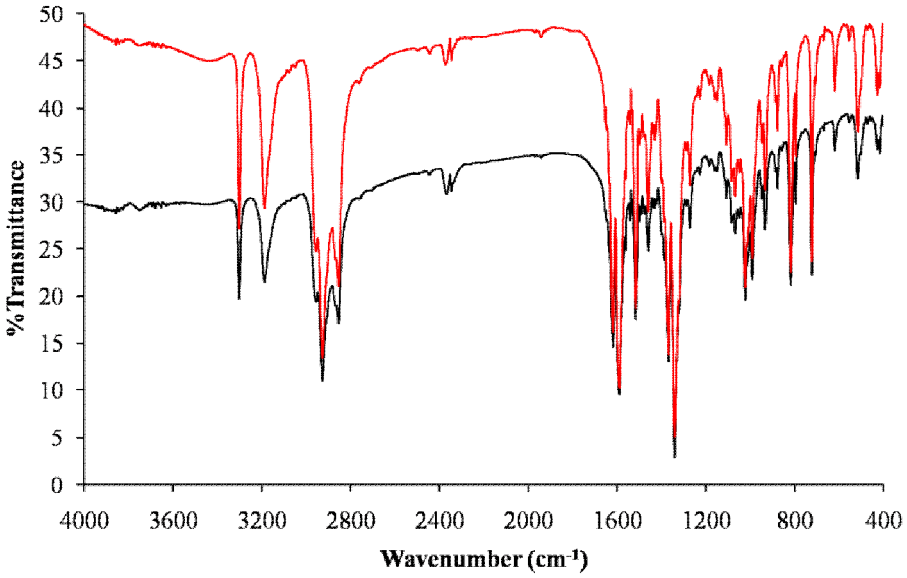

Figure 119. FT-IR spectra of complex **(14)** before (Black) and after (Red) 5 recycles.

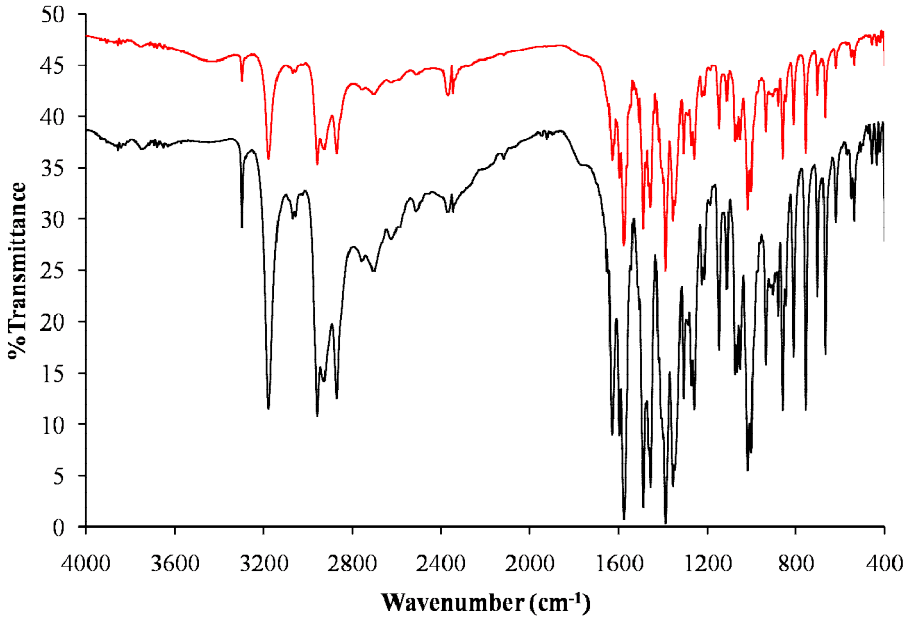

Figure 120. FT-IR spectra of complex **(15)** before (Black) and after (Red) 5 recycles.

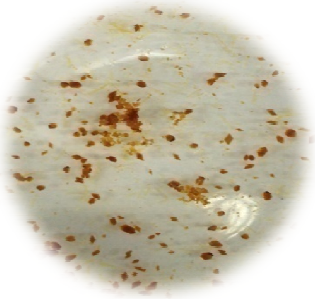

Before UV irradiation of **(13)**

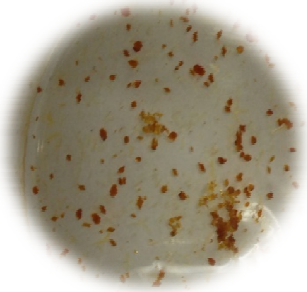

After UV irradiation of **(13)**

Before UV irradiation of **(14)**

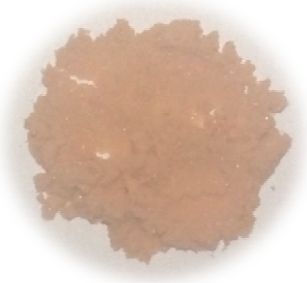

After UV irradiation of **(14)**

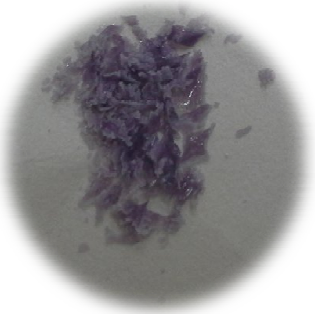

Before UV irradiation of **(15)**

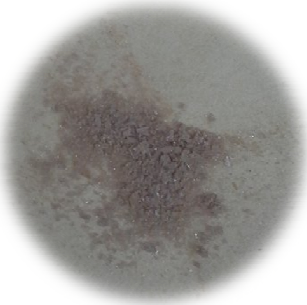

After UV irradiation of **(15)**

Figure 121. Physical appearance of catalysts **(13)** - **(15)**.

3.10 Antibacterial activities

The *in vitro* antibacterial activity of the complexes **(3) - (10)** were investigated against the gram positive (*S. aureus*) and gram negative (*E. coli* and *P. aeruginosa*) using agar disc diffusion method by using DMSO as medium.

The results of the antibacterial activity of the complexes **(3) - (10)** showed lower activity compared to the standard drugs are shown in **Table 28**. Among the synthesized complexes, **(5)** and **(10)** showed higher activity than the others possibly due to the presence of the octylamine and 2-ethyl-1-hexylamine acting as pendant arms in the structure. It is interesting to note the low activity of complex **(6)** with *iso*-butylamine moiety which could be responsible for the low lipophilicity. The lipophilicity relates well with the antibacterial activity and is a very important molecular structure indicator. Lipophilic behavior of complexes plays an important role in their biological activity (Arslan *et al*., 2009). Therefore, the increasing activities of the metal chelates can be described on the basis of Tweedy's chelation theory and Overtone's concept (Tweedy, 1964). According to the Overtone's concept of cell permeability the lipid membrane that surrounds the cell favors the passage of only lipid soluble materials due to which liposolubility is an important factor that controls antibacterial activity. On chelation theory, the polarity of metal ion is degreased to a greater extent because the overlap of the ligand orbital and partial sharing of the positive charge of metal ion with donor groups (Gurumoorthy *et al*., 2012). In addition, it increases the delocalization of the π-electron over the whole chelate ring and enhances the lipophilicity of the complex. This increased lipophilicity enhances the penetration of the metal complexes into lipid membrane and thus blocks the metal binding sites on enzymes of microorganisms (Mounika *et al*., 2010). These metal complexes also badger the respiration process of the cell and thus block the synthesis of proteins, which constrains further growth of the organism (Gupta *et al*., 2012). The modification in the activity of different metal complexes against different organism depend either on the impermeability of the cells of the microbes or difference in ribosomes of microbial cells. There are also other factors that affect the effectiveness of bacterial activity, such as labile of the ligands, nature of the metal

ions or ligands, geometry of the complexes, conductance, electron density, dipole moment, and cell permeability (Jain *et al*., 2016 and Kaushal *et al*., 2013).

Table 28. Inhibition zones and % inhibition of *S. aureus, E. coli,* and *P. aeruginosa* of the complexes **(3) - (10)**.

Complexes	Inhibition zones (mm)			% inhibition		
	S. aureus	*E. coli*	*P. aeruginosa*	*S. aureus*	*E. coli*	*P. aeruginosa*
$[CuL^3(ClO_4)_2]$ **(3)**	12	9.5	11	70.6	63.3	64.7
$[NiL^3](ClO_4)_2$ **(4)**	13	10	12.5	76.5	66.7	73.5
$[CuL^4(ClO_4)_2]$ **(5)**	15	12.5	14	88.2	88.3	82.4
$[CuL^5(ClO_4)_2]$ **(6)**	9.5	9	10	55.9	60.0	58.8
$[NiL^5](ClO_4)_2$ **(7)**	10	10.5	13	58.9	70.0	76.5
$[CuL^6(ClO_4)_2]$ **(8)**	13	10.5	12	76.5	70.0	70.6
$[CuL^7(ClO_4)_2]$ **(9)**	14	11	13.5	82.4	73.3	79.4
$[NiL^7](ClO_4)_2$ **(10)**	14.5	13.5	15	85.3	90.0	88.2
Penicillin	15	14	16	-	-	-
Gentamicin	17	15	17	100	100	100

CHAPTER 4

CONCLUSIONS

This thesis describes the syntheses and characterizations of eleven novel complexes of copper(II) and nickel(II) with hexaazamacrocyclic ligands with primary amines as pendant-arms and perchlorate anions. Three novel nickel(II) complexes were obtained by replacing *p*-nitrobenzoate (or aspirin) in the precursor Ni(II) complexes. Likewise, novel copper(II) complex was obtained from replacing with hexacyanoferrate(III) anion on the precursor Cu(II) complex. The complexes **(3)** - **(10)** were screened for antibacterial activity on gram positive and gram negative bacterial. The complexes **(13)** - **(15)** were tested for catalytic properties on degradation of methyl orange dye with activation of persulfate under UV light irradiation.

Several physicochemical properties and crystal structures of the complexes were measured, i.e., molar conductivity, elemental analyses, thermal analysis, FT-IR, UV-Vis, ESI-mass spectroscopy, powder X-ray diffraction, and single crystal X-ray diffraction. The mass spectra confirmed the proposed structures of the complexes **(1)** - **(11)** by comparing the *m/z* values checked in ESI-mass spectra with the mass of fragments obtained.

The data supported by FT-IR spectra of the complexes **(1)** - **(15)** showed that the hexaazamacrocyclic ligands coordinated to metal ions and it also suggested the presence of perchlorate, carboxylate, and hexaazacyanoferrate(III) anions. In addition, the thermal analysis supported the proposed formula, the nature of water molecules, and the thermal stability of the complexes by giving data concerning the stages corresponding to the thermal releasing with weight loss of them.

The single crystal X-ray determination of the complexes **(5)**, **(7)**, **(8)**, and **(12)** - **(15)** confirmed the crystallographic data, bond distances, bond angles, coordination geometry around metal ions, and weak interactions. Moreover, the purity of the as-synthesized complexes **(5)**, **(7)**, **(8)**, and **(12)** - **(15)** were confirmed by

powder X-ray diffraction. The results showed that the PXRD patterns were identical with the calculated pattern derived from the single crystal data using Mercury 3.8 program, indicating phase purity of the bulk sample.

Antibacterial activities were tested in order to determine inhibition zone (IZ) by agar diffusion method. The results showed that the complexes $[CuL^3(ClO_4)_2]$ **(3)**, $[NiL^3](ClO_4)_2$ **(4)**, $[CuL^4(ClO_4)_2]$ **(5)**, $[CuL^5(ClO_4)_2]$ **(6)**, $[NiL^5](ClO_4)_2$ **(7)**, $[CuL^6(ClO_4)_2]$ **(8)**, $[CuL^7(ClO_4)_2]$ **(9)**, and $[NiL^7](ClO_4)_2$ **(10)** were more active than the starting materials. The complexes with hexaazamacrocyclic ligands derived from *iso*-butyl as pendant arm and ethylenediamine, namely complexes **(6)** and **(7)**, were less active. This action probably related with their low lipophilicity, which resulted in permeation through the cell membrane lipids of microorganisms to cause disease being difficult to occur.

The catalytic properties of the complexes **(13)** - **(15)** with persulfate activation to degrade of methyl orange showed that methyl orange could not be effectively degraded by complexes **(13)** - **(15)** or persulfate anions alone under UV light irradiation. However, the photodegradation of methyl orange was clearly improved when nickel(II) complexes and persulfate anions were used together. The coexistence of the two agents enhanced the generation of hydroxyl and sulfate free radicals, which are the active oxidizing agents for organic dyes.

REFERENCES

Addison, A. W.; Rao, T. N.; Reedijk, J.; Rijn, J. V.; Verschoor, G. C. Synthesis, structure, and spectroscopic properties of copper(II) compounds containing nitrogen-sulphur donor ligands; the crystal and molecular structure of aqua[1,7-bis(*N*-methylbenzimidazol-2′-yl)-2,6-dithiaheptane]copper(II) perchlorate. *J. Chem. Soc., Dalton Trans*. **1984**, 7, 1349-1356.

Arslan, H.; Duran, N.; Borekci, G.; Ozer, C. K.; Akbay, C. Antimicrobial activity of some thiourea derivatives and their nickel and copper complexes. *Molecules*. **2009**, 14(1), 519-527.

Beltrán, A.; Andrés, J. Structure and bonding of chlorine oxides and peroxides: ClO_x, ClO_x^- (x = 1-4), and Cl_2O_x (x = 1-8). *J. Phys. Chem. A*. **1999**, 103(16), 3078-3088.

Bourdolle, A.; Allali, M.; Mulatier, J.-C.; Guennic, B. L.; Zwier, J. M.; Baldeck, P. L.; Büunzli, J.-C. G.; Andraud, C.; Lamarque, L.; Maury, O. Modulating the photophysical properties of azamacrocyclic europium complexes with charge-transfer antenna chromophores. *Inorg. Chem*. **2011**, 50(11), 4987-4999.

Bullen, T. D. Stable isotopes of transition and post-transition metals as tracers in environmental studies. *Handbook of environmental isotope geochemistry, advances in isotope geochemistry*; Springer-Verlag Berlin Heidelberg, 2011; pp 177-203.

Busch, D. H. Reactions of ligands in metal complexes. *Reactions of coordinated ligands and homogeneous catalysis*; American Chemical Society, 1963; pp 1-18.

Cha, M. J.; Shin, J. W.; Shin, Y. H.; Kim, Y.; Kim, B. G.; Min K. S. Structure and magnetic properties of a novel branch-like one-dimensional cyano-bridged assembly $[Cu(L)]_3[Fe(CN)_6]_2 \cdot 8H_2O$ (L = 6,13-dimethyl-6-nitro-1,4,8,11-

tetraazabicyclo[11.1.1]pentadecane). *Inorg. Chem. Commun*. **2009**, 12(6), 520-522.

Chandra, S.; Jain, D.; Sharma, A. K.; Sharma, P. Coordination modes of a Schiff base pentadentate derivative of 4-aminoantipyrine with cobalt(II), nickel(II) and copper(II) metal ions: Synthesis, spectroscopic and antimicrobial studies. *Molecules*. **2009**, 14(1), 174-190.

Cho, J.; Lough, A. J.; Kim, J. C. Monomeric and polymeric copper(II) hexaaza macrocyclic complexes with btc anions (btc = 1,2,4,5-benzenetetra-carboxylic acid). *Inorg. Chim. Acta*. **2003**, 342, 305-310.

Choi, H. J.; Suh, M. P. Self-assembly of molecular brick wall and molecular honey-comb from nickel(II) macrocycle and 1,3,5-benzenetricarboxylate: Guest-dependent host structures. *J. Am. Chem. Soc*. **1998**, 120(41), 10622-10628.

Choi, H. J.; Suh, M. P. Synthesis, crystal structure, and properties of a 3-D network assembled by nickel(II) macrocyclic complex and terephthalato bridge. *J. Am. Chem. Soc*. **1999**, 38(26), 6309-6312.

Christensen, J. J.; Eatough, D. J.; Izatt, R. M. The synthesis and ion bindings of synthetic multidentate macrocyclic compounds. *Chem. Rev*. **1974**, 74(3), 351-384.

Chu, I. K.; Rodriguez, C. F.; Hopkinson, A. C.; Siu, K. W. M. Formation of molecular radical cations of enkephalin derivatives *via* collision-induced dissociation of electrospray-generated copper(II) complex ions of amines and peptides. *J. Am. Soc. Mass Spectrom*. **2001**, 12(10), 1114-1119.

Curtis, N. F.; House, D. A. Structure of some aliphatic Schiff base complexes of nickel(II) and copper(II). *Chem. Ind*. **1961**, 42, 1708-1709.

Degagsa, B.; Faye, G.; Fernandez, N. Synthesis, characterization and antimicrobial activity of hexamethylenetetramine copper(II) complex. *World J. Pharm. Pharma. Sci*. **2013**, 2(6), 6391-6404.

Elizbarashvili, E.; Matitaishvili, T.; Topuria, K. Synthesis of macrocyclic polyazomethines. *J. Braz. Chem. Soc*. **2007**, 18(6), 1254-1258.

Feng, Z.-Q.; Yang, X.-L.; Ye, Y.-F. Synthesis, crystal structures, luminescence, biological and catalytic properties of two d^{10} metal-organic coordination polymers constructed from mixed ligands. *J. Inorg. Organomet. Polym*. **2014**, 24(4), 684-693.

Fukuzumi, S.; Jung, J.; Yamada, Y.; Kojima, T.; Nam, W. Homogeneous and heterogeneous photocatalytic water oxidation by persulfate. *Chem. Asian J*. **2016**, 11(8), 1138-1150.

Gaikwad, V. K.; Yadav, U. M. Metal complexes of Schiff bases. *Scholarly Res. J. Int. Stud*. **2016**, 3(24), 2225-2234.

Goeta, A. E.; Howard, J. A. K.; Maffeo, D.; Puschmann, H.; Williams, J. A. G.; Yufit, D. S. Copper(II) complexes of the isomeric tetraazamacrocyclic ligands 1,11- and 1,8-bis(2-pyridylmethyl)-1,4,8,11-tetraazacyclotetradecane and of the 1,4,8,11-tetraazacyclotetradecane-5,12-dione analogue at neutral and basic pH. *J. Chem. Soc., Dalton Trans*. **2000**, 12, 1873-1880.

Gokulakrishnan, S.; Parakh, P.; Prakash, H. Degradation of malachite green by potassium persulphate, its enhancement by 1,8-dimethyl-1,3,6,8,10,13-hexaazacyclotetradecane nickel(II) perchlorate complex, and removal of antibacterial activity. *J. Hazard. Mater*. **2012**, 213-214, 19-27.

Gokulakrishnan, S.; Nalawade, P.; Hinder, S. J.; Pillai, S. C.; Prakash, H. Nickel azamacrocyclic complex activated persulphate based oxidative degradation of methyl orange: Recovery and reuse of complex using adsorbents. *RSC. Adv*. **2015**, 5, 31716-31724.

Gupta, R.; Agrawal, N.; Gupta, K. C. Synthesis, IR spectral studies and biological activities of some rare earth metal complexes with biochemically relevant ligand. *Res. J. Pharm., Bio. Chem. Sci*. **2012**, 3(2), 50-56.

Gurumoorthy, P.; Ravichandran, J; Karthikeyan, N.; Palani, P.; Rahiman, A. K. Template synthesis of polyaza macrocyclic copper(II) and nickel(II) complexes: Spectral characterization and antimicrobial studies. *Bull. Korean Chem. Soc*. **2012**, 33(7), 2279-2286.

Haines, R. I.; Rowley, J. E. Structure and kinetics of oxidation of amphiphilic nickel(II) pentaazamacrocycles by peroxodisulfate and by a nickel(III) pendant-arm macrocycle. *J. Incl. Phenom. Macrocycl. Chem*. **2003**, (47), 25-32.

Han, J. H.; Cha, M. J.; Kim, B. G.; Kim, S. K.; Min, K. S. Synthesis and characterization of macrocyclic nickel(II) complexes with α-methylbenzyl groups as chiral pendants. *Inorg. Chem. Commun*. **2008**, 11(7), 745-748.

Han, S.; Kim, T.; Lough, A. J.; Kim, J. C. Synthesis, structures and properties of macrocyclic nickel(II) supramolecules with imidazole pendants. *Inorg. Chim. Acta*. **2011**, 370(1), 170-174.

Hathaway, B. J.; Billing, D. E. The electronic properties and stereochemistry of mono-nuclear complexes of the copper(II) ion. *Cooridin. Chem. Rev*. **1970**, 5(2), 143-207.

He, Y.; Kou, H.-Z.; Li, Y.; Zhou, B. C.; Xiong, M.; Li, Y. One-pot template synthesis and crystal structure of two new polyaza copper(II) complexes. *Inorg. Chem. Commun*. **2003**, 6(1), 38-42.

Huan, D.-H.; Zhao, Y.-Q.; Dong, G.-Y.; Yin, F.-J.; Wang, S.-C. Synthesis, crystal structures and photocatalytic properties of four silver(I) coordination polymers based on semirigid bis(pyrazole) and carboxylic acid co-ligands. *Transit. Met. Chem*. **2016**, 41(6), 701-712.

Huang, K. C.; Zhao, Z., Hoag, G. E.; Dahmani, A.; Block, P. A. Degradation of volatile organic compounds with thermally activated persulfate oxidation. *Chemosphere*. **2005**, 61(4), 551-560.

Husain, A.; Nami, S. A. A.; Siddiqi, K. S. The synthesis, crystal structures and antimicrobial studies of *C*-methyl-substituted hexaaza macrocycle of Cu(II) having aromatic pendant arm. *Appl. Organometal. Chem*. **2011**, 25(10), 761-768.

Husain, A.; Moheman, A.; Nami, S. A. A.; Siddiqi, K. S. Fourteen membered hexaaza copper macrocycle: Synthesis, characterization, crystal structures and the consequence of anion coordination. *Inorg. Chim. Acta*. **2012**, 384, 309-317.

Jain, P.; Singh, V. Pharmacological activity of newly synthesized and characterized N, O-donor tetraaza macrocyclic metal complexes. *Asian J. Pharm*. **2016**, 10(4), 612-622.

Jiao, C.-H.; He, C.-H.; Geng, J.-C.; Cui, G.-H. Synthesis, crystal structures and catalytic properties of two 1D cobalt(II) coordination polymers. *Transit. Met. Chem*. **2012**, 37(1), 17-23.

Kamboj, M.; Singh, D. P. Macrocyclic complexes: Potent molecules against drug resistant microbes. *Int. J. Curr. Res. Chem. Pharm. Sci*. **2016**, 3(4), 15-22.

Kang, S.-G.; Jung, S.-K.; Kweon, J. K. Synthesis and characterization of new nickel(II) and copper(II) complexes of the hexaaza macrobicyclic ligand 8-methyl-1,3,6,8,10,13-hexaazabicyclo[11,2,1] hexadecane. *Bull. Korean Chem. Soc*. **1990**, 11(5), 431-434.

Kang, S.-G.; Ryu, K.; Jung, S.-K.; Kim, J. Template synthesis, crystal structure, and solution behavior of a hexaaza macrocyclic nickel(II) complex containing two *N*-aminoethyl pendant arms. *Inorg. Chim. Acta*. **1999**, 293(2), 140-146.

Kaushal, R.; Kumar, N.; Awasthi, P.; Nehra, K. Syntheses, characterization, and antibacterial study of titanium complexes. *Turk. J. Chem*. **2013**, 37(6), 936-945.

Kim, J. C.; Lough, A. J.; Kim, H. Structurally different nickel(II) hexaazamacrocyclic complexes with the same btc^{2-} anions (btc^{2-} = 1,2,4,5-benzenetetra-carboxylic acid dianion). *Inorg. Chem. Commun*. **2002**, 5(10), 771-776.

Kim, J. C.; Kim, J. A.; Kang, Y. C. Synthesis, characterization and single crystal structures of one-dimensional coordination polymers formed with $[Ni(L)]\cdot 2ClO_4$ and polycarboxylate ligands. *Transit. Met. Chem*. **2006**, 31(6), 829-833.

Kim, T.; Lough, A. J.; Kim, J. C. Template syntheses, crystal structures and supramolecular assembly of hexaaza macrocyclic copper(II) complexes. *Bull. Korean Chem. Soc*. **2013**, 34(6), 1913-1916.

Kongchoo, S.; Kantacha, A.; Saithong, S.; Wongnawa, S. Synthesis, crystal structure, and spectroscopic properties of Cu(II) complex with 14-membered hexaaza macrocyclic ligands. *J. Chem. Crystallogr*. **2016**, 46(5), 222-229.

Kou, H.-Z.; Gao, S.; Bai, O.; Wang, Z.-M. Magnetic characteristics of new cyano-bridged two-dimensional honeycomb-like bimetallic assemblies containing Ni(II)-N≡C-Cr(III) or Ni(II)-N≡C-Cr(I) linkages. *Inorg. Chem*. **2001**, 40(24), 6287-6294.

Kou, H.-Z.; Gao, S.; Ma, B.-Q.; Liao, D.-Z. A cyano-bridged molecular magnet with a novel two-dimensional brick wall structure. *Chem. Commun*. **2000**, 1309-1310.

Kou, H.-Z.; Jiang, Y.-B.; Zhou, B. C.; Wang, R.-J. Cyano-bridged 2D Cu^{II}-Cr^{III} coordination polymers: Structural evidence for formation of a polymeric macrocyclic metallic compound. *Inorg. Chem*. **2004**, 43(10), 3271-3276.

León-Rodríguez, L. M. D.; Ortiz, A.; Weiner, A. L.; Zhang, S.; Kovacs, Z.; Kodadek, T.; Sherry, A. D. Magnetic resonance imaging detects a specific peptide-protein binding event. *J. Am. Chem. Soc*. **2002**, 124(14), 3514-3515.

Li, X.-Z.; Yang, G.-M.; Liao, D.-Z.; Jiang, Z.-H.; Yan, S.-P. Crystal and molecular structure of a nickel(II) complex with a macrocyclic $[14]N_4$ ligand. *J. Chem. Crystallogr*. **2003**, 33(1), 5-9.

Li, Y.-W.; Xiang, H.; Lu, T.-B.; Ng, S. W. [1,8-Bis(2-benzyl)-1,3,6,8,10,13-hexaaza cyclotetradecane]nickel(II) diperchlorate. *Acta Crystallogr. E*. **2004**, 60, 309-311.

Li, Y.-W.; Xiang, H.; Lu, T.-B.; Ng, S. W. (1,8-Di-*n*-propyl-1,3,6,8,10,13-hexaaza cyclotetradecane)nickel(II) diperchlorate. *Acta Crystallogr. E*. **2004**, 60, 312-313.

Li, H. H.; Ma, Y. J.; Zhao, Y. Q.; Cui, G. H. Synthesis and characterization of three cobalt(II) coordination polymers with tetrabromoterephthalic acid and flexible bis(benzimidazole) ligands. *Transit. Metal Chem*. **2015**, 40(1), 21-29.

Lim, J. H.; Yoon, J. H.; Choi, S. Y.; Ryu, D. W.; Koh, E. K.; Hong, C. S. Cyano-bridged pentanuclear and honeycomblike $M^{III}Cu^{II}$ (M = Fe, Cr) bimetallic assemblies: Structural variations modulated by side groups of macrocyclic ligands and magnetic properties. *Inorg. Chem*. **2011**, 50(5), 1749-1757.

Lindoy, L. F. Synthetic procedures. *Molecular Biology, Biochemistry, and Structural Biology, Inorganic Chemistry, Chemistry, Life Sciences*. Cambridge University Press. 1989: pp 21-50.

Liu, Y.; Zhang, G.; Fang, S.; Chong, S.; Zhu, J. Degradation of aniline by heterogeneous Fenton's reaction using a Ni-Fe oxalate complex catalyst. *J. Environ. Manage*. **2006**, 182, 367-373.

Lu, T.-B.; Xiang, H.; Chen, S.; Su, C.; Yu, K.; Mao, Z.; Cheng, P.; Ji, L. $[CuL(H_2O)_2]\{[CuL][Fe(CN)_6]\}_2 \cdot 2H_2O$ (L=3,10-Bis(2-hydroxyethyl-1,3,5,-8,10,12-hexaazacyclotetradecane): A novel three-dimensional coordination polymer via H-bonded linkages of one-dimensional zigzag chain. *J. Inorg. Organomet. P*. **1999**, 9(3), 165-178.

Lu, T.-B.; Xiang, H.; Luck, R. L.; Mao, Z.-W.; Chen, X.-M.; Ji, L.-N. Molecular architecture via coordination and multi-intermolecular interactions Synthesis, structures and magnetic properties of one-dimensional

coordination polymers of macrocyclic nickel(II) complexes with terephthalate and *trans*-butene dicarboxylate. *Inorg. Chim. Acta*. **2003**, 355, 229-241.

Min, K. S.; Suh, M. P. Construction of various supramolecules by π-π interactions: Self-assembly of nickel(II) macrocyclic complexes containing pyridine pendant arms with bidentate ligands. *Eur. J. Inorg. Chem*. **2001**, 2001(2), 449-455.

Min, K. S.; Park, M. J.; Ryoo, J. J. Synthesis and chiral recognition of nickel(II) macrocyclic complex with (*R*)-naphthylethyleneamine pendant groups and its self-assembled framework. *Chirality*. **2013**, 25(1), 54-58.

Ming, C.-L.; Hao, Z.-C.; Yu, B.-Y.; Hecke, K. V.; Cui, G.-H. Synthesis, structures, and catalytic properties of three new metal-organic coordination polymers constructed from flexible benzimidazole-based and *cis*-1,2-cyclohexane-dicarboxylate synthons. *J. Inorg. Organomet. Polym*. **2015**, 25(3), 559-568.

Mohammed, A. A.; Al-daher, A. G. M.; Mohamad, H. A.; Harrison, R. G. Synthesis and characterization of polydentate macrocyclic Schiff bases (18-membered atoms) and their complexes with cobalt (II), nickel (II), copper (II) and zinc (II) ions. *Int. J. Enh. Res. Sci. Tech. & Eng*. **2015**, 4(6), 440-447.

Mounika, K.; Anupama, B.; Pragathi, J.; Gyanakumari, C. Synthesis, characterization and biological activity of a Schiff base derived from 3-ethoxy salicylalde-hyde and 2-amino benzoic acid and its transition metal complexes. *J. Sci. Res*. **2010**, 2(3), 513-524.

Mulaudzi, R. B.; Ndhlala, A. R.; Kulkarni, M. G.; Finnie, J. E.; Staden, J. V. Antimicrobial properties and phenolic contents of medicinal plants used by the Venda people for conditions related to venereal diseases. *J. Ethnopharmacol*. **2011**, 135(2), 330-337.

Nair, M. L. H.; Lalitha, K. P. Synthesis, physicochemical characterization and structure determination of some novel nickel (II) complexes. *IOSR. J. Appl. Chem*. **2014**, 6(6), 15-20.

Odola, A. J.; Woods, J. A. O. New nickel(II) mixed ligand complexes of dithiocarbamates with Schiff base. *J. Chem. Pharm. Res*. **2011**, 3(6), 865-871.

Olar, R.; Badea, M.; Marinescu, D.; Iorgulescu, E. E.; Frunza, E.; Lazar, V.; Chifiriuc, C. Thermal, spectral and antimicrobial study on some Cu(II) complexes with ligands bearing biguanide moieties. *J. Therm. Anal. Calorim*. **2010**, 99(3), 815-821.

Park, J. H.; Jeong, A. R.; Hastuti, D. K. A. K.; Jeong, M. J.; Min, K. S. Self-assembly of functional macrocyclic metal complexes and 4-(phenylazo)benzoic acid: preparation, structure, and photoluminescence. *J. Incl. Phenom. Macrocycl. Chem*. **2015**, 82(1), 153-162.

Park, J. H.; Jeong, A. R.; Shin, J. W.; Jeong, M. J.; Cho, C. S.; Min, K. S. Self-assembly and guest binding of nickel(II) macrocyclic complex with pentyl groups and *cis,cis*-1,3,5-cyclohexanetricarboxylic acid. *Inorg. Chem. Commun*. **2015**, 57, 44-46.

Pătraşcu, F.; Badea, M.; Grecu, M. N.; Stanică, N.; Măruțescu, L.; Marinescu, D.; Spînu, C.; Tigae, C.; Olar, R. Thermal, spectral, magnetic and antimicrobial behaviour of new Ni(II), Cu(II) and Zn(II) complexes with a hexaaza-macrocyclic ligand. *J. Therm. Anal. Calorim*. **2013**, 113(3), 1421-1429.

Peternel, I.; Kusic, H.; Marin, V.; Koprivanac, N. UV-assisted persulfate oxidation: the influence of cation type in the persulfate salt on the degradation kinetics of an azo dye pollutant. *Reac. Kinet. Mech. Cat*. **2013**, 108(1), 17-39.

Pokrovsky, O. S.; Viers, J.; Emnova, E. E.; Kompantseva, E. I.; Freydier, R. Copper isotope fractionation during its interaction with soil and aquatic

microorganisms and metal oxy(hydr)oxides: Possible structural control. *Geochim. Cosmochim. Acta*. **2008**, 72(7), 1742-1757.

Qin, L.; Liu, L.-W.; Du, X.; Cui, G.-H. Two dinuclear copper(II) complexes based on 5,6-dimethylbenzimidazole ligands: synthesis, crystal structures, and catalytic properties. *Transit. Met. Chem*. **2013**, 38(1), 85-91.

Ramesh, P.; Revathi, M.; Ammar, A.; Mohammeda, N. A. A.; Siddappa, S.; Reddy, P. M.; Pasha, C. Copper(II) complexes of new carboxyamide ligands: Synthesis, spectroscopic and antibacterial study. *Int. J. Adv. Res. Chem. Sci*. **2016**, 3(8), 1-8.

Samanta, B.; Chakraborty, J.; Shit, S.; Batten, S. R.; Jensen, P.; Mitra, S. Synthesis, characterization and crystal structure of a copper(II) dichromate complex with the *N,N'*-bis(2-pyridylmethylene)butane-1,4-diamine Schiff base ligand. *Z. Naturforsch*. **2007**, 62(4), 495-500.

Sánchez-Polo, M.; Salhi, E.; Rivera-Utrilla, J.; Gunten, U. V. Combination of ozone with activated carbon as an alternative to conventional advanced oxidation processes. *Ozone Sci. Eng*. **2006**, 28(4), 237-245.

Shakir, M.; Azim, Y.; Chishti, H. T. N.; Begum, N.; Chingsubam, P.; Siddiqi, M. Y. Synthesis, physico-chemical and antimicrobial screening studies on 14 and 16-membered hexaazamacrocyclic complexes bearing pendant amine groups. *J. Braz. Chem. Soc*. **2006**, 17(2), 272-278.

Shen, L.; Wang, H.-T.; Zhang, Y.-J.; Jin, Z.-M. *catena*-Poly[[[1,8-bis(2-hydroxyethyl)-1,3,6,8,10,13-hexaazacyclotetradecane]copper(II)]-μ-cyano-[tricyanonitrosoiron(III)]-μ-cyano]. *Acta Crystallogr. C*. **2004**, 60, 180-182.

Shen, X.-P.; Xu, Y.; Zhou, H.; Shu, H.-Q.; Yuan, A.-H. Crystal structure and magnetic properties of a cyano-bridged bimetallic assembly $[CuL^4]_3$-$[Fe(CN)_6]_2 \cdot 2H_2O$ (L^4 = 3,10-dibutyl-1,3,5,8,10,12-hexaazacyclotetradecane). *J. Mol. Struct*. **2008**, 892(1-3), 58-62.

Shih, M.-H.; Xu, Y.-Y.; Yang, Y.-S.; Lin, T.-T. Syntheses of nickel (II) complexes from novel semicarbazone ligands with chloroformylarylhydrazine, benzimidazole and salicylaldehyde moieties. *Molecules*. **2015**, 20(3), 5184-5201.

Shin, J. W.; Yeo, S. M.; Min, K. S. Copper(II) coordination compounds containing chiral functional groups as pendants: Syntheses, crystal structures, and physical properties. *Inorg. Chem. Commun*. **2012**, 22, 162-166.

Shin, J. W.; Kim, D.-W.; Moon, D. Syntheses and characterization of various supramolecular compounds from the self-assembly of nickel(II) hexaaza macrocyclic complex with carboxylic acid derivatives. *Polyhedron*. **2016**, 105, 62-70.

Singh, C.; Rakesh, M. Oxidation of phenol using $LaMnO_3$ perovskite, TiO_2, H_2O_2 and UV radiation. *Indian J. Chem. Technol*. **2010**, 17(6), 451-454.

Stănilă, A.; Braicu, C.; Stănilă, S.; Pop, R. M. Antibacterial activity of copper and cobalt amino acids complexes. *Not. Bot. Horti. Agrobo*. **2011**, 39(2), 124-129.

Su, Y.-H.; Liu, J.; Li, J.; Si, X.-Z. Synthesis, crystal structures and properties of two novel macrocyclic nickel(II) and copper(II) complexes. *J. Mol. Struct*. **2007**, 837(1-3), 257-262.

Suh, M. P.; Kang, S.-G. Synthesis and properties of nickel(II) and copper(II) complexes of 14-membered hexaaza macrocycle, 1,8-dimethyl- and 1,8-diethyl-1,3,6,810,13-hexaazacyclotetradecane. *Inorg. Chem*. **1988**, 27(14), 2544-2546.

Sujatha, S.; Balasubramanian, S.; Varghese, B. Synthesis, structural, spectral, electrochemical and spin equilibrium studies of hexaaza macrotricyclic complexes. *Polyhedron*. **2009**, 28(17), 3723-3730.

Taner, B. Novel *vic*-dioxime ligand containing calix[4]pyrrole moiety: synthesis, characterization, anion binding studies and complexation with Ni(II). *J. Incl. Phenom. Macrocycl. Chem*. **2014**, 79(1), 75-81.

Tao, B.; Cheng, F.; Jiang, X.; Xia, H. Synthesis, crystal structures and luminescent properties of nickel(II) and copper(II) hexaazamacrocyclic compounds with 1,3,5-benzenetricarboxylate ligands. *J. Mol. Struct*. **2012**, 1028, 176-180.

Taraszewska, J.; Sadlo, J.; Michalik, J.; Korybut-Daszkiewicz, B. Stability and ESR spectra of Ni(III) tetraazamacrocyclic complexes in nitrate and chloride solutions. *Polish J. Chem*. **2000**, 74(6), 813-822.

Tweedy, B. G. Plant extracts with metal ions as potential antimicrobial agents. *Phytopathology*. **1964**, 55, 910-914.

Uddin, M. N.; Akter, J.; Manchur, M. A. Cyano bridged bimetallic compounds of the type M^{2+}-NC-Fe^{3+} (M = Co, Ni, Cu, Zn, Cd) using the $[Fe(CN)_6]^{3-}$ building block and their antibacterial evaluation. *Orbital: Electron. J. Chem*. **2013**, 5(4), 257-263.

Uddin, M. N.; Chowdhury, D. A.; Akter, J. Bimetallic heteronuclear complexes bridged with ferrichexathiocyanate: synthesis, characterization and antibacterial properties. *J. Pure App. Chem. Res*. **2014**, 3(3), 99-107.

Wang, X. X.; Zhao, Y. N.; Li, G. Y.; Cui, G. H. Self-assembly of two 2D cobalt(II) coordination polymers constructed from 5-*tert*-butyl isophthalic acid and flexible bis(benzimidazole)-based ligands. *Transit. Met. Chem*. **2014**, 39(6), 653-660.

Xiang, H.; Lu, T.-B.; Chen, S.; Mao, Z.-W.; Feng, X.-L.; Yu, K.-B. Macrocyclic nickel(II) complexes with a folded conformation. Synthesis, properties and structures of $[NiL(en)][Ni(en)_3](ClO_4)_4$ and $[(NiL)_2(\mu\text{-}ox)](ClO_4)_2$ (L = 3,10-bis(2-hydroxyethyl)-1,3,5,8,10,12-hexaazacyclotetradecane, en = ethylenediamine, ox = oxalate anion). *Polyhedron*. **2001**, 20(3-4), 313-319.

Xiao-Bing, L.; Ze-Ting, Z.; Yan-Yan, W.; Rui, L. Hydrothermal syntheses, crystal structures, and characterization of two zinc(II) complexes containing flexible bis(benzimidazole) ligands. *Chinese J. Struct. Chem*. **2016**, 35(11), 1745-1753.

Yang, R.; Zompa, L. J. Metal complexes of cyclic triamines. Complexes of 1,4,7-triazacyclononane ([9]aneN_3) with nickel(II), copper(II), and zinc(II). *Inorg. Chem*. **1976**, 15(7), 1499-1502.

Zelĕnák, V.; Vargova, Z.; Gÿoryova, K. Correlation of infrared spectra of zinc(II) carboxylates with their structures. *Spectrochimica Acta A*. **2007**, 66(2), 262-272.

Zhang, K.-L.; Xu, Y.; Wang, Z.; Jin, C.-M.; You, X.-Z. Synthesis, crystal structure and magnetic properties of the first dinuclear copper(II)-iron(II) complex [Cu(L)Fe$(CN)_5$NO] based on nitroprusside. *Transit. Met. Chem*. **2002**, 27(1), 95-98.

Zhou, B.-C.; Kou, H.-Z.; Li, Y.; Xiong, M.; Wang, R.-J. Synthesis, characterization and crystal structure of the first trinuclear MFe_2 (M = Cu and Ni) complexes based on nitroprusside. *Chiese J. Chem*. **2003**, 21(9), 1159-1164.

APPENDICES

PACCON 2015

Proceedings

"Innovative Chemistry for Sustainability of the AEC and Beyond"

21st - 23rd January 2015

Amari Watergate Hotel
Bangkok, Thailand

Organized by The Chemical Society of Thailand
under the Patronage of Her Royal Highness Princess Chulabhorn Mahidol

Coorganized by Department of Chemistry Faculty of Science
King Mongkut's University of Technology Thonburi

PACCON
PURE AND APPLIED CHEMISTRY INTERNATIONAL CONFERENCE 2015

"Innovative Chemistry for Sustainability of the AEC and Beyond"

26 November, 2014

Notification of acceptance of the PACCON 2015

The abstract ID 81 Title "Synthesis and Characterization of Copper(II) and Nickel(II) Complexes of Hexaazamacrocyclic Ligands"

Dear Mr.Surachai Kongchoo

First of all, thank you for your interest in joining the Pure and Applied Chemistry International Conference (PACCON 2015) on January 21-23, 2015 in Bangkok, Thailand. We are delighted to inform you that your abstract has been accepted for Poster presentation in "Inorganic Chemistry" session at PACCON 2015.

For your registration, please do finish important 2 steps on time as follows:

1. Finish the payment by 28th November 2014 to guarantee your highlight abstract published in the highlight abstract book.
2. Upload a copy of your payment documentation to your registration account. (Students are required to attach a copy of student ID card or a certification letter from their institutions/supervisors confirming the respective condition to the registration account.)

If you have any questions, please feel free to contact us via paccon2015@kmutt.ac.th.

For the most updated information on the conference, please visit the conference website at http://paccon2015.kmutt.ac.th .

Again, congratulations. We are looking forward to meeting you in Bangkok.

Yours sincerely,

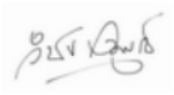

Assoc. Prof. Dr. Winai Somboon
Chairperson, Local Organization Committee PACCON2015
King Mongkut's University of Technology Thonburi

Pure and Applied Chemistry International Conference Organizer
126 Pracha Uthit Rd, Bangmod, Thung Khru, Bangkok 10140, THAILAND

Tel: +662 470 8843 and +662 270 8840 E-mail: paccon2015@kmutt.ac.th

SYNTHESIS AND CHARACTERIZATION OF COPPER(II) AND NICKEL(II) COMPLEXES OF HEXAAZA MACROCYCLIC LIGANDS

Surachai Kongchoo[1], Anob Kantacha[2], and Sumpun Wongnawa[1*]

[1] Department of Chemistry, Faculty of Science, Prince of Songkla University, Hat Yai, Songkhla, 90112, Thailand
[2] Department of Chemistry, Faculty of Science, Thaksin University, Patthalung, 93110, Thailand

* E-mail for Corresponding Author; E-mail: sumpun.w@psu.ac.th, Tel. +66 7428 8443, Fax. +66 7455 8841

Abstract: Two new complexes, $[CuL](ClO_4)_2$ (1) and $[NiL](ClO_4)_2$ (2), of the hexaaza macrocyclic ligand 3,10-dioctyl-1,3,5,8,10,12-hexaazacyclotetradecane (L), were synthesized by one-pot condensation of ethylenediamine, formaldehyde, and octylamine in the presence of copper(II) and nickel(II) salts, respectively. The complexes were characterized by elemental analyses (CHN/O), liquid chromatography-mass spectrometry (LC-MS), Fourier-transformed infrared spectroscopy (FT-IR), and UV-Vis spectroscopy. Data from these techniques indicated that each metal ion combined with one ligand L and two perchlorate anions. The structures of these two complexes were then proposed to consist of metal-ion center, Ni(II) or Cu(II), coordinated to a square-planar geometry by four secondary amine nitrogen donors of the hexaaza macrocyclic ligand with two perchlorato ligands to counter ion molecule the square planar geometry.

1. Introduction

N-donor atoms hexaaza macrocyclic complexes bearing pendant arms connected by an additional bridge (e.g. $-(CH_2)_n-$) at one or two pairs of nitrogen atoms of a macrocycle have received much attention [1] due to possible applications in catalysis [2-3], photocatalytic [4], magnetic properties [5], and antimicrobial activity [6]. Macrocyclic complexes of transition metals, particular, nickel(II) and copper(II), are currently widely used as building blocks for construction of new materials. One of the obvious advantages of such compounds along with their high thermodynamic stability and kinetic inertness is the possibility of synthetically convenient chemical modification of macrocyclic framework using the one-pot condensation methods [7]. The metal ions as templates and many macrocyclic ligands have been prepared by the condensation of formaldehyde with amide. Template synthesis of macrocyclic complexes is simple reaction as formaldehyde links between two amine moieties to form methylenediamine linkages ($-N-CH_2-N-$). The methylenediamine linkage is unstable when it contains primary amines, $R-NH_2$, in which R is either aromatic or aliphatic group which can condense with formaldehyde to form a new N-C bond [8].

In this work, we report the syntheses of the complexes of Cu(II) and Ni(II) with hexaaza macrocyclic ligand, and characterizations by spectroscopy techniques.

2. Materials and Methods

2.1 Materials and physical measurements

All chemicals were obtained from commercial sources and were reagent grade. Absolute ethanol was used throughout this synthesis. Infrared spectra of solid samples as KBr pellets were recorded on a Perkin-Elmer Spectrum One FT-IR spectrophotometer in the range 4000-400 cm^{-1}. Electronic absorption spectra were obtained on a Shimadzu Lambda-1600 UV-Vis spectrophotometer. Elemental analysis of CHNO was performed using a CE instruments Flash EA 1112 series, Thermo Quest analyzer. Mass spectra were recorded by electro-spray ionization (ESI) technique operating in the positive ion mode, the solution was injected directly in mass spectrometer (Waters micromass).

Caution! Perchlorate salts are potentially explosive and should be handled in small quantities.

2.2 Synthesis of $[CuL](ClO_4)_2$ (1)

To a stirred solution of copper(II) chloride dihydrate (1 mmol) and ethylenediamine (2 mmol) in absolute ethanol added dropwise a solution of formaldehyde (4 mmol) and octylamine (2 mmol) in absolute ethanol (15 mL). The reaction mixture was refluxed for 24 h. The hot solution was filtered, cooled and perchloric acid was added slowly. The precipitate formed was filtered off, washed with absolute ethanol, and dried in air. Yield: ~75%. *Anal.* Calc. for $C_{24}H_{54}N_6O_8Cl_2Cu$: C, 41.72; H, 7.88; N, 12.17; O, 17.78. Found C, 41.45; H, 7.81; N, 12.52; O, 17.88%.

2.3 Synthesis of $[NiL](ClO_4)_2$ (2)

Complex **2** was prepared similarly to that of complex **1** except that nickel(II) chloride hexahydrate was used instead of copper(II) salt. Yield: ~50%. *Anal.* Calc. for $C_{24}H_{54}N_6O_8Cl_2Ni$: C, 41.92; H, 7.87; N, 12.25; O, 24.68. Found C, 41.62; H, 7.81; N, 12.36; O, 24.74%.

3. Results and Discussion

The hexaaza macrocyclic complexes were synthesized in a one-pot condensation from the starting materials: copper(II) chloride dihydrate (or nickel(II) chloride hexahydrate), ethylenediamine, formaldehyde, and octylamine with in molar ratio 1:2:4:2 according to Scheme 1. The powder products

were soluble in organic solvents such as DMSO, MeCN, DMF, and acetone. Unfortunately, all efforts failed to grow single crystal suitable for X-ray crystallography.

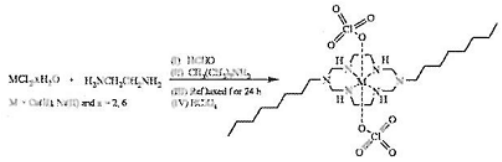

Scheme 1. The preparation of **1** and **2** complexes

3.1 FT-IR spectra of **1** and **2**

The preliminary investigation of the hexaaza-macrocyclic complexes was done from their FT-IR spectra (Figure 1.). The FT-IR of **1** and **2** showed the absence of a strong band in the range 1720-1740 cm^{-1} assignable to carbonyl group of aldehydic moiety confirming the condensation reaction [9]. However, the both complexes a weak band at 1638 cm^{-1} was assigned to δ(O-H) of the moisture. The complexes showed the presence of sharp band around 3241 and 3206 cm^{-1} corresponding to ν(N-H) of the coordinated secondary amine of the **1** and **2**, respectively. A medium intensity band appearing in the range 2927-2857 cm^{-1} was assigned to ν(sp^3 C-H) [10]. In the region 1100 cm^{-1}, splitting to two peaks at 1121-1118 and 1093-1167 cm^{-1} could be assigned to perchlorate ions. The splitting of this peak clearly explained the presence of coordinated perchlorate. In both complexes, a band seen at 485-471 cm^{-1} was probably due to the formation of M-N bonds [6].

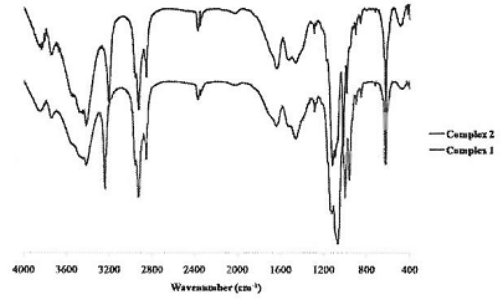

Figure 1. The FT-IR spectra of **1** and **2**

3.2 Mass spectra of **1** and **2**

The electro-spray ionization mass spectra of the perchlorate salts of copper(II) and nickel(II) complexes were studied in positive mode. Complex **1** showed an intense signal of *m/z* values at 588.3 (100%) and 590.3 (85%) corresponding to $[CuL(ClO_4)]^+$ and $[CuL(ClO_4)\text{-}2H]^+$ (Figure 2.) whereas complex **2** showed peaks at 583.3 (100%) and 585.3 (80%) corresponding to $[NiL(ClO_4)]^+$ and $[NiL(ClO_4)\text{-}2H]^+$ (Figure 3.). Similar type of mass spectra patterns have been observed in hexaaza macrocyclic complexes reported by Sujatha and co-workers [11-12].

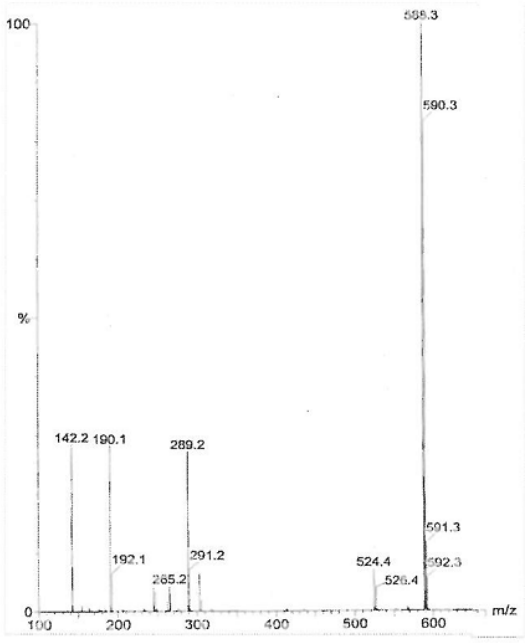

Figure 2. The mass spectra of **1**

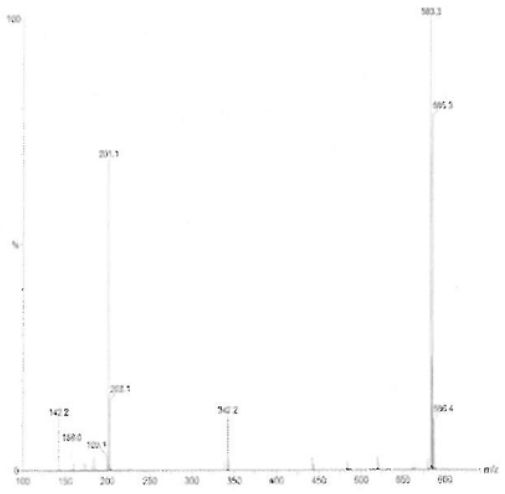

Figure 3. The mass spectra of **2**

3.3 UV-Vis spectra of **1** and **2**

The electronic spectra of **1** (Figure 4) showed a broad band at 502 nm consistent with that reported for square planar geometry and, thus, was assigned to the $^2E_g \rightarrow {}^2T_{2g}$ [6]. In general, due to Jahn-Teller distortion Cu^{2+} complexes give absorption band between 599-699 nm [13]. No absorption bands are observed in the

region near UV any complex under study which rules out the possibility of tetrahedral geometry [14].

The electronic spectra of **2** (Figure 5) exhibited two bands at 452 and 625 nm which could be assigned to $^3A_{2g}$ (F) $\rightarrow$ $^3T_{2g}$ (F) and $^3A_{2g}$ (F) $\rightarrow$ $^3T_{1g}$ (P) transitions, respectively [6], for the square planar Ni^{2+} complex [13].

The electronic spectra found in **1** and **2** were of the *d-d* transition type similar to those reported by Firdaus and co-workers [15].

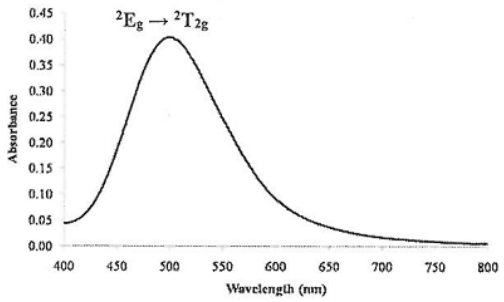

Figure 4. Electronic absorption spectra of **1**

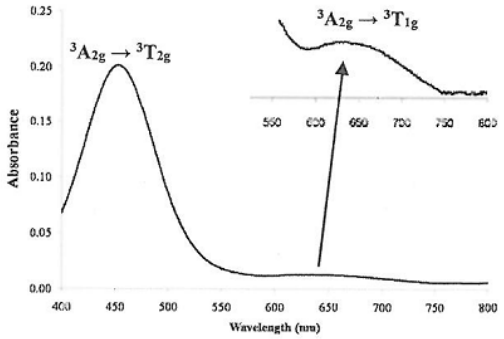

Figure 5. Electronic absorption spectra of **2**

From spectroscopic data the structure of both complexes can be proposed as follows (Figure 6.).

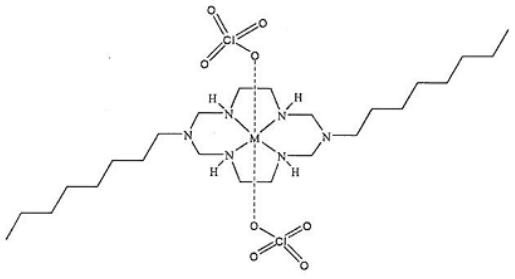

Figure 6. The proposed structure for **1** and **2** (M = Cu(II) or Ni(II))

In the proposed structures, the coordination geometry about each metal-ion center, Ni(II) or Cu(II), is square planar composed of four secondary amine nitrogen atoms of the hexaaza macrocyclic ligand and two oxygen atoms from perchlorate anions. The hexaaza macrocyclic occupies the equatorial sites to form a square-planar geometry leaving the two oxygen atoms (from two perchlorates) at the axial sites to counter ion molecule. The macrocyclic itself contains two each of five- and six-membered rings. A similar structure was presented in previous research [16-18].

4. Conclusions

Copper(II) and nickel(II) complexes have been synthesized by the one-pot condensation reaction. The elemental analyses and LC-MS revealed the stoichiometry and composition while FT-IR and UV-visible spectra confirmed the bonding features and stereochemistry of the hexaaza macrocyclic complexes.

Acknowledgements

This work was supported by the Songklanagarind Scholarship for Graduate Studies from the Prince of Songkla University.

References

[1] Firdaus, F., Fatma, K., Azam, M., Khan, S.N., Khan, A.U. and Shakir, M., 2008, *Transition. Met. Chem.*, 33, 467-473.
[2] Salavati-Niasari, M., 2004, *J. Mol. Catal. A: Chem.*, 217, 87-92.
[3] Salavati-Niasari, M., 2004, *Inorg. Chem. Commun.*, 7, 963-966.
[4] Gokulakrishnan, S., Parakh, P. and Prakash, H., 2012, *J. Hazard. Mater.*, 213-214, 19-27.
[5] Kou, H.-Z., Jiang, Y.-B., Zhou, B.C. and Wang, R.-J., 2004, *Inorg. Chem.*, 43, 3271-3276.
[6] Husain, A., Nami, S.A.A. and Siddiqi, K.S., 2011, *Appl. Organometal. Chem.*, 25, 761-768.
[7] Tsymbal, L.V., Andriichuk, I.L., Lampeka, Y. D. and Pritzkow, H., 2010, *Russ. Chem. Bull.*, 59, 1572-1581.
[8] He, Y., Kou, H.-Z., Li, Y., Zhou, B.C., Xiong, M. and Li, Y., 2006, *Inorg. Chem. Commun.*, 6, 38-42.
[9] Shakir, M., Azim, Y., Chishti, H.T.N., Begum, N., Chingsubam, P. and Siddiqi, M.Y., 2006, *J. Braz. Chem. Soc.*, 17, 272–278.
[10] Raman, N., Raja, J.D. and Sakthivel, A., 2008, *J. Chill. Chem. Soc.*, 53, 1568–1571.
[11] Sujatha, S., Balasubramanian, S. and Varghese, B., 2009, *Polyhedron.*, 28, 3723-3730.
[12] Sujatha, S., Balasubramanian, S., Varghese, B., Jayaprakashvel, M. and Mathivanan, N., 2012, *Inorg. Chim. Acta.*, 386, 109-115.
[13] El-Sherif, A. A., 2009, *Inorg. Chim. Acta.*, 362, 4991-5000.
[14] Patel, M.N., Patel, C.B and Patel, R.P., 1974, *J. Inorg. Nucl. Chem.* 36, 3868-3870.
[15] Firdaus, F., Fatma, K., Azam, M., Khan, S.N., Khan, A.U., and Shakir, M., 2008, *Transition. Met. Chem.*, 33, 467-473.
[16] Husain, A., Moheman, A., Nami, S. A.A. and Siddiqi, K.S., 2012, *Inorganica Chimica Acta.*, 384, 309-317.
[17] Min, K.S., Park, M.J., and Ryoo, J.J., 2013, *Chirality*, 25, 54-58.


TCEB
THAILAND CONVENTION & EXHIBITION BUREAU
PACCON 2016
PURE AND APPLIED CHEMISTRY INTERNATIONAL CONFERENCE
PROCEEDINGS
'THAILAND: One Hundred Years of Advancement in Chemistry'
100 Years
9-11 February 2016
BITEC
Bangkok, Thailand

PURE AND APPLIED CHEMISTRY INTERNATIONAL CONFERENCE 2016

9 - 11 February 2016 Bangkok, Thailand

Date: January 14, 2016

Subject: Acceptance of Abstract for PACCON 2016

Dear Participant,

I am pleased to inform you that your abstract entitled "Supramolecular Architecture of Nickel(II) Macrocyclic Complex Containing i-butylamine Pendant Arms with p-nitrobenzoic Acid Ligand" has been accepted for poster presentation.

THE ACCEPTED ABSTRACTS WILL BE PUBLISHED IN THE ON-LINE ABSTRACT BOOK IF THE EARLY BIRD REGISTRATION AND FULL PAYMENT ARE MADE BEFORE **DECEMBER 21, 2015**.

Having your abstract accepted, you may optionally submit the proceedings paper for further review. The deadline for proceedings submission is **January 18, 2016**. The instruction for proceedings preparation is available on our website (http://www.paccon2016.com). Please note that acceptance of the abstract does not guarantee acceptance of the proceedings.

If you have any further inquiries, please do not hesitate to contact us via e-mail at paccon2016@gmail.com.

Yours sincerely,

Associate Professor Dr.Vudhichai Parasuk
Chairperson of PACCON 2016

PACCON Proceedings 2016: Chemical and Biological Crystallography (CBC-0514)

Supramolecular architecture of nickel(Ⅱ) macrocyclic complex containing *i*-butylamine pendant arms with *p*-nitrobenzoic acid ligand

Surachai Kongchoo,[1] Kittipong Chainok,[2] Anob Kantacha,[3] Sumpun Wongnawa*,[1]
[1]*Department of Chemistry, Faculty of Science, Prince of Songkla University, Songkhla 90112, Thailand*
[2]*Department of Physics, Faculty of Science and Technology, Thammasart University, Phatum Thani 12121, Thailand*
[3]*Department of Chemistry, Faculty of Science, Thaksin University, Patthalung 93110, Thailand*
*e-mail: sumpun.w@psu.ac.th

Abstract:

The reaction of $[NiL](ClO_4)_2$ (L = 3,10-diisobutyl-1,3,5,8,10,12-hexaazacyclotetradecane) with *p*-nitrobenzoate (4-nba) in mixed solvent $MeCN/H_2O$ at room temperature yielded $[Ni(L)(4\text{-nba})_2]\cdot H_2O$ which crystallized in the monoclinic system *C2/c* with *a* = 31.0572(12) Å, *b* = 12.8285(4) Å, *c* = 18.1320(7) Å, β = 90.7760(10)°, *V* = 7223.44 Å^3, and Z = 4. This structure was characterized by combined analytical, spectroscopic, and X-ray crystallographic methods. The X-ray crystal structure shows the distorted octahedral coordination geometry around the Ni(II) ion with secondary amines of the macrocycle at the equatorial positions and two molecules of *p*-nitrobenzoate at the axial positions. This complex displays infinite 1D chains using the intra- and intermolecular hydrogen bonding as well as the intrachain face-to-face π-π stacking interaction between phenyl rings of the macrocycle and the *p*-nitrobenzoate ion in plane of the adjacent molecules.

1. Introduction

Cu(II) and Ni(II) complexes of hexaazamacrocyclic ligands as building blocks for constructing supramolecular networks, which received interests due to their inherited novel properties such as porosity, photoluminescence,[1] magnetism,[2] and non-linear optical behavior. Among these, hexaazamacro- cyclic complexes have been used as very useful building blocks because they have vacant sites in axial position. Coordination polymer of organic ligands to hexaaza- macrocyclic metal(II) complexes, a variety of inter- and intramolecular interactions.[3–6] Moreover, supramolecular species could be coordination interaction, weak intra- and intermolecular interactions, such as hydrogen bonding, as well as π-π stacking, and C-H···π interactions provide supramolecular assemblies through the creation of 1D, 2D, and 3D networks.[7] For example, one-dimension coordination polymers $[Ni(L)(mal)_2]_n$ (mal = malonate and L = 3,14-dimethyl-2,6,13,17-tetraaza-tricyclo[14,4,- $0^{1.18},0^{7.12}$]docosane)[8] was assembled by square-planar nickel(II) macrocyclic complex $[Ni(L)]Cl_2\cdot 2H_2O$ and malonate ligand, which shows the distorted octahedral geometries and revealed weak antiferromagnetic interactions.

In the present study, we report the synthesis, spectroscopic properties and crystal structure of nickel(II) complex $[Ni(L)(4\text{-nba})_2]\cdot H_2O$ (L = 3,10-diisobutyl-1,3,5,8,10,12-hexaazacyclotetradecane and 4-nba = *p*-nitrobenzoate).

2. Materials and Methods

2.1 Materials and physical methods

All chemicals and solvents were reagent grade and used without further purification. The complex $[NiL](ClO_4)_2$

was initially prepared for use in another project. Elemental analyses (C, H and N) were performed using a CE instruments Flash EA 1112 series, Thermo Quest analyzer. FT-IR spectra of solid samples as KBr pellets were recorded on a Perkin-Elmer, Spectrum One FT-IR spectrophotometer in the range 4000–400 cm^{-1}. Powder X-ray diffraction (PXRD) patterns were recorded on a X'Pert, Philips diffractometer with CuKα radiation. The simulation of PXRD spectrum was carried out with the Mercury 3.6 software.

2.2 Synthesis of [Ni(L)(4-nba)$_2$·H$_2$O

$[NiL](ClO_4)_2$ (50.3 mg, 0.088 mmol) was dissolved in 10 mL of MeCN and was added to a solution of *p*-nitrobenzoic acid (30.1 mg, 0.180 mmol) in 8 mL of mixed MeCN/H_2O (1:1 v/v) followed by addition of an excess triethylamine (0.02 mL). The mixture was stirred for 3 hour at ambient temperature and was filtered to remove insoluble material. The filtrate was left to stand at ambient temperature until the orange crystals formed. Yield: 63%. *Anal.* Calc. for $C_{60}H_{92}N_{16}O_{17}Ni_2$: C, 50.51; H, 6.49; N, 15.71. Found: C, 50.55; H, 6.53; N, 15.77%.

2.3 X-ray crystallographic analysis

Suitable single crystal with dimension 0.35 x 0.24 x 0.20 mm was selected for single-crystal X-ray diffraction analysis. Data were collected on a Bruker Smart Apex-II CCD diffracto- meter with graphite monochromated MoKα radiation (λ = 0.71073 Å) in the ω scanning mode at 296(2) K. Structure determination was carried out with OLEX^2 [9], the structure was solved with the ShelXS^{10} structure solution program using Direct Methods and refined with the ShelXL^{11} refinement package using Least Squares minimization. All non-hydrogen atoms were refined anisotropically, while the hydrogen were located geometrically and refined isotropically. The selected bond distances and angles are present in Table 1.

3. Results & Discussion

3.1 Synthesis and characterization

The nickel(II) complex was characterized by elemental analysis, infrared spectrum, powder X-ray diffraction and single crystal X-ray diffraction analysis. The hexaaza-macrocyclic of nickel(II) complex was synthesized in MeCN/H_2O from the reaction of $[NiL](ClO_4)_2$ with 4-nba in the presence of triethylamine. The complex is insoluble in organic solvents. The FT-IR spectrum (Figure 1) of complex showed medium strong absorption at 3158 and 3258 cm^{-1} attributed to the secondary amine groups of macrocyclic ligands. The bands of the C-H sp^3 of the macrocyclic ligand appeared at 2927 and 2871 cm^{-1} and that of the C-H of the benzene ring at 2957 cm^{-1}. The bands of the N-O asymmetric and symmetric stretching of 4-nba ligand occurred at 1521 and 1573 cm^{-1}, respectively. The bands of the C-O and very strong band of the C=O of 4-nba ligand showed up at 1592 and 1341 cm^{-1}, respectively. In the complex, the secondary amine peaks are splitted due to the hydrogen bonds. The bands of the Cl-O of perchlorate ions disappeared due to the perchlorate being replaced by 4-nba ion.

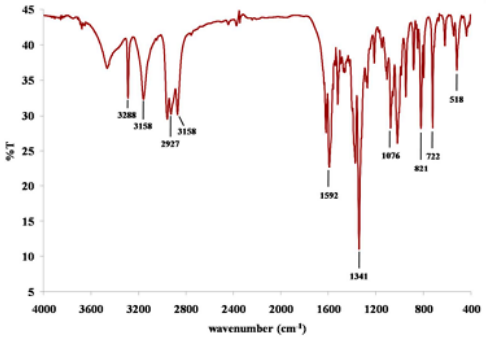

Figure 1. FT-IR spectrum of [Ni(L)(4-nba)$_2$•H$_2$O

The simulated (red line) and experimental (blue line) PXRD patterns of complex at ambient temperature are shown in Figure 2. Their peaks positions are in good consistency with each other,

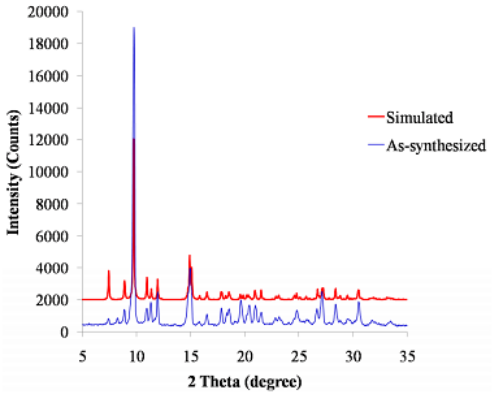

Figure 2. PXRD patterns of [Ni(L)(4-nba)$_2$•H$_2$O.

indicating the phase purity of the as-synthesized samples.

3.2 Description of the structure

An ORTEP representation of two independent molecules in the asymmetric unit of [Ni(L)(4-nba)$_2$·H$_2$O with the atomic numbering scheme are shown in Figure 3 and the unit cell packing is shown in Figure 4. The complex crystallized in the monoclinic *C2/c* space group. The nickel(II) ion displays a distorted octahedral coordination geometry by binding to the four secondary nitrogen atoms of the macrocycle [Ni(1)-N(4) = 2.0608(16), Ni(1)-N(5) = 2.0668(17), Ni(2)-N(1) = 2.0577(18), and Ni(2)-N(2) = 2.0478(18) Å] forming the equatorial plane in a square planar fashion. Two oxygen atoms from two 4-nba anions are located at the axial positions [Ni(1)-O(4) = 2.1310(13) and Ni(2)-O(5) = 2.1320(14) Å]. The geometry of the tertiary nitrogen atom [N(3) and N(6)] shows C-N distances averaged about 1.435(18) Å and C-N-C angles were in the range 111.09(6)-116.18(8)◦, indicating significant contribution of sp^2 hybridization of the bridgehead nitrogen atoms. The six-membered chelate rings involving the C(3), C(4), C(16), and C(17) atoms adopted a chair conformation, whereas five-membered rings involving the C(1), C(2), C(18), and C(19) atoms assumed a gauche conformation.[12,13]

The oxygen atoms of the 4-nba ligand forms the intramolecular hydrogen bonds with secondary amine of the macrocycle [N(2)-H(2)···O(6) = 2.039 Å and N(5)-H(5)···O(3) = 2.081 Å] and intermolecular interactions [N(4)-H(4)···O(2) = 2.651 Å and N(1)-H(1)···O(8) = 2.604 Å], which leads to a 1D chain running along *c* axis as shown in Figure 5. The pendant *i*-butylamine groups of the macrocycles are not involved in any interactions.

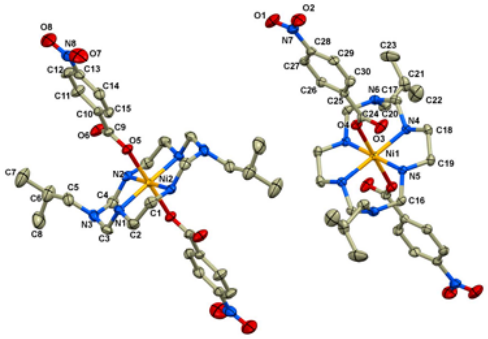

Figure 3. Two independent molecular structure of [Ni(L)(4-nba)$_2$•H$_2$O with atom labeling scheme. Hydrogen atoms and water molecule are omitted for clarity.

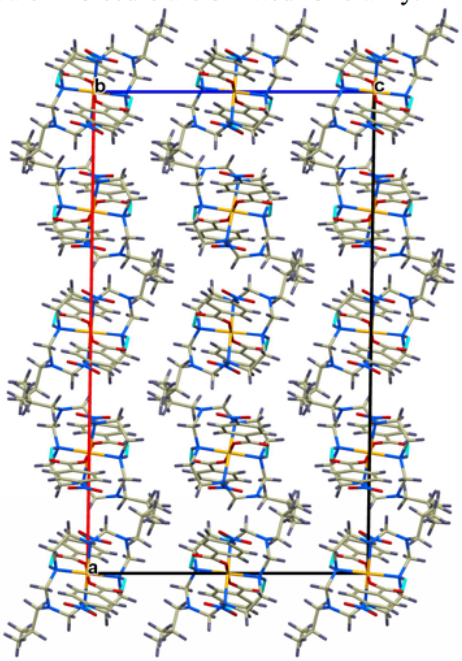

Figure 4. View of the unit cell packing of [Ni(L)(4-nba)$_2$•H$_2$O, plotted down *b* axis.

Table 1. Selected bond distances (Å) and angles (°) for $[Ni(L)(4\text{-nba})_2 \cdot H_2O]$.

Bond distances (Å)	
Ni(1) – N(4)	2.0608(16)
Ni(1) – N(5)[a]	2.0668(17)
Ni(2) – N(1)	2.0577(18)
Ni(2) – N(2)	2.0478(18)
Ni(1) – O(4)[a]	2.1310(13)
Ni(2) – O(5)	2.1320(14)
Bond angle (°)	
O(4)[a] – Ni(1) – O(4)	180.00(8)
O(5) – Ni(2) – O(5)[b]	180.00(0)
N(4) – Ni(1) – O(4)	92.89(6)
N(4) – Ni(1) – N(5)	93.96(7)
N(5) – Ni(1) – O(4)	86.75(6)
N(1) – Ni(2) – O(5)[b]	87.52(7)
N(2) – Ni(2) – O(5)	92.44(6)

Symmetry transformations used to generate equivalent atoms: (a) -x, -y, -z and (b) $^1/_2$ - x, $^3/_2$ - y, -z.

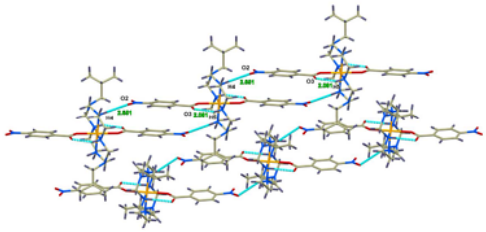

Figure 5. One-dimension of $[Ni(L)(4\text{-nba})_2] \cdot H_2O$ showing the intra- and intermolecular hydrogen bonds [(N-H···O) are indicated by dotted lines].

The linear chains are linked by the off-set interchain face-to-face π-π stacking interaction between phenyl rings of the macrocycle and the *p*-nitrobenzoate ligand in plane of the adjacent molecules, as shown in Figure 6.

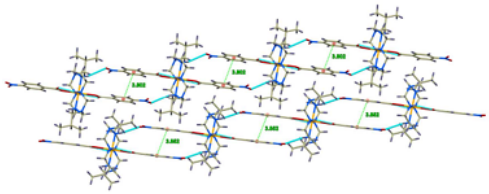

Figure 6. One-dimension of $[Ni(L)(4\text{-nba})_2] \cdot H_2O$ showing the π-π stacking interactions are indicated by dotted lines.

4. Conclusion

In summary, we have prepared and characterized a supramolecular structure of nickel(II) macrocyclic complex. The complex was synthesized by the reaction of nickel(II) macrocyclic complex containing *i*-butyl- amine as pendant arms with *p*-nitrobenzoic acid ligand. The nickel(II) ion has a distorted octahedral geometry with the four nitrogen atoms of the macrocycle occupy the equatorial positions and two oxygen atoms of the 4-nba ions in the axial positions. The structure shows 1D chain using the intra- and intermolecular H-bonding. Moreover, the interchain face-to-face π-π stacking interaction between phenyl rings of the macrocycle and the *p*-nitrobenzoate ion in plane of the adjacent molecules.

Acknowledgements

This work was supported by the Songklanagarind Scholarship for Graduate Studies from the Prince of Songkla University.

References

1. Tao, B.; Cheng, F.; Jiang, X.; Xia, H. *J. Mol. Struct.* **2012**, *1028*, 176–180.
2. Choi, K.-Y.; Ryu, H.; Lee, K.-C.; Lee, H.-H.; Hong, C.-P.; Kim, J.-H.; Sung, N.-D. *Bull. Korean Chem. Soc.* **2003**, *24*, 1150–1154.
3. Park, J. H.; Jeong, A. R.; Hastuti, D. K. A. K.; Jeong, M. J.; Min, K. S. *J. Incl. Phenom. Macrocycl. Chem.* **2015**, *82*, 153–162.
4. Choi, K.-Y.; Chun, K. M.; Suh, I.-H. *Polyhedron* **2001**, *20,* 57–65.
5. Choi, K.-Y.; Kim, K.-J. *Polyhedron* **2008**, *27,* 1311–1317.
6. Min, K. S.; Suh, M. P. *Eur. J. Inorg. Chem.* **2001**, *2001,* 449–455.
7. Lu, T.-B.; Xiang, H.; Luck, R. L.; Mao, Z.-W.; Chen, X.-M.; Ji, L.-N. *Inorg. Chim. Acta* **2003**, *355,* 229–241.
8. Choi, K.-Y. *J. Chem. Crystallogr.* **2010**, *40*, 477–481.

9. Dolomanov, O. V.; Bourhis, L. J.; Gildea, R. J.; Howard, J. A. K.; Puschmann, H. *J. Appl. Cryst.* **2009**, *42*, 339–341.
10. Sheldrick, G. M. *Acta Cryst.* **2008**, *A64*, 112–122.
11. Sheldrick, G. M. *Acta Cryst.* **2015**, *C71*, 3–8.
12. Husain, A.; Nami, S. A. A.; Siddiqi, K. S. *Appl. Organometal. Chem.* **2011**, *25*, 761–768.
13. Husain, A.; Turnbull, M. M.; Nami, S. A. A.; Moheman, A.; Siddiqi, K. S. *J. Coord. Chem.* **2012**, *65*, 2593–2611.

Synthesis, Crystal Structure, and Spectroscopic Properties of Cu(II) Complex with 14-Membered Hexaazamacrocyclic Ligands

Surachai Kongchoo, Anob Kantacha, Saowanit Saithong & Sumpun Wongnawa

Journal of Chemical Crystallography

ISSN 1074-1542

J Chem Crystallogr
DOI 10.1007/s10870-016-0649-8

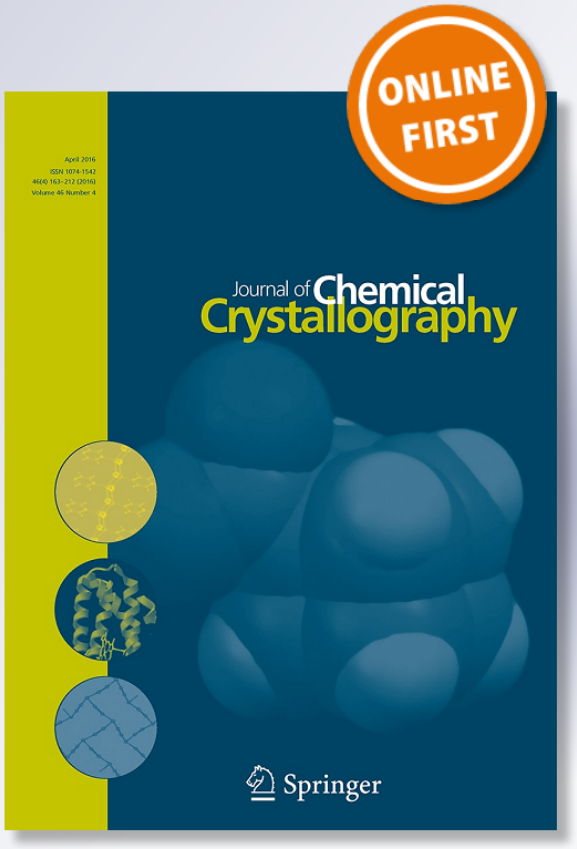

Springer

J Chem Crystallogr (2016) 46:222–229
DOI 10.1007/s10870-016-0649-8

ORIGINAL PAPER

Synthesis, Crystal Structure, and Spectroscopic Properties of Cu(II) Complex with 14-Membered Hexaazamacrocyclic Ligands

Surachai Kongchoo[1] · Anob Kantacha[2] · Saowanit Saithong[1] · Sumpun Wongnawa[1]

Received: 13 October 2015 / Accepted: 28 April 2016 / Published online: 6 May 2016

Abstract $[CuL(ClO_4)_2]$ complex of 14-membered hexaazamacrocyclic ligand (L = 6,13-dimethyl-3,10-dioctyl-1,3,5,8,10,12-hexaazacyclotetradecane) was synthesized by template condensation reaction of 1,2-diaminopropane, octylamine, and formaldehyde in ethanol. The product was characterized by elemental analysis, Fourier-transformed infrared spectroscopy (FT-IR), ultraviolet–visible spectroscopy (UV–vis), diffused reflectance spectroscopy (DRS), liquid chromatography-mass spectrometry (LC–MS), and X-ray crystallographic technique. Thermal behavior of this complex was studied by thermogravimetric analysis (TGA). The IR and other spectral properties were consistent with the result from X-ray diffraction. The electronic absorption spectra of $[CuL(ClO_4)_2]$ complex showed one band at 500 nm corresponding to $^2B_{1g} \rightarrow {}^2B_{2g}$ transition. The complex crystallized in the triclinic space group of $P\bar{1}$ with $a = 8.1307(6)$ Å, $b = 9.3579(7)$ Å, $c = 13.3930(10)$ Å, $\alpha = 95.932(2)°$, $\beta = 98.579(2)°$, and $\gamma = 114.478(2)°$. The copper(II) ion of the macrocyclic cation displayed a tetragonally distorted octahedral geometry with four nitrogen atoms in the equatorial plane and two oxygen atoms from the perchlorate ions weakly coordinated to the copper(II) ion in the axial positions. The complex exhibited only weak luminescent property.

✉ Sumpun Wongnawa
sumpun.w@psu.ac.th

[1] Department of Chemistry and Center of Excellence for Innovation in Chemistry, Faculty of Science, Prince of Songkla University, Hat Yai, Songkhla 90112, Thailand

[2] Department of Chemistry, Faculty of Science, Thaksin University, Papayom, Phatthalung 93110, Thailand

Graphical Abstract A new macrocyclic complex that can be easily obtained from the one-pot synthesis.

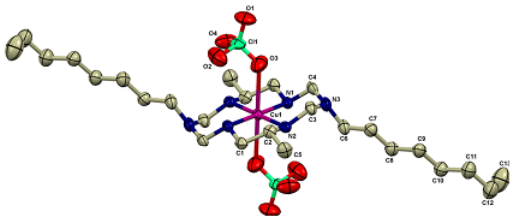

Keywords Macrocycles · Copper(II) complexes · One-pot reactions · Template condensation · Hexaazamacrocyclic complexes · 14-Membered macrocyclic complexes · Pendant arm

Introduction

The complexes of transition metals with macrocyclic ligands are of particular interest because of their similarity to many natural systems like porphyrins, cobalamines (vitamin B12), hemoglobin, and chlorophyll [1, 2]. Hexaazamacrocyclic complexes are of great importance with potential applications in antimicrobial activity [1, 3–6], photosynthesis [7], catalysis [8–11], gas sorption [12, 13], and molecular magnetism [14–18]. Copper(II) and nickel(II) having received much attention because of their high thermodynamic stability and kinetic inertness can provide the possibility of synthetically convenient chemical modification of macrocyclic ligand using the template synthetic method [19]. Metal template condensation reaction is simple "one-pot" reaction and has been generally utilized

due to its ease of use, low cost, and high yield. Macrocyclic complexes are best prepared with the aid of metal ion as template to direct the condensation reaction which ultimately ends with ring closure [20]. In addition, formaldehyde can serve as a link for two amine moieties and, therefore, metal-directed reaction of coordinated amines and formaldehyde is useful for the preparation of various types of fully saturated hexaazamacrocyclic complexes containing *N*–CH_2–*N* linkings [21]. Typical examples of primary amines side chain, the "pendant arm", that have been used so far include propylamine [22, 23], ethanolamine [24, 25], 1,4-phenylenediamine [26], hydrazine [27], 2-thiophenemethylamine [28], nicotinamide [5], 4-aminobutyric acid [29, 30], ethylamine [31], (*R*)-(+)-1-(1-naphthyl)ethylamine [32], ethylenediamine [33], 1-(3-aminopropyl)-imidazole [34], benzylamine [1, 35], and (*R/S*)-α-methylbenzylamine [36–39].

Following this path, herein, we report the synthesis of a new complex of Cu(II) ion containing 14-membered hexaazamacrocyclic ligand obtained by condensation reaction of 1,2-diaminopropane, octylamine, and formaldehyde followed by structure determination and spectral studies.

Experimental

Materials and Physical Measurements

All chemicals were of reagent grade and obtained from commercial sources. Absolute ethanol was used throughout this synthesis. Infrared spectra of solid samples (KBr pellets) were recorded on a Perkin-Elmer Spectrum One FT-IR spectrophotometer in the range 4000–400 cm^{-1}. Electronic absorption spectra were obtained on a Shimadzu Lambda-1600 UV–Vis spectrophotometer. Solid state UV–Vis diffused reflectance spectra (sample diluted with $BaSO_4$) were recorded with a Shimadzu 2450 PC UV–Vis recording spectrophotometer. Fluorescence spectra were recorded with a Perkin Elmer LS55 Luminescence spectrometer at room temperature. Elemental analysis of CHNO was performed using a CE instruments Flash EA 1112 series, Thermo Quest analyzer. Mass spectra were recorded by electro-spray ionization (ESI) technique operating in the positive ion mode by directly injecting the solution into mass spectrometer (Waters Micromass). The thermal curves (TGA and DTA) were recorded using a TGA7 Perkin Elmer, USA, with a sample mass of 4.1 mg over the temperature range 50–1000 °C and a heating rate 10 °C min^{-1}.

Caution! Perchlorate salts are potentially explosive and should be handled in small quantities.

Synthesis of $[CuL(ClO_4)_2]$

To a stirred solution of copper(II) acetate monohydrate (1 mmol) and 1,2-diaminopropane (2 mmol) in absolute ethanol was added dropwise a solution of formaldehyde (4 mmol) and octylamine (2 mmol) in absolute ethanol (15 mL). The reaction mixture was refluxed for 48 h. The hot solution was filtered and cooled then perchloric acid was added slowly. The purple-red crystals formed was filtered off, washed with absolute ethanol, and dried in air. The yield was ~35 %, *anal. calc*. for $C_{26}H_{58}C_{l2}CuN_6O_8$: C, 43.54; H, 8.15; N, 11.71; O, 17.84, *found* C, 43.95; H, 8.08; N, 11.84; O, 17.16 %.

Crystal Structure Determination and Refinements

The diffraction data for $[CuL(ClO_4)_2]$ were collected at 25 °C on a Bruker APEX CCD area-detector equipped with graphite-monochromated Mo K_α radiation (λ = 0.71073 Å) at 293(2) K. The lattice parameters were identified by the auto-matrix indexing routine of the diffractometer (*SMART* Program) [40]. Data reduction was carried out by using *SIANTV8.30C* Program [40] and a semi-empirical absorption-correction (multi-scan, *SADABS* [41]) based on the intensities of equivalent reflections. The structure was solved by direct method using SHELXL [41] and refined by a full-matrix least-squares procedure based on F^2. All non-hydrogen atoms were found from the different map and refined with anisotropic displacement parameters. All hydrogen atoms on carbon atoms were constrained at calculated positions and refined as riding atoms. The hydrogen atoms on nitrogen atoms were located in a different map and restrained. The molecular structure with atomic labeling scheme and the crystal packing was plotted by Mercury 3.8 program [42]. The crystallographic data are given in Table 1. The selected bond lengths (Å) and bond angles (°) are presented in Table 2.

Results and Discussion

$[CuL(ClO_4)_2]$ was synthesized in ethanol by the template condensation reaction of $Cu(CH_3COO)_2{\cdot}H_2O$, 1,2-diaminopropane, formaldehyde, and octylamine (Scheme 1). The complex was soluble in organic solvents such as acetonitrile (MeCN), dimethylformamide (DMF), dimethylsulfoxide (DMSO), and acetone. According to the Scheme 1, the reaction proceeded by the formation of an imine (C = N) coordinated to a copper(II) ion. The imine was attacked by octylamine (as pendant arm) to yield a

Table 1 Crystal data, data collection, and structure refinement for the complex $[CuL(ClO_4)_2]$

Molecular formula	$C_{26}H_{58}Cl_2CuN_6O_8$
Molecular weight	717.22
Crystal system	Triclinic
Space group	$P\bar{1}$
Unit cell dimension	
a (Å)	8.1307(6)
b (Å)	9.3579(7)
c (Å)	13.3930(10)
α (°)	95.932(2)
β (°)	98.579(2)
γ (°)	114.478(2)
V (Å^3)	901.48(12)
Z	1
D_{cal} (g cm^{-3})	1.321
μ (mm^{-1})	0.804
F (000)	383
Crystal size (mm)	0.335 × 0.107 × 0.071
θ range for data collection	1.564–24.997°
Index ranges	$-9 \le h \le 9$, $-11 \le k \le 11$, $-15 \le l \le 15$
Reflections collected	9673
Independent reflections	3185 [$R_{int} = 0.0308$]
Refinement method	Full-matrix least-squares on F^2
Data/restraints/parameters	3185/2/204
Goodness-of-fit on F^2	1.042
Final R indices [$I > 2\sigma(I)$]	$R1 = 0.0559$, $wR2 = 0.1459$
R indices (all data)	$R1 = 0.0681$, $wR2 = 0.1561$
Largest diff. peak and hole (e Å^{-3})	0.568 and −0.381
Completeness to $\theta = 25.00$ (%)	100.0

Table 2 Selected bond lengths (Å) and bond angles (°) of the $[CuL(ClO_4)_2]$

Bond lengths			
Cu(1)–N(1)	2.002(3)	N(2)–C(2)	1.488(5)
Cu(1)–N(2)	2.013(3)	N(3)–C(3)	1.419(5)
Cu(1)–O(3)	2.592(3)	Cl(1)–O(1)	1.376(4)
Bond angles			
N(1)–Cu(1)–N(2)		94.14(13)	
C(1)–N(1)–C(4)		112.0(3)	
O(3#)–Cu(1)–O(3)		180.0(3)	
C(2)–N(2)–C(3)		113.8(3)	

gem-diamine and then condensed with a neighboring imine group producing a five- and six-membered ring.

Crystal Structure Description of $[CuL(ClO_4)_2]$

The complex contained $[CuL]^{2+}$ cationic part (L = 6, 13-dimethyl-3,10-dioctyl-1,3,5,8,10,12,-hexaazacyclotetradecane) and two perchlorate anions as depicted in Fig. 1. The Cu^{2+} ion coordinated to four N atoms of the hexaazacyclotetradecane macrocycle ligand and was in the crystallographic $\bar{1}$ inversion center where one half of cation could be generated from the other half by inverting through the metal center.

The copper(II) ion bound to four secondary amine atoms in a square-planar fashion in the equatorial plane at the distances of 2.002(3) Å for Cu1–N1 and 2.013(3) Å for Cu1–N2 which were comparable to those of hexaaza-macrocycle Cu(II) complexes with Cu–N distances in the range of 1.985(7)–2.017(6) Å [33, 43]. In the axial plane, copper(II) ion bound to two oxygen atoms of perchlorate anions at a distance of 2.592(3) Å which was significantly longer than those to the N atoms in the equatorial position, however, slightly shorter than Cu–O distances in $[Cu(L^{R,R})(ClO_4)_2]$ and $[Cu(L^{S,S})(ClO_4)_2]$ at 2.610(7)–2.659(7) Å [43] and $[Cu(L1)(ClO_4)_2]$ at 2.7418(13) Å [54]. This was due to the Jahn–Teller distortion of the copper(II) ion in the z-axis with the elongation of the Cu–O bonding [45–47]. The geometry of copper(II) ion for this complex could be described as a distorted octahedral geometry like those reported complexes [33, 43]. The six-membered chelate rings (N1–Cu1–N2 = 94.14(13)° and N1–Cu1–

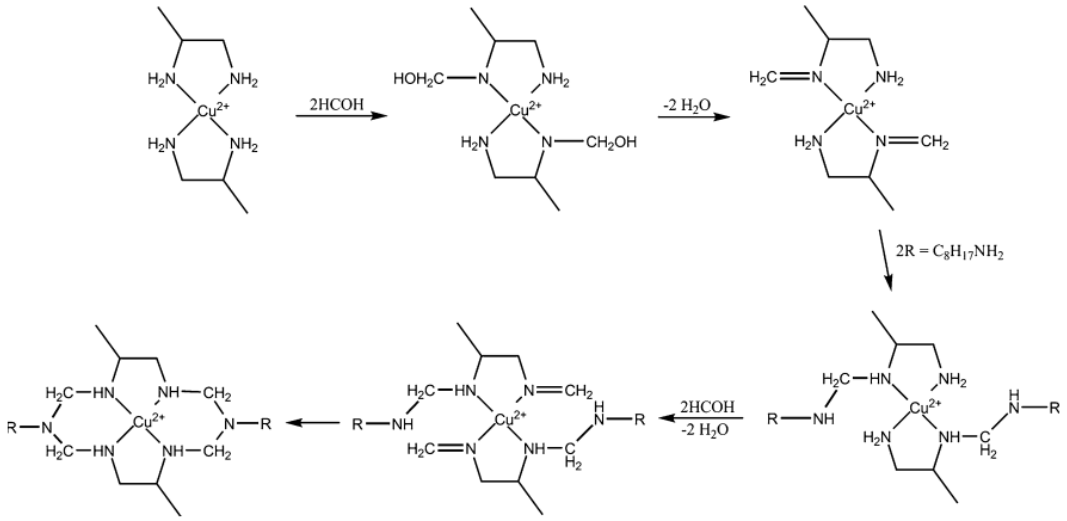

Scheme 1 Proposed mechanism for the formation of $[CuL(ClO_4)_2]$

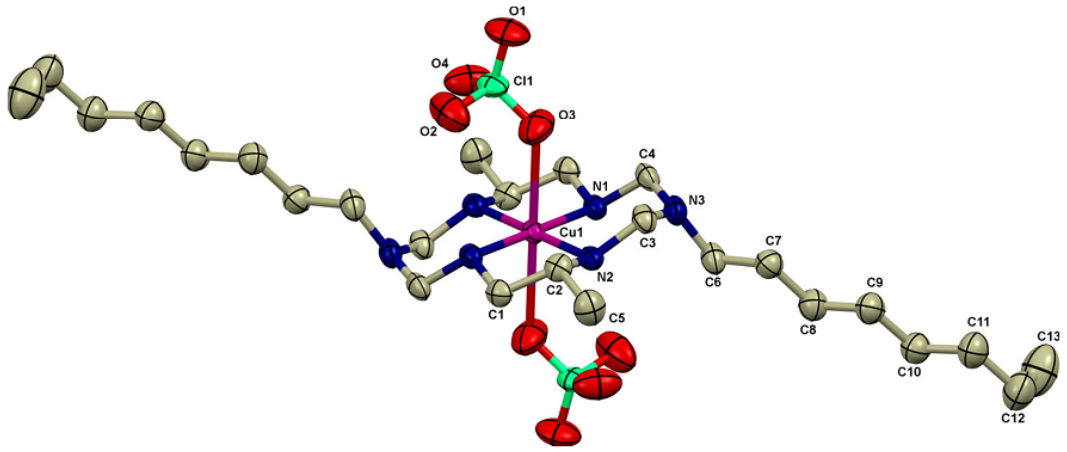

Fig. 1 The molecular structure plot of the $[CuL(ClO_4)_2]$, along with the atomic numbering scheme (H atoms omitted for clarity)

N2#1 = 85.86(13)°) adopted the chair conformation and the five-membered chelate rings assumed the gauche conformation (N1#1–Cu1–N2 = 85.86(13)° and N1#1–Cu1–N2#1 = 94.14(13)°) [48]. The C–N–C angles of the tertiary nitrogen atoms (N3 and its equivalent atom) were in the range of 116.6(3)–117.7(4)° which were larger than the ideal tetrahedral angle (109.5°). Thus, the tertiary nitrogen atoms (N3) could use the sp^2-like hybridization similar to the other polyazamacrocyclic complexes containing uncoordinated tertiary amino groups [33, 39, 43, 44]. The secondary amines of the macrocycle formed N–H···O molecular hydrogen bond interactions with the O atoms of neighboring perchlorate anions: N1···O2 = 3.369(6) Å, N1–H1···O2 = 153(4)°; N1···O2#2 = 3.099(5) Å, N1–H···O2#2 = 138(4)°; N2···O4 = 3.078(5) Å, N2–H2···O4 = 164(4)°; C3···O3#1 = 3.374(6) Å, C3–H3B···O3#1 = 122.8°; C4···O3#1 = 3.232(6) Å, C4–H4A···O3#1 = 124.6° (#1: −x + 2, −y + 2, −z + 1, #2: −x + 1, y + 2, −z + 1) as shown in Fig. 2.

These hydrogen bonding interactions between the adjacent cationic part and anionic part alternately linked to generate one dimensional supramolecular interaction

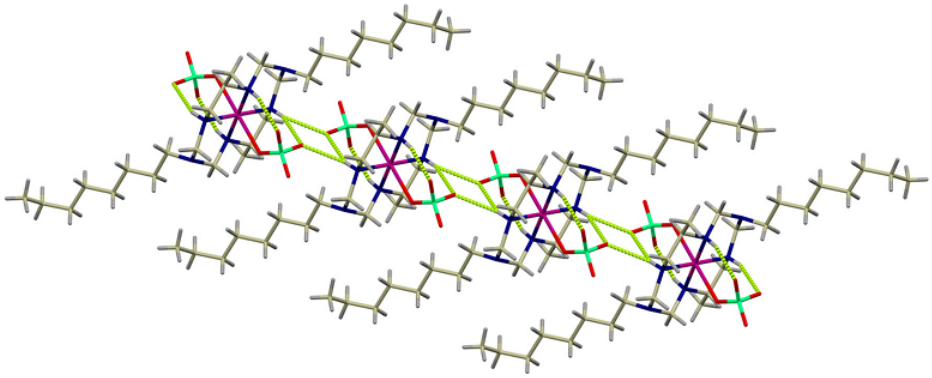

Fig. 2 View of the contacts made by an individual complex molecule with hydrogen bonding interactions drawn as *dashed lines*

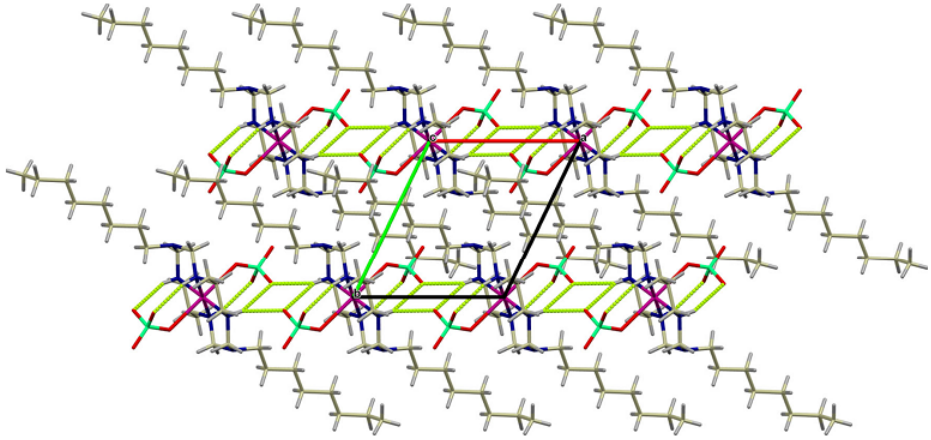

Fig. 3 Two views of 1D hydrogen bonding interaction chains plotted down *c* axes (shown as *dashed lines*)

chains running along *c*-axis as depicted in Fig. 3. The octyl pendant groups of the hexaazamacrocycle did not involve in either intra- or inter-molecular interactions.

FT-IR Spectra

The FT-IR spectrum (Fig. 4) of $[CuL(ClO_4)_2]$ showed a sharp band at 3235 cm^{-1} assignable to the coordinated secondary amine stretching mode. The presence of this band together with the absence of the ν(C=O) of aldehyde in the range 1740–1720 cm^{-1} supported the occurrence of the condensation reaction [49]. The bands around 2927–2855 cm^{-1} could be assigned to sp^2 C–H stretching mode of long chain pendant arms. The broad vibration band at 1100 cm^{-1} which split into two bands at 1140 and 1068 cm^{-1} was assigned to perchlorate ions (ClO_4^-). The

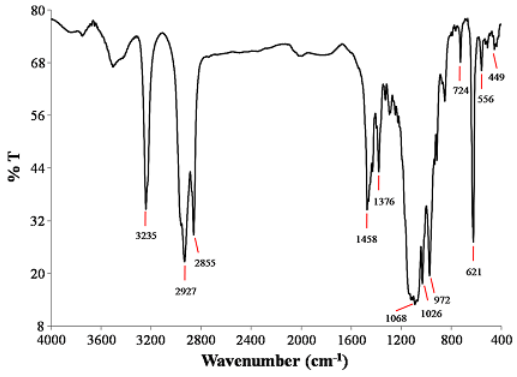

Fig. 4 FT-IR spectra of $[CuL(ClO_4)_2]$

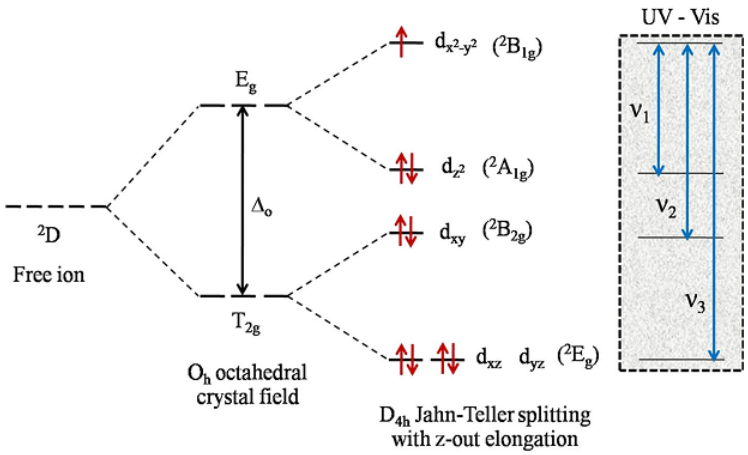

Fig. 5 The crystal field of octahedral and tetragonally distorted octahedral of Cu^{2+} ion

splitting of this band clearly indicated the presence of coordinated perchlorate [1, 50, 51]. As a result, the perchlorate bending vibration was seen as a sharp band at 621 cm^{-1} [35]. The weak bands at 724, 556 and 449 cm^{-1} were assigned to δ(C–H) long chain of alkyl group of pendant arm, ν(Cu–O), and ν(Cu–N), respectively.

Electronic Absorption Spectra

Generally, the six coordinated d^9 Cu(II) complex exists in either the D_{4h} or C_{4v} symmetry with the E_g and T_{2g} levels of the ^2D free ion term split into B_{1g}, A_{1g}, B_{2g} and E_g levels, respectively. Thus, the three spin allowed transitions were expected in the visible or near infrared region. These bands arise from the following transitions, in order of increasing energy $^2B_{1g} \rightarrow {}^2A_{1g}$ ($d_{x^2-y^2} \leftarrow d_z^2$), $^2B_{1g} \rightarrow {}^2B_{2g}$ ($d_{x^2-y^2} \leftarrow d_{xy}$) and $^2B_{1g} \rightarrow {}^2E_g$ ($d_{x^2-y^2} \leftarrow d_{xy}, d_{yz}$) as shown in Fig. 5. The energy level sequence will depend on the amount of tetragonal distortion due to ligand field and Jahn–Teller effects [2, 50, 52].

The electronic absorption spectrum of $[CuL(ClO_4)_2]$ in DMSO solution showed the *d–d* transition of Cu(II) ion in the complex under approximate D_{4h} symmetry at 500 nm corresponding to $^2B_{1g} \rightarrow {}^2B_{2g}$ transition which was consistent with a tetragonally distorted octahedral. This distortion was supported by the single X-ray diffraction data that the axial bonds Cu–O was longer

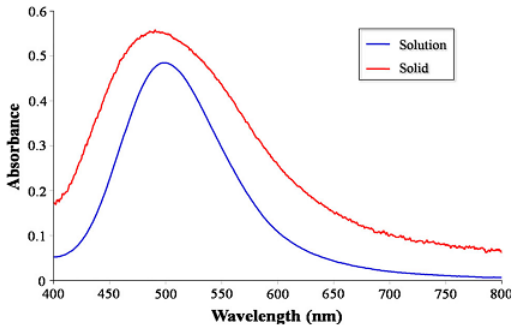

Fig. 6 Electronic absorption spectra of $[CuL(ClO_4)_2]$

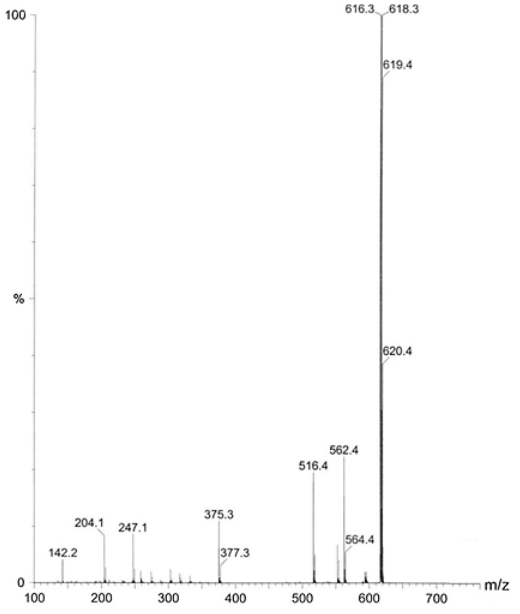

Fig. 7 ESI mass spectrum of $[CuL(ClO_4)_2]$

Scheme 2 Fragmentation pattern of the mass spectrum of $[CuL(ClO_4)_2]$

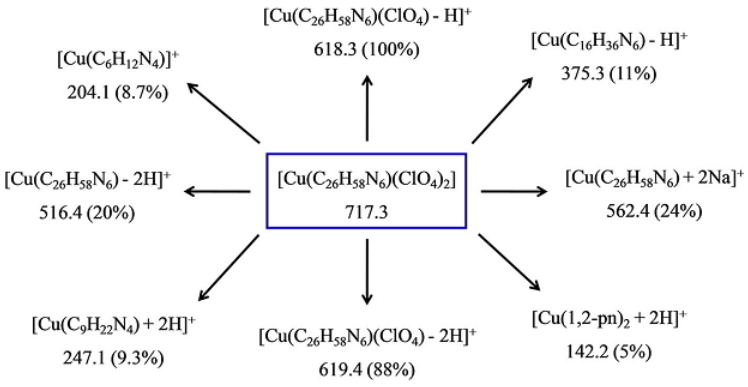

than the Cu–N bonds of the square-planar basal plane as a result from the Jahn–Teller effect with z-out elongation [1, 35, 50, 53].

The solid state electronic absorption band was measured using the diffused reflectance technique and was similar to the spectrum obtained in liquid state above indicating the environment around the metal ion was under similar field strength in both states (Fig. 6).

Thermal Gravimetric Analysis

The thermogram of the $[CuL(ClO_4)_2]$ complex showed no weight loss up to 100 °C indicating the complex was free from lattice water molecules. The TGA curve indicated that the thermal decomposition of this complex involved elimination of perchlorate moiety and finally resulting in the formation of copper oxide [5, 50, 54–56]. The first weight loss of 28.9 % (calculated 27.8 %) was in the range of 120–250 °C corresponding to the loss of two perchlorate molecules. On further heating, the second weight loss was observed in the range 250–860 °C with the loss of macrocyclic ligands. After decomposition of the complex at high temperature above 1000 °C, the weight of the residue (taken as CuO) was 25.1 % (calculated 24.4 %).

LC–MS Spectra

The electro-spay ionization mass spectrometry (ESI–MS) of the complex was studied in positive mode and showed the parent ion peak indicating the stability of the structure in a solution phase (Fig. 7) [20, 50]. The experimental result showed an intense signal corresponding to $[M\text{-anion}]^+$ at *m/z* 618.3 (100 %) (Scheme 2). The different fragments of the complex gave peaks with various intensities at different *m/z* values. The mass spectral data of complex agreed with the formula of the complex with molecular structure obtained from X-ray crystallography.

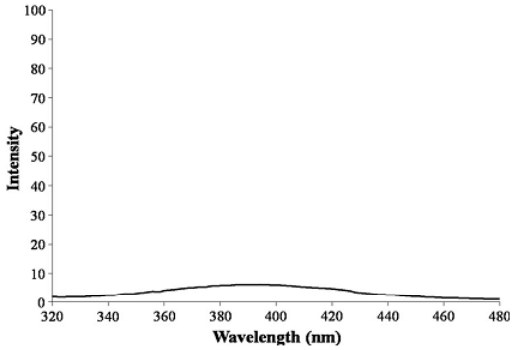

Fig. 8 Emission spectrum of $[CuL(ClO_4)_2]$ at room temperature (excitation at 290 nm)

Luminescent Property

The solid state luminescent spectrum of complex was investigated at room temperature. As shown in Fig. 8, the complex exhibited very faint emission peak at 390 nm ($\lambda_{ex} = 290$ nm) due to the σ–σ* transitions in the side chain alkyl group as a result of lacking n and π electrons [57].

Conclusion

$[CuL(ClO_4)_2]$ complex was synthesized by template condensation reaction. The product was investigated and confirmed by the elemental analysis, FT-IR, UV–Vis, DRS, TGA, and mass spectral techniques. From data the single crystal X-ray diffraction revealed that the Cu(II) ion is in a tetragonally distorted octahedral geometry with macrocyclic ligands in a planar conformation and two perchlorate ions in the axial positions. The solid state UV–vis

absorption spectrum also supported the octahedral structure of complex.

Supplementary Materials

CCDC 1402069 contain the supplementary crystallographic data for this paper. The data can be obtained free of charge via http://www.ccdc.cam.ac.uk, or from the Cambridge Crystallographic Data Centre (CCDC), 12 Union Road, Cambridge, CB2 1EZ, UK; fax: +44(0)1223-336033; e-mail: deposit@ccdc.cam.ac.uk.

Acknowledgments This work was supported by the Songklanagarind Scholarship for Graduate Studies from the Prince of Songkla University. We also thank the Department of Chemistry, Faculty of Science, Prince of Songkla University for the support of all facilities needed in this study.

References

1. Husain A, Nami SAA, Siddiqi KS (2011) Appl Organomet Chem 25(10):761
2. Chandra S, Sharma S (2007) Transit Met Chem 32(2):150
3. Olar R, Badea M, Marinescu D et al (2010) J Therm Anal Calorim 99(3):815
4. Reddy PM, Rohini R, Krishna ER et al (2012) Int J Mol Sci 13(4):4982
5. Pătraşcu F, Badea M, Grecu MN et al (2013) J Therm Anal Calorim 113(3):1421
6. Reddy PM, Prasad AVSS, Shanker K et al (2007) Spectrochim Acta A 68(3):1000
7. Gokulakrishnan S, Parakh P, Prakash H (2012) J Hazard Mater 213–214:19
8. Salavati-Niasari M (2004) Inorg Chem Commun 7(8):963–966
9. Salavati-Niasari M (2004) J Mol Catal A: Chem 217(1–2):87
10. Salavati-Niasari M (2006) Inorg Chem Commun 9(6):628
11. Salavati-Niasari M (2006) Microporous Mesoporous Mater 92(1–2):173
12. Jiang L, Meng X-R, Xiang H et al (2012) Inorg Chem 51(3):1874
13. Lu T-B, Xiang H, Luck RL et al (2002) New J Chem 26:969
14. Shen X, Zhou H, Zhang Q et al (2012) Eur J Inorg Chem 31:5050
15. Kim JC, Lough AJ, Fettinger JC et al (2000) Inorg Chim Acta 303(2):163
16. Lampeka YD, Lightfoot P, Maloshtan IM et al (2001) Theor Exp Chem 37(4):247
17. Liu H, Gu W, Xu G et al (2007) Inorg Chem Commun 10(9):1099
18. Kou H-Z, Gao S, Bai O et al (2001) Inorg Chem 40(24):6287
19. Tsymbal LV, Andriichuk IL, Lampeka YD et al (2010) Russ Chem Bull 59(8):1572
20. Gurumoorthy P, Ravichandran J, Karthikeyan N et al (2012) Bull Korean Chem Soc 33(7):2279
21. Lee Y-T, Kang S-G (2012) Bull Korean Chem Soc 33(8):2517
22. Ou G-C, Zou L-S, Yuan Z-H (2011) Z Kristallogr NCS 226(4):543
23. Li Y-W, Hua Xiang H, Lu TB et al (2004) Acta Crystallogr E 60(3):m312
24. Lampeka YD, Maloshtan IM, Lightfoot Ph et al (1998) Theor Exp Chem 34(6):327
25. Shen L (2002) Acta Crystallogr C 58(12):m588
26. Firdaus F, Fatma K, Azam M et al (2008) Transit Met Chem 33(4):467
27. Cao S, Li H, Chen T et al (2009) J Solut Chem 38(12):1520
28. Su Y-H, Liu J, Li J et al (2007) J Mol Struct 837(1–3):257
29. Lu T-B, Ou G-C, Jiang L et al (2005) Inorg Chim Acta 358(11):3241
30. Ou GC, Su C-Y, Yao J-H et al (2005) Inorg Chem Commun 8(5):421
31. Li Y-W, Xiang H, Lu T-B et al (2004) 2004. Acta Crystallogr E 60(3):m317
32. Min KS, Park MJ, Ryoo JJ (2013) Chirality 25(1):54
33. He Y, Kou H-Z, Li Y et al (2003) Inorg Chem Commun 6(1):38
34. Kim T, Lough AJ, Kim JC (2013) Bull Korean Chem Soc 34(6):1913
35. Husain A, Moheman A, Nami SAA et al (2012) Inorg Chim Acta 384:309
36. Shin JW, Min KS (2009) 2009. Acta Crystallogr E 65(2):m234
37. Shin JW, Rowthu SR, Ryoo JJ et al (2010) Acta Crystallogr E 66(8):m919
38. Li Y-W, Xiang H, Lu T-B et al (2004) Acta Crystallogr E 60(3):m309
39. Han JH, Cha MJ, Kim BG et al (2008) Inorg Chem Commun 11(7):745
40. Bruker (2003) APEX II, SAINT and SADABS. Bruker AXS Inc., Madison
41. Sheldrick GM (2008) Acta Crystallogr A: Found Crystallogr 64(1):112
42. Macrae CF, Bruno IJ, Chisholm JA et al (2008) J Appl Crystallogr 41(2):466
43. Shin JW, Yeo SM, Min KS (2012) Inorg Chem Commun 22:162
44. Hay RW, Crayston JA, Cromic TJ et al (1997) Polyhedron 16(20):3557
45. Cordero B, Gómez V, Platero-Prats AE et al (2008) Dalton Trans 21:2832
46. Pyykkö P, Atsumi M (2009) Chem Eur J 15(1):186
47. Orpen AG, Brammer L, Allen FH et al (1989) J Chem Soc Dalton Trans 12:S1
48. Kim D-W, Shin JW, Moon D (2015) Acta Crystallogr E 71(6):m136
49. Shakir M, Azim Y, Chishit HTN et al (2006) J Braz Chem Soc 17(2):272
50. Sujatha S, Balasubramanian S, Varghese B (2009) Polyhedron 28(17):3723
51. Sujatha S, Balasubramanian S, Varghese B et al (2012) Inorg Chim Acta 386:109
52. Patel KA, Patel SK, Patel CJ et al (2014) J Club Appl Sci 1:1
53. Cho J, Alan J, Lough AJ et al (2003) Inorg Chim Acta 342:305
54. Han S, Lough J, Kim JC (2012) Bull Korean Chem Soc 33(7):2381
55. Kim JA, Park H, Kim JC et al (2008) Inorg Chim Acta 361(7):2087
56. Tao B, Cheng F, Jiang X et al (2012) J Mol Struct 1028:176
57. Subhan MA, Choi J-H (2014) Spectrochim Acta A 123:410

J. Chem. Sci. Vol. 129, No. 4, April 2017, pp. 431–440. © Indian Academy of Sciences.
DOI 10.1007/s12039-017-1255-9

REGULAR ARTICLE

Copper(II) complex as a precursor for formation of cyano-bridged pentanuclear Fe^{III}-Cu^{II} bimetallic assembly: Synthesis, characterization, crystal structure and antibacterial activity

SURACHAI KONGCHOO[a], KITTIPONG CHAINOK[b], ANOB KANTACHA[c] and SUMPUN WONGNAWA[a,*]

[a]Department of Chemistry, Faculty of Science, Prince of Songkla University, Hat Yai, Songkhla, 90112, Thailand
[b]Department of Physics, Faculty of Science and Technology, Thammasat University, Khlong Luang, Pathum Thani, 12120, Thailand
[c]Department of Chemistry, Faculty of Science, Thaksin University, Papayom, Phatthalung, 93110, Thailand
Email: surachai016@yahoo.co.th; kc@tu.ac.th; k_anob@hotmail.com; sumpun.w@psu.ac.th

MS received 17 November 2016; revised 12 February 2017; accepted 22 February 2017

Abstract. $[CuL(ClO_4)_2]$ (**1**) (L = 3,10-diisobutyl-1,3,5,8,10,12-hexaazacyclotetradecane) was synthesized by condensation reaction of ethylenediamine, formaldehyde and *iso*-butylamine in absolute ethanol. Characterization of **1** utilized various spectroscopic techniques, *viz*. elemental analysis, electrospray ionization-mass spectrometry (ESI-MS), Fourier-transform infrared spectroscopy (FT-IR), ultraviolet-visible spectroscopy (UV-Vis), diffuse reflectance spectroscopy (DRS) and thermogravimetric analysis (TGA). Based on these techniques, the structure of **1** was proposed as Cu(II) ion occupying octahedral geometry with four secondary amine nitrogens of the hexaazamacrocyclic ligand and two perchlorato anions. **1** was used as a precursor in the preparation of cyano-bridged bimetallic compound, $[CuL]_3[Fe(CN)_6]_2{\cdot}5H_2O$ (**2**), by reaction with $K_3[Fe(CN)_6]$ in aqueous solution. Single-crystal X-ray analysis indicated that **2** crystallized in the monoclinic system with space group $P2_1/n$. The structure of **2** consisted of cyano-bridged Fe^{III}-Cu^{II} pentanuclear molecules having two $[Fe(CN)_6]^{3-}$ anions connected to three *cis*-$[CuL]^{2+}$ cations *via* two *cis*-cyanide ligands from each ferrate unit. In each of pentanuclear unit, the central $[CuL]^{2+}$ cation exhibited a distorted octahedral geometry while the other two units exhibited a distorted square pyramidal geometry. The room temperature magnetic moments of both complexes were measured to be 1.92 B.M. for **1** and 5.61 B.M. for **2**. The *in vitro* antibacterial activity of **1** against *Staphylococcus aureus* ATCC 25923, *Escherichia coli* ATCC 25922, and *Pseudomonas aeruginosa* ATCC 27853 strains were studied and compared with standard drugs, which showed moderate antibacterial activity compared with Penicillin and Gentamicin.

Keywords. Hexacyanoferrate(III); copper(II) complex; cyano-bridged complex; crystal structure; antibacterial activity.

1. Introduction

The coordination chemistry of hexaazamacrocyclic complexes has become an attractive topic of research because of their various applications in biological field. The importance of these hexaazamacrocyclic ligands and their complexes lie in the fact that they display the structural similarities to the natural hexaazamacrocyclic complexes such as heme in human red blood cell, chlorophyll A and B, and vitamin B12.[1] Especially, the copper(II), nickel(II) and zinc(II) complexes[2,3] of the hexaazamacrocyclic with nitrogen-donor ligands have received much attention recently because of the enhanced thermodynamic and kinetic stability of the resulting complexes[4] and their applications as antifungal,[5] antibacterial,[6] antitumor,[7] and antiviral agents.[8]

Furthermore, the bridged-cyanide bimetallic assemblies based upon hexacyanometalate building blocks $[M(CN)_6]^{n-}$, such as, $[Fe(CN)_6]^{3-}$ or $[Cr(CN)_6]^{3-}$, have several types of molecular-based materials with interesting magnetic properties.[9] The terminal nitrogen atoms of the cyanide ligands of hexacyanoferrate(III) are strong donor atoms that could link two metal ions. Bridged-cyanide transition metal complexes of 3d-3d or 4f-3d electron configurations have received much interest due to the possible uses as magnetic, catalytic, and magneto-optical materials.[10] Recently, six-coordinate hexazamacrocyclic copper(II) complexes were used as the complex ligand to construct a dinuclear (CuFe),[11,12] trinuclear ($CuFe_2$),[13] and pentanuclear (Cu_3Fe_2)[14]

*For correspondence

complexes. It is expected that the coordinated $[CuL]^{2+}$ cation (L = macrocyclic ligands) could accept donor atoms at the axial planes giving rise to a five- or six-coordinate environment around the copper(II) ion.

In this paper, we report part of our work in the realm of copper(II) complexes and bridged-cyanide complexes covering the synthesis, spectroscopic characterization, antibacterial study of $[CuL(ClO_4)_2]$ **(1)**, and X-ray crystal structure of $[CuL]_3[Fe(CN)_6]_2{\cdot}5H_2O$ **(2)** (L = 3,10-diisobutyl-1,3,5,8,10,12-hexaazacyclotetradecane).

2. Experimental

2.1 *Materials and physical measurements*

All chemicals and solvents were of reagent grade and used without further purification. Complex **1** was prepared according to the method previuosly reported.[15] Mass spectrum of **1** was recorded by electrospray ionization (ESI) technique operating in the positive ion mode by directly injecting the solution into the mass spectrometer (Waters Micromass). The simulated isotopic pattern of **1** was generated by mMass version 5.5 - Open Source Mass Spectrometry Tool (http://www.mmass.org/). Electronic absorption spectrum of **1** was obtained on a Shimadzu Lambda-1600 UV-Vis spectrophotometer in the range 400–800 nm. Solid state UV-Vis diffuse reflectance spectra (sample diluted with $BaSO_4$) were recorded with a Shimadzu 2450 PC UV-Vis recording spectrophotometer in the range 400–800 nm. Infrared spectra of solid samples (in KBr pellets) were recorded on a Perkin-Elmer Spectrum One FT-IR spectrophotometer in the range 4000–400 cm^{-1}. Elemental analysis of CHN was performed using a CE instruments Flash EA 1112 series, Thermo Quest analyzer. The thermal curves (TGA) were recorded using a TGA7 Perkin Elmer, USA, with sample mass of 1.96 mg for complex **1** and 0.50 mg for complex **2** over the temperature range 50–1000°C and a heating rate 10°C min^{-1}. Powder X-ray diffraction (PXRD) patterns were recorded on a X'Pert, Philips diffractometer with CuKα radiation. The simulation of PXRD patterns was carried out with the Mercury 3.8 software. Magnetic measurements were performed at room temperature on Lake Shore's fully integrated Vibrating Sample Magnetometer (VSM) system 7400.

Synthesis safety note! Perchlorate salts of metal complexes with organic ligands are potentially explosive and should be handled with great caution.

2.2 *Synthesis of $[CuL(ClO_4)_2]$ (1)*

To a stirred solution of copper(II) chloride dihydrate (0.171 g, 1 mmol) and ethylenediamine (2 mmol) in absolute ethanol (10 mL) was added dropwise a solution of formaldehyde (4 mmol) and *iso*-butylamine (2 mmol) in absolute ethanol (10 mL). The reaction mixture was refluxed for 24 h. The hot solution was filtered, cooled, and perchloric acid was added slowly. The pink color precipitate formed was filtered off, washed with absolute ethanol, and dried in air. The yield was 0.489 g (~75%). M.p.: 262–264°C. Anal. calc. for $C_{16}H_{38}CuN_6O_8C_{12}$: C, 33.32; H, 6.59; N, 14.58%. Found: C, 33.23; H, 6.51; N, 14.77%.

2.3 *Synthesis of $[CuL]_3[Fe(CN)_6]_2{\cdot}5H_2O$ (2)*

To an aqueous solution (15 mL) of $K_3[Fe(CN)_6]$ (0.033 g, 0.10 mmol) was added a DMF solution (15 mL) containing complex **1** (0.056 g, 0.10 mmol) with stirring at room temperature. The resulting brown color precipitate was filtered off and washed several times with water, and dried in air. Well shaped brown single crystals suitable for X-ray structure analysis were grown at room temperature by the slow diffusion of two solutions of the reactants into a H-tube. The yield was 0.039 g (~44%). M.p.: 289–291°C. Anal. calc. for $C_{60}H_{122}Cu_3Fe_2N_{30}O_5$: C, 43.74; H, 6.80; N, 25.51%. Found: C, 43.71; H, 6.78; N, 25.49%.

2.4 *Antibacterial activity of $[CuL(ClO_4)_2]$ (1)*

The *in vitro* antibacterial activity of **1** was tested using agar disc diffusion method and each testing was performed in triplicate. The tests were carried out with three species of Gram-positive and Gram-negative bacteria, namely: *Staphylococcus aureus* (*S. aureus* ATCC 25923), *Escherichia coli* (*E. coli* ATCC 25922), and *Pseudomonas aeruginosa* (*P. aeruginosa* ATCC 27853). Solution of **1** (1 mg mL^{-1}) in dimethylsulfoxide (DMSO) was compared with standard drugs, Penicillin (10 μg $disc^{-1}$) and Gentamicin (10 μg $disc^{-1}$), as the positive control. The inoculums were prepared using a 4–6 h broth culture of each bacterium and adjusted to a turbidity equivalent to a 0.5 McFarland of standard containing approximately 10^4–10^6 CFU mL^{-1}. A sterile cotton swab was dipped into the inoculums and the surface of the nutrient agar (NA) was inoculated by streaking the swab. The paper disks impregnated with the test complex **1** was placed on the solidified medium. The plates were incubated immediately at 37°C for 24 h. The antibacterial activity was evaluated by measuring the diameter of zones showing complete inhibition (mm). Percentage of inhibition was determined by comparing between the distance of the complex **1** and positive control (Penicillin and Gentamicin) as follows:[16]

$$\%\text{inhibition} = \left(\frac{\text{Diameter of the sample}}{\text{Diameter of the positive control}}\right) \times 100$$

2.5 *Crystal structure determination and refinement*

Selected crystallographic data for **2** are given in Table 1. X-ray data were collected on a Bruker APEXII D8 QUEST CMOS diffractometer, using graphite-monochromated Mo K_α radiation (λ = 0.71073 Å) in the ω scanning mode at 298(2) K. Data reduction was carried out by using *SAINT* Program[17] and a semi-empirical absorption-correction (multi-scan,

Table 1. Crystal data and structure refinement parameters of **2**.

Complex	**2**
Empirical formula	$C_{60}H_{112}Cu_3Fe_2N_{30}$
Formula weight	1556.12
Crystal system, space group	Monoclinic, $P2_1/n$
Unit cell dimension	a = 11.8658(5) Å, $\alpha = 90°$ b = 9.7447(3) Å, $\beta = 96.8990(12)°$ c = 37.7968(14) Å, $\gamma = 90°$
V (Å^3)	4338.7(3)
Z	2
D_{cal} (g·cm^{-3})	1.191
μ (mm^{-1})	1.100
F (000)	1642
Crystal size (mm)	0.30 × 0.28 × 0.20
θ range for data collection	3.01−25.75°
Index ranges	$-14 \le h \le 14$, $-11 \le k \le 11$ $-46 \le l \le 46$
Reflections collected	57347
Independent reflections	8205 [$R_{int} = 0.0737$]
Data / restraints / parameters	8205 / 135 / 430
Goodness-of-fit on F^2	1.021
Final R indices [$I > 2\sigma(I)$]	$R_1 = 0.0491$, $wR2 = 0.1241$
R indices (all data)	$R1 = 0.0775$, $wR2 = 0.1340$
Largest diff. peak and hole (eÅ^3)	0.57 and −0.40
Completeness to θ	98.8% ($\theta = 25.75°$)

SADABS[18]) based on the intensities of equivalent reflections. The structures were solved by direct methods using *OLEX2* program[19] and refined by a full-matrix least-squares procedure based on F^2. All non-hydrogen atoms were found from the different map and refined with anisotropic displacement parameters. All hydrogen atoms on carbon atoms were constrained at calculated positions and refined as riding atoms. The molecular structure with atomic labeling scheme and the crystal packing were plotted by Mercury 3.8 program.[20] The crystal structure of **2** displayed disordered solvent water molecules occupancy. An acceptable model for the disordered solvent water molecules was not found, so the disordered density was masked out by using solvent mask route in *OLEX2*. The *OLEX2* program revealed two voids per unit cell at (0.0, 0.5, 0.5) and (0.5, 0.0, 0.0) of 401.3 Å^3 with total electron count per unit cell of 13.2 electrons each. Furthermore, this structure was implicated by the orientation disorder of carbon atoms. The molecule was refined at two positions, the major position of the atoms C16A (51%), C17A (51%), C18A (51 %), C20A (56.7%), C21A (56.7%), C22A (56.7%) and the minor position of the atoms C16B (49%), C17B (49%), C18B (49%), C20B (43.3%), C21B (43.3%), C22B (43.3%).

3. Results and Discussion

3.1 *Synthesis of the complexes*

The condensation reaction of **1** began with the reaction of copper(II)-ethylenediamine complex with formaldehyde to form an imine (C=N) with the loss of two water molecules. Further reaction with *iso*-butylamine which acted as pendant arms yielded a *gem*-diamine to give the first six-membered ring. The same reaction path could also take place on the other side to form the second six-membered ring. Finally, the target hexaazamacrocyclic complex **1** was obtained. For complex **2**, the complex **1** was used as a precursor to react with hexacyanoferrate(II) ion. The cyanide ions replaced the perchlorate anions due to its stronger ligand field power in spectrochemical series resulting in a new structure that is different from those ever reported in the literatures.

3.2 *FT-IR spectroscopy*

The FT-IR spectrum (Figure S1, in Supplementary Information) of **1** showed the absence of a strong band in the range 1720–1740 cm^{-1} corresponding to carbonyl group of aldehydic moiety confirming the completion of condensation reaction.[3] A sharp band around 3244 cm^{-1} was assigned to ν(N-H) stretching vibration of the secondary amine groups of the hexaazamacrocyclic ligands. A medium band appearing in the range 2872–2961 cm^{-1} was assigned to $\nu(sp^3$ C-H). In the region 1100 cm^{-1}, splitting to two bands at 1080 and 1119 cm^{-1} corresponded to ν(Cl-O) stretching and a sharp band at 627 cm^{-1}, was assigned to δ(Cl-O) bending vibration of the perchlorate ions. The splitting of ν(Cl-O) band clearly indicated the presence of coordinated perchlorate.[21] In complex **2**, the FT-IR spectrum (Figure S2, in Supplementary Information) showed strong band at 3247 cm^{-1} which was assigned to secondary amine group. The vibrations from cyanide ligand may vary depending on the bonding mode,[22–24] the two absorption bands observed at 2117 and 2097 cm^{-1} were assigned to the terminal cyanide and the bridging cyanide ions, respectively. The assignment of the former was based on the comparison with that of $K_3[Fe(CN)_6]$ which shows a sharp band at 2117 cm^{-1} while the bridging mode of the type M-C≡N-M' appears at the lower energy[25]. The bands of the ν(Cl-O) of perchlorate ions disappeared due to the perchlorate being replaced by hexacyanoferrate(III) ions.

3.3 *ESI-MS spectroscopy*

The ESI mass spectrum (Figure S3, in Supplementary Information) of **1** showed the parent ion peaks of $[CuL(ClO_4)-2H]^+$ at m/z 476.1 (100%). This molecular ion underwent fragmentation in two ways. First, with the release of C_3N_2 radical, the new fragment ion cooresponding to $[Cu(C_{13}H_{38}N_4)-ClO_4)]^+$ species was observed with m/z 412.2 (28%). The other path was the release of perchlorate anion which gave fragment ion peak at m/z 376.2 (5%) cooresponding to $[Cu(C_{16}H_{38}N_6)]^{2+}$ species, which on further release of $C_5H_{11}N$ radical gave a fragment ion peak at m/z 291.2 (5%) cooresponding to $[Cu(C_{11}H_{27}N_5)]^{2+}$ species. Fragmentation of the last species continued to $[Cu(C_9H_{20}N_4)]^{2+}$ with m/z = 247.1 (10%), $[Cu(C_8H_{18}N_4)]^{2+}$ with $m/z = 233.1$ (8%), and $[Cu(C_6H_{13}N_3)]^{2+}$ with $m/z = 190.0$ (35%), respectively. Further confirmation for the proposed structure of **1** came from the appearance of other peaks containing ^{65}Cu besides the peaks due to successive degradation of the target complex to various fragments.[26] The simulated isotopic pattern is in good agreement with the measured spectrum (Figure S4, in Supplementary Information). Similar type of ESI mass spectral pattern was also observed in the hexaazamacrocyclic copper(II) complex reported previously.[21] Based on the physico-chemical and the spectral studies, the structure proposed for **1** is shown in Figure 1.

3.4 *Electronic absorption spectra*

Complex **1** showed a distinct single *d–d* transition band (Figure S5, in Supplementary Information) which could be assigned to $^2T_{2g} \leftarrow {}^2E_g$ transition. In solution, λ_{max} appeared at 514 nm (ε = 38 L mol^{-1} cm^{-1}) while in the solid state it was at 512 nm. The peak was slightly unsymmetrical as a result of the Jahn-Teller distortion inherited with the d^9 configuration of Cu^{2+} ion. Distorted octahedral geometry due to Jahn-Teller distortion normally shows weak absorption bands at around 625 nm and often a broad band in the near infrared region.[27] Solid state DRS of complex **2** exhibited a shoulder absorption band at 530 nm in the visible region which could be attributed to *d–d* transition occurred from overlay between Cu^{2+} and Fe^{3+} ions. The shift to longer wavelengths was assigned to stabilization of the Fe^{3+} *d*-orbital because the weakening of the σ-donor types of the cyanide ligands.[28,29] Other absorption bands below 380 nm were assigned to $\pi \rightarrow \pi^*$, $n \rightarrow \pi^*$, and $n \rightarrow \sigma^*$ transitions, and the maximum absorption band at 431 nm was assigned to the ligand-to-metal charge transfer (LMCT) due to the presence of $[Fe(CN)_6]^{3-}$ ions.[30]

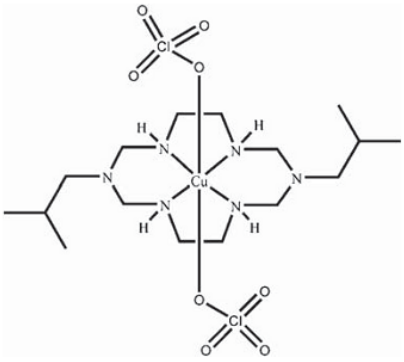

Figure 1. The proposed structure of $[CuL(ClO_4)_2]$ (**1**).

3.5 *Thermal analysis*

Thermogravimetric analyses (TGA) of **1** and **2** were recorded in N_2 atmosphere in the temperature range 50–1000°C (Figure S6, in Supplementary Information). TGA curve of **1** revealed three steps of weight losses. The first weight loss (47.5%) appeared in the range 200–260°C corresponding to the loss of one *iso*-butyl molecule and two perchlorate anion (calculated 47.60%). The second stage at 260–650°C with a weight loss of 27.83% corresponded to the weight loss of one *iso*-butyl molecule and hexaazamacrocycle (calculated 22.88%). The final residue, presumably CuO, was obtained with weight loss of 24.64% (calculated 24.71%). Complex **2** also exhibited four steps of dissociation in TGA curve. The first decomposition started in the temperature range 120–200°C with the weight loss of 5.06% (calculated 5.46%) corresponding to release of five lattice water molecules. The second weight loss of 40.37% took place at 200–285°C was attributed to the loss of hexaazamacrocyclic ligand and cyanide group (calculated 40.20%). The third step of 20.54% at 285–600°C corresponded to loss of one hexaazamacrocyclic ligand (calculated 20.15%). The remaining mass of 2.47% (calculated 2.51%), mixture product of CuO + FeO, was obtained above 600°C.

3.6 *Crystal structure of $[CuL]_3[Fe(CN)_6]_2 \cdot 5H_2O$ (**2**)*

Selected bond lengths and bond angles are listed in Table 2. The molecular structure of **2** is presented in Figure 2, together with the atomic labeling scheme and the unit cell packing diagram are illustrated in Figure 3. X-ray crystallographic study revealed that complex **2** belonged to the monoclinic system with space group

$P2_1/n$. The asymmetric unit of **2** consisted of core structure of three $[CuL]^{2+}$ cations, two $[Fe(CN)_6]^{3-}$ anions and five water molecules as lattice solvent. Addison *et al.*,[31] have suggested the angular structural parameter (τ) to differentiate between trigonal bipyramidal (TBP, $\tau = 1$) and square pyramidal (SP, $\tau = 0$) in five-coordinated metal complexes. The parameter τ is defined as $\tau = (\beta - \alpha)/60$ where α and β are the two largest coordination angles. In our case, the five-coordinated Cu1 center exhibited $\tau = 0.115$ which favored the square pyramidal geometry defined by the bondings to four nitrogen atoms of the macrocyclic ligand with the average Cu1-$N_{macrocyclic}$ bond length of 2.013(3) Å and one nitrogen atom of cyanide ligand from $[Fe(CN)_6]^{3-}$ anion with the Cu1-N1 distance of 2.303(3) Å. The Cu2 center showed distorted octahedral geometry with the equatorial planes composed of four nitrogen atoms of the macrocyclic ligand with the average Cu2-N_{eq} bond distance of 2.009(3) Å and the axial sites coordinated to two nitrogen atoms from cyanide ions with the Cu2-N_{ax} distance of 2.579(3) Å. The fact that the Cu2-N_{ax} distances were much longer than the Cu2-N_{eq} distances could be attributed to the Jahn-Teller distortion of the d^9 configuration of the Cu^{2+} ion.[32–35] In the crystal structure, each Fe^{3+} ion coordinated to six carbon atoms from the cyanide ligands in an octahedral geometry. The bond angles of the *cis*-N-C-Fe for the terminal cyanide ligands were ~177.0° and those for the bridging cyanide ligands were slightly bent to ~176.2°. The average bond distance of cyanide-bridge was 1.147(4) Å while those of the terminal cyanide ligands were in the range 1.146–1.154 Å which were in the normal range for low spin cyanide complexes of Fe^{3+} ion.[36,37] Hydrogen bonding interactions were observed between the hydrogen atoms (H9, H11 and H14) from the secondary amine (N9, N11 and N14) of the macrocyclic ligand with the nitrogen atoms (N3 and N4) of the terminal cyanide ligands with the contacts of N9-H9···N3 = 2.453 Å, N11-H11···N4 = 2.565 Å, and N14-H14···N3 = 2.419 Å generating a 2D supramolecular interactions as depicted in Figure 4 (plotted along *a*-axis).

Table 2. The selected bond lengths (Å) and bond angles (°) of **2**.

Bond lengths			
Cu1-N1	2.303(3)	Cu2-N2	2.579(3)
Cu1-N8	2.009(3)	Cu2-N14[1]	2.011(3)
Cu1-N9	2.013(3)	Cu2-N15[1]	2.007(3)
Cu1-N11	2.008(3)	Fe1-C3	1.942(3)
Cu1-N12	2.022(3)	Fe(1)-C4	1.944(3)
Fe1-C0AA	1.941(3)	Fe(1)-C5	1.941(5)
Fe1-C1AA	1.944(3)	Fe(1)-C6	1.940(5)
Bond angles			
N8-Cu1-N1	92.85(11)	N14[1]-Cu2-N14	179.99(1)
N9-Cu1-N1	93.13(10)	N15[1]-Cu2-N15	180.00(1)
N9-Cu1-N12	170.77(10)	N15-Cu2-N2	86.61(12)
N11-Cu1-N8	170.07(11)	C0AA-Fe1-C4	93.55(12)
N14-Cu2-N2	92.17(10)	C1AA-Fe1-C4	175.67(13)

Symmetry transformations used to generate equivalent atoms: 1 = 1−x,1−y,1−z.

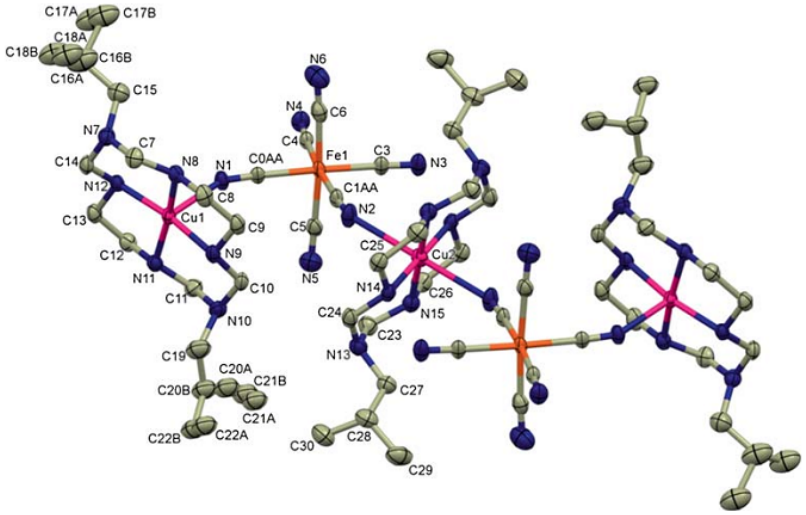

Figure 2. Crystal structure of **2** with the atomic labeling scheme. Solvent molecules and all hydrogen atoms are omitted for clarity. Thermal ellipsoids are drawn at the 40% probability level.

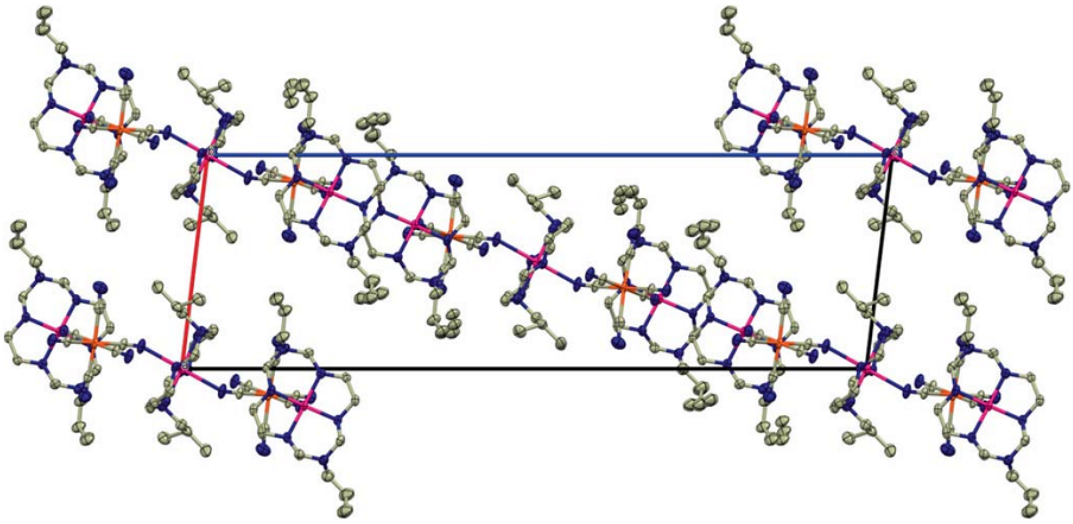

Figure 3. The molecular packing arrangement of **2** plotted along the *b* axis.

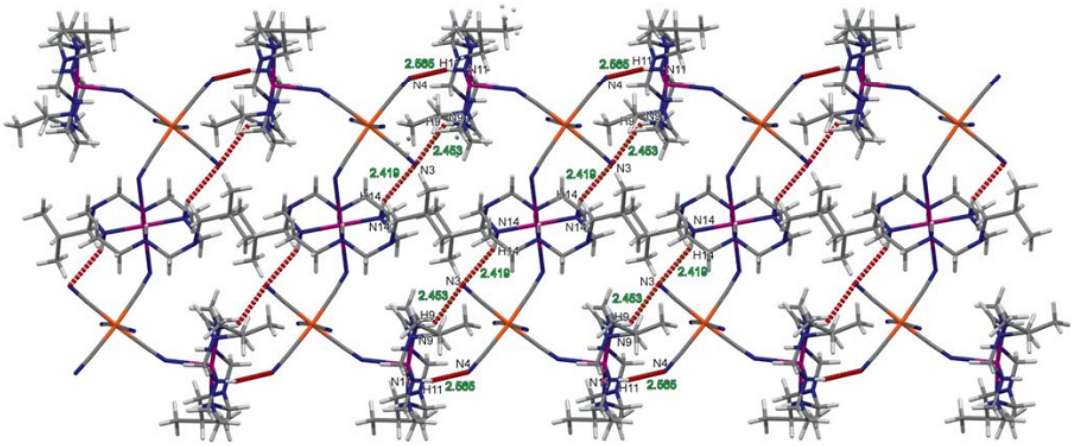

Figure 4. The 2D supramolecular structure of **2**, showing hydrogen bonding (N-H· · · N) indicated by dotted lines.

In addition, the structural parameters of the hexaazamacrocyclic ligand were similar to those found in linked metal complexes reported in literatures. It should be indicated that in the $[ML]^{2+}$ cation and $[Fe(CN)_6]^{3-}$ anions (where M = Cu(II) or Ni(II) and L = 3,10-dialkyl-1,3,5,8,10,12-hexaazacyclotetradecane), the $[Fe(CN)_6]^{3-}$ revealed different coordination styles depending on pendant arms of the hexaazamacrocyclic ligand. In the work by Shen *et al.*,[33] on the complex $[CuL^4]_3[Fe(CN)_6]_2 \cdot 2H_2O$ (L^4 = 3,10-dibutyl-1,3,5,8,10,12-hexaazacyclotetradecane), each $[Fe(CN)_6]^{3-}$ anion linked to three $[CuL^4]^{2+}$ cations *via* three *mer*-C≡N and each $[CuL^4]^{2+}$ cation was connected to two $[Fe(CN)_6]^{3-}$ anions in *trans* positions resulting in a 2D ring-like structure. Yuan *et al.*,[38] reported the complex $[CuL]_2[Fe(CN)_6]ClO_4 \cdot H_2O$ (L = 3,10-dipropyl-1,3,5,8,10,12-hexaazacyclotetradecane) where each $[Fe(CN)_6]^{3-}$ anion connected to four $[CuL]^{2+}$ cations using four co-planar cyanide groups to axially bind to the $[CuL]^{2+}$ cations in the *trans* position forming *trans*-$CuL(N{\equiv}C)_2$ moieties resulting in a novel 3D honeycomb-like structure. Thus, by resonably designing the organic ligands, it

is possible to synthesize complexes with a variety of crystal structures giving advantage in searching for the expected physicochemical properties.

3.7 *Powder X-ray diffraction of $[CuL]_3[Fe(CN)_6]_2 \cdot 5H_2O$ (**2**)*

Complex **2** was characterized by powder X-ray diffraction and compared with the simulated one based on the single crystal data (Figure S7, in Supplementary Information). Both spectra are identical indicating that the bulk synthesized material and the as-grown crystals were homogeneous.

3.8 *Magnetic measurements*

The effective magnetic moment (μ_{eff}) of **1** was 1.92 B.M. corresponding to the d^9 electronic configuration. The observed value is slightly higher than the spin-only value of one unpaired electron 1.73 B.M. suggesting the octahedral coordination geometry.[39] The μ_{eff} values of copper(II) octahedral complexes normally lie between 1.8-2.2 B.M. depending on the magnitudes of orbital contribution and spin-orbit coupling.[40–42] The μ_{eff} of **2** was 5.61 B.M. which was higher than the combined magnetic moment one would expect in the multinuclear complexes calculated from the simple relation:[43] $\mu_{eff\_T} = \{3(\mu_{eff} \text{ of } \mathbf{1})^2 + 2(\mu_{eff} \text{ of } K_3[Fe(CN)_6])^2\}^{1/2}$, where the magnetic moment of $K_3[Fe(CN)_6]$ is 2.31 B.M. The observed value of **2** indicated that the ferromagnetic interaction in μ_{eff_T} was much greater than $\mu_{spin-only}$ due to the combination effect of the spins coupling in parallel which occured between the Cu^{2+} and the low-spin configuration Fe^{3+} as a result of the strict orthogonality.[44] From the crystal structure of **2**, Cu^{2+} ions in square-pyramidal and octahedral surrounding had one unpaired electron (per each ion) in $d^2_{x^2-y^2}$ orbital which interacted with the molecular orbitals of bridged-cyanide having appropriate symmetry giving a magnetic orbital with σ type.[43] Meanwhile, each low-spin Fe^{3+} ion in octahedral geometry environment had one unpaired electron in d_{xy}, d_{xz}, and d_{yz} which interacted with other molecular orbitals of bridged-cyanide of the same symmetry to give a magnetic orbital with π type.[45] From this scenario, we may expect the ferromagnetic behaviour in this pentanuclear complex **2**.

3.9 *Antibacterial activity*

Complex **1** was tested for antibacterial activity *in vitro* using one Gram-positive (*S. aureus*) and two Gram-negative (*E. coli* and *P. aeruginosa*) bacteria. The sensibility of the bacterial strains to **1** evaluated by measuring the diameter of the inhibition zone and % inhibition are shown in Figures 5 and 6. The results showed moderate activity against all bacteria under investigation compared with inert non-complexed starting materials. The increase in activity upon coordination formation could be described on the basis of Overtone's concept[46] and Tweedy's chelation theory.[47,48] According to the Overtone's concept of cell permeability, the lipid membrane that surrounds the cell favors the passage of only lipid-soluble materials owing to liposolubility is considered to be an important factor controlling antimicrobial activity. On Tweedy's chelation, the polarity of metal ion will be reduced to a greater extent due to the overlap of the ligand orbital and the partial sharing of the positive charge of the metal ion with the ligand donor atoms.[49] Besides, it increases the delocalization of electrons over the whole chelate ring. This may increase the lipophilic feature of the metal complex, enabling it to permeate the lipid membrane of the bacteria and thus killing them more effectively. Also, factors such as

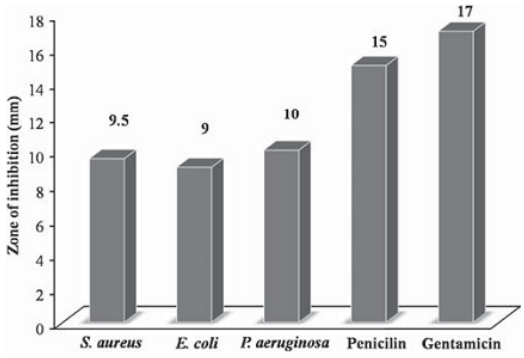

Figure 5. The antibacterial activity of $[CuL(ClO_4)_2]$ (**1**).

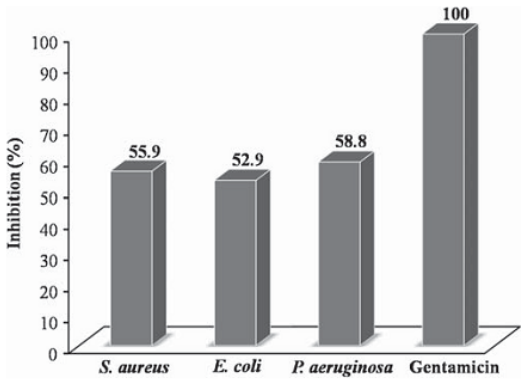

Figure 6. Percentage of inhibition of $[CuL(ClO_4)_2]$ (**1**).

solubility, different dipole moments and cell permeability mechanisms may be affected by the presence of the different anions and this affects the mechanism of permeation through the lipid layer of the organisms killing more of them effectively.[50]

4. Conclusions

In summary, we have reported the synthesis of a new hexaazamacrocyclic copper(II) complex, $[CuL(ClO_4)_2]$ (**1**), and bimetallic pentanuclear complex, $[CuL]_3[Fe(CN)_6]_2{\cdot}5H_2O$ (**2**). The structural characterizations of the synthesized complexes were investigated by elemental analyses, spectroscopic techniques, and X-ray diffraction. The proposed structure of **1** was octahedral geometry in which the copper(II) ion is coordinated to four nitrogen atoms from hexaazamacrocyclic ligand and two oxygen atoms from perchlorate anions. In the crystal structure of **2**, one of the $[Fe(CN)_6]^{3-}$ ions used two *cis*-cyanide ligands to link with *cis*-$[CuL]^{2+}$ cations in which each of the copper(II) ion had a five- or six-coordinated geometry leading to the formation of a pentanuclear Cu_3Fe_2 bimetallic structure. Complex **1** simply showed a paramagnetic property while **2** showed strong paramagnetism which very likely puts it in the ferromagnetic class. With regard to application, **1** displayed moderate antibacterial activity against *S. aureus*, *E. coli* and *P. aeruginosa*, thus, the exploitation of this complex could be in the treatment of bacterial infections.

Supplementary Information (SI)

CCDC 1510377 contains the supplementary crystallographic data for this paper. These data can be obtained free of charge *via* http://www.ccdc.cam.ac.uk, or from the Cambridge Crystallographic Data Centre (CCDC), 12 Union Road, Cambridge, CB2, 1EZ, UK; fax: +44(0)1223-336033; email: deposit@ccdc.cam.ac.uk. FT-IR spectra (Figures S1, S2), ESI-MS spectrum (Figure S3), simulated isotopic pattern (Figure S4), electronic absorption spectrum (Figure S5), TGA curves (Figure S6), and PXRD pattern (Figure S7) are given in Supplementary Information, available at www.ias.ac.in/chemsci.

Acknowledgements

This work was supported by the Songklanagarind Scholarship for Graduate Studies from the Prince of Songkla University. We also thank the Department of Chemistry, Faculty of Science, Prince of Songkla University for support of all research utilities.

References

1. Biswas F B, Roy T G, Rahman M A and Emran T B 2014 An *in vitro* antibacterial and antifungal effects of cadmium(II) complexes of hexamethyltetraazacyclotetradecadiene and isomers of its saturated analogue *Asian Pac. J. Trop. Med.* **7** 534
2. Husain A, Nami S A A and Siddiqi K S 2011 The synthesis, crystal structures and antimicrobial studies of *C*-methyl-substituted hexaaza macrocycle of Cu(II) having aromatic pendant arm *Appl. Organomet. Chem.* **25** 761
3. Shakir M, Azim Y, Chishti H T N, Begum N, Chingsubam P and Siddiqi M Y 2006 Synthesis, physico-chemical and antimicrobial screening studies on 14 and 16-membered hexaazamacrocyclic complexes bearing pendant amine groups *J. Braz. Chem. Soc.* **17** 272
4. Degagsa B, Faye G and Fernandez N 2013 Synthesis, characterization and antimicrobial activity of hexamethylenetetramine copper(II) complex *World J. Pharm. Pharm. Sci.* **2** 6391
5. Kumar U and Chandra S 2011 Synthesis, spectral and antifungal studies of some coordination compounds of cobalt(II) and copper(II) of a novel 18-membered octaaza $[N_8]$ tetradentate macrocyclic ligand *J. Saudi Chem. Soc.* **15** 187
6. Singh J, Kanojia R and Tyagi M 2014 Template synthesis and spectral studies of biologically active Ni(II), and Cu(II) transition metal complexes of tetradentate azaoxo (N_2O_2) macrocyclic ligand *Int. J. Pharm. Sci. Res.* **5** 3903
7. Singh J, Jain P and Tyagi M 2014 Synthesis, IR, EPR, UV-Visible characterization and in vitro antimicrobial activity of macrocyclic schiff's base and its metal complexes of Mn(II) and Co(II) *World J. Pharm. Pharm. Sci.* **3** 953
8. Colette A, Ondoh A M, Yufanyi D M and Gaelle D S Y 2015 Synthesis, crystal structure and antimicrobial properties of an anhydrous copper(II) complex of pyridine-2-carboxylic acid *Int. J. Chem.* **7** 10
9. Bellouard F, Miguel C-L, Coronado E, José R G-M, Carlos J G-G, Romero F and Dunbar K R 2002 Unusual magnetic behavior in the layered ferromagnet $[Ni(C_6H_{14}N_2)_2]_3$-$[Fe(CN)_6]_2{\cdot}2H_2O$ *Eur. J. Inorg. Chem.* **2002** 1603
10. Kou H-Z, Zhou B C, Gao S and Wang R-J 2003 A 2D cyano- and oxamidato-bridged heterotrimetallic Cr^{III}-Cu^{II}-Gd^{III} complex *Angew. Chem. Int. Ed.* **42** 3288
11. Zhang K-L, Xu Y, Wang Z, Jin C-M and You X-Z 2002 Synthesis, crystal structure and magnetic properties of the first dinuclear copper(II)–iron(II) complex $[Cu(L)Fe(CN)_5NO]$ based on nitroprusside *Transition Met. Chem.* **27** 95
12. Shen L, Wang H-T, Zhang Y-J and Jin Z-M 2004 *catena*-Poly [[[1,8-bis(2-hydroxy- ethyl)-1,3,6,8,10,13-hexaazacyclotetradecane]copper(II)]-μ-cyano-[tricyano-nitroso iron(III)]-μ-cyano] *Acta Crystallogr. Sect. C* **60** 180
13. Zhou B-C, Kou H-Z, Li Y, Xiong M and Wang R-J 2003 Synthesis, characterization and crystal structure of the first tri-nuclear MFe_2 (M = Cu and Ni) complexes based on nitroprusside *Chin. J. Chem.* **21** 1159

14. Lim J H, Yoon J H, Choi S Y, Ryu D W, Koh E K and Hong C S 2011 Cyano-bridged pentanuclear and honeycomblike $M^{III}Cu^{II}$ (M = Fe, Cr) bimetallic assemblies: Structural variations modulated by side groups of macrocyclic ligands and magnetic properties *Inorg. Chem.* **50** 1749
15. Suh M P and Kang S-G 1988 Synthesis and properties of nickel(II) and copper(II) complexes of 14-membered hexaaza macrocycles, 1,8-dimethyl- and 1,8-diethyl-1,3,6,8,-10,13-hexaazacyclotetradecane *Inorg. Chem.* **27** 2544
16. Mulaudzi R B, Ndhlala A R, Kulkarni M G, Finnie J F and Staden J V J 2011 Antimicrobial properties and phenolic contents of medicinal plants used by the Venda people for conditions related to venereal diseases *J. Ethnopharmacol.* **135** 330
17. APEX II, SAINT and SADABS 2008 Madison, (WI, USA): Bruker AXS Inc.
18. Sheldrick G M 2008 A short history of SHELX *Acta Crystallogr. Sect. E* **64** 112
19. Dolomanov O V, Bourhis L J, Gildea R J, Howard J A K and Puschmann H J 2009 OLEX2: A complete structure solution, refinement and analysis program *J. Appl. Crystallogr.* **42** 339
20. Macrae C F, Bruno I J J, Chisholm A, Edgington P R, McCabe P, Pidcock E, Rodriguez-Monge L, Taylor R, Streek J V D and Wood P A 2008 *Mercury CSD 2.0*-new features for the visualization and investigation of crystal structures *J. Appl. Crystallogr.* **41** 466
21. Kongchoo S, Kantacha A, Saithong S and Wongnawa S 2016 Synthesis, crystal structure, and spectroscopic properties of Cu(II) complex with 14-membered hexaazamacrocyclic ligands *J. Chem. Crystallogr.* **46** 222
22. Mock M T, Matthew T K-E, Popescu C V, Gasda P, Yap G P A and Riordan C G 2009 A series of cyanide-bridged binuclear complexes *Inorg. Chim. Acta* **362** 4553
23. Li G-L, Zhang L-F, Ni Z-H, Kou H-Z and Cui A-L 2012 Cyanide-bridged Cr^{III}-Mn^{II} binuclear complexes based on $[Mn(phen)_2]^{2+}$ and dicyanidechromate(III) building blocks: Syntheses, crystal structures, and magnetic properties *Bull. Korean Chem. Soc.* **33** 1675
24. Şenocak A, Karadağ A, Yerli Y, Andaç Ö and Şahin E 2010 Two novel bimetallic cyano-bridged coordination polymers containing the 2,2′-(ethylenedioxy)bis (ethylamine): Syntheses, structural, thermal, and magnetic properties *J. Inorg. Organomet. Polym.* **20** 628
25. Nakamoto K 1978 In *Infrared and Raman Spectra of Inorganic and Coordination Compounds* (New York: Wiley) p. 110
26. Hassan N H, Ali N M, Yamin B M, Karim N H A and Ghani N A A 2014 Synthesis and characterization of 5,5,7,12,12,14-hexamethyl-1,4,8,11-tetraazacyclotetradeca-7,14-dienium diperchlorate copper(II) complex *Malaysian J. Anal. Sci.* **18** 562
27. Prakash N B 2014 Synthesis and studies of tetraaza macrocyclic complexes of transition metal ions *Scholarly J. Phys. Appl. Chem.* **1** 17
28. Uddin M N, Chowdhury D A and Akter J 2014 Bimetallic heteronuclear complexes bridged with ferrichexathiocyanate: Synthesis, characterization and antibacterial properties *J. Pure Appl. Chem. Res.* **3** 99
29. Uddin M N, Akter J and Manchur M A 2013 Cyano bridged bimetallic compounds of the type M^{2+}-NC-Fe^{3+} (M = Co, Ni, Cu, Zn, Cd) using the $[Fe(CN)_6]^{3-}$ building block and their antibacterial evaluation *Orbital: Electron. J. Chem.* **5** 257
30. Smékal Z and Biler M 1998 The complexes of iron(II,III) and copper(II) or nickel(II) with cyanide as bridging ligand *Acta Univ. Palack. Olomuc. Fac. Rerum. Natur.* **37** 49
31. Addison A W, Rao T N, Reedijk J, Rijn J V and Verschoor G C 1984 Synthesis, structure, and spectroscopic properties of copper(II) compounds containing nitrogen-sulphur donor ligands; the crystal and molecular structure of aqua[1,7-bis(*N*-methylbenzimidazol-2′-yl)-2,6-dithiaheptane]copper(II) perchlorate *J. Chem. Soc., Dalton Trans.* **7** 1349
32. Cha M J, Shin J W, Lee Y H, Kim Y, Kim B G and Min K S 2009 Structure and magnetic properties of a novel branch-like one-dimensional cyano-bridged assembly $[Cu(L)]_3[Fe(CN)_6]_2{\cdot}8H_2O$ (L = 6,13-dimethyl-6-nitro-1,4,8,11-tetraazabicyclo[11.1.1]-pentadecane) *Inorg. Chem. Commun.* **12** 520
33. Shen X-P, Gao S, Yin G, Yu K-B and Xu Z 2004 Crystal structure and magnetic behavior of a three-dimensional cyano-bridged assembly $[CuL^1]_2[Cr(CN)_6]ClO_4{\cdot}0.5H_2O$ (L^1 = 3,10-dipropyl-1,3,5,8,10,12-hexaazacyclotetradecane) *New J. Chem.* **28** 996
34. Shen X-P, Xu Y, Zhou H, Shu H-Q and Yuan A-H 2008 Crystal structure and magnetic properties of a cyano-bridged bimetallic assembly $[CuL^4]_3[Fe(CN)_6]_2{\cdot}2H_2O$ (L^4 = 3,10-dibutyl-1,3,5,8,10,12-hexaazacyclotetradecane) *J. Mol. Struct.* **892** 58
35. Lu T, Xiang H, Chen S, Su C, Yu K, Mao Z, Cheng P and Ji L J 1999 $[CuL(H_2O)_2]$- $\{[CuL][Fe(CN)_6]\}_2{\cdot}2H_2O$ (L=3,10-Bis(2-hydroxyethyl-1,3,5,8,10,12-hexaazacyclotetra- decane): A novel three-dimensional coordination polymer *via* H-bonded linkages of one-dimensional zigzag Chain *Inorg. Organomet. P* **9** 165
36. Zhang S-W, Duan C-Y, Sun W-Y, Fu D-G and Tang W-X 2001 A 2-D bimetallic assembly with bridging cyanide ions *Transit. Metal Chem.* **26** 127
37. Dogaru A, Dechambenoit P, Shova S and Aandruh M 2015 Synthesis and crystal structures of three new cyanide-bridged heterometallic complexes *Rev. Roum. Chim.* **60** 371
38. Yuan A-H, Shen A-P and Zhou H 2008 Crystal structure and magnetic properties of a three-dimensional complex constructed from $[CuL]^{2+}$ and $[Fe(CN)_6]^{3-}$ precursors *Transit. Metal Chem.* **33** 133
39. Nagesh G Y, Mahadev U D and Mruthyunjayaswamy B H M 2015 Mononuclear metal(II) Schiff base complexes derived from thiazole and o-vanillin moieties: Synthesis, characterization, thermal behaviour and biological evaluation *Int. J. Pharm. Sci. Rev. Res.* **31** 190
40. Rajakumar R, Raman N and Rajeswari S 2012 Preparation, characterization, antibacterial and DNA binding studies of phenylenediamine mixed ligand complex of copper (II) benzoate *J. Chem. Bio. Phys. Sci. Sec. A* **2** 1717
41. Ekennia A C, Onwudiwe D C, Olasunkanmi L O, Osowole A A and Ebenso E E 2015 Synthesis, DFT calculation, and antimicrobial studies of novel Zn(II),

Co(II), Cu(II), and Mn(II) heteroleptic complexes containing benzoylacetone and dithiocarbamate *Bioinorg. Chem. Appl.* **2015** 1

42. Spinu C and Kriza A Co(II), Ni(II) and Cu(II) Complexes of bidentate Schiff bases *Acta Chim. Slov.* **47** 179
43. Kou H-Z, Liao D-Z, Cheng P, Jiang Z-H, Yan S-P, Wang G-L, Yao X-K and Wang H-G 1997 Crystal structure and magnetic behaviour of a two-dimensional step-shaped cyano-bridged complex $[Cu(dien)]_3[Fe(CN)_6]_2{\cdot}6H_2O$ (dien=diethylenetriamine) *J. Chem. Soc., Dalton Trans.* **9** 1503
44. Li Y-T, Yan C-W and Liao D-Z 1999 Synthesis and ferromagnetic interaction in oxamido-bridged heterodinuclear copper(II)-chromium(III) complexes *Chin. J. Chem.* **17** 24
45. Ohba M, Ohkawa H, Fukita N and Hashimoto Y 1997 Bimetallic magnetic material $[Ni(diamine)_2]_2[Fe(CN)_6]X$ with two-dimensional network extended by Fe(III)-CN-Ni(II) linkages *J. Am. Chem. Soc.* **119** 1011
46. Agwara M O, Yufanyi M D, Foba-Tendo J N, Atamba M A and Ndinteh D T J 2011 Synthesis, characterization and biological activities of Mn(II), Co(II) and Ni(II) complexes of hexamethylenetetramine *Chem. Pharm. Res.* **3** 196
47. Gupta R and Gupta K C 2012 Synthesis, IR spectral studies and antimicrobial studies of some rare earth metal complexes with meso 2,3-dimercaptosuccinic acid *Natl. Acad. Sci. Lett.* **35** 249
48. Alyar S, Özbek N, İskeleli N O and Karacan N 2013 Synthesis, characterization, and antimicrobial activity of copper(II) complexes with N,N′-propanediyl-bis benzenesulfo-namide and N,N′-ethanediyl-bis-2- methylbenzenesulfonamide *Med. Chem. Res.* **22** 2051
49. Mounika K, Anupama B, Pragathi J and Gyanakumari C 2010 Synthesis, characterization and biological activity of a schiff base derived from 3-ethoxy salicylaldehyde and 2-amino benzoic acid and its transition metal complexes *J. Sci. Res.* **2** 513
50. Gupta R, Agrawal N and Gupta K C 2012 Synthesis, IR spectral studies and biological activities of some rare earth metal complexes with biochemically relevant ligand *Res. J. Pharm. Biol. Chem. Sci.* **3** 50

VITAE

Name Mr. Surachai Kongchoo

Student ID 5510230029

Educational Attainment

Degree	Name of Institution	Year of Graduation
B. Sc. (Chemistry)	Thaksin University	2009
M. Sc. (Applied Chemistry)	Thaksin University	2012

Scholarship Awards during Enrolment

1. Songklanagarind Scholarship for Graduate Studies, Prince of Songkla University
2. The Thesis Research Fund through the Graduate School, Prince of Songkla University

List of Publications and Proceedings

Publications

1. Kongchoo, S.; Kantacha, A.; Saithong, S; Wongnawa, S. Synthesis, crystal structure, and spectroscopic properties of Cu(II) complex with 14-membered hexaazamacrocyclic ligands. *J. Chem. Crystallogr.* 2016, 46(5), 222-229.

2. Kongchoo, S.; Chainok, K; Kantacha, A.; Wongnawa, S. Copper(II) complex as a precursor for formation of cyano-bridged pentanuclear Fe^{III}-Cu^{II} bimetallic assembly: Synthesis, characterization, crystal structure, and antibacterial activity. *J. Chem. Sci.* 2017, 129(4), 431-440.

3. Kongchoo, S.; Kantacha, A.; Chainok, K; Wongnawa, S. Syntheses, crystal structures, spectroscopy, and catalytic properties of two nickel-based hexaaza-macrocyclic complexes with carboxylate ligands. Manuscript submitted to Inorganic Chemistry Communications. (April, 2017)

Proceedings

1. Kongchoo, S.; Kantacha, A.; Wongnawa, S. Synthesis and characterization of copper(II) and nickel(II) complexes of hexaazamacrocyclic ligands. Proceeding of the Pure and Applied Chemistry International Conference (PACCON2015), Amari Watergate Hotel, Bangkok, Thailand, January 21-23, 2015.

2. Kongchoo, S.; Chainok, K; Kantacha, A.; Wongnawa, S. Supramolecular architecture of nickel(II) macrocyclic complex containing *i*-butylamine pendant arms with *p*-nitrobenzoic acid ligand. Proceeding of the Pure and Applied Chemistry International Conference (PACCON2016), Bangkok International Trade & Exhibition Centre (BITEC), Bangkok, Thailand, February 9-11, 2016.